frontiers | Research Topics

Improving responses to immunotherapy in glioblastoma multiforme

Edited by
Stephanie E. B. McArdle, Divya Nagarajan and Michael Barish

Coordinated by
Joshua Pearson

Published in
Frontiers in Immunology

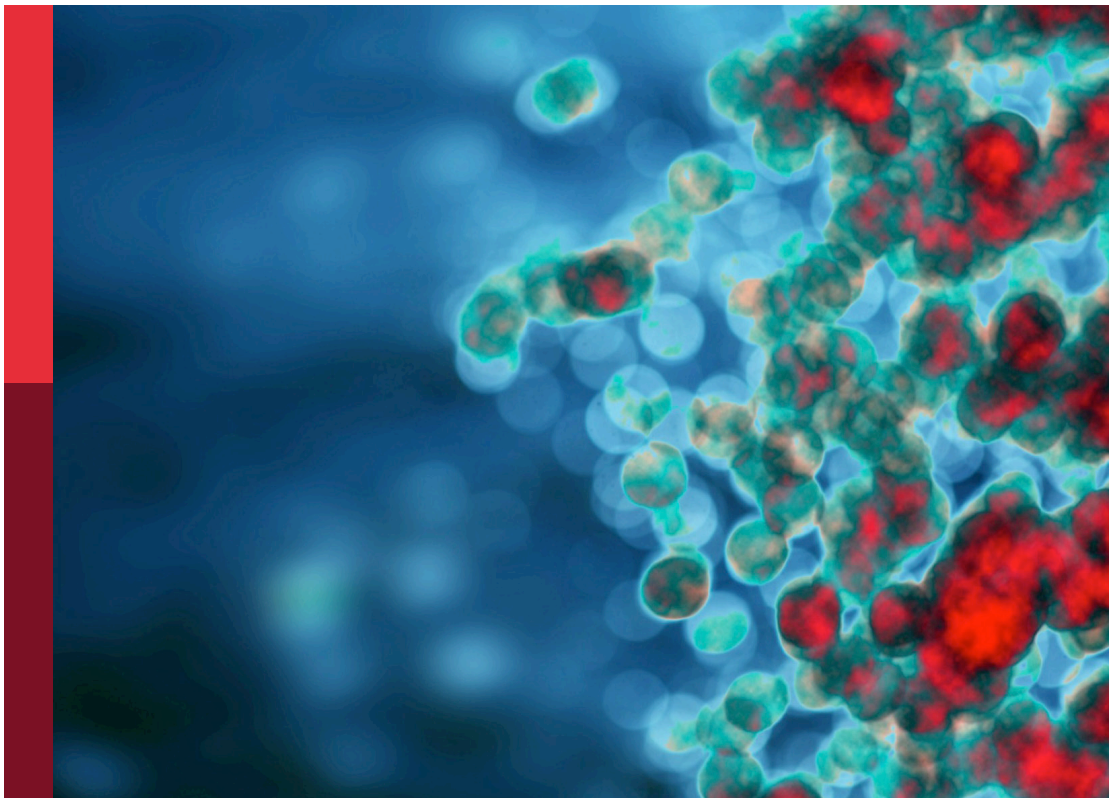

ISSN 1664-8714
ISBN 978-2-8325-4856-1
DOI 10.3389/978-2-8325-4856-1

About Frontiers

Frontiers is more than just an open access publisher of scholarly articles: it is a pioneering approach to the world of academia, radically improving the way scholarly research is managed. The grand vision of Frontiers is a world where all people have an equal opportunity to seek, share and generate knowledge. Frontiers provides immediate and permanent online open access to all its publications, but this alone is not enough to realize our grand goals.

Frontiers journal series

The Frontiers journal series is a multi-tier and interdisciplinary set of open-access, online journals, promising a paradigm shift from the current review, selection and dissemination processes in academic publishing. All Frontiers journals are driven by researchers for researchers; therefore, they constitute a service to the scholarly community. At the same time, the *Frontiers journal series* operates on a revolutionary invention, the tiered publishing system, initially addressing specific communities of scholars, and gradually climbing up to broader public understanding, thus serving the interests of the lay society, too.

Dedication to quality

Each Frontiers article is a landmark of the highest quality, thanks to genuinely collaborative interactions between authors and review editors, who include some of the world's best academicians. Research must be certified by peers before entering a stream of knowledge that may eventually reach the public - and shape society; therefore, Frontiers only applies the most rigorous and unbiased reviews. Frontiers revolutionizes research publishing by freely delivering the most outstanding research, evaluated with no bias from both the academic and social point of view. By applying the most advanced information technologies, Frontiers is catapulting scholarly publishing into a new generation.

What are Frontiers Research Topics?

Frontiers Research Topics are very popular trademarks of the *Frontiers journals series*: they are collections of at least ten articles, all centered on a particular subject. With their unique mix of varied contributions from Original Research to Review Articles, Frontiers Research Topics unify the most influential researchers, the latest key findings and historical advances in a hot research area.

Find out more on how to host your own Frontiers Research Topic or contribute to one as an author by contacting the Frontiers editorial office: frontiersin.org/about/contact

Improving responses to immunotherapy in glioblastoma multiforme

Topic editors
Stephanie E. B. McArdle — Nottingham Trent University, United Kingdom
Divya Nagarajan — Uppsala University, Sweden
Michael Barish — Department of Developmental and Stem Cell Biology, Beckman Research Institute, City of Hope, United States

Topic coordinator
Joshua Pearson — Nottingham Trent University, United Kingdom

Citation
McArdle, S. E. B., Nagarajan, D., Barish, M., Pearson, J., eds. (2024). *Improving responses to immunotherapy in glioblastoma multiforme*.
Lausanne: Frontiers Media SA. doi: 10.3389/978-2-8325-4856-1

Table of contents

05 Editorial: Improving responses to immunotherapy in glioblastoma multiforme
Stephanie E. B. McArdle, Divya Nagarajan and Michael E. Barish

07 Optimizing T Cell-Based Therapy for Glioblastoma
Aida Karachi, Farhad Dastmalchi, Saina Nazarian, Jianping Huang, Elias J. Sayour, Linchun Jin, Changlin Yang, Duane A. Mitchell and Maryam Rahman

19 Surfaceome Proteomic of Glioblastoma Revealed Potential Targets for Immunotherapy
Mélanie Rose, Tristan Cardon, Soulaimane Aboulouard, Nawale Hajjaji, Firas Kobeissy, Marie Duhamel, Isabelle Fournier and Michel Salzet

30 Comprehensive Analysis of the Tumor Immune Microenvironment Landscape in Glioblastoma Reveals Tumor Heterogeneity and Implications for Prognosis and Immunotherapy
Rongrong Zhao, Ziwen Pan, Boyan Li, Shulin Zhao, Shouji Zhang, Yanhua Qi, Jiawei Qiu, Zijie Gao, Yang Fan, Qindong Guo, Wei Qiu, Shaobo Wang, Qingtong Wang, Ping Zhang, Xing Guo, Lin Deng, Hao Xue and Gang Li

49 Glioma-derived CCL2 and CCL7 mediate migration of immune suppressive CCR2^{+}/CX3CR1^{+} M-MDSCs into the tumor microenvironment in a redundant manner
Gregory P. Takacs, Christian J. Kreiger, Defang Luo, Guimei Tian, Julia S. Garcia, Loic P. Deleyrolle, Duane A. Mitchell and Jeffrey K. Harrison

65 The diversity and dynamics of tumor-associated macrophages in recurrent glioblastoma
Lingyun Zhang, Yu Jiang, Gao Zhang and Shiyou Wei

79 $\gamma\delta$ T cells as a potential therapeutic agent for glioblastoma
In Kang, Yumin Kim and Heung Kyu Lee

93 Antigen presentation deficiency, mesenchymal differentiation, and resistance to immunotherapy in the murine syngeneic CT2A tumor model
J. Bryan Iorgulescu, Neil Ruthen, Ryuhjin Ahn, Eleni Panagioti, Prafulla C. Gokhale, Martha Neagu, Maria C. Speranza, Benjamin K. Eschle, Kara M. Soroko, Raziye Piranlioglu, Meenal Datta, Shanmugarajan Krishnan, Kathleen B. Yates, Gregory J. Baker, Rakesh K. Jain, Mario L. Suvà, Donna Neuberg, Forest M. White, E. Antonio Chiocca, Gordon J. Freeman, Arlene H. Sharpe, Catherine J. Wu and David A. Reardon

111 Adoptive cell therapy for high grade gliomas using simultaneous temozolomide and intracranial mgmt-modified γδ t cells following standard post-resection chemotherapy and radiotherapy: current strategy and future directions
L. B. Nabors, L. S. Lamb, T. Goswami, K. Rochlin and S. L. Youngblood

118 Targeting Wnt signaling for improved glioma immunotherapy
Margarita Gutova, Jonathan C. Hibbard, Eric Ma, Heini M. Natri, Vikram Adhikarla, Nyam-Osor Chimge, Runxiang Qiu, Cu Nguyen, Elizabeth Melendez, Brenda Aguilar, Renate Starr, Holly Yin, Russel C. Rockne, Masaya Ono, Nicholas E. Banovich, Yate-Ching Yuan, Christine E. Brown and Michael Kahn

frontiers | Frontiers in Immunology

TYPE Editorial
PUBLISHED 23 April 2024
DOI 10.3389/fimmu.2024.1407930

OPEN ACCESS

EDITED AND REVIEWED BY
Peter Brossart,
University of Bonn, Germany

*CORRESPONDENCE
Stephanie E. B. McArdle
stephanie.mcardle@ntu.ac.uk

RECEIVED 27 March 2024
ACCEPTED 10 April 2024
PUBLISHED 23 April 2024

CITATION
McArdle SEB, Nagarajan D and Barish ME (2024) Editorial: Improving responses to immunotherapy in glioblastoma multiforme. *Front. Immunol.* 15:1407930. doi: 10.3389/fimmu.2024.1407930

Editorial: Improving responses to immunotherapy in glioblastoma multiforme

Stephanie E. B. McArdle[1,2]*, Divya Nagarajan[3] and Michael E. Barish[4]

[1]John van Geest Cancer Research Centre, Nottingham Trent University, Nottingham, United Kingdom, [2]School of Science and Technology, Department of Biosciences, Nottingham Trent University, Nottingham, United Kingdom, [3]Pencil Biosciences Limited, Macclesfield, United Kingdom, [4]Department of Stem Cell Biology and Regenerative Medicine, Beckman Research Institute, City of Hope, Duarte, CA, United States

KEYWORDS

glioblastoma multiforme (GBM), immunotherapy, responses, improve, future

Editorial on the Research Topic
Improving responses to immunotherapy in glioblastoma multiforme

Glioblastoma multiforme (GBM), WHO grade 4 glioma, IDH-wildtype, is essentially a uniformly fatal primary brain tumour. Whilst many therapeutic interventions have been studied pre-clinically, and tantalizing observations have emerged from clinical trials, very few have matured to the level required for clinical use as therapies for patients with GBM, and unfortunately nearly all GBM tumours relapse.

These tumours are uniquely challenging due to their location within the brain, making delivery of therapeutic interventions difficult. Further, the GBM tumour microenvironment is highly immunosuppressive, dominated by tumour-associated macrophages (TAMs) and myeloid suppressor cells. Here, Takacs et al., who previously reported the existence of three populations of myeloid cells within the glioma microenvironment based on expression of chemokine receptors CCR2 and CX3CR1, demonstrate that myeloid-derived suppressor cells (MDSCs) expressing both CCL2 and CCL7 represent a potent and migratory T cell suppressive population, and that a therapeutic strategy targeting CCR2 might help limit recruitment of this population to the brain. Wei et al. discuss therapy-induced changes of the tumor microenvironment (TME) in recurrent GBM (rGBM), with large infiltration of CD68+ macrophages following anti-angiogenic therapy together with the almost (82%) complete loss of the immunogenetic epidermal growth factor receptor variant III (EGFRvIII). These macrophages are the dominant non-malignant cells in the TME of rGBM, are far more diverse than a simple binary M1/M2 polarisation and are very plastic cells that need to be taken into consideration when applying immunotherapies to treat rGBM as reviewed by Wei et al. This immunosuppressive microenvironment also affects tumour-infiltrating lymphocytes (TILs), which have been found to exhibit exhausted phenotypes, expressing PD-1, TIM-3, LAG-3, TIGIT, and CD39, or are otherwise dysfunctional. Zhao et al. describe 25 immune cell types in 796 GBM samples, find patterns associated with different clinical outcomes, and identify novel dysregulated signalling pathways that could be used as prognosticators of treatment outcomes. In this regard, Gutova et al. focus on one such pathway, the Wnt signalling pathway, using the

small molecule inhibitor ICG-001, and find that it has pleotropic effects on a GL261 tumour model: increased TIL recruitment and activation, modulation of the tumour stroma, and differentiation of self-renewing glioma stem cells. However, as demonstrated by Iorgulescu et al., murine GL261 and CT2A glioma models, in contrast to human GBM, have high mutational loads, and neither cell line shares the essential genetic or histologic features of human GBM. As such, these results warrant confirmation using better suited GBM models.

Adoptive transfer of chimeric antigen receptor (CAR) T cells are a potentially interesting avenue. Karachi et al. discuss this approach in their review, considering ongoing clinical trials and the hurdles faced by CAR T cell strategies. One challenge is antigen loss in the context of highly heterogeneous tumors, rendering single antigen-targeted T cells useless. Indeed, antigen escape has been demonstrated, and may be one of several mechanisms underlying tumour recurrence. One could envisage adoptive transfer of CAR T cells recognising more than one antigen, or CAR T cells recognizing targets expressed by most or all cells within a tumour, or strategies incorporating additional CAR T cells to be injected once the tumour recurs. Relevant to this approach, Rose et al. identify multiple surface proteins, including some that are mutated proteins, some that are targeted by existing drugs, and some novel proteins not yet targeted.

In this Research Topic, two groups, Kang et al. and Nabors et al., discuss γδ T cells as vehicles for CAR expression and as a potential alternative to the more abundant αβ T cells. γδ T cells are a small (0.5-5%) subset of all T cells, whose T cell receptors (TCRs) consist of γ and δ chains, hence their name. Contrary to αβ TCRs, antigen recognition by γδ TCRs is independent of class I major histocompatibility complex (MHC) molecules, and therefore potentially obviate the very expensive requirement for patient-specific autologous adoptive transfer. Further, γδ T cells produce high numbers of cytokines and are the most abundant T cell in the gut mucosa. Nabors et al. previously showed that GBM cells constitutively express low levels of the stress associated NKG2D ligands (NKG2DL) recognised by γδ T cells. They show here that NKG2DL expression is increased by temozolomide (TMZ) treatment, but also that TMZ is toxic to γδ T cells. However, by rendering their γδ T cells resistant to TMZ, these cells could be administrated to patients receiving TMZ treatment in a first-in-human phase 1 clinical trial (NCT04165941). CAR engineered γδ T cells could both be an alternative approach to CAR T cell immunotherapy, and a complementary approach to be considered on tumour recurrence.

One hopes that the efforts described here, and others, will collectively begin to help patients with GBM that presently lack effective treatment options.

Author contributions

SM: Writing – original draft, Writing – review & editing. DN: Writing – review & editing. MB: Writing – review & editing.

Conflict of interest

The authors declare that the research was conducted in the absence of any commercial or financial relationships that could be construed as a potential conflict of interest.

Publisher's note

frontiers in Immunology

REVIEW
published: 05 August 2021
doi: 10.3389/fimmu.2021.705580

Optimizing T Cell-Based Therapy for Glioblastoma

Aida Karachi, Farhad Dastmalchi, Saina Nazarian, Jianping Huang, Elias J. Sayour, Linchun Jin, Changlin Yang, Duane A. Mitchell and Maryam Rahman*

Lillian S. Wells Department of Neurosurgery, University of Florida (UF) Brain Tumor Immunotherapy Program, University of Florida, Gainesville, FL, United States

Evading T cell surveillance is a hallmark of cancer. Patients with solid tissue malignancy, such as glioblastoma (GBM), have multiple forms of immune dysfunction, including defective T cell function. T cell dysfunction is exacerbated by standard treatment strategies such as steroids, chemotherapy, and radiation. Reinvigoration of T cell responses can be achieved by utilizing adoptively transferred T cells, including CAR T cells. However, these cells are at risk for depletion and dysfunction as well. This review will discuss adoptive T cell transfer strategies and methods to avoid T cell dysfunction for the treatment of brain cancer.

Keywords: T cell dysfunction, exhaustion, glioblastoma, glioma, CAR T cells, adoptive T cell transfer

OPEN ACCESS

Edited by:
Rodabe N. Amaria, University of Texas MD Anderson Cancer Center, United States

Reviewed by:
Andrew Sloan, Case Western Reserve University, United States
Pedro Lowenstein, University of Michigan, United States

****Correspondence:***
Aida Karachi
Aida.karachi@neurosurgery.ufl.edu

Specialty section:
This article was submitted to Cancer Immunity and Immunotherapy, a section of the journal Frontiers in Immunology

Received: *05 May 2021*
Accepted: *20 July 2021*
Published: *05 August 2021*

Citation:
Karachi A, Dastmalchi F, Nazarian S, Huang J, Sayour EJ, Jin L, Yang C, Mitchell DA and Rahman M (2021) Optimizing T Cell-Based Therapy for Glioblastoma. Front. Immunol. 12:705580. doi: 10.3389/fimmu.2021.705580

INTRODUCTION

T cells are the key players of the adaptive immune response, and their potency is being leveraged for the treatment of cancer. T cells represent a diverse population of immune cells in the peripheral blood and lymphoid organs, and their overarching function is to rid the host of "non-self" or antigen expressing cells. Many studies have shown a positive correlation between the presence of tumor infiltrating T cells and prognosis in solid tissue malignancies (1–3) including glioblastoma (GBM) (4). T cell immunotherapeutic platforms have had success in certain hematologic and solid tissue cancers (5). However, T cell dysfunction is a major limitation for the efficacy of these strategies in the treatment of GBM (6).

Dysfunctional T cells are defined by loss of effector function, including loss of cytotoxicity, decreased secretion of inflammatory cytokines such as interleukin-2 (IL-2), tumor necrosis factor-α (TNF-α), or interferon- γ (IFN-γ) (7). These cells often develop due to chronic antigen exposure with loss of the ability to respond to antigen with cytolysis **(Figure 1).** Dysfunctional T cells can limit the efficacy of immunotherapeutic strategies for patients with GBM. Infusion of potent T cells educated against particular antigens is an attractive strategy to overcome the dysfunction and sequestration seen in host T cells in patients with GBM. Several platforms are being developed, including adoptive transfer of autologous T cells followed by vaccination and autologous T cells engineered for improved anti-tumor efficacy such as chimeric antigen receptor (CAR) T cells. These platforms have shown some response rates in early trials. However, these therapies are limited by issues with engraftment, a hostile tumor microenvironment, and induced T cell dysfunction. In this review, we will discuss adoptive transfer of T cells for the treatment of GBM and factors that affect the potency of these approaches.

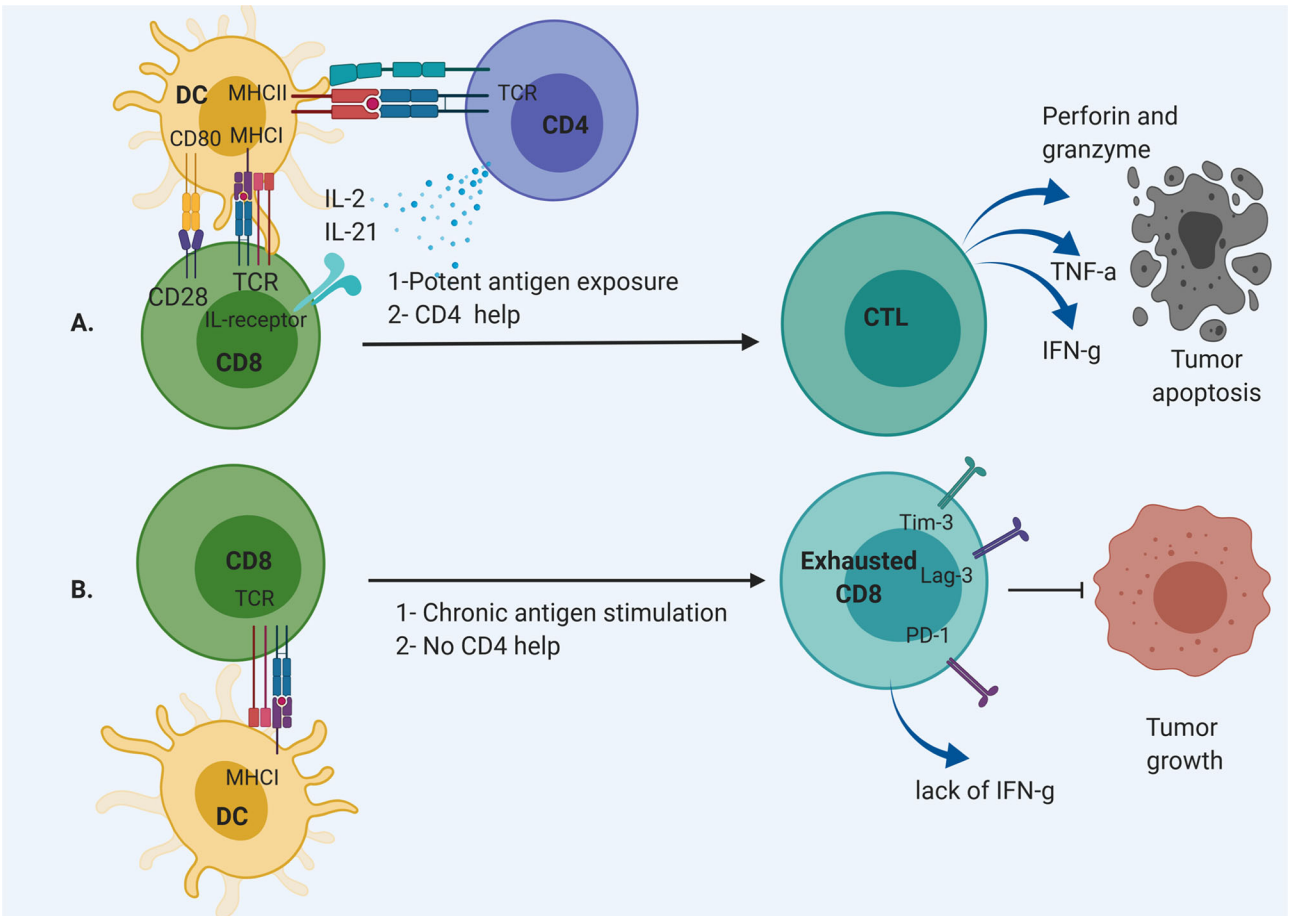

FIGURE 1 | CD8 T cell differentiation pathway. **(A)** CD8 T cell are activated through MHC I by dendritic cells (DCs) with CD4 "help" *via* IL-2 and IL-21 secretion. This results in the development of CD8 effector T cells that can cause cytolysis. **(B)** Chronic antigen exposure and lack of appropriate support from T helpers result in exhausted CD8 T cells without effector function to remove tumor cells.

EXOGENOUS T CELLS FOR GBM

Adoptive T cell infusion provides the host with a bolus of functional T cells primed against a particular antigen. Approaches to generate tumor specific T cells are 1) infusion of autologous, expanded T cells primed against the antigen of interest, or 2) infusion of autologous, engineered T cells such as chimeric antigen receptor (CAR) T cells **(Figure 2).** Autologous T cells are typically harvested from the peripheral blood (8). Tumor infiltrating lymphocytes (TILs) are intrinsically tumor specific, but in patients with GBM, are too few and dysfunctional, and therefore do not represent a viable source of cells (9, 10). Peripheral circulating T cells must be primed against antigens by co-culturing with antigen loaded dendritic cells (DCs) or through genetic engineering. After detecting antigen specific T cell clones, these cells are expanded and infused into the patients as adoptive T cell transfer.

These strategies are being tested in early phase trials (**Table 1**). A phase I/II study (NCT00331526) in 2004 studied the safety of implantation of lymphocytes into the tumor resection cavity in patients with newly diagnosed or recurrent glioma (11, 12). The lymphocytes were generated from PBMCs and grown with IL-2. The investigators called these cells lymphokine activated killer (LAK) cells. They found that this approach was safe in 40 patients. However, the analysis did not evaluate the engraftment or persistence of the cells. An on-going phase I/II study is testing autologous cytotoxic T cells primed against pp65 CMV antigen in patients with newly diagnosed GBM (NCT02661282). In this study, patients receive dose intensified temozolomide to induce lymphopenia and leverage the homeostatic lymphoproliferation that ensues after temozolomide induced lymphopenia. Patients receive up to 4 cycles of temozolomide followed by T cell infusion. The results so far have found that the production of large numbers of T cells from patients with GBM is feasible, and the treatment has been safe. Results on engraftment and clinical efficacy are still underway (13). The ERaDICATe clinical trial (NCT00693095) is also testing CMV targeting T cells with temozolomide and is adding DC vaccines to one of the cohorts to determine if this improves the persistence of T cells (14).

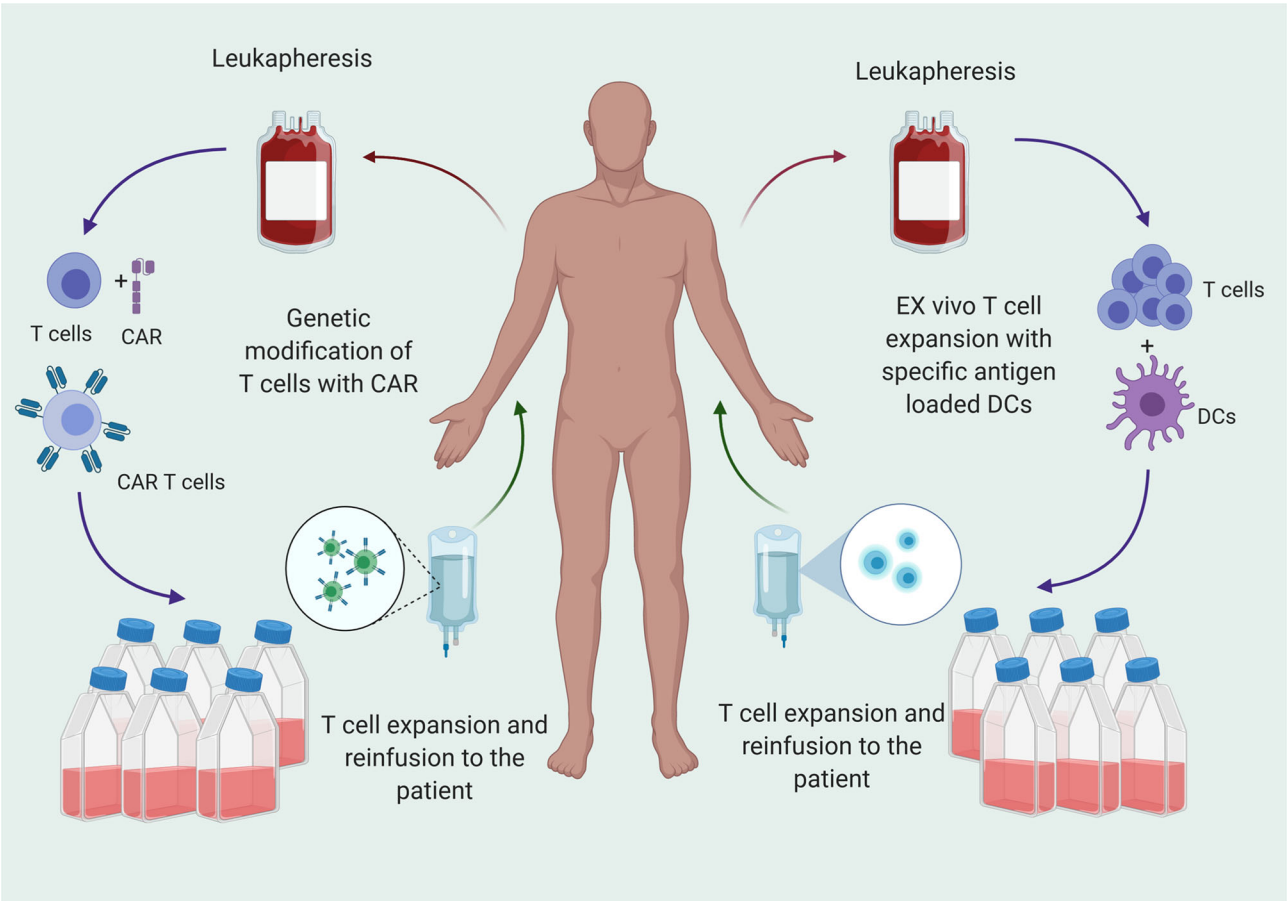

FIGURE 2 | T cell therapy for cancer treatment is transfer of T cells that are specific for tumor antigens to the patients after *ex vivo* expansion. T cells are matured from peripheral blood mononuclear cells (PBMCs) and primed against antigen or genetically engineered to express CARs that specific for the antigen and reinfused to patients after *ex vivo* expansion.

Similarly, adoptive transfer of clonally selected T cells targeting tumor has been described for the treatment of recurrent primitive neuroectodermal tumors (PNETs) (19). Blood was drawn and tumor biopsies were obtained from 10 patients for vaccine preparation. Autologous T cells were isolated from patients' blood and were primed and expanded *ex vivo* by exposure to dendritic cells loaded with total tumor RNA extracted from tumor biopsies. The T cells were infused back to the patients after conditioning chemotherapy. Some patients received non myeloablative chemotherapy, and others received myeloablation followed by stem cell rescue. These conditioning regimens have significant implications for the potential for T cell proliferation and are further discussed in the following sections of this review. Patients subsequently received three dendritic cell (DC) vaccines. T cell receptor (TCR) RNA sequencing of peripheral blood mononuclear cells (PBMCs) after treatment demonstrated a large clonal expansion of T cells, which correlated with clinical outcomes. This platform is now also being tested in high-grade pediatric glioma (NCT03334305) and diffuse intrinsic pontine glioma (DIPG) (NCT03396575).

Alternatively, T cells can be engineered to provide a more potent population of cells. Autologous patient derived T cells isolated from patients can be modified with a CAR gene. CAR T cells are designed to express artificial T cell receptor using viral transfection to recognize cancer antigens. CARs are composed of extracellular, transmembrane and intracellular domain. The extracellular domain, also known as tumor targeting domain, is composed of single chain variable fragment (scVF) that is made up of the variable regions of the heavy and light chains (20). The tumor targeting domains are not restricted by MHC bound antigens. They can recognize non-MHC cell surface proteins. Intracellular domain composed of CD3ζ to direct T cells for performing the primary cytolytic activity. However, cytotoxic T cells require further signaling when they encounter a cognate foreign antigen to induce expansion, persistence, and cytokine secretion (21). To address this issue, 2nd and 3rd generation of CAR T cells developed with the 2nd generation composed of co-stimulatory domains such as CD28, 4-1BB to improve proliferation and cytokine production of CAR T cells. The 3rd generation of CAR T cells, composed of multiple signaling

TABLE 1 | T cell clinical trials for brain tumors.

Title/ Trial NCT	Phase	Disease	T cell product	Interventions	n	OS	Status	Reference
Cellular Adoptive Immunotherapy in Treating Patients with Glioblastoma Multiforme (NCT00331526)	II	Brain and CNS tumors, newly diagnosed or recurrent glioma	PBMC derived lymphocytes grown with IL-2 (lymphokine activated killer cells)	**Biologic:** 1. Aldesleukin	86	Median survival of 20.5 months with a 1-year survival rate of 75%)	Completed	(11) (12)
Autologous CMV-Specific Cytotoxic T Cells and Temozolomide in Treating Patients with Glioblastoma (NCT02661282)	I/II	Newly diagnosed CMV positive GBM	*Ex vivo* expanded polyclonal CD8+ and CD4+ CMV T cells from peripheral blood of GBM patients	**Drug:** 1. Dose-intensified Temozolomide	65 (34 were screened)	N/A	Active, not recruiting	(13)
Evaluation of Recovery from Drug-Induced Lymphopenia Using Cytomegalovirus-specific T-cell Adoptive Transfer (ERaDICATe) (NCT00693095)	I	GBM	CMV-autologous lymphocyte transfer	**Biologic:** 1. CMV-DC vaccine	22	N/A	Completed	(14)
Adoptive Cellular Therapy in Pediatric Patients with High-grade Gliomas (ACTION) (NCT03334305)	I	GBM	Total tumor RNA primed autologous T cells	**Biologic:** 1. TTRNA-DC vaccines with GM-CSF 2.Autologous Hematopoietic Stem cells (HSCs) **Drug:** 1. Dose-intensified Temozolomide 2.Td vaccine	18	N/A	Recruiting	NCT03334305
Brain Stem Gliomas Treated With Adoptive Cellular Therapy During Focal Radiotherapy Recovery Alone or With Dose-intensified Temozolomide (BRAVO) (NCT03396575)	I	Diffuse intrinsic pontine glioma (DIPG)	Total tumor RNA primed autologous T cells	**Biologic:** 1. TTRNA-DC vaccines with GM-CSF 2.Autologous hematopoietic stem cells (HSCs) **Drug:** 1. Cyclophosphamide + Fludarabine 2.Td vaccine	21	N/A	Recruiting	NCT03396575
CAR T Cell Receptor Immunotherapy Targeting EGFRvIII for Patients with Malignant Gliomas Expressing EGFRvIII (NCT01454596)	I/II	Recurrent GBM	A single infusion of EGFRvIII CAR T cells	**Drug:** 1. Aldesleukin 2. Fludarabine 3. Cyclophosphamide	10	8	Completed	(20)
Genetically Modified T-cells in Treating Patients with Recurrent or Refractory Malignant Glioma (NCT02208362)	I	Recurrent or Refractory GBM	Intratumoral Infusion of IL13R alpha 2-specific CAR T cells followed by infusions into the ventricular system	**N/A**	92	N/A	Recruiting	(21)
IL13Ralpha2-Targeted Chimeric Antigen Receptor (CAR) T Cells with or Without Nivolumab and Ipilimumab in Treating Patients with Recurrent or Refractory Glioblastoma (NCT 04003649)	I	Recurrent or Refractory GBM	Intratumoral Infusion of IL13R alpha 2-specific CAR T cells followed by infusions into the ventricular system	**Drug:** 1. Ipilimumab 2. Nivolumab	60	N/A	Recruiting	NCT 04003649
CMV-specific Cytotoxic T Lymphocytes Expressing CAR Targeting HER2 in Patients With	I	Recurrent GBM	Infusion of autologous CMV-specific cytotoxic T-lymphocytes genetically modified to	**N/A**	17	24.5	Completed	22

(Continued)

TABLE 1 | Continued

Title/ Trial NCT	Phase	Disease	T cell product	Interventions	n	OS	Status	Reference
GBM (NCT01109095)			express CAR19 targeting the HER2 molecule					
3rd Generation GD-2 Chimeric Antigen Receptor and iCaspase Suicide Safety Switch **(GRAIN)** (NCT01822652)	I	Relapsed or refractory Neuroblastoma	Infusion of third generation GD2-CAR (GD2-CAR3) generated from patients' PBMC	**Drug:** 1. Cyclophosphamide 2. Fludarabine 3. Pembrolizumab	11	16.8	Active, not recruiting	(41)
Pembrolizumab in Patients Failing to Respond to or Relapsing After CAR T Cell Therapy for Relapsed or Refractory Lymphomas (NCT02650999)	I/II	CD19 Diffuse Large B-cell Lymphomas, Follicular Lymphomas, Mantle Cell Lymphomas	Infusion of PBMC derived CAR T cells specific for CD19	**Drug:** Pembrolizumab	12	N/A	Active, not recruiting	(42)
Study of DC Vaccination Against Glioblastoma (NCT01567202)	II	GBM	Infusion of DC vaccine loaded with glioblastoma stem cell-like (GSC) antigens	**Biologic:** 1. DC vaccination **Drug:** 1. Temozolomide **Radiation:** 1. Radiotherapy	43	13.7	Recruiting	
Chemotherapy, Radiation Therapy, and Vaccine Therapy With Basiliximab in Treating Patients With Glioblastoma Multiforme That Has Been Removed by Surgery (NCT00626015)	I	GBM	N/A	**Biologic:** 1.PEP-3-KLH conjugate vaccine **Drug:** 1. Daclizumab 2. Temozolomide	16		Completed	NCT00626015
EGFRvIII CAR T Cells for Newly-Diagnosed WHO Grade IV Malignant Glioma (NCT02664363)	I	GBM	EGFRvIII CAR T cells	**Drug:** 1. Dose-intensified temozolomide	3	N/A	Terminated	NCT02664363

CMV, cytomegalovirus; DC, dendritic cells; TTRNA, Total tumor RNA; GM-CSF, Granulocyte-macrophage colony-stimulating factor; TD vaccine, tetanus; diphtheria vaccine.

domains such as CD28 and 4-1BB or Ox40. The most current generation CAR T cells, T cells redirected for universal cytokine-mediated killing (TRUCKS), have co-stimulatory molecules and are armed with transgenes to express a synthetic protein of interest such as immune stimulatory cytokines of IL-2, IL-5, IL-12 to exhibit an improved anti-tumor function and resistance to immunosuppressive tumor microenvironment (22, 23).

Two FDA approved CAR T cell therapies are available for treatment of acute lymphoblastic leukemia (ALL) and diffuse large B cell lymphoma (DLBCL), Tisagenlecleucel (CTL019, Kymriah©) and axicabtagene ciloleucel (Yescarta©). Three single antigen CAR T cell therapies are under investigation for GBM targeting EGFRvIII, IL13Rα2, and HER2. A single infusion of EGFRvIII CAR T cells was tested in 10 patients with recurrent GBM in a phase I study (NCT01454596) that required EGFRvIII expression in tumor samples (15). Patients did not receive conditioning with chemotherapy prior to infusion. Cells were detectable by flow cytometry or PCR but declined significantly (2-10 fold) within 14 days post infusion. The level of existing lymphopenia did not correlate with peak engraftment. EGFRvIII CAR T cells were detectable in the tumor specimens of patients who had early surgery after infusion (within two weeks). However, some of the specimens also had infiltration of immunosuppressive regulatory T cells and upregulation of IDO1, PD-L1, and IL-10, suggesting that the infiltration of EGFRvIII cells within the tumor incited a compensatory immunosuppressive response.

IL13Rα2 targeting CAR T cells are also being tested in patients with recurrent GBM either as monotherapy (NCT02208362) or in combination with immune checkpoint blockade (NCT 04003649). A report of a single patient with multiple intracranial and spinal lesions of recurrent, wide-spread GBM demonstrated regression when treated with intrathecal delivery of IL13Rα2 CAR T cells developed from autologous cells (16). The patient eventually succumbed to disease progression. Similarly, HER2 CAR T cells were tested in a phase I study in patients with recurrent GBM with HER2 expression (24). No conditioning regimen was given prior to infusion. Most patients had the highest concentrations of detectable HER2 CAR T cells in the peripheral blood within two weeks of infusion. Six weeks after infusion, detectable CAR T cells declined significantly. The median overall survival was 24.5 months after diagnosis and was 11.1 months after T cell infusion.

BARRIERS TO T CELL-BASED THERAPY

Engraftment

A major hurdle for T cell therapy is the engraftment of cells. Engraftment for T cell therapy in brain tumors refers to presence of the cells in the peripheral blood and migration within the tumor microenvironment for sustained anti-tumor responses. This definition is different from the traditional concept of engraftment of hematopoietic stem cells, which are expected to take residence

in the bone marrow for cellular production. The kinetics of autologous T cells after the infusion is a decline as they distribute in the tissues, an increase as they proliferate, and a subsequent decline that persists (25, 26). As discussed in the previous section, most patients do not have detectable levels of infused T cells within two weeks after infusion. Approaches to improve engraftment are pre-conditioning with chemotherapy to induce lymphopenia. This allows for the infused T cells to have less "competition" for cytokines and also to leverage the homeostatic lymphoproliferation that results from the lymphopenia (27–29). Another alternative strategy is the use of DC vaccination following T cell infusion. In a pilot study, 17 patients with newly diagnosed GBM were randomized to receive CMV targeting T cells alone or with DC vaccines (14). The patients who received vaccines had significant increases (~1.5-fold, p=0.04) in T cells that expressed IFN gamma, TNF alpha, and CCL3. However, this analysis was performed only seven days after T cell infusion. Therefore, the persistence of cells after DC vaccination was not evaluated.

Another method to overcome issues with loss of T cell frequency in the circulation is to force cells to accumulate in the tumor microenvironment. This technique was utilized successfully in pre-clinical models testing a CD70 CAR T cell (30). The CD70 CAR T cell was modified to express IL-8 receptors (CXCR-1 and CXCR-2) (31). In the setting of CD70 expressing tumors treated with radiotherapy (RT), the modified CD70 CAR T cells had much greater trafficking to the tumors due to IL-8 upregulation after RT. The improved CAR T cell tumor infiltration resulted in long term survivors compared to only 35 days of survival in untreated animals, and a strong memory T cell response that prevented regrowth of tumors on re-challenge.

Potency

One of the limiting factor of transferred T cells' potency is exhaustion. Exhaustion is a T cell state that develops gradually in both transferred and host T cells due to repeated stimulation of the T cell from persistent antigen exposure (32). Exhaustion has distinct signatures but one of the most important characteristics of exhausted T cells is persistent over-expression of inhibitory checkpoints. The over-expression of immune checkpoints is also present in activated T cells. However, activated T cells experience a transient upregulation of immune checkpoints while exhausted T cells have a persistent upregulation of immune checkpoints.

Exhausted T cells are heterogeneous and include two different cell populations: progenitor exhausted T cells and terminally differentiated exhausted T cells. Progenitor exhausted T cells can be generated from both effector T cells or directly from naïve T cells. Progenitor exhausted T cells have some stem cell like characters similar to central memory T cells as they have the potential to proliferate and expand and also reverse to effector T cells after vaccination or PD-1 blockade (33, 34). Although these cells have a high expression of PD-1 and T cell factor-1(TCF-1), which is a self-renewal marker, they have a limited expression of other inhibitory molecules and lack expression of markers like Tim-3 (35).

Terminally differentiated exhausted T cells are generated from high PD-1 expressing cells with expression of multiple immune checkpoints and lack of responsiveness to immune checkpoint blockade (36). Persistent antigen exposure leads to upregulation of transcription factor TOX and alterations of nuclear factor activated T cells (NFAT), which is required for formation of exhausted T cells (37, 38). In GBM, TILs expressing high levels of Tim-3, Lag-3 and PD-1 that fail to secrete IFN-g, IL-2 and TNF-α are considered terminally exhausted (9).

Exhaustion can also be seen in transferred CAR T cells that results in reduced anti-tumor efficacy. In elegant experiments performed by Dr. Rao's group, CD19 reactive CAR T cells were found to have gene expression and chromatin accessibility associated with NFAT pathway including activation of NR4A1-3 (37). When the three NR4A binding motifs were knocked out in the CAR T cells, the gene expression profiles and chromatin regions of effector CD8 T cells were characterized, and they caused tumor regression and prolonged survival in tumor bearing mice (75% in triple knockout CAR T cells versus <5% wild type CAR T cells, p<0.0001).

Other potential strategies to avoid exhaustion of CAR T cells include combining with immune checkpoint blockade (39). Pre-clinical models have demonstrated enhanced anti-tumor efficacy when PD-1 blockade is added to CAR T cells in murine models of lung cancer and breast cancer (40–42). In a small study of patients with neuroblastoma, the addition of PD-1 blockade to lymphodepletive chemotherapy did not enhance the expansion or persistence of third generation GD2 CAR T cells (17). Administration of PD-1 blockade in 10 adult patients with high grade gliomas resulted in blockade of PD-1 on both host T cells and intracranial injected CAR T cells with reduction of PD-1 on T cell surface from 39.3% to 3.8% (18). In this study the effect of PD-1 blockade on T cell function and phenotype were not evaluated. Therefore, T cells engineered to secrete immune checkpoint antibodies are being developed (43, 44).

Another strategy is having the CAR induced only when the antigen is present. Choe et al. developed a CAR T cell that has CAR activation only when a synNotch receptor interacts with the tumor antigen (45). They utilized EGRvIII and myelin oligodendrocyte glycoprotein (MOG) targeting CARs to demonstrate that these particular CAR T cells were more likely to be in a naïve/stem cell memory state. This correlated with better anti-tumor efficacy. NCG mice implanted with GBM6 PDX GBM were treated with α-EGFRvIII synNotch–α-EphA2/IL13Rα2 CAR T cells which resulted in long-term remission of all tumors. In other studies, CAR T cells targeting alkaline phosphatase placental-like 2 (ALPPL2) in murine models of human ovarian and mesotheliomas tumors had longer persistence and better tumor control when synNotch was added (46). Animals bearing M28 mesotheliomas tumors were treated with ALPPL2-synNotch-MCAM CAR T cells and demonstrated complete responses in the majority of animals with less PD-1+/CD39+ exhausted CD8 T cells (~60%) compared to MCAM CAR T cells (~75%).

T cell-based therapies have been limited thus far due to the inability to target all antigen-expressing tumor cells. Strategies to overcome issues with T cell effector function began with the development of 2nd and 3rd generation CAR T cells. First generation CAR T cells only had CD3ζ intracellular domain signaling, which limited the ability of complete activation signaling and secretion of cytokines long-term as the signaling

diminished over time (47). Second and third generation CAR T cells added 4-1BB and CD28, which are co-stimulatory factors that improved activation and expansion (22). Fourth generation CAR T cells provide the ability to secrete a protein of interest such as cytokines and chemokines with enhanced T cell persistence and anti-tumor function (23).

In GBM, CAR T cells have also been modified to improve activation. IL13Rα2-CAR T cells were engineered to overexpress IL-15 to enhance effector function (48). Transgenic IL-15 expressing IL13Rα2-CAR T cells had greater expansion and enhanced anti-tumor effector function as measured by cytokine production. IL-15 secreting CAR T cells showed enhanced intracranial persistence with resultant tumor regression in the U373 human glioblastoma orthotopic xenograft mouse GBM model. However, tumors recurred after 40 days due to IL13Rα2 antigen loss (48).

Antigen Loss

Tandem and trivalent CAR T cells have been developed in an attempt to overcome the issue of antigen loss post CAR T cell therapies that has been seen with both EGFRvIII CAR T cell therapy in patients with GBM (15) and IL13Rα2 CAR T cell therapy in a xenograft GBM mouse model (48). In a murine GBM model, tandem CAR T cells targeting HER2 and IL13Rα (two specific antigen targeting domains within one CAR construct) displayed enhanced activation and anti-tumor function without being more exhaustible than co-expressed HER2 and IL13Rα CAR T cells (biCAR T cells) or pool of single antigen HER2 or IL13Rα CAR T cells (49) (**Figure 3**). These tandem CAR T cells had moderate increases in IFN-gamma and IL-2 secretion and improved tumor-killing capacity (~60% in tandem CAR *vs*~20% in biCAR in U373 model, $p<0.05$). The animals treated with tandem CAR T cells had a survival of >140 days compared to biCAR (85 days) ($p<0.0001$).

Due to the heterogeneity of GBM tumor cells, the expression of surface antigens significantly varies between patients, and targeting two antigens may not be an effective treatment for all patients. CAR T cells targeting HER2, IL13Rα2, and ephrin-A2 (EphA2) have been developed to provide antigenic "coverage" for almost all patients (50). This trivalent CAR T cell demonstrated improved anti-tumor activity and survival in GBM patient derived xenografts compared to biCAR (IL13Rα2, andEphA2) and single IL13Rα2 CAR T cells, while lower T cell doses were required to control tumor growth. The ability of the trivalent CAR to overcome tumor antigen loss is still unknown.

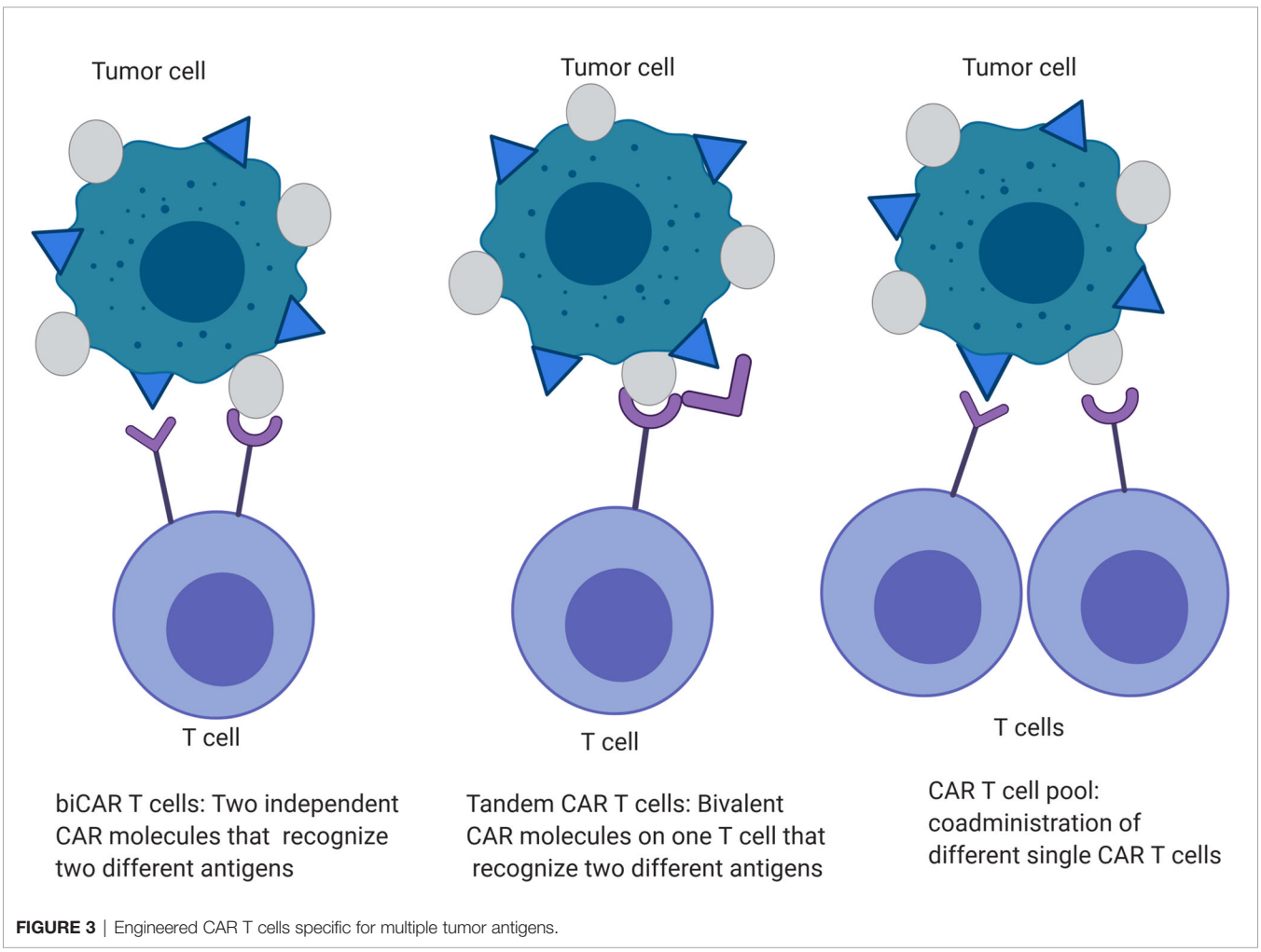

FIGURE 3 | Engineered CAR T cells specific for multiple tumor antigens.

Peptide based CAR T cells exploit the binding potential of the peptides to target diverse heterogeneous tumor cells without a shared specific antigen. Researchers complexed a peptide [chlorotoxin (CLTX) extracted from the scorpion's venom] to the CD28 end of the CAR (51). Although the specific tumor cell surface receptor for CLTX has not been identified, this study found that the CLTX CAR T cells tumor recognition was mediated by expression of membrane-bound matrix metalloproteinase-2 (MMP-2) on the tumor cells. These peptide targeting CAR T cells resulted in anti-tumor effects in orthotopic xenograft models including tumors that did not express typical GBM associated tumor antigens such as IL13Rα2. Therefore, CARs targeting peptides have the potential to overcome the limitations of CARs that target 1 or 2 antigens with recurrence of tumors due to antigen loss.

Immunosuppressive Microenvironment

In addition to intrinsic problems with infused T cell function, these cells are limited by the immunosuppressive tumor microenvironment (TME). Macrophages and microglia within the murine GBM tumor microenvironment produce CCL2 cytokine to recruit CCR4+ Tregs and CCR2+ Ly6C+ myeloid cells (52). Overexpression of immunosuppressive cytokines and the recruitment of Tregs and myeloid derived suppressor cells (MDSCs) create a hostile environment for engraftment or effector function of cytotoxic T cells (53, 54). This environment is hostile not only locally but also peripherally as T cells have been shown to be sequestered within the bone marrow of patients with GBM (53). These data suggest that T cell egress and trafficking into intracranial malignancies are additional inhibitory mechanisms that must be overcome to initiate and perpetuate a cycle of self-sustaining cancer immunotherapy.

Myeloid cells compose 30-50% of GBM tumor mass and accumulate in the peripheral blood sabotaging the efficacy of T cells (54, 55). Tumor associated myeloid cells express high levels of PD-L1 (55). The majority of PD-L1 expression in the tumor microenvironment results from myeloid cells and not tumor cells (56). In a murine study, radiation therapy was used to upregulate the expression of PD-L1 on myeloid cells to produce synergy when combined with PD-L1 blockade (55). Targeting of myeloid cells and PD-1 expression on T cells leads to reversal of immune resistance to DC vaccination and abundance of T cell infiltration within the tumor with resultant long-term survival in GL-261 GBM bearing mice (56). However, these strategies have not yet been tested in combination with T cell infusion therapies.

Other signaling pathways except than PD-1/PD-L1 are also involved in the dysfunction of T cells mediated by tumor associated myeloid cells. B7 superfamily membrane 1 (B7S1), also known as B7-H4, is an inhibitory molecule expressed by tumor associated myeloid cells that negatively regulates activation of T cells and promotes exhaustion of tumor infiltrating CD8 T cells (57). Inhibition of B7S1 on tumor infiltrating myeloid cells and PD-1 on T cells improves CD8 T cell anti-tumor immune responses in murine cancer models (57). In phase II randomized trial investigating DCs loaded with lysates from GBM cells cultured in stem cell media, patients with low B7-H4 expression had prolonged survival (58). This increase in survival was associated with higher T cell infiltration in the tumors.

Adoptive transfer of autologous T cells is also limited by immunosuppression from circulating Tregs (59–61). Patients with GBM have natural, or thymus derived Tregs and induced Tregs (62, 63). Tregs are associated with reduced survival and are linked to tumor recurrence in patients with GBM (64). IDO expression on tumor cells and CCL-2 secretion from microglia and macrophages in the tumor microenvironment contribute to recruiting Tregs (CD4 +CD25+ FOXP3+) (52, 60, 65). Targeting Tregs may have the potential to be synergistic with T cell infusions, but this has not been tested. Treatment targeting Tregs has thus far only been tested alone or in combination with standard chemotherapy or radiation. For example, glucocorticoid-induced TNFR-related protein (GITR) are receptors expressed on Tregs, and antibody blockade of GITR has been shown to have efficacy in murine models (66). Intratumoral treatment with an antibody against GITR was found to have a survival benefit in a murine GBM model (30 days compare to 19 days in control, $p<0.01$, and 10% of mice being long-term survivors). However, this benefit was only seen when treatment was delivered within the tumor through FcγR-mediated destruction of Tregs. Systemic delivery did not deplete intratumoral Tregs and did not extend survival significantly. Anti-GITR, non-depleting antibodies combined with stereotactic radiation also increases overall survival in murine GL-261 Luc glioma model (67). In GBM patients, selective depletion of Tregs with anti-IL-2Rα mAb during lymphopenia, enhanced response to an EGFRVIII peptide vaccine and improve anti-tumor humoral immunity (68). The effects of anti-Treg therapy in combination with infusion of cytotoxic T cells has not been tested.

OPTIMIZING EXPANSION, ENGRAFTMENT, AND FUNCTION OF T CELLS

Current treatment strategies for GBM all have effects on the host immune system. Although many of these effects are immunosuppressive, some of the immune-related changes can be leveraged for improved efficacy of immunotherapy. Experimental data of cancer models and results from metastatic cancer patients suggest addition of radiotherapy to immunotherapy contributes to systemic anti-tumor immunity (69). In murine models, GL261 tumor bearing mice had a median survival of 53 days when treated with PD-1 blockade combined with stereotactic radiosurgery compared to 25-28 days in control animals or those treated with monotherapy (70). In a pre-clinical study evaluating a second generation NKG2D targeting CAR T cell, investigators found that the addition of a single dose of 4 Gy radiation to the tumor resulted in significantly more intra-tumor T cell migration (71). This was associated with increased long-term survival in the SMA-560 glioma model (42% versus 14% with CAR alone, $p<0.001$). In patients with newly diagnosed high grade glioma, radiation was given 9 days after intra-tumoral administration of adenoviral vector (ADV-TK) as preclinical studies suggest increased efficacy with the combination (72). Twelve patients were treated and 4/4 tumors were found to have CD3 T cell infiltrates on H&E analysis. This was a phase IB study and further investigation is ongoing.

Chemotherapy has also been described to improve engraftment after T cell infusions. Using a murine melanoma tumor model treated with OT-1 T cell infusion followed by OVA peptide

vaccination, myeloablation using temozolomide led to a 70-fold expansion of antigen specific T cells compared to controls (28). In the same model, temozolomide-induced lymphopenia increased antigen specific T cell expansion in a dose dependent fashion (73). Interestingly, the immune effects of temozolomide vary based on the dosing schedule. When combined with PD-1 blockade, standard dosing of temozolomide abrogated the survival benefit of PD-1 blockade in murine GL-261 glioma models (74). When the same total dose was delivered in smaller individual doses over a longer period of time (metronomic schedule), the survival benefit of PD-1 blockade was preserved due to avoidance of T cell dysfunction. In a phase II study of DCs loaded with GBM lysate combined with adjuvant temozolomide, CD8 T cells expanded, but the effector memory (CCR7 low, CD45RO high) decreased after the first adjuvant temozolomide dose (75).

The ideal conditioning chemotherapy regimen prior to T cell infusion is controversial. Myeloablative dosing has been shown to increase T cell engraftment. However, myeloablation requires stem cell rescue and is more toxic. A myeloablative dose of temozolomide was tested in B16 F10-OVA melanoma model, in combination with T cell transfer and OVA peptide vaccine improved survival by 10 days compare to non-myeloablative dose (28). The improved survival was mediated by elevated levels of IL-2 post chemotherapy. Higher levels of IL-2 contributed to a significant expansion of transferred T cells and differentiation of naïve T cells to effector T cells with a higher capacity for pro inflammatory cytokine secretion.

Lymphodepletion without myeloablation may be enough. Lymphodepletion prior to CAR T cells targeting EGFRvIII was found to cause regression of tumors and resulted in 50% long term survivors (over 200 days) (29). Animals that received higher temozolomide doses (dose intensified) had enhanced proliferation and persistence of CAR T cells compared to animals receiving the standard dose. Based on this study, phase I clinical trial had been designed to evaluate the anti-tumor efficacy of EGFRvIII CAR T cells after host precondition with dose intensified temozolomide for newly diagnosed GBM patients (NCT02664363). In another phase I clinical trial for patients with recurrent central PNETs, the efficacy of T cell transfer targeting total tumor RNA combined with DC vaccine was evaluated post non myeloablative doses of cyclophosphamide and fludarabine (19). Massive clonal expansion of T cells were found using TCR sequencing. However, the function of these expanded T cells has not been described.

T cell dysfunction is a major limitation of any T cell-based therapy. One strategy to avoid T cell dysfunction is replacement of exhausted and senescent T cells with effector and memory T cells. This replacement can be performed by promoting apoptosis by targeting FOXO4/p53 peptide in senescent T cells (76) and substituting the exhausted T cells with effector and memory T cells using stem cell transplantation (77). Alternatively, dysfunctional T cells can be replaced by T cells recruited by hematopoietic stem cell (HSC) infusion. In a murine GBM model, HSCs were shown migrate to the tumor microenvironment (78). Secretion of chemoattractants such as growth factors and cytokines from tumor cells attract HSCs where HSCs can recruit tumor-specific T cells. A study by Flores et al. demonstrated that HSC infusion after myeloablative RT resulted in homing of tumor specific lymphocytes to the tumor (KR158) *via* CCL3 secretion and tumor control with improved survival (doubling of median survival compared to control) (79).

An alternative is use of induced pluripotent stem cells (iPS) which differentiate into functional T cells (80). For example, murine embryonic fibroblasts were used to create iPS cells using Flt-3 and IL-7 (81). These iPS cells were used to create T cells which were able to reconstitute a normal pool of T cells in a T cell deficient mouse model. Differentiation of T cells from iPS cells can be used as a strategy to produce "rejuvenated" T cells with high proliferative capacity and elongated telomeres (82). Moreover, iPS grown T cells can be transduced with CARs or engineered TCRs specific for tumor antigens (83).

Restoration strategy is another novel area of research. This technique requires harvesting of a functional thymus from cadaveric donor, isolation of thymus organoids and bioengineering them with growth promoting factors and thymo-stimulatory cytokines such as IL-21 (84). These thymic organoids can be transduced with recipient HLA molecules followed by recellularization of bioengineered organoid scaffold to be prepared for transplanting into the recipients (85, 86). These strategies are still experimental and require further study to determine their role in the treatment of patients with GBM.

Preventing or reversing T cell dysfunction will be the key to the future of immunotherapy in the treatment of GBM. Importantly, the effects of standard treatment modalities on the host and exogenously derived T cells will be critical. Manipulation of the peripheral and intra-tumoral immune microenvironment, optimizing the timing and duration of T cell antigen exposure, and providing sufficient T cell activation have the potential to improve responses to immunotherapy. Furthermore, adoptive T cell therapy with antigen specific T cells including CAR T cells or hematopoietic stem cells, are promising approaches to replace dysfunctional T cells in patients with GBM.

CONCLUSION

Patients with GBM present with several mechanisms of immunosuppression and T cell dysfunction. Targeted efforts to improve T cell function will result in greater efficacy of platforms such as adoptive T cell transfer and CAR T cell infusion. These efforts include designing T cells that target the major tumor antigens, improving persistence and effector function of T cells, and optimization of tumor microenvironment for the efficacious T cell response in the immunosuppressive tumor setting. The efficacy of immunotherapy for GBM rests on the ability to overcome T cell dysfunction.

AUTHOR CONTRIBUTIONS

AK and MR researched data and wrote the article. FD, JH, ES, SN, CY, LJ, and DM contributed to scientific discussion and critical review of the manuscript. SN generated the figures. All authors contributed to the article and approved the submitted version.

REFERENCES

1. Denkert C, Loibl S, Noske A, Roller M, Muller BM, Komor M, et al. Tumor-Associated Lymphocytes as an Independent Predictor of Response to Neoadjuvant Chemotherapy in Breast Cancer. *J Clin Oncol* (2010) 28 (1):105–13. doi: 10.1200/JCO.2009.23.7370
2. Hendry S, Salgado R, Gevaert T, Russell PA, John T, Thapa B, et al. Assessing Tumor-Infiltrating Lymphocytes in Solid Tumors: A Practical Review for Pathologists and Proposal for a Standardized Method From the International Immuno-Oncology Biomarkers Working Group: Part 2: TILs in Melanoma, Gastrointestinal Tract Carcinomas, Non-Small Cell Lung Carcinoma and Mesothelioma, Endometrial and Ovarian Carcinomas, Squamous Cell Carcinoma of the Head and Neck, Genitourinary Carcinomas, and Primary Brain Tumors. *Adv Anat Pathol* (2017) 24(6):311–35. doi: 10.1097/PAP.0000000000000161
3. Idos GE, Kwok J, Bonthala N, Kysh L, Gruber SB, Qu C. The Prognostic Implications of Tumor Infiltrating Lymphocytes in Colorectal Cancer: A Systematic Review and Meta-Analysis. *Sci Rep* (2020) 10(1):3360. doi: 10.1038/s41598-020-60255-4
4. Han S, Zhang C, Li Q, Dong J, Liu Y, Huang Y, et al. Tumour-Infiltrating CD4(+) and CD8(+) Lymphocytes as Predictors of Clinical Outcome in Glioma. *Br J Cancer* (2014) 110(10):2560–8. doi: 10.1038/bjc.2014.162
5. Maude SL, Frey N, Shaw PA, Aplenc R, Barrett DM, Bunin NJ, et al. Chimeric Antigen Receptor T Cells for Sustained Remissions in Leukemia. *N Engl J Med* (2014) 371(16):1507–17. doi: 10.1056/NEJMoa1407222
6. Mohme M, Schliffke S, Maire CL, Runger A, Glau L, Mende KC, et al. Immunophenotyping of Newly Diagnosed and Recurrent Glioblastoma Defines Distinct Immune Exhaustion Profiles in Peripheral and Tumor-Infiltrating Lymphocytes. *Clin Cancer Res* (2018) 24(17):4187–200. doi: 10.1158/1078-0432.CCR-17-2617
7. Ahmadzadeh M, Johnson LA, Heemskerk B, Wunderlich JR, Dudley ME, White DE, et al. Tumor Antigen-Specific CD8 T Cells Infiltrating the Tumor Express High Levels of PD-1 and Are Functionally Impaired. *Blood* (2009) 114(8):1537–44. doi: 10.1182/blood-2008-12-195792
8. Topalian SL, Muul LM, Solomon D, Rosenberg SA. Expansion of Human Tumor Infiltrating Lymphocytes for Use in Immunotherapy Trials. *J Immunol Methods* (1987) 102(1):127–41. doi: 10.1016/S0022-1759(87)80018-2
9. Woroniecka K, Chongsathidkiet P, Rhodin K, Kemeny H, Dechant C, Farber SH, et al. T-Cell Exhaustion Signatures Vary With Tumor Type and Are Severe in Glioblastoma. *Clin Cancer Res* (2018) 24(17):4175–86. doi: 10.1158/1078-0432.CCR-17-1846
10. Sims JS, Grinshpun B, Feng Y, Ung TH, Neira JA, Samanamud JL, et al. Diversity and Divergence of the Glioma-Infiltrating T-Cell Receptor Repertoire. *Proc Natl Acad Sci USA* (2016) 113(25):E3529–37. doi: 10.1073/pnas.1601012113
11. Dillman RO, Duma CM, Schiltz PM, DePriest C, Ellis RA, Okamoto K, et al. Intracavitary Placement of Autologous Lymphokine-Activated Killer (LAK) Cells After Resection of Recurrent Glioblastoma. *J Immunother* (2004) 27 (5):398–404. doi: 10.1097/00002371-200409000-00009
12. Dillman RO, Duma CM, Ellis RA, Cornforth AN, Schiltz PM, Sharp SL, et al. Intralesional Lymphokine-Activated Killer Cells as Adjuvant Therapy for Primary Glioblastoma. *J Immunother* (2009) 32(9):914–9. doi: 10.1097/CJI.0b013e3181b2910f
13. Penas-Prado M, Weathers S-PS, Zhou S, Kamiya-Matsuoka C, O'Brien B , Loghin M, et al. A Phase I/II Clinical Trial of Autologous CMV-Specific Cytotoxic T Cells (CMV-TC) for Glioblastoma: Dose Escalation and Correlative Results. *Neuro Oncol* (2018) 20(Supplement 6):vi2–3. doi: 10.1093/neuonc/noy148.006
14. Reap EA, Suryadevara CM, Batich KA, Sanchez-Perez L, Archer GE, Schmittling RJ, et al. Dendritic Cells Enhance Polyfunctionality of Adoptively Transferred T Cells That Target Cytomegalovirus in Glioblastoma. *Cancer Res* (2018) 78 (1):256–64. doi: 10.1158/0008-5472.CAN-17-0469
15. O'Rourke DM, Nasrallah MP, Desai A, Melenhorst JJ, Mansfield K, Morrissette JJD, et al. A Single Dose of Peripherally Infused EGFRvIII-Directed CAR T Cells Mediates Antigen Loss and Induces Adaptive Resistance in Patients With Recurrent Glioblastoma. *Sci Transl Med* (2017) 9(399). doi: 10.1126/scitranslmed.aaa0984
16. Brown CE, Alizadeh D, Starr R, Weng L, Wagner JR, Naranjo A, et al. Regression of Glioblastoma After Chimeric Antigen Receptor T-Cell Therapy. *N Engl J Med* (2016) 375(26):2561–9. doi: 10.1056/NEJMoa1610497
17. Heczey A, Louis CU, Savoldo B, Dakhova O, Durett A, Grilley B, et al. CAR T Cells Administered in Combination With Lymphodepletion and PD-1 Inhibition to Patients With Neuroblastoma. *Mol Ther* (2017) 25(9):2214–24. doi: 10.1016/j.ymthe.2017.05.012
18. Portnow J, Wang D, Blanchard MS, Tran V, Alizadeh D, Starr R, et al. Systemic Anti-PD-1 Immunotherapy Results in PD-1 Blockade on T Cells in the Cerebrospinal Fluid. *JAMA Oncol* (2020) 6(12):1947–51. doi: 10.1001/jamaoncol.2020.4508
19. Gururangan S, Grant G, Driscoll T, Archer G, Herndon J, Friedman H, et al. ImmU-27. Re-Match Protocol: Phase I Study of Autologous Tumor Specific Lymphocyte Trtansfer (ALT) + DC Vaccine (DCV) During Recovery From Myeloablative Chemotherapy (MAC) and Autologous Stem Cell Rescue (HDC + ASCR) or Non-Myeloablative Chemotherapy (NMAC) In Patients With Recurrent Central PNETs (R-PNET). *Neuro Oncol* (2018) 20(Suppl 2): i104. doi: 10.1093/neuonc/noy059.343
20. Wu L, Wei Q, Brzostek J, Gascoigne NRJ. Signaling From T Cell Receptors (TCRs) and Chimeric Antigen Receptors (CARs) on T Cells. *Cell Mol Immunol* (2020) 17(6):600–12. doi: 10.1038/s41423-020-0470-3
21. Gururangan S, Sayour E, Mitchell DA. Total Tumor RNA Pulsed Dendritic Cells Plus Adoptive Transfer of Ex-Vivo Enriched Autologous T-Lymphocytes in the Treatment of Children With Primary Brain Tumors. *Neuroimmunol Neuroinflam* (2018) 4(45). doi: 10.20517/2347-8659.2018.44
22. Weinkove R, George P, Dasyam N, McLellan AD. Selecting Costimulatory Domains for Chimeric Antigen Receptors: Functional and Clinical Considerations. *Clin Transl Immunol* (2019) 8(5):e1049. doi: 10.1002/cti2.1049
23. Land CA, Musich PR, Haydar D, Krenciute G, Xie Q. Chimeric Antigen Receptor T-Cell Therapy in Glioblastoma: Charging the T Cells to Fight. *J Transl Med* (2020) 18(1):428. doi: 10.1186/s12967-020-02598-0
24. Ahmed N, Brawley V, Hegde M, Bielamowicz K, Kalra M, Landi D, et al. HER2-Specific Chimeric Antigen Receptor-Modified Virus-Specific T Cells for Progressive Glioblastoma: A Phase 1 Dose-Escalation Trial. *JAMA Oncol* (2017) 3(8):1094–101. doi: 10.1001/jamaoncol.2017.0184
25. Porter DL, Hwang WT, Frey NV, Lacey SF, Shaw PA, Loren AW, et al. Chimeric Antigen Receptor T Cells Persist and Induce Sustained Remissions in Relapsed Refractory Chronic Lymphocytic Leukemia. *Sci Transl Med* (2015) 7(303):303ra139. doi: 10.1126/scitranslmed.aac5415
26. Scholler J, Brady TL, Binder-Scholl G, Hwang WT, Plesa G, Hege KM, et al. Decade-Long Safety and Function of Retroviral-Modified Chimeric Antigen Receptor T Cells. *Sci Transl Med* (2012) 4(132):132ra53. doi: 10.1126/scitranslmed.3003761
27. Sanchez-Perez L, Suryadevara CM, Choi BD, Reap EA, Sampson JH. Leveraging Chemotherapy-Induced Lymphopenia to Potentiate Cancer Immunotherapy. *Oncoimmunology* (2014) 3(7):e944054. doi: 10.4161/21624011.2014.944054
28. Sanchez-Perez LA, Choi BD, Archer GE, Cui X, Flores C, Johnson LA, et al. Myeloablative Temozolomide Enhances CD8(+) T-Cell Responses to Vaccine and Iis Required for Efficacy Against Brain Tumors in Mice. *PloS One* (2013) 8 (3):e59082. doi: 10.1371/journal.pone.0059082
29. Suryadevara CM, Desai R, Abel ML, Riccione KA, Batich KA, Shen SH, et al. Temozolomide Lymphodepletion Enhances CAR Abundance and Correlates With Antitumor Efficacy Against Established Glioblastoma. *Oncoimmunology* (2018) 7(6):e1434464. doi: 10.1080/2162402X.2018.1434464
30. Jin L, Ge H, Long Y, Yang C, Chang YE, Mu L, et al. CD70, A Novel Target of CAR T-Cell Therapy for Gliomas. *Neuro Oncol* (2018) 20(1):55–65. doi: 10.1093/neuonc/nox116
31. Jin L, Tao H, Karachi A, Long Y, Hou AY, Na M, et al. CXCR1- or CXCR2-Modified CAR T Cells Co-Opt IL-8 for Maximal Antitumor Efficacy in Solid Tumors. *Nat Commun* (2019) 10(1):4016. doi: 10.1038/s41467-019-11869-4
32. Wherry EJ, Blattman JN, Murali-Krishna K, van der Most R, Ahmed R. Viral Persistence Alters CD8 T-Cell Immunodominance and Tissue Distribution and Results in Distinct Stages of Functional Impairment. *J Virol* (2003) 77 (8):4911–27. doi: 10.1128/JVI.77.8.4911-4927.2003
33. Gattinoni L, Zhong XS, Palmer DC, Ji Y, Hinrichs CS, Yu Z, et al. Wnt Signaling Arrests Effector T Cell Differentiation and Generates CD8+ Memory Stem Cells. *Nat Med* (2009) 15(7):808–13. doi: 10.1038/nm.1982

34. Gattinoni L, Lugli E, Ji Y, Pos Z, Paulos CM, Quigley MF, et al. A Human Memory T Cell Subset With Stem Cell-Like Properties. *Nat Med* (2011) 17 (10):1290–7. doi: 10.1038/nm.2446
35. Wu T, Ji Y, Moseman EA, Xu HC, Manglani M, Kirby M, et al. The TCF1-Bcl6 Axis Counteracts Type I Interferon to Repress Exhaustion and Maintain T Cell Stemness. *Sci Immunol* (2016) 1(6). doi: 10.1126/sciimmunol.aai8593
36. Li H, van der Leun AM, Yofe I, Lubling Y, Gelbard-Solodkin D, van Akkooi ACJ, et al. Dysfunctional CD8 T Cells Form a Proliferative, Dynamically Regulated Compartment Within Human Melanoma. *Cell* (2019) 176(4):775–89 e18. doi: 10.1016/j.cell.2018.11.043
37. Chen J, Lopez-Moyado IF, Seo H, Lio CJ, Hempleman LJ, Sekiya T, et al. NR4A Transcription Factors Limit CAR T Cell Function in Solid Tumours. *Nature* (2019) 567(7749):530–4. doi: 10.1038/s41586-019-0985-x
38. Seo H, Chen J, Gonzalez-Avalos E, Samaniego-Castruita D, Das A, Wang YH, et al. TOX and TOX2 Transcription Factors Cooperate With NR4A Transcription Factors to Impose CD8(+) T Cell Exhaustion. *Proc Natl Acad Sci USA* (2019) 116(25):12410–5. doi: 10.1073/pnas.1905675116
39. Chong EA, Melenhorst JJ, Lacey SF, Ambrose DE, Gonzalez V, Levine BL, et al. PD-1 Blockade Modulates Chimeric Antigen Receptor (CAR)-Modified T Cells: Refueling the CAR. *Blood* (2017) 129(8):1039–41. doi: 10.1182/blood-2016-09-738245
40. Moon EK, Ranganathan R, Eruslanov E, Kim S, Newick K, O'Brien S, et al. Blockade of Programmed Death 1 Augments the Ability of Human T Cells Engineered to Target NY-ESO-1 to Control Tumor Growth After Adoptive Transfer. *Clin Cancer Res* (2016) 22(2):436–47. doi: 10.1158/1078-0432.CCR-15-1070
41. John LB, Devaud C, Duong CP, Yong CS, Beavis PA, Haynes NM, et al. Anti-PD-1 Antibody Therapy Potently Enhances the Eradication of Established Tumors by Gene-Modified T Cells. *Clin Cancer Res* (2013) 19(20):5636–46. doi: 10.1158/1078-0432.CCR-13-0458
42. John LB, Kershaw MH, Darcy PK. Blockade of PD-1 Immunosuppression Boosts CAR T-Cell Therapy. *Oncoimmunology* (2013) 2(10):e26286. doi: 10.4161/onci.26286
43. Tanoue K, Rosewell Shaw A, Watanabe N, Porter C, Rana B, Gottschalk S, et al. Armed Oncolytic Adenovirus-Expressing PD-L1 Mini-Body Enhances Antitumor Effects of Chimeric Antigen Receptor T Cells in Solid Tumors. *Cancer Res* (2017) 77(8):2040–51. doi: 10.1158/0008-5472.CAN-16-1577
44. Suarez ER, Chang de K, Sun J, Sui J, Freeman GJ, Signoretti S, et al. Chimeric Antigen Receptor T Cells Secreting Anti-PD-L1 Antibodies More Effectively Regress Renal Cell Carcinoma in a Humanized Mouse Model. *Oncotarget* (2016) 7(23):34341–55. doi: 10.18632/oncotarget.9114
45. Choe JH, Watchmaker PB, Simic MS, Gilbert RD, Li AW, Krasnow NA, et al. SynNotch-CAR T Cells Overcome Challenges of Specificity, Heterogeneity, and Persistence in Treating Glioblastoma. *Sci Transl Med* (2021) 13(591). doi: 10.1126/scitranslmed.abe7378
46. Hyrenius-Wittsten A, Su Y, Park M, Garcia JM, Alavi J, Perry N, et al. SynNotch CAR Circuits Enhance Solid Tumor Recognition and Promote Persistent Antitumor Activity in Mouse Models. *Sci Transl Med* (2021) 13 (591). doi: 10.1126/scitranslmed.abd8836
47. Elahi R, Khosh E, Tahmasebi S, Esmaeilzadeh A. Immune Cell Hacking: Challenges and Clinical Approaches to Create Smarter Generations of Chimeric Antigen Receptor T Cells. *Front Immunol* (2018) 9:1717. doi: 10.3389/fimmu.2018.01717
48. Krenciute G, Prinzing BL, Yi Z, Wu MF, Liu H, Dotti G, et al. Transgenic Expression of IL15 Improves Antiglioma Activity of IL13Ralpha2-CAR T Cells But Results in Antigen Loss Variants. *Cancer Immunol Res* (2017) 5 (7):571–81. doi: 10.1158/2326-6066.CIR-16-0376
49. Hegde M, Mukherjee M, Grada Z, Pignata A, Landi D, Navai SA, et al. Tandem CAR T Cells Targeting HER2 and IL13Ralpha2 Mitigate Tumor Antigen Escape. *J Clin Invest* (2016) 126(8):3036–52. doi: 10.1172/JCI83416
50. Bielamowicz K, Fousek K, Byrd TT, Samaha H, Mukherjee M, Aware N, et al. Trivalent CAR T Cells Overcome Interpatient Antigenic Variability in Glioblastoma. *Neuro Oncol* (2018) 20(4):506–18. doi: 10.1093/neuonc/nox182
51. Wang D, Starr R, Chang WC, Aguilar B, Alizadeh D, Wright SL, et al. Chlorotoxin-Directed CAR T Cells for Specific and Effective Targeting of Glioblastoma. *Sci Transl Med* (2020) 12(533). doi: 10.1126/scitranslmed.aaw2672
52. Chang AL, Miska J, Wainwright DA, Dey M, Rivetta CV, Yu D, et al. CCL2 Produced by the Glioma Microenvironment Is Essential for the Recruitment of Regulatory T Cells and Myeloid-Derived Suppressor Cells. *Cancer Res* (2016) 76(19):5671–82. doi: 10.1158/0008-5472.CAN-16-0144
53. Chongsathidkiet P, Jackson C, Koyama S, Loebel F, Cui X, Farber SH, et al. Sequestration of T Cells in Bone Marrow in the Setting of Glioblastoma and Other Intracranial Tumors. *Nat Med* (2018) 24(9):1459–68. doi: 10.1038/s41591-018-0135-2
54. Raychaudhuri B, Rayman P, Ireland J, Ko J, Rini B, Borden EC, et al. Myeloid-Derived Suppressor Cell Accumulation and Function in Patients With Newly Diagnosed Glioblastoma. *Neuro Oncol* (2011) 13(6):591–9. doi: 10.1093/neuonc/nor042
55. Zhang P, Miska J, Lee-Chang C, Rashidi A, Panek WK, An S, et al. Therapeutic Targeting of Tumor-Associated Myeloid Cells Synergizes With Radiation Therapy for Glioblastoma. *Proc Natl Acad Sci USA* (2019) 116 (47):23714–23. doi: 10.1073/pnas.1906346116
56. Antonios JP, Soto H, Everson RG, Moughon D, Orpilla JR, Shin NP, et al. Immunosuppressive Tumor-Infiltrating Myeloid Cells Mediate Adaptive Immune Resistance *via* a PD-1/PD-L1 Mechanism in Glioblastoma. *Neuro Oncol* (2017) 19(6):796–807. doi: 10.1093/neuonc/now287
57. Li J, Lee Y, Li Y, Jiang Y, Lu H, Zang W, et al. Co-Inhibitory Molecule B7 Superfamily Member 1 Expressed by Tumor-Infiltrating Myeloid Cells Induces Dysfunction of Anti-Tumor CD8(+) T Cells. *Immunity* (2018) 48 (4):773–86.e5. doi: 10.1016/j.immuni.2018.03.018
58. Yao Y, Luo F, Tang C, Chen D, Qin Z, Hua W, et al. Molecular Subgroups and B7-H4 Expression Levels Predict Responses to Dendritic Cell Vaccines in Glioblastoma: An Exploratory Randomized Phase II Clinical Trial. *Cancer Immunol Immunother* (2018) 67(11):1777–88. doi: 10.1007/s00262-018-2232-y
59. Fecci PE, Mitchell DA, Whitesides JF, Xie W, Friedman AH, Archer GE, et al. Increased Regulatory T-Cell Fraction Amidst a Diminished CD4 Compartment Explains Cellular Immune Defects in Patients With Malignant Glioma. *Cancer Res* (2006) 66(6):3294–302. doi: 10.1158/0008-5472.CAN-05-3773
60. El Andaloussi A, Lesniak MS. An Increase in CD4+CD25+FOXP3+ Regulatory T Cells in Tumor-Infiltrating Lymphocytes of Human Glioblastoma Multiforme. *Neuro Oncol* (2006) 8(3):234–43. doi: 10.1215/15228517-2006-006
61. Dieckmann D, Plottner H, Berchtold S, Berger T, Schuler G. Ex Vivo Isolation and Characterization of CD4(+)CD25(+) T Cells With Regulatory Properties From Human Blood. *J Exp Med* (2001) 193(11):1303–10. doi: 10.1084/jem.193.11.1303
62. Wainwright DA, Sengupta S, Han Y, Lesniak MS. Thymus-Derived Rather Than Tumor-Induced Regulatory T Cells Predominate in Brain Tumors. *Neuro Oncol* (2011) 13(12):1308–23. doi: 10.1093/neuonc/nor134
63. Curotto de Lafaille MA, Lafaille JJ. Natural and Adaptive Foxp3+ Regulatory T Cells: More of the Same or a Division of Labor? *Immunity* (2009) 30(5):626–35. doi: 10.1016/j.immuni.2009.05.002
64. Sayour EJ, McLendon P, McLendon R, De Leon G, Reynolds R, Kresak J, et al. Increased Proportion of FoxP3+ Regulatory T Cells in Tumor Infiltrating Lymphocytes Is Associated With Tumor Recurrence and Reduced Survival in Patients With Glioblastoma. *Cancer Immunol Immunother* (2015) 64(4):419–27. doi: 10.1007/s00262-014-1651-7
65. Wainwright DA, Balyasnikova IV, Chang AL, Ahmed AU, Moon KS, Auffinger B, et al. IDO Expression in Brain Tumors Increases the Recruitment of Regulatory T Cells and Negatively Impacts Survival. *Clin Cancer Res* (2012) 18(22):6110–21. doi: 10.1158/1078-0432.CCR-12-2130
66. Miska J, Rashidi A, Chang AL, Muroski ME, Han Y, Zhang L, et al. Anti-GITR Therapy Promotes Immunity Against Malignant Glioma in a Murine Model. *Cancer Immunol Immunother* (2016) 65(12):1555–67. doi: 10.1007/s00262-016-1912-8
67. Patel MA, Kim JE, Theodros D, Tam A, Velarde E, Kochel CM, et al. Agonist Anti-GITR Monoclonal Antibody and Stereotactic Radiation Induce Immune-Mediated Survival Advantage in Murine Intracranial Glioma. *J Immunother Cancer* (2016) 4:28. doi: 10.1186/2051-1426-3-S2-P194
68. Sampson JH, Schmittling RJ, Archer GE, Congdon KL, Nair SK, Reap EA, et al. A Pilot Study of IL-2Ralpha Blockade During Lymphopenia Depletes Regulatory T-Cells and Correlates With Enhanced Immunity in Patients With Glioblastoma. *PloS One* (2012) 7(2):e31046. doi: 10.1371/journal.pone.0031046
69. Formenti SC, Demaria S. Combining Radiotherapy and Cancer Immunotherapy: A Paradigm Shift. *J Natl Cancer Inst* (2013) 105(4):256–65. doi: 10.1093/jnci/djs629

70. Zeng J, See AP, Phallen J, Jackson CM, Belcaid Z, Ruzevick J, et al. Anti-PD-1 Blockade and Stereotactic Radiation Produce Long-Term Survival in Mice With Intracranial Gliomas. *Int J Radiat Oncol Biol Phys* (2013) 86(2):343–9. doi: 10.1016/j.ijrobp.2012.12.025
71. Weiss T, Weller M, Guckenberger M, Sentman CL, Roth P. NKG2D-Based CAR T Cells and Radiotherapy Exert Synergistic Efficacy in Glioblastoma. *Cancer Res* (2018) 78(4):1031–43. doi: 10.1158/0008-5472.CAN-17-1788
72. Chiocca EA, Aguilar LK, Bell SD, Kaur B, Hardcastle J, Cavaliere R, et al. Phase IB Study of Gene-Mediated Cytotoxic Immunotherapy Adjuvant to Up-Front Surgery and Intensive Timing Radiation for Malignant Glioma. *J Clin Oncol* (2011) 29(27):3611–9. doi: 10.1200/JCO.2011.35.5222
73. Mitchell DA, Cui X, Schmittling RJ, Sanchez-Perez L, Snyder DJ, Congdon KL, et al. Monoclonal Antibody Blockade of IL-2 Receptor Alpha During Lymphopenia Selectively Depletes Regulatory T Cells in Mice and Humans. *Blood* (2011) 118(11):3003–12. doi: 10.1182/blood-2011-02-334565
74. Karachi A, Yang C, Dastmalchi F, Sayour EJ, Huang J, Azari H, et al. Modulation of Temozolomide Dose Differentially Affects T-Cell Response to Immune Checkpoint Inhibition. *Neuro Oncol* (2019) 21(6):730–41. doi: 10.1093/neuonc/noz015
75. Pellegatta S, Eoli M, Cuccarini V, Anghileri E, Pollo B, Pessina S, et al. Survival Gain in Glioblastoma Patients Treated With Dendritic Cell Immunotherapy Is Associated With Increased NK But Not CD8(+) T Cell Activation in the Presence of Adjuvant Temozolomide. *Oncoimmunology* (2018) 7(4): e1412901. doi: 10.1080/2162402X.2017.1412901
76. Baar MP, Brandt RMC, Putavet DA, Klein JDD, Derks KWJ, Bourgeois BRM, et al. Targeted Apoptosis of Senescent Cells Restores Tissue Homeostasis in Response to Chemotoxicity and Aging. *Cell* (2017) 169(1):132–47.e16. doi: 10.1016/j.cell.2017.02.031
77. Rueff J, Medinger M, Heim D, Passweg J, Stern M. Lymphocyte Subset Recovery and Outcome After Autologous Hematopoietic Stem Cell Transplantation for Plasma Cell Myeloma. *Biol Blood Marrow Transplant* (2014) 20(6):896–9. doi: 10.1016/j.bbmt.2014.03.007
78. Bryukhovetskiy IS, Dyuizen IV, Shevchenko VE, Bryukhovetskiy AS, Mischenko PV, Milkina EV, et al. Hematopoietic Stem Cells as a Tool for the Treatment of Glioblastoma Multiforme. *Mol Med Rep* (2016) 14(5):4511–20. doi: 10.3892/mmr.2016.5852
79. Flores C, Pham C, Snyder D, Yang S, Sanchez-Perez L, Sayour E, et al. Novel Role of Hematopoietic Stem Cells in Immunologic Rejection of Malignant Gliomas. *Oncoimmunology* (2015) 4(3):e994374. doi: 10.4161/2162402X.2014.994374
80. Karagiannis P, Iriguchi S, Kaneko S. Reprogramming Away From the Exhausted T Cell State. *Semin Immunol* (2016) 28(1):35–44. doi: 10.1016/j.smim.2015.10.007
81. Lei F, Haque R, Weiler L, Vrana KE, Song J. T Lineage Differentiation From Induced Pluripotent Stem Cells. *Cell Immunol* (2009) 260(1):1–5. doi: 10.1016/j.cellimm.2009.09.005
82. Nishimura T, Kaneko S, Kawana-Tachikawa A, Tajima Y, Goto H, Zhu D, et al. Generation of Rejuvenated Antigen-Specific T Cells by Reprogramming to Pluripotency and Redifferentiation. *Cell Stem Cell* (2013) 12(1):114–26. doi: 10.1016/j.stem.2012.11.002
83. Themeli M, Kloss CC, Ciriello G, Fedorov VD, Perna F, Gonen M, et al. Generation of Tumor-Targeted Human T Lymphocytes From Induced Pluripotent Stem Cells for Cancer Therapy. *Nat Biotechnol* (2013) 31 (10):928–33. doi: 10.1038/nbt.2678
84. Al-Chami E, Tormo A, Pasquin S, Kanjarawi R, Ziouani S, Rafei M. Interleukin-21 Administration to Aged Mice Rejuvenates Their Peripheral T-Cell Pool by Triggering *De Novo* Thymopoiesis. *Aging Cell* (2016) 15 (2):349–60. doi: 10.1111/acel.12440
85. Tajima A, Pradhan I, Trucco M, Fan Y. Restoration of Thymus Function With Bioengineered Thymus Organoids. *Curr Stem Cell Rep* (2016) 2(2):128–39. doi: 10.1007/s40778-016-0040-x
86. Tuckett AZ, Thornton RH, O'Reilly RJ, van den Brink MRM, Zakrzewski JL. Intrathymic Injection of Hematopoietic Progenitor Cells Establishes Functional T Cell Development in a Mouse Model of Severe Combined Immunodeficiency. *J Hematol Oncol* (2017) 10(1):109. doi: 10.1186/s13045-017-0478-z

Conflict of Interest: The authors declare that the research was conducted in the absence of any commercial or financial relationships that could be construed as a potential conflict of interest.

Publisher's Note: All claims expressed in this article are solely those of the authors and do not necessarily represent those of their affiliated organizations, or those of the publisher, the editors and the reviewers. Any product that may be evaluated in this article, or claim that may be made by its manufacturer, is not guaranteed or endorsed by the publisher.

frontiers in Immunology

ORIGINAL RESEARCH
published: 27 September 2021
doi: 10.3389/fimmu.2021.746168

Surfaceome Proteomic of Glioblastoma Revealed Potential Targets for Immunotherapy

Mélanie Rose[1], Tristan Cardon[1], Soulaimane Aboulouard[1], Nawale Hajjaji[1,2], Firas Kobeissy[3], Marie Duhamel[1], Isabelle Fournier[1,4]* and Michel Salzet[1,4]**

[1] Université Lille, Inserm, CHU Lille, U1192, Laboratoire Protéomique, Réponse Inflammatoire et Spectrométrie de Masse (PRISM), Lille, France, [2] Breast Cancer Unit, Oscar Lambret Center, Lille, France, [3] Department of Biochemistry and Molecular Genetics, Faculty of Medicine, American University of Beirut, Beirut, Lebanon, [4] Institut Universitaire de France, Paris, France

Glioblastoma (GBM) is the most common and devastating malignant brain tumor in adults. The mortality rate is very high despite different treatments. New therapeutic targets are therefore highly needed. Cell-surface proteins represent attractive targets due to their accessibility, their involvement in essential signaling pathways, and their dysregulated expression in cancer. Moreover, they are potential targets for CAR-based immunotherapy or mRNA vaccine strategies. In this context, we investigated the GBM-associated surfaceome by comparing it to astrocytes cell line surfaceome to identify new specific targets for GBM. For this purpose, biotinylation of cell surface proteins has been carried out in GBM and astrocytes cell lines. Biotinylated proteins were purified on streptavidin beads and analyzed by shotgun proteomics. Cell surface proteins were identified with Cell Surface Proteins Atlas (CSPA) and Gene Ontology enrichment. Among all the surface proteins identified in the different cell lines we have confirmed the expression of 66 of these in patient's glioblastoma using spatial proteomic guided by MALDI-mass spectrometry. Moreover, 87 surface proteins overexpressed or exclusive in GBM cell lines have been identified. Among these, we found 11 specific potential targets for GBM including 5 mutated proteins such as RELL1, CYBA, EGFR, and MHC I proteins. Matching with drugs and clinical trials databases revealed that 7 proteins were druggable and under evaluation, 3 proteins have no known drug interaction yet and none of them are the mutated form of the identified proteins. Taken together, we discovered potential targets for immune therapy strategies in GBM.

Keywords: surfaceome proteomic, glioblastoma, immune therapy, surface proteins, mutated proteins, drugs, clinical trials

OPEN ACCESS

Edited by:
Nurit Hollander, Tel Aviv University, Israel

Reviewed by:
Evelyne Maes, AgResearch Ltd., New Zealand
Michael C. Burger, Goethe University Frankfurt, Germany

****Correspondence:***
Melanie Rose
melanie.rose@univ-lille.fr
Michel Salzet
michel.salzet@univ-lille.fr
Isabelle Fournier
isabelle.fournier@univ-lille.fr

Specialty section:
This article was submitted to Cancer Immunity and Immunotherapy, a section of the journal Frontiers in Immunology

Received: *23 July 2021*
Accepted: *08 September 2021*
Published: *27 September 2021*

Citation:
Rose M, Cardon T, Aboulouard S, Hajjaji N, Kobeissy F, Duhamel M, Fournier I and Salzet M (2021) Surfaceome Proteomic of Glioblastoma Revealed Potential Targets for Immunotherapy. Front. Immunol. 12:746168. doi: 10.3389/fimmu.2021.746168

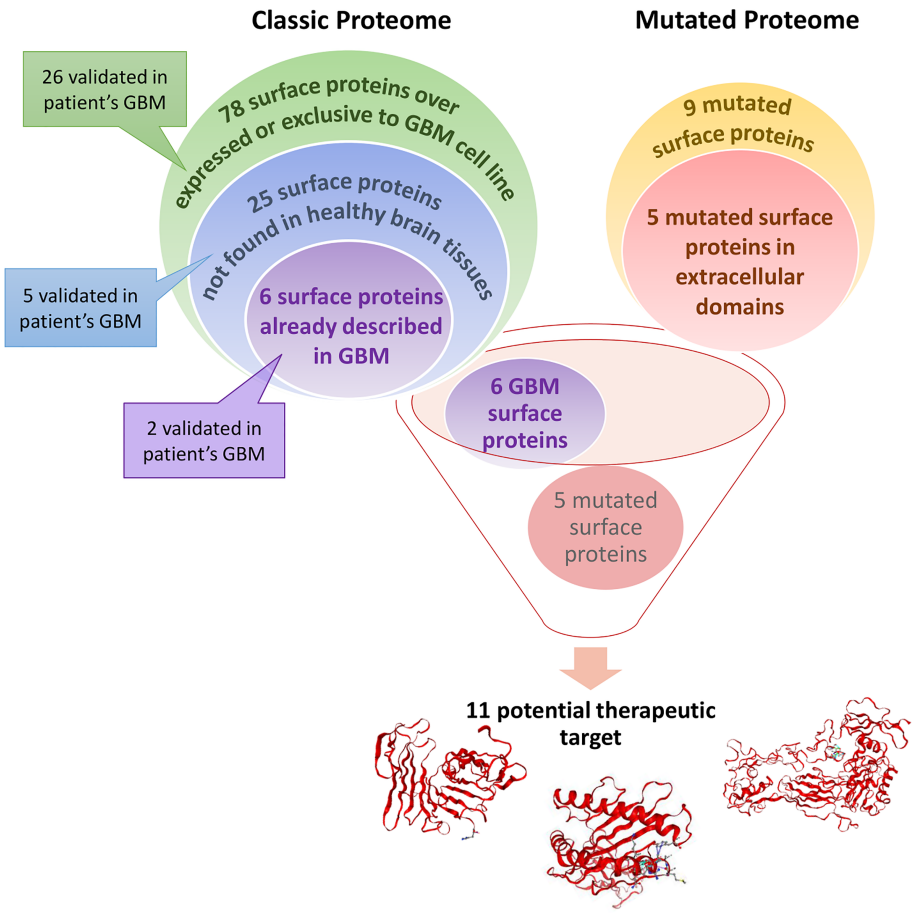

GRAPHICAL ABSTRACT | Glioblastoma (GBM) cell line surface proteome was compared to healthy astrocytes cell line surface proteome. A total of 78 surface proteins are identified as over-expressed or exclusive to the GBM cell line. According to Human Protein Atlas, 25 of these surface proteins are not found in healthy brain tissues. Among these 25 surface proteins, 6 are already described in (GBM) and could be potential therapeutic target. Some of the proteins described above have also been found in a cohort of 50 GBM patients. Moreover, we identified 9 mutated proteins only expressed by GBM cell lines in which 5 are mutated in their extracellular domains which is interesting for targeted therapy. Thus, these 11 proteins could be potential therapeutic targets for CAR-based immunotherapy or mRNA vaccine strategies.

INTRODUCTION

Glioblastoma represents the main malignant primary brain tumor with an incidence of 3.22 per 100,000 population (1). The prognosis is poor with median survival estimated at 16 months in clinical studies if treated with at least a near-total resection (QTR) and followed by the Stupp protocol (SP) (2–8) and around 12 months in contemporary population-based studies (9). Approximately 7% of patients survive more than 5 years after diagnosis (1). Favorable therapy-independent prognostic factors include lower age and higher neurological performance status at diagnosis. Furthermore, low postoperative residual tumor volume has been associated with improved outcomes. Moreover, GBM treatment options such as oncogenic signaling pathways including RTK/Ras/PI3K (88%), p53 (87%) and pRB signaling pathways (78%), or VEGF-targeting monoclonal antibody Bevacizumab, DNA alkylating agents such as lomustine and carmustine implants, and the checkpoint blockade inhibitor have been underwhelming in GBM (10, 11). For immunotherapy, resistance is due to strong local immunosuppression and to the difficulty of identifying highly specific tumor antigens. Very few GBM-specific antigens have been identified so far and they show a very limited potential as targets for immunotherapy.

In this context, several strategies tried to identify surface protein targets. In fact, 10 to 20% of all genes in the human genome encode cell surface proteins and due to their subcellular localization, these proteins represent excellent targets for cancer diagnosis and therapeutics. Recent studies have integrated transcriptomic and proteomic data for such a purpose in GBM (12). 395 genes were classified as coding for surface proteins and 6 were identified with high confidence i.e. HLA-DRA, CD44, SLC1A5, EGFR, ITGB2, PTPRJ, which are upregulated in GBM (12). Bausch-Fluck et al. (13) have developed a mass spectrometric-derived cell surface Atlas (CSPA) integrating GBM cell lines (13, 14). Thus, it is now possible to compare

new surfaceome proteomic dataset provided experimentally to CSPA database and from mutated peptides from XMan v.2 database (15). In this context, we compared astrocytoma GBM cell lines to normal astrocytes cell line. We could identify 11 specific potential targets for GBM including 5 mutated proteins (PLAUR, ITGB3, and MHC I proteins). The specificity of these proteins to GBM has been validated using the human protein atlas and a cohort of 50 GBM patients.

MATERIALS AND METHODS

Experimental Design and Statistical Rationale

Shotgun proteomics experiments were conducted in biological triplicates (n=3). For the proteomics statistical analysis, extracted proteins presenting as significant by the ANOVA test analysis were used (p-value < 0.05). Normalization was achieved using a Z-score with matrix access by rows.

Chemicals and Reagents

Water (H^2O), formic acid (FA), acetonitrile (ACN), and trifluoroacetic acid (TFA) were obtained from Biosolve B. V. (Valkenswaard, Netherlands). DL-dithiothreitol (DTT), Hydrochloric acid (HCl), and Triton X-114 were purchased from Sigma-Aldrich (Saint-Quentin Fallavier, France). Trypsin was purchased from Promega (Charbonnieres, France). Tris was purchased from Interchim (Montluçon, France). EZ-Link Sulfo-NHS-SS-Biotin, Streptavidin UltraLink Resin (Pierce), Sodium chloride (NaCl), Dulbecco's Modified Eagle's Medium (DMEM), DMEM high glucose GlutaMAX™ Supplement, heat-inactivated fetal bovine serum (FBS), trypsin, phosphate buffer saline (PBS), penicillin and streptomycin were purchased from Thermo Fisher Scientific (Massachusetts, USA). U-87 MG (ATCC® HTB-14™) cell lines were purchased from ATTC (Manassas, Virginia, USA). Immortalized Human Astrocytes (Ref: P10251-IM) and astrocyte medium were obtained from Innoprot (Derio, Spain). Human NCH82 stage IV glioma cells were obtained from Dr Regnier-Vigouroux.

Cell Culture

Human glioma cell line NCH82 and U-87 MG were grown in DMEM and DMEM high glucose GlutaMAX™ Supplement respectively supplemented with 10% FBS, 1% L-glutamine (2 mM), and 1% penicillin/streptomycin (100 units per ml). Immortalized human astrocytes were grown in an appropriate medium purchased from Innoprot. All cell lines were cultured at 37°C in a humidified atmosphere (5% CO2).

Cell Surface Protein Biotinylation and Triton X-114 Phase Partitioning

The same amount of cells (20.10^6) were plated on sterile 15 cm dish and cultured until they reached ≃ 80% confluence. Cells were washed three times with ice-cold PBS and incubate 30 min at room temperature with 0.25 mg/ml EZ-Link Sulfo-NHS-SS-Biotin with gentle agitation. The reaction was quenched with 50 mM Tris-HCl and cells were washed two times with ice-cold PBS. Cells were then scraped and resuspended in aqueous 2% (w/v) Triton X-114, containing 10 mM Tris–HCl, pH 7.5, and 150 mM NaCl and incubated 30 min at 4°C with frequent vortexing. Cell debris was removed with centrifugation at 10,000 x g at 4°C for 10 min. Supernatants were collected and incubated for 15 min at 37°C to achieve phase partitioning. The suspension was then centrifuged at 5,000 x g at 25°C for 30 min. The upper aqueous phase was discarded, and the lower detergent phase was carefully collected.

Purification of Biotinylated Proteins

Prior to experiments, the beads were pre-equilibrated with lysis buffer. The lower detergent phase was incubated with 40 µl of a 50% slurry of pre-equilibrated Streptavidin UltraLink Resin (Pierce) for 3 hrs at 4°C on a rotating well. After 6 washes with 50 mM ammonium bicarbonate buffer, biotinylated proteins were eluted with 50mM DTT 30 minutes at 50°C.

Protein Digestion

The proteins were digested with 1 µg Trypsin (Promega) overnight at 37°C. The digestion was stopped with 0.5% TFA. The samples were desalted using ZipTip C-18 (Millipore) and eluted with a solution of ACN/0.1% TFA (7:3, v/v). The samples were dried with SpeedVac and resuspended in 20 µL of ACN/0.1% formic acid (0.2:9.8, v/v) just before processing using LC-MS/MS. Experiments were done in biological triplicate (n=3).

LC-MS/MS Analysis

Mass spectrometry proteomics analysis of digested proteins was performed using a nano Acquity UPLC system (Waters) coupled with the Q-Exactive Orbitrap mass spectrometer (Thermo Scientific) *via* a nanoelectrospray source. The samples were separated using online reversed-phase, using a preconcentration column (nanoAcquity Symmetry C18, 5 µm, 180 µm x 20 mm) and an analytical column (nanoAcquity BEH C18, 1.7 µm, 75 µm x 250 mm). The peptides were separated by applying a linear gradient of acetonitrile in 0.1% formic acid (5%-35%) for 2h, at a flow rate of 300 nl/min. The Q- Exactive was operated in data-dependent mode defined to analyze the ten most intense ions of MS analysis (Top 10). The MS analysis was performed with an m/z mass range between 300 to 1 600, resolution of 70,000 FWHM, AGC of 3e6 ions, and maximum injection time of 120ms. The MS/MS analysis was performed with an m/z mass range between 200 to 2,000; AGC of 5e4 ion; maximum injection time of 60 ms and resolution set at 17,500 FWHM.

Protein ID and Data Analysis

Proteins were identified by comparing all MS/MS data with the proteome database of the complete reviewed proteome of Homo sapiens (Uniprot, release November 2020; 20,370 entries), using the MaxQuant software version 1.6.10.43 (16, 17). Trypsin specificity was used for the digestion mode with two missed cleavages. N-terminal acetylation and methionine oxidation were selected as the variable modifications. For MS spectra, an initial mass tolerance of 6 ppm was selected, and the MS/MS tolerance was set to 20 ppm for HCD data (18). For identification, the FDR at the peptide spectrum matches (PSMs) and protein level was set to 0.01, and a

minimum of 2 peptides per protein in which 1 was unique. Relative, label-free quantification of proteins was performed using the MaxLFQ algorithm integrated into MaxQuant with the default parameters. This algorithm performed the normalization of the MS-data in the total peptide ion signals. The normalization factors is calculated between the different cell condition and replicates (19). Analysis of the proteins identified was performed using Perseus software (http://www.perseus-framework.org/) (version 1.6.5.0) (20). The file containing the information from identification was used with hits to the reverse database, and proteins identified with modified peptides and potential contaminants were removed. Then, the LFQ intensity was logarithmized (log2[x]). Categorical annotation of rows was used to define different groups depending on the cell line. Multiple-samples tests were performed using an ANOVA test with a p-value of 0.05 and preserved grouping in randomization. The results were normalized by Z-score and represented as hierarchical clustering. Functional annotation and characterization of identified proteins were obtained using STRING (version 11.0, http://string-db.org). Surface proteins were then identified with the lists of surface proteins provided by the cell surface protein atlas (CSPA) (13) and the list of predicted surfaceome proteins (14). Gene Ontology enrichment allows the identification of some additional surface proteins. To identify surface protein already described in GBM we grouped the surface proteins described in the CSPA of primary brain tumor and GBM cells and in the CSPA of GBM cell lines LN18, LN229, U251-MG, U87-MG, and T98G GBM cell line (13). Venn diagram analysis was performed using "the InteractiVenn" (21).

Sub-Network Enrichment Pathway Analysis

Using Elsevier's Pathway Studio (version 11.0//Elsevier), all relationships between the differentially expressed proteins among all conditions were depicted based on the Ariadne ResNet (22) For proteins identified in the shotgun analysis, the Subnetwork Enrichment Analysis (SNEA) algorithm was used to detect the statistically significant altered biological pathways in which the identified proteins are involved. This algorithm uses Fisher's statistical test to detect any non-random associations between two categorical variables organized by a specific relationship. Also, this algorithm starts by creating a central "seed" from all the relevant identities in the database and builds connections with associated entities based on their relationship with the seed. SNEA compares the sub-network distribution to the background distribution using one-sided Mann-Whitney U-Test and calculates a p-value; thus, representing a statistical significance between different distributions. In all analyses that we performed, the GenBank ID was used to form experimental groups based on the different conditions present for analysis. The pathway networks were reconstructed based on biological processes and molecular functions for every single protein, along with its associated targets.

Mutation Identification

Protein identification was also performed using the mutation-specific database.32 XMan v2 database contains 2 539 031 mutated peptide sequences from 17 599 Homo sapiens proteins (2 377 103 are missense and 161 928 are nonsense mutations). The interrogation was performed with Proteome Discoverer 2.3 software and Sequest HT package, using an iterative method. The precursor mass tolerance was set to 15 ppm and the fragment mass tolerance was set to 0.02 Da. For high confidence results, the false discovery rate (FDR) values were specified to 1%. A filter with a minimum Xcorr of 2 was applied. The generated result file was filtered using a Python script to remove unmutated peptides. All mutations were then manually checked based on MSMS spectra profile. The structure of mutated proteins was constructed with PremPS (https://lilab.jysw.suda.edu.cn/research/PremPS/) (23).

Druggable Genome Database and Clinical Trials

To identify drug candidates targeting the surfaceome proteins specific to GBM, the relationship between protein-coding genes and drugs was analyzed from different sources including Drug Central (https://drugcentral.org), DrugBank (https://go.drugbank.com/), ApexBio (https://www.apexbt.com/), DGIdb (https://www.dgidb.org/), FDA Approved Drugs (https://www.accessdata.fda.gov/scripts/cder/daf/), ClinicalTrials.gov, and/or PharmGKB (https://www.pharmgkb.org/).

To determine whether drug candidates were investigated in therapeutic trials for GBM patients, ClinicalTrials.gov web-based resource was used (https://clinicaltrials.gov/ct2/home). This resource provides information on publicly and privately supported clinical studies on a wide range of diseases and conditions and is maintained by the National Library of Medicine at the National Institutes of Health (US). Information on ClinicalTrials.gov is provided and updated by the sponsor or principal investigator of the clinical study. Among the clinical trials conducted in patients, children, and adults, with glioblastoma, the search was conducted among the trials corresponding to interventional studies with a status recruiting, not yet recruiting, active, not recruiting, enrolling by invitation, or completed, which represented a list of 1750 clinical trials.

Patient Samples and Consent

Patients with newly diagnosed glioblastoma were prospectively enrolled between September 2014 and November 2018 at Lille University Hospital, France. Patients were adult, had no medical history of other cancers or previous cancer treatment, no known genetic disease potentially leading to cancer and no neurodegenerative disease. Tumors samples were processed within 2 hours after sample extraction in the surgery room to limit the risk of degradation of proteins. Characteristic of the cohort has been published in (24) (**Supplementary Table 1**). Approval was obtained from the research ethics committee (ID-RCB 2014-A00185-42) before initiation of the study. The study adhered to the principles of the Declaration of Helsinki and the Guidelines for Good Clinical Practice and is registered at NCT02473484. Informed consent was obtained from patients.

RESULTS

Malignant cells adopt a complete proteomic makeover, especially on their surface. Surfaceome study allows emphasizing the

changes in the interactions between cells and with their environment. Here, we compared the surfaceome of two different human glioblastoma cell lines, U87 and NCH82, with a human astrocyte cell line. Cell-surface proteins were labelled and captured with membrane-impermeable EZ-Link Sulfo-NHS-SS-Biotin from intact cells. Shotgun proteomic analysis of these three cell lines yielded 2,920 protein identifications across all the samples (**Supplementary Data 1**). We applied a filter to retain only the proteins found in at least two of the three replicates. Then, the variations in protein expression were analyzed between the three cell lines. As a criterion of significance, we applied an ANOVA test with a significance threshold of $p < 0.05$. A heatmap was created from which 190 proteins showed a significant difference in LFQ expression between astrocytes, NCH82, and U87 cell lines (**Figure 1A**, **Supplementary Data 2**, **3**). Surface proteins were then identified by cross-checking the total list of heatmap proteins with the lists of surface proteins provided by the cell surface protein atlas (CSPA) (13) and the list of predicted surfaceome proteins (14). Gene Ontology enrichment allowed the identification of some additional surface proteins. We found 57 surface proteins thanks to CSPA and *in silico* databases and 14 additional proteins being described as membrane proteins for a total of 71 surface proteins with differential expression between the three cell lines (**Figure 1B**). Four clusters were highlighted, cluster 1 regroups under-expressed surface proteins in the two GBM cell lines and cluster 2 overexpressed proteins (**Figure 1A**). The cluster 3 represents NCH82 over-expressed proteins and the U87 over-expressed proteins are in the cluster 4 (**Figure 1A**).

Over-Expressed and Exclusive Surface Proteins in Immortalized Astrocyte Cell Line

We were first interested in the proteins under-expressed or unexpressed in GBM cells compared to astrocytes. On the heatmap (**Figure 1A**), cluster 1 includes 21 proteins that are under-expressed in NCH82 and U87 compared to the astrocyte cell line (**Supplementary Data 2**). Among these proteins, 12 are known to be expressed at the plasma membrane. We compared these proteins to the surface proteins described in GBM cell line and primary culture in CSPA (GBM CSPA) database. Four proteins were found in GBM CSPA databases and 8 additional proteins were found in astrocyte cell line (**Figure 1C**, **Supplementary Data 2**). Among these proteins, we found Cell adhesion molecule 3 (*cadm3*) involved in intercellular adhesion and Fibrillin-2 (*fbn2*), an extracellular matrix component. Stomatin (*stom*) which regulates ion transport was also found in this cluster of under-expressed surface proteins. We then examined the proteins exclusive to each cell line and among the 15 proteins only expressed by astrocytes cell line, 11 were membrane-bound and so, unexpressed in GBM cell lines (**Figure 2A**). 7 of these 11 surface proteins are described in GBM CSPA databases (**Supplementary Data 4**, **Figure 2B**). In addition to these proteins, we also found 4 more cell surface proteins not described in the lists above (**Supplementary Data 4**). Among these proteins, we found the desmosomal protein plakoglobin (*jup*) which plays a central role in the structure and function of submembranous plaques (25). We have also identified NHE-RF1 (*slc9a3r1*), known to be localized

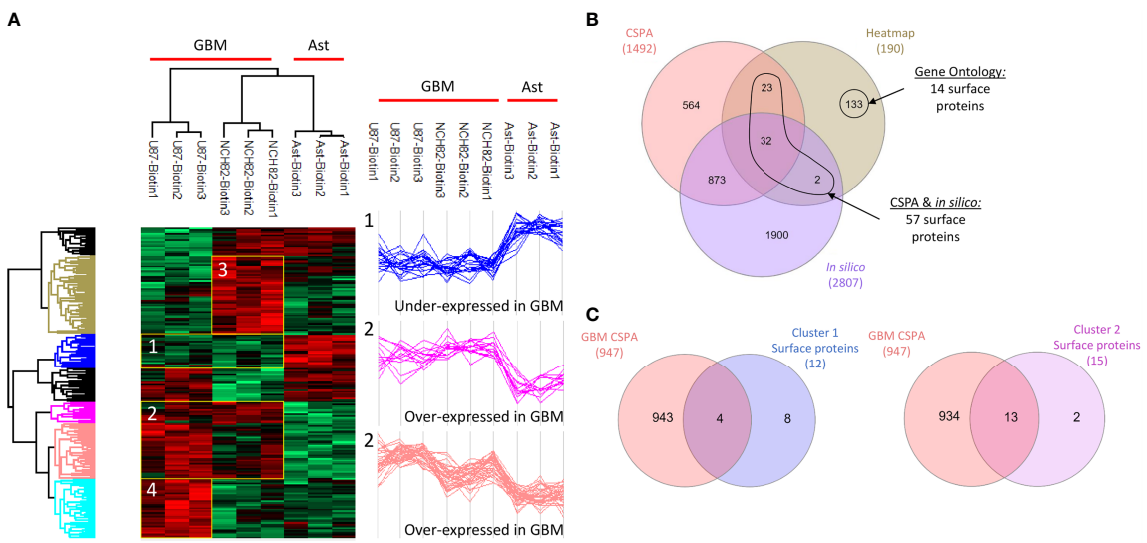

FIGURE 1 | Healthy astrocyte cell line, U87 and NCH82 GBM cell lines were biotinylated and lysed. Biotinylated surface proteins were purified on streptavidin beads, digested, and analyzed with LC-MS/MS. MaxQuant and Perseus software were used for the statistical analysis. **(A)** A heatmap was generated to show proteins with expression significantly different between cell lines. Two clusters are highlighted (1 and 2). **(B)** Venn diagram was performed between the 190 proteins of the heatmap and the surface proteins from CSPA and in silico CSPA databases to identify 57 surface proteins. Analysis of Gene Ontology of the different proteins allowed the discovery of 14 additional surface proteins. **(C)** Proteins from cluster 1 and cluster 2 were compared to surface proteins described for different GBM cell lines in CSPA (GBM CSPA).

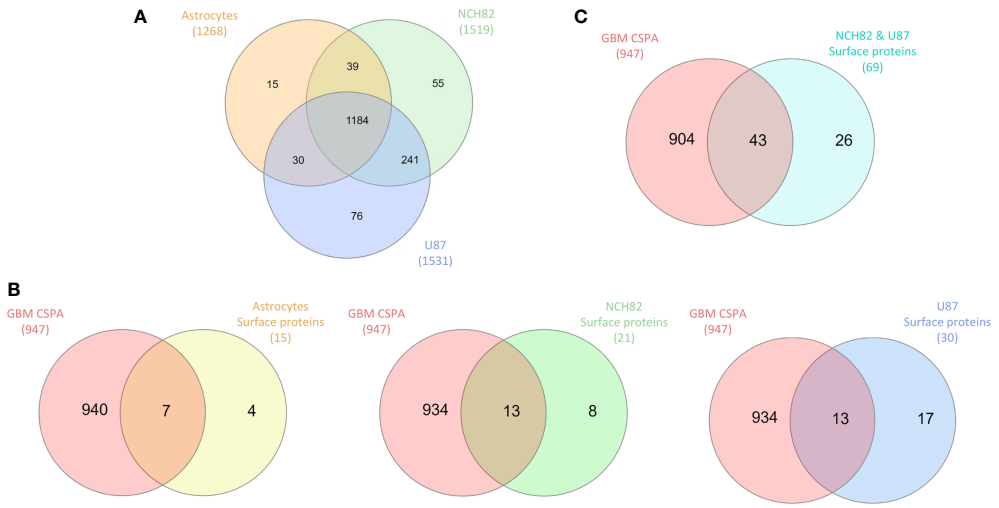

FIGURE 2 | **(A)** Proteins identified in all cell lines are compared in Venn diagram to highlight exclusive proteins to each cell line and common proteins to GBM cell lines. **(B)** Exclusive surface proteins from each cell line were compared to surface proteins from GBM cell lines in CSPA (CSPA GBM). **(C)** Common proteins to NCH82 and U87 GBM cell lines were compared to surface proteins from GBM cell lines in CSPA (CSPA GBM).

to the plasma membrane in normal astrocytes and showing a cytoplasmic shift within GBM tumor cells (26).

Over-Expressed and Exclusive Surface Proteins in GBM Cell Lines

Overexpressed and exclusive proteins to GBM cell lines were abundant in our data. Indeed, cluster 2 of the heatmap includes 47 proteins overexpressed in GBM cell lines compared to astrocytes cell line. Among these proteins, we counted 15 proteins described to localize at the plasma membrane including 13 proteins already described in GBM CSPA and 2 additional surface proteins (**Figure 1C**, **Supplementary Data 2**). Some of these membrane proteins are involved in tumor progression such as Neurogenic locus notch homolog protein 2 (*notch2*) (27), Aspartyl/asparaginyl beta-hydroxylase (*asph*) (28) and Procathepsin L (*ctsl*) for which high expression is unfavorable in glioma (29). We also found the proteins Prostaglandin F2 receptor negative regulator (*ptgfrn*) and Collagen alpha-1(VI) chain (*col6a1*), which correlate with a poor prognosis in GBM (30, 31). Two more clusters of over-expressed proteins in each GBM cell line are highlighted. In the cluster 3, we found 15 surface proteins over-expressed in NCH82 cell line (**Figure 1A**) in which 5 are not described in GBM CSPA (**Supplementary Data 2**). Finally, cluster 4 contains 10 surface proteins over-expressed in U87 cell line among which one protein is not found in GBM CSPA (**Figure 1A**, **Supplementary Data 2**). We have also identified 21 surface proteins only expressed by NCH82 among the 55 proteins identified (**Supplementary Data 4**, **Figure 2B**). Among these cell surface proteins, 13 were already described in GBM CSPA (**Supplementary Data 4**).

We identified 8 additional surface proteins in NCH82 cell line. Among these proteins we found, Guanylate-binding protein 1 (*gbp1*) and Pro-neuregulin-1 (*nrg1*) which are key players in glioblastoma progression (32, 33). We have also identified Raftlin (*rftn1*) which is involved in the cell entry of poly(I:C), ligand of TLR3 (34). It could therefore be a target in therapies involving TLRs (35).

Regarding the 76 proteins only expressed by U87 cell line, 30 surface proteins have been identified (**Supplementary Data 4**, **Figure 2B**). 13 of these proteins are found in GBM CSPA. We have also identified 17 other proteins that are described as membrane-bound in the literature (**Supplementary Data 4**). Among these proteins, we found Calpain-5 (*capn5*) which is already described in surgical biopsies of glioblastoma (36). We also found Paxillin (*pxn*) which is associated with a poor prognosis of glioblastoma (37). Sodium-dependent phosphate transporter 1 (*slc20a1*) is described to be over-expressed in high grade gliomas (38) and Integrin-linked protein kinase (*ilk*) to promote glioblastoma invasion (39). Finally, Caveolin-1 (*cav1*) could serve as a biomarker to predict response to chemotherapy. Indeed, its over-expression seems to confer sensitivity to the most commonly used chemotherapy for glioblastoma, temozolomide (40). Moreover, 69 proteins described as membrane proteins were found among the 241 proteins common to both NCH82 and U87 glioblastoma cell lines and not expressed by astrocyte cell line (**Supplementary Data 4**, **Figure 2C**). Among these proteins, 43 are found in the GBM CSPA database. We found 26 additional surface proteins that are not included in the lists of surface proteins previously mentioned (**Supplementary Data 4**). Among them, we found Glioma pathogenesis-related protein 1 (*glipr1*), Receptor of activated protein C kinase 1 (*rack1* or *gnb2l1*), Protein disulfide-isomerase (*p4hb*), and Carbonic anhydrase 9 (*ca9*) known to be over-expressed in glioblastoma and to promote tumor growth (41–44). We also find Microtubule-actin cross-linking factor 1 (*macf1*) recently described as a novel radiosensitization target in

glioblastomas (45) and Protein NDRG1 (*ndrg1*) which is over-expressed in glioma resistant to antiangiogenic therapy (46).

Most of GBM cell Surface Proteins Are Linked to Tumor Growth and Immune Regulation

As described before, several surface proteins identified in GBM cell lines are involved in tumor growth. Biological pathways analyses highlighted several proteins only expressed by NCH82 or U87 cell line linked to cell invasion or cell spreading, two key processes for GBM development and drug resistance (**Figure 3**, **Supplementary Figure 1**). Moreover, most of the cell surface proteins are related to cell contact and cell adhesion pathway, another main process for tumor growth (**Figure 3**, **Supplementary Figure 1**). The two GBM cell lines also over-expressed surface proteins linked to the vascularization and proliferation pathways (**Supplementary Figure 1**). Biological pathways analyses also established that several common proteins for GBM cell line and proteins only expressed by U87 (**Figure 3**) are involved in immune regulation processes such as negative regulation of CD8-positive, alpha-beta T cell activation (*hfe*), negative regulation of activated T cell proliferation (*pdcd11g2, cd274*) or negative regulation of interferon-gamma production (*c1qbp*).

Expression of Mutated Surface Proteins in the Glioblastoma Cell Lines

Several studies have reported the high number of protein mutations related to tumor progression in GBM (47–49). In this context, we investigated the mutations of surface proteins in GBM cell lines. For that purpose, we used a human database combined with the XMan v.2 database (15). This database contains information about mutated peptides that can be found in some cancers, extracted from the COSMIC database. After applying statistic filters, 114 mutations were identified. The MSMS spectra of these 114 mutations were manually checked for specific fragmentation of the mutated amino acid. Thus, thirty-three mutated peptides were identified among which 9 are only detected in both NCH82 and U87 GBM cell lines compared to astrocyte cell line. Among the proteins from which mutated peptides were identified, we retrieved RELT-like protein 1 (*rell1*), Cytochrome b-245 light chain (*cyba*), Epidermal growth factor receptor (*egfr*) and Cytochrome b reductase 1 (*cybrd1*) for which missense mutations are found in their intracellular domains. Other proteins mutated this time in their extracellular domain have been identified such as Urokinase plasminogen activator surface receptor (*plaur*), Integrin beta-3 (*itgb3*), and different subunit of HLA class I and II histocompatibility antigen such as B-41 alpha chain (*hla-b*), A-24 alpha chain (*hla-a*) and DP beta 1 chain (*hla-dpb1*) (**Figure 4**).

Tracking Identified Surface Proteins in Patients

In this study, proteomic analyses were performed on three different replicates of cell samples. Some variation in the protein expression can be observed between replicates of a same cell sample (**Figure 1A**). Since the number of replicates was limited, we wanted to validate the expression in GBM patients of all the surface proteins identified in this study. To do so, we compared the proteins of each heatmap clusters (**Figure 1A**, **Supplementary Data 2**) as well as the proteins exclusive to each cell line and the proteins common to both NCH82 and U87 cell line (**Figure 2A**, **Supplementary Data 4**) to the ones identified in patient's glioblastoma using spatial proteomic guided by MALDI-mass spectrometry (24). Characteristics of the GBM cohort are presented in (**Supplementary Table 1**). It has allowed to identify 66 of our surface proteins expressed in at least 70% patient's GBM from this cohort.

Of all the surface proteins we identified in this study (**Supplementary Data 2** and **4**), 67 are not described in the GBM cell lines in the CSPA database. It was therefore necessary to confirm the expression of these additional surface proteins in patient's GBMs. Thus, we can confirm the expression of 32 surface proteins in 70% of the GBM patients cohort (24) among the 67 additional proteins not founded in the GBM CSPA data (**Supplementary Data 2** and **4**). Finally, among the surface

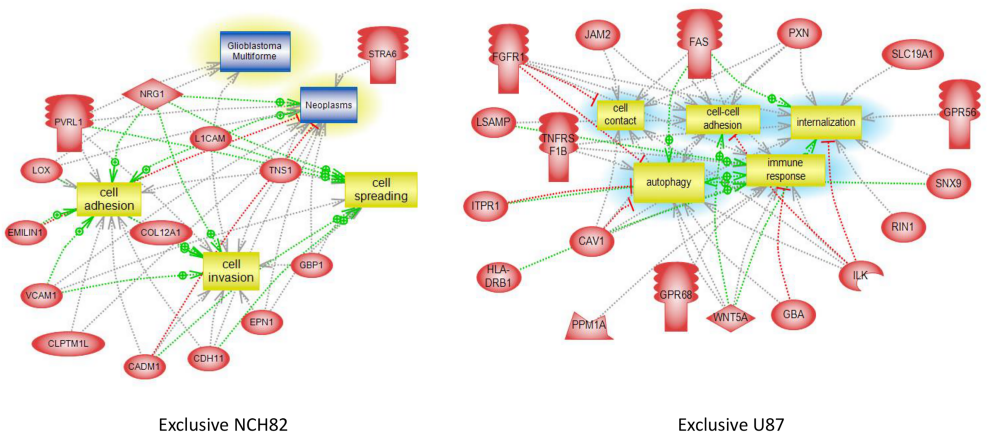

FIGURE 3 | Global pathway analyses of proteins only expressed by NCH82 and U87 GBM cell lines.

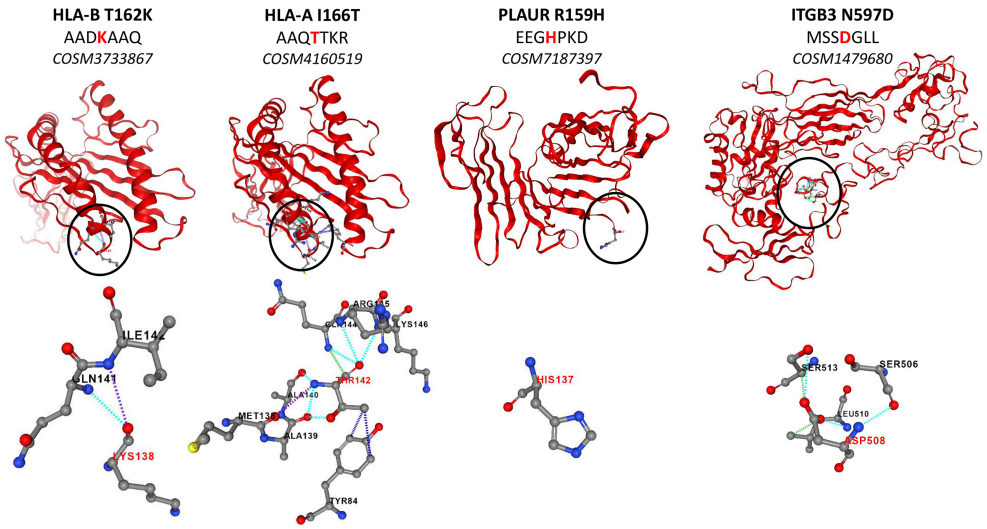

FIGURE 4 | Structure of mutated proteins according to PremPS.

proteins identified in the GBM cell lines and in the patient's GBM we found 5 proteins not described in healthy brain tissues according to human protein atlas (**Table 1**, **Supplementary Table 3**). In which we have HSPD1 already used in clinical trials as described before and LGALS3BP which have no known drug interaction yet. The two proteins are associated with a bad overall survival (**Supplementary Figure 2**).

Moreover, the mutation of HLA class I histocompatibility antigen A and B are also found in several patient's GBM (50) (**Table 1**).

Clinical Investigation for the Selected Specific Glioblastoma Targets

We selected 78 surface proteins only found in each GBM cell lines (**Figure 2C**) or overexpressed (**Cluster 2, Figure 1A**) in both NCH82 and U87 GBM cell lines (**Supplementary Table 2**) and the 9 mutated surface proteins only expressed by NCH82 or U87. We analyzed the expression of these proteins inside healthy tissues and cancers thanks to Human Protein Atlas and Catalogue Of Somatic Mutation In Cancer (COSMIC) databases. Thus we highlighted 25 proteins not expressed in healthy brain tissues (**Supplementary Table 3**). The druggability of the selected surface proteins specific to GBM was assessed using drug and compound databases as described in methods. Our approach identified among targetable proteins CPM, CYBA, EGFR, HLA-A, HLA-B, HSPD-1, P4HA2 which were druggable with either chemotherapy, tyrosine kinase inhibitors, vaccines, anti-CTLA4 or vitamins. A non-exhaustive list of clinical studies detailing the trials investigating the antitumor efficacy of these strategies in GBM patients is in **Supplementary Table 3**. These proteins also had interactions with other drugs or compounds not yet under clinical investigation such as antiepileptics to target CPM or HLA, lipid-lowering drugs to target CYBA, or antibiotics to target HSPD1, thus showing the potential for drug repurposing to treat GBM. Moreover, our approach identified C1orf159, CD151, and LGALS3BP which have no known drug interaction yet.

DISCUSSION

In this work, we compared the surfaceome of glioblastoma cell lines to an immortalized astrocyte cell line. We were able to

TABLE 1 | Expression of surface proteins in GBM patients.

Protein Ids	Gene names	Protein names	Astrocytes	NCH82	U87	Glioma patients
P12109	**COL6A1**	Collagen alpha-1(VI) chain	0	X	X	49/50 (24)
P12110	**COL6A2**	Collagen alpha-2(VI) chain	0	X	X	39/50 (24)
P12111	**COL6A3**	Collagen alpha-3(VI) chain	0	X	X	50/50 (24)
Q08380	**LGALS3BP**	Galectin-3-binding protein	0	X	X	45/50 (24)
P10809	**HSPD1**	60 kDa heat shock protein, mitochondrial	0	X	X	50/50 (24)
P30479	**HLA-B**	HLA class I histocompatibility antigen, B-41 alpha chain *Mutated for T162K*	0	0	X	7/17 (50)
P05534	**HLA-A**	HLA class I histocompatibility antigen, A-24 alpha chain *Mutated for I166T*	0	0	X	4/17 (50)

highlight the different changes in the surface proteins expressed in cancer cells. Among these changes, we found an under-expression of proteins involved in cell adhesion in glioblastoma cell lines compared to immortalized astrocytes. Indeed, NCH82 and U87 underexpress proteins such as CADM3, CADM4, or NRCAM involved in intercellular adhesion. Impairment of cell-cell adhesion is one of the processes allowing tumor escape and metastasis. Alteration of adhesion protein expression is a common event in many types of cancer. Many of these proteins are being studied as potential biomarkers or therapeutic targets (51). The extracellular matrix organization and integrity is another crucial aspect of the metastasis process. Several proteins related to the extracellular matrix organization are overexpressed in GBM cell lines compared to astrocytes cell line. These results suggest a complete extracellular matrix reorganization by cancer cells. On the other hand, some surface proteins overexpressed in GBM cells compared to immortalized astrocytes are involved in the generation of metabolic energy. The immune system regulation by cancer cells can also be investigated by surfaceome study. Indeed, some proteins expressed only in GBM cells are involved in the negative regulation of the immune response. Moreover, we highlight changes in protein localization within cancer cells. NHE-RF1 previously described as showing a cytoplasmic shift within GBM tumor cells compared to healthy cells (26), is only found in the membrane of immortalized astrocytes. Thus, this protein known to be membrane-bound shows intracellular localization in glioblastoma cells. This suggests that commonly intracellular proteins may be expressed at the cell surface within cancer cells. In fact, protein mislocalization is known to be a less emphasized mechanism in cancer (52). We also identified several mutations in surface proteins only expressed by GBM cell lines. Among these mutated proteins we find RELT-like protein 1 (*rell1*), Cytochrome b-245 light chain (*cyba*), Epidermal growth factor receptor (*egfr*), and Cytochrome b reductase 1 (*cybrd1*). These mutations are found in the cytoplasmic domain and could alter the signaling pathways in which these proteins are involved. Thus, we have demonstrated that the study of surface proteins allows us to highlight different processes used by cancer cells to modify their environment and metabolism to increase tumor growth. It is a new tool to explore specific tumor development mechanisms through a non-traditional approach.

The surfaceome study is a useful tool for fundamental research to understand the mechanisms of tumor growth. It also enables the discovery of new biomarkers for clinical purposes. Indeed, in this data, we found 78 surface proteins over-expressed or exclusive to GBM cell lines compared to astrocyte cell lines (**Cluster 2, Figures 1A**, **2C**, and **Figure 2C**). Among these proteins, 28 are not described in GBM CSPA database. It may be an opportunity to complete databases after localization validation of these proteins with the literature. On the other hand, we screened the human protein atlas for these 78 surface proteins to highlight potential therapeutic targets for immunotherapy. Thus, 25 surface proteins showed low expression on brain-healthy tissues (**Table S1**, proteins highlighted in blue), and 6 of these proteins are described in GBM tissues (**Table S1**, proteins highlighted in purple) according to the human protein atlas. Moreover, among mutated surface proteins identified, some are mutated in their extracellular domain (**Table S1**, proteins highlighted in red). Among these proteins we found Urokinase plasminogen activator surface receptor (*plaur*), Integrin beta-3 (*itgb3*) and the different subunits of HLA class I and II histocompatibility antigen such as B-41 alpha chain (*hla-b*), A-24 alpha chain (*hla-a*) and DP beta 1 chain (*hla-dpb1*). These 5 proteins present extracellular mutations unique to GBM cell lines and described in the literature in very few cancers. As it is the case for mutated HLA-B and HLA-A previously described within GBM tissues (50). Thus, we identified 11 surface proteins which could be used as a therapeutic target in immunotherapy against GBM. Among these 11 targets, 7 are already used in clinical trials (**Table S2**), for example, HSPD1 is also described in GBM tissues (24). Moreover, C1orf159, CD151, LGALS3BP, and mutated proteins described above are not yet used in clinical trials but worth interest, notably LGALS3BP also found in GBM tissue (24) like mutated HLA-A and HLA-B (50). We also identified from spatial proteomic studies of 50 GBM patients, twelve proteins in common with our data including LGALS3BP and HLA-A2. Nine of the twelve have been associated with worse overall survival (50). LGALS3BP is included in the nine proteins which is in line with other data observed in breast cancer. LGALS3BP inhibits the differentiation of monocyte-derived fibrocytes through CD209/SIGN-R1 in mouse spleen and is secreted from breast cancer for metastasis (53).

Taken together, our data suggest that these surface proteins could be candidate targets for alternative therapeutic strategies such as new CARs against mutated GBM-specific proteins, which would reduce the immune response and off-target effect. This work showed that exploring the surfaceome of GBM cells has the potential to identify new therapeutic targets including mutated surface proteins exclusive to GBM. However, it is important to be aware that these results are derived from surfaceome analyses of immortalized cell lines in a limited range of replicates. The cross-validation of our results with GBM patients proteomics data and with the Human Protein Atlas data helped us to select the more specific potential targets which still need to be validated on a more relevant study model such as patients'-derived organoids and an increased number of replicates. Using patients' derived tumoroids in order to select the right antigens expressed by the tumor cells could help to translate this kind of approach into the clinic in order to perform personalized therapies.

DATA AVAILABILITY STATEMENT

Proteomics data including MaxQuant files and annotated MS/MS have been deposited to the ProteomeXchange Consortium *via* the PRIDE partner repository with the dataset identifier PXD027110.

ETHICS STATEMENT

The studies involving human participants were reviewed and approved by ID-RCB 2014-A00185-42. The patients/participants

provided their written informed consent to participate in this study.

AUTHOR CONTRIBUTIONS

Conceptualization, IF and MS. Methodology, MR. Software, FK, NH, MR, TC, and SA. Validation, MR, TC, and SA. Formal analysis, MR and MS. Investigation, IF, NH, MD, MR, and MS. Resources, IF and MS. Data curation, MR. Writing—original draft preparation, MR and MS. Writing—review and editing, IF, FK, MD, MR, and MS. Visualization, MR. Supervision, IF and MS. Project administration, MD and MS. Funding acquisition, IF, NH, MS, and TC. All authors contributed to the article and approved the submitted version.

FUNDING

This research was funded by Institut national de la Santé et de la recherche Médicale (Inserm), Canceropole Nord.

SUPPLEMENTARY MATERIAL

The Supplementary Material for this article can be found online at: https://www.frontiersin.org/articles/10.3389/fimmu.2021.746168/full#supplementary-material

Supplementary Table 1 | Expression in healthy and cancers tissues of surface proteins over-expressed or exclusive to GBM cell lines according to Human Protein Atlas.

Supplementary Table 2 | Drug candidates targeting genes specific to glioma and existing therapeutic clinical trials in glioma patients.

Supplementary Data Sheet 1 | Raw data before the application of any filters.

Supplementary Data Sheet 2 | Proteins list for the clusters of the heatmap **Figure 1**.

Supplementary Data Sheet 3 | p-value of proteins presented on the heatmap.

Supplementary Data Sheet 4 | Exclusive proteins list for each cell line.

Supplementary Figure 1 | Global pathways analyses for clusters 1, 2, 3 & 4.

Supplementary Figure 2 | Overall survival studies and HIS results for LGALS3BP and HSPD1.

REFERENCES

1. Ostrom QT, Cioffi G, Gittleman H, Patil N, Waite K, Kruchko C, et al. CBTRUS Statistical Report: Primary Brain and Other Central Nervous System Tumors Diagnosed in the United States in 2012-2016. *Neuro Oncol* (2019) 21: v1–100. doi: 10.1093/neuonc/noz150
2. Chinot O, Wick W, Mason W, Henriksson R, Saran F, Nishikawa R, et al. Bevacizumab Plus Radiotherapy-Temozolomide for Newly Diagnosed Glioblastoma. *N Engl J Med* (2014) 370:709–22. doi: 10.1056/NEJMOA1308345
3. Gilbert M, Liu Y, Neltner J, Pu H, Morris A, Sunkara M, et al. Autophagy and Oxidative Stress in Gliomas With IDH1 Mutations. *Acta Neuropathol* (2014) 127:221–33. doi: 10.1007/S00401-013-1194-6
4. Stupp R, Roila FESMO Guidelines Working Group. Malignant Glioma: ESMO Clinical Recommendations for Diagnosis, Treatment and Follow-Up. *Ann Oncol* (2009) 20 Suppl 4:iv126–8. doi: 10.1093/ANNONC/MDP151
5. Stupp R, Taillibert S, Kanner A, Read W, Steinberg D, Lhermitte B, et al. Effect of Tumor-Treating Fields Plus Maintenance Temozolomide vs Maintenance Temozolomide Alone on Survival in Patients With Glioblastoma: A Randomized Clinical Trial. *JAMA* (2017) 318:2306–16. doi: 10.1001/JAMA.2017.18718
6. Stupp R, Hegi M, Mason W, Van Den Bent M, Taphoorn M, Janzer R, et al. Effects of Radiotherapy With Concomitant and Adjuvant Temozolomide Versus Radiotherapy Alone on Survival in Glioblastoma in a Randomised Phase III Study: 5-Year Analysis of the EORTC-NCIC Trial. *Lancet Oncol* (2009) 10:459–66. doi: 10.1016/S1470-2045(09)70025-7
7. Weller M, Van Den Bent M, Tonn J, Stupp R, Preusser M, Cohen-Jonathan-Moyal E, et al. European Association for Neuro-Oncology (EANO) Guideline on the Diagnosis and Treatment of Adult Astrocytic and Oligodendroglial Gliomas. *Lancet Oncol* (2017) 18:e315–29. doi: 10.1016/S1470-2045(17)30194-8
8. Weller M, Roth P, Preusser M, Wick W, Reardon DA, Platten M, et al. Vaccine-Based Immunotherapeutic Approaches to Gliomas and Beyond. *Nat Rev Neurol* (2017) 13:363–74. doi: 10.1038/NRNEUROL.2017.64
9. Gramatzki D, Dehler S, Rushing EJ, Zaugg K, Hofer S, Yonekawa Y, et al. Glioblastoma in the Canton of Zurich, Switzerland Revisited: 2005 to 2009. *Cancer* (2016) 122:2206–15. doi: 10.1002/CNCR.30023
10. Ito H, Nakashima H, Chiocca EA. Molecular Responses to Immune Checkpoint Blockade in Glioblastoma. *Nat Med* (2019) 25:359–61. doi: 10.1038/s41591-019-0385-7
11. Roth P, Mason WP, Richardson PG, Weller M. Proteasome Inhibition for the Treatment of Glioblastoma. *Expert Opin Investig Drugs* (2020) 29:1133–41. doi: 10.1080/13543784.2020.1803827
12. Effendi Syafruddin S, Fahmi Wan Mohamad Nazarie W, Ashikin Moidu N, Hong Soon B, Aiman Mohtar M. Integration of RNA-Seq and Proteomics Data Identies Glioblastoma Multiforme Surfaceome Signature. *BMC Cancer* (2021) 21:1–13. doi: 10.21203/rs.3.rs-46071/v2
13. Bausch-Fluck D, Hofmann A, Bock T, Frei AP, Cerciello F, Jacobs A, et al. A Mass Spectrometric-Derived Cell Surface Protein Atlas. *PLoS One* (2015) 10:121314. doi: 10.1371/journal.pone.0121314
14. Bausch-Fluck D, Goldmann U, Müller S, van Oostrum M, Müller M, Schubert OT, et al. The in Silico Human Surfaceome. *Proc Natl Acad Sci USA* (2018) 115:E10988–97. doi: 10.1073/pnas.1808790115
15. Flores MA, Lazar IM. XMAn V2-A Database of Homo Sapiens Mutated Peptides. *Bioinformatics* (2020) 36:1311–3. doi: 10.1093/bioinformatics/btz693
16. Cox J, Mann M. MaxQuant Enables High Peptide Identification Rates, Individualized P.P.B.-Range Mass Accuracies and Proteome-Wide Protein Quantification. *Nat Biotechnol* (2008) 26:1367–72. doi: 10.1038/nbt.1511
17. Tyanova S, Temu T, Cox J. The MaxQuant Computational Platform for Mass Spectrometry-Based Shotgun Proteomics. *Nat Protoc* (2016) 11:2301–19. doi: 10.1038/nprot.2016.136
18. Cox J, Neuhauser N, Michalski A, Scheltema RA, Olsen JV, Mann M. Andromeda: A Peptide Search Engine Integrated Into the MaxQuant Environment. *J Proteome Res* (2011) 10:1794–805. doi: 10.1021/pr101065j
19. Cox J, Hein MY, Luber CA, Paron I, Nagaraj N, Mann M. Accurate Proteome-Wide Label-Free Quantification by Delayed Normalization and Maximal Peptide Ratio Extraction, Termed MaxLFQ. *Mol Cell Proteomics* (2014) 13:2513–26. doi: 10.1074/mcp.M113.031591
20. Tyanova S, Temu T, Sinitcyn P, Carlson A, Hein MY, Geiger T, et al. The Perseus Computational Platform for Comprehensive Analysis of (Prote) Omics Data. *Nat Methods* (2016) 13:731–40. doi: 10.1038/nmeth.3901
21. Heberle H, Meirelles VG, da Silva FR, Telles GP, Minghim R. InteractiVenn: A Web-Based Tool for the Analysis of Sets Through Venn Diagrams. *BMC Bioinf* (2015) 16:1–7. doi: 10.1186/s12859-015-0611-3
22. Yuryev A, Kotelnikova E, Daraselia N. Ariadne's ChemEffect and Pathway Studio Knowledge Base. *Expert Opin Drug Discov* (2009) 4:1307–18. doi: 10.1517/17460440903413488

23. Chen Y, Lu H, Ning Z, Zhu Z, Wang S, Li M. PremPS: Predicting the Impact of Missense Mutations on Protein Stability. *PLoS Comput Biol* (2020) 16:1–22. doi: 10.1371/JOURNAL.PCBI.1008543
24. Drelich L, Duhamel M, Wisztorski M, Aboulouard S, Gimeno J-P, Caux P-D, et al. Overall Patient's Survival of Glioblastoma Associated to Molecular Markers: A Pan-Proteomic Prospective Study. *bioRxiv* (2020) 2020.11.24.397117:1–38. doi: 10.1101/2020.11.24.397117
25. Kirchner F, Schuetz A, Boldt LH, Martens K, Dittmar G, Haverkamp W, et al. Molecular Insights Into Arrhythmogenic Right Ventricular Cardiomyopathy Caused by Plakophilin-2 Missense Mutations. *Circ Cardiovasc Genet* (2012) 5:400–11. doi: 10.1161/CIRCGENETICS.111.961854
26. Molina JR, Morales FC, Hayashi Y, Aldape KD, Georgescu MM. Loss of PTEN Binding Adapter Protein NHERF1 From Plasma Membrane in Glioblastoma Contributes to PTEN Inactivation. *Cancer Res* (2010) 70:6697–703. doi: 10.1158/0008-5472.CAN-10-1271
27. Bazzoni R, Bentivegna A. Role of Notch Signaling Pathway in Glioblastoma Pathogenesis. *Cancers (Basel)* (2019) 11:1–25. doi: 10.3390/cancers11030292
28. Sturla LM, Tong M, Hebda N, Gao J, Thomas JM, Olsen M, et al. Aspartate-β-Hydroxylase (ASPH): A Potential Therapeutic Target in Human Malignant Gliomas. *Heliyon* (2016) 2:1–31. doi: 10.1016/j.heliyon.2016.e00203
29. Fei Y, Xiong Y, Shen X, Zhao Y, Zhu Y, Wang L, et al. Cathepsin L Promotes Ionizing Radiation-Induced U251 Glioma Cell Migration and Invasion Through Regulating the GSK-3β/CUX1 Pathway. *Cell Signal* (2018) 44:62–71. doi: 10.1016/j.cellsig.2018.01.012
30. Aguila B, Morris AB, Spina R, Bar E, Schraner J, Vinkler R, et al. The Ig Superfamily Protein PTGFRN Coordinates Survival Signaling in Glioblastoma Multiforme. *Cancer Lett* (2019) 462:33–42. doi: 10.1016/j.canlet.2019.07.018
31. Turtoi A, Blomme A, Bianchi E, Maris P, Vannozzi R, Naccarato AG, et al. Accessibilome of Human Glioblastoma: Collagen-VI-Alpha-1 Is a New Target and a Marker of Poor Outcome. *J Proteome Res* (2014) 13:5660–9. doi: 10.1021/pr500657w
32. Ji X, Zhu H, Dai X, Xi Y, Sheng Y, Gao C, et al. Overexpression of GBP1 Predicts Poor Prognosis and Promotes Tumor Growth in Human Glioblastoma Multiforme. *Cancer Biomarkers* (2019) 25:275–90. doi: 10.3233/CBM-171177
33. Lin WW, Ou GY, Lin JZ, Yi SJ, Yao WC, Pan HC, et al. Neuregulin 1 Enhances Cell Adhesion Molecule L1 Like Expression Levels and Promotes Malignancy in Human Glioma. *Oncol Lett* (2020) 20:326–36. doi: 10.3892/ol.2020.11548
34. Watanabe A, Tatematsu M, Saeki K, Shibata S, Shime H, Yoshimura A, et al. Raftlin Is Involved in the Nucleocapture Complex to Induce Poly(I:C)-Mediated TLR3 Activation. *J Biol Chem* (2011) 286:10702–11. doi: 10.1074/jbc.M110.185793
35. Rose M, Duhamel M, Aboulouard S, Kobeissy F, Tierny D, Fournier I, et al. Therapeutic Anti-Glioma Effect of the Combined Action of PCSK Inhibitor With the Anti-Tumoral Factors Secreted by Poly (I:C)-Stimulated Macrophages. *Cancer Gene Ther* (2021) 1–15. doi: 10.1038/s41417-020-00286-1
36. Polisetty RV, Gautam P, Sharma R, Harsha HC, Nair SC, Gupta MK, et al. LC-MS/MS Analysis of Differentially Expressed Glioblastoma Membrane Proteome Reveals Altered Calcium Signaling and Other Protein Groups of Regulatory Functions. *Mol Cell Proteomics* (2012) 11:1–15. doi: 10.1074/mcp.M111.013565
37. Sun LH, Yang FQ, Zhang CB, Wu YP, Liang JS, Jin S, et al. Overexpression of Paxillin Correlates With Tumor Progression and Predicts Poor Survival in Glioblastoma. *CNS Neurosci Ther* (2017) 23:69–75. doi: 10.1111/cns.12606
38. Pan YB, Wang S, Yang B, Jiang Z, Lenahan C, Wang J, et al. Transcriptome Analyses Reveal Molecular Mechanisms Underlying Phenotypic Differences Among Transcriptional Subtypes of Glioblastoma. *J Cell Mol Med* (2020) 24:3901–16. doi: 10.1111/jcmm.14976
39. Louca M, Zaravinos A, Stylianopoulos T, Gkretsi V. ILK Silencing Inhibits Migration and Invasion of More Invasive Glioblastoma Cells by Downregulating ROCK1 and Fascin-1. *Mol Cell Biochem* (2020) 471:143–53. doi: 10.1007/s11010-020-03774-y
40. Quann K, Gonzales DM, Mercier I, Wang C, Sotgia F, Pestell RG, et al. Caveolin-1 Is a Negative Regulator of Tumor Growth in Glioblastoma and Modulates Chemosensitivity to Temozolomide. *Cell Cycle* (2013) 12:1510–20. doi: 10.4161/cc.24497
41. Scheuring UJ, Ritter S, Martin D, Schackert G, Temme A, Tietze S. GliPR1 Knockdown by RNA Interference Exerts Anti-Glioma Effects In Vitro and In Vivo. *J Neurooncol* (2021) 1:1–10. doi: 10.1007/s11060-021-03737-3
42. Yan Y, Jiang Y. RACK1 Affects Glioma Cell Growth and Differentiation Through the CNTN2-Mediated RTK/Ras/MAPK Pathway. *Int J Mol Med* (2016) 37:251–7. doi: 10.3892/ijmm.2015.2421
43. Zou H, Wen C, Peng Z, Shao YY, Hu L, Li S, et al. P4HB and PDIA3 Are Associated With Tumor Progression and Therapeutic Outcome of Diffuse Gliomas. *Oncol Rep* (2018) 39:501–10. doi: 10.3892/or.2017.6134
44. Proescholdt MA, Merrill MJ, Stoerr EM, Lohmeier A, Pohl F, Brawanski A. Function of Carbonic Anhydrase IX in Glioblastoma Multiforme. *Neuro Oncol* (2012) 14:1357–66. doi: 10.1093/neuonc/nos216
45. Bonner K, Borlay D, Kutten O, Quick QA. Inhibition of the Spectraplakin Protein Microtubule Actin Crosslinking Factor 1 Sensitizes Glioblastomas to Radiation. *Brain Tumor Res Treat* (2020) 8:43. doi: 10.14791/btrt.2020.8.e1
46. Broggini T, Wüstner M, Harms C, Stange L, Blaes J, Thomé C, et al. NDRG1 Overexpressing Gliomas Are Characterized by Reduced Tumor Vascularization and Resistance to Antiangiogenic Treatment. *Cancer Lett* (2016) 380:568–76. doi: 10.1016/j.canlet.2015.06.026
47. Masica DL, Karchin R. Correlation of Somatic Mutation and Expression Identifies Genes Important in Human Glioblastoma Progression and Survival. *Cancer Res* (2011) 71:4550–61. doi: 10.1158/0008-5472.CAN-11-0180
48. Yan W, Zhang W, You G, Bao Z, Wang Y, Liu Y, et al. Correlation of IDH1 Mutation With Clinicopathologic Factors and Prognosis in Primary Glioblastoma: A Report of 118 Patients From China. *PLoS One* (2012) 7:30339. doi: 10.1371/journal.pone.0030339
49. Xu J, Li Z, Wang J, Chen H, Fang JY. Combined PTEN Mutation and Protein Expression Associate With Overall and Disease-Free Survival of Glioblastoma Patients. *Transl Oncol* (2014) 7:196–205.e1. doi: 10.1016/j.tranon.2014.02.004
50. Shankar GM, Lelic N, Gill CM, Thorner AR, Van Hummelen P, Wisoff JH, et al. BRAF Alteration Status and the Histone H3F3A Gene K27M Mutation Segregate Spinal Cord Astrocytoma Histology. *Acta Neuropathol* (2016) 131:147–50. doi: 10.1007/s00401-015-1492-2
51. Makrilia N, Kollias A, Manolopoulos L, Syrigos K. Cell Adhesion Molecules: Role and Clinical Significance in Cancer. *Cancer Invest* (2009) 27:1023–37. doi: 10.3109/07357900902769749
52. Wang X, Li S. Protein Mislocalization: Mechanisms, Functions and Clinical Applications in Cancer. *Biochim Biophys Acta - Rev Cancer* (2014) 1846:13–25. doi: 10.1016/j.bbcan.2014.03.006
53. White MJV, Roife D, Gomer RH. Galectin-3 Binding Protein Secreted by Breast Cancer Cells Inhibits Monocyte-Derived Fibrocyte Differentiation. *J Immunol* (2015) 195:1858–67. doi: 10.4049/JIMMUNOL.1500365

Conflict of Interest: The authors declare that the research was conducted in the absence of any commercial or financial relationships that could be construed as a potential conflict of interest.

frontiers in Immunology

ORIGINAL RESEARCH
published: 02 March 2022
doi: 10.3389/fimmu.2022.820673

Comprehensive Analysis of the Tumor Immune Microenvironment Landscape in Glioblastoma Reveals Tumor Heterogeneity and Implications for Prognosis and Immunotherapy

Rongrong Zhao[1,2†], Ziwen Pan[1,2†], Boyan Li[1,2], Shulin Zhao[1,2], Shouji Zhang[1,2], Yanhua Qi[1,2], Jiawei Qiu[1,2], Zijie Gao[1,2], Yang Fan[1,2], Qindong Guo[1,2], Wei Qiu[1,2], Shaobo Wang[1,2], Qingtong Wang[1,2], Ping Zhang[1,2], Xing Guo[1,2], Lin Deng[1,2], Hao Xue[1,2] and Gang Li[1,2*]*

[1] Department of Neurosurgery, Qilu Hospital, Cheeloo College of Medicine and Institute of Brain and Brain-Inspired Science, Shandong University, Jinan, China, [2] Shandong Key Laboratory of Brain Function Remodeling, Qilu Hospital, Shandong University, Jinan, China

Background: Glioblastoma (GBM) is a fatal brain tumor with no effective treatment. The specific GBM tumor immune microenvironment (TIME) may contribute to resistance to immunotherapy, a tumor therapy with great potential. Thus, an in-depth understanding of the characteristics of tumor-infiltrating immune cells is essential for exploring biomarkers in GBM pathogenesis and immunotherapy.

Methods: We estimated the relative abundances of 25 immune cell types in 796 GBM samples using single sample gene set enrichment analysis (ssGSEA). Unsupervised clustering was used to identify different GBM-associated TIME immune cell infiltration (GTMEI) patterns. The GTMEIscore system was constructed with principal component analysis (PCA) to determine the immune infiltration pattern of individual tumors.

Results: We revealed three distinct GTMEI patterns with different clinical outcomes and modulated biological pathways. We developed a scoring system (GTMEIscore) to determine the immune infiltration pattern of individual tumors. We comprehensively analyzed the genomic characteristics, molecular subtypes and clinicopathological features as well as proteomic, phosphoproteomic, acetylomic, lipidomic and metabolomic properties associated with the GTMEIscore and revealed many novel dysregulated pathways and precise targets in GBM. Moreover, the GTMEIscore accurately quantified the immune status of many other cancer types. Clinically, the GTMEIscore was found to have significant potential therapeutic value for chemotherapy/radiotherapy, immune checkpoint inhibitor (ICI) therapy and targeted therapy.

OPEN ACCESS

Edited by:
Eiichi Ishikawa, University of Tsukuba, Japan

Reviewed by:
Ming Yi, Huazhong University of Science and Technology, China
Dan Liu, Tianjin Medical University, China

***Correspondence:**
Gang Li
dr.ligang@sdu.edu.cn
Hao Xue
xuehao@sdu.edu.cn

†These authors have contributed equally to this work

Specialty section:
This article was submitted to Cancer Immunity and Immunotherapy, a section of the journal Frontiers in Immunology

Received: *23 November 2021*
Accepted: *14 February 2022*
Published: *02 March 2022*

Citation:
Zhao R, Pan Z, Li B, Zhao S, Zhang S, Qi Y, Qiu J, Gao Z, Fan Y, Guo Q, Qiu W, Wang S, Wang Q, Zhang P, Guo X, Deng L, Xue H and Li G (2022) Comprehensive Analysis of the Tumor Immune Microenvironment Landscape in Glioblastoma Reveals Tumor Heterogeneity and Implications for Prognosis and Immunotherapy. Front. Immunol. 13:820673. doi: 10.3389/fimmu.2022.820673

Conclusions: For the first time, we employed a multilevel and multiplatform strategy to construct a multidimensional molecular map of tumors with different immune infiltration patterns. These results may provide theoretical basises for identifying more effective predictive biomarkers and developing more effective drug combination strategies or novel immunotherapeutic agents for GBM.

Keywords: glioblastoma, tumor immune microenvironment, proteomics, metabolomics, immunotherapy, target therapy

INTRODUCTION

Glioblastomas (GBMs) are the most common aggressive primary brain tumors and the most lethal central nervous system (CNS) tumors due to their high proliferation rate, high aggressiveness, highly heterogeneous immunosuppressive microenvironment, and resistance to chemotherapy and targeted therapies (1, 2). Recently, immune checkpoint blockade (ICB) therapy has made outstanding achievements in improving the treatment of certain types of tumors. However, the unique immune microenvironment of the brain makes immunotherapy for GBM more challenging than that for other cancers (3). The tumor microenvironment (TME) is a key mediator of tumor malignant progression, plays an important role in clinical survival and response to therapy. In the TME, immune cells infiltrating into tumor tissue form the tumor immune microenvironment (TIME), which helps tumor cells achieve immune escape and promote tumor malignancy and is closely related to the response rate of immunotherapy (4, 5). Therefore, characteristics of the GBM immune microenvironment are expected to serve as biomarkers to guide clinical treatment and to identify GBM patients who can benefit from immunotherapy.

Mounting evidence suggests that cancer patients who receive personalized therapy show better clinical outcomes, and precision medicine promises to revolutionize universal therapy for oncology, but numerous studies still focus on abnormal changes in the genome (6, 7). As the understanding of tumor mechanisms deepens, the focus on tumor treatment is gradually shifting from tumor cells to the interaction between the tumor and the surrounding tissues. The TME is a key mediator of tumor progression and therapeutic outcome. Tumor cells are able to escape surveillance and recognition of the immune system and the killing of T cells without the combined effect of the immune microenvironment (8–11). The present classification schemes used for the TIME and the establishment of immune scoring systems in multiple tumors have greatly improved the current understanding of TIME subtypes (12–15). Strategies to further identify the ideal population and optimize immune combination strategies for specific populations are urgently needed in the era of precision medicine, and such strategies are popular areas of research in the field of immunotherapy at present. However, the recent integrated genomic and transcriptomic analyses and overall assessments of the GBM immune microenvironment have often been unsystematic, and effective immune models are lacking.

In this study, we integrated transcriptome information from 796 GBM samples, used single sample gene-set enrichment analysis (ssGSEA) to estimate the relative abundances of 25 immune cell types based on annotated immune cell gene expression profiles (16–18), and provided a comprehensive outlook on the immune landscape within GBM tumors. We revealed three distinct GTMEI patterns with different clinical outcomes and modulated biological pathways. In addition, we developed a scoring system to quantify the immune infiltration pattern of individual tumors, termed GTMEIscore. To understand the intrinsic tumor characteristics and tumor immune infiltration patterns associated with the GTMEIscore, we comprehensively analyzed the genomic characteristics, molecular subtypes and clinicopathological features as well as proteomic, phosphoproteomic, acetylomic, lipidomic and metabolomic properties associated with the GTMEIscore, revealing lots of novel dysregulated pathways and precise targets in GBM. Moreover, GTMEIscore accurately quantified the immune status of many other cancer types. Clinically, GTMEIscore was found to have significant potential therapeutic value for chemotherapy/radiotherapy, immune checkpoint inhibitor (ICI) therapy and targeted therapy. These findings might provide a theoretical basis for identifying more effective GBM predictive biomarkers and developing more effective, targeted clinical treatment strategies, ultimately guiding GBM clinical treatment and achieving precision medicine.

METHODS

Collection and Preprocessing of Publicly Available Expression Datasets

A total of 796 GBM patients with clinical prognostic information from 6 cohorts, including 153 from the TCGA RNA-seq dataset, 374 from 2 CGGA RNA-seq datasets (237 from one cohort and 137 from the other cohort), 155 from the Gravendeel microarray dataset, 97 from the Wang RNA-seq dataset (19) and 17 patients treated with anti-PD1 therapy from the Zhao/PD1 RNA-seq dataset (20), were included in this study. TCGA RNA-seq data (FPKM format) and clinical information were downloaded from the TCGA database (https://portal.gdc.cancer.gov/repository) and transformed into TPM format. The 2 CGGA RNA-seq datasets and their clinical information were downloaded from the CGGA database (http://www.cgga.org.cn/), the Gravendeel microarray dataset and clinical information were downloaded from the GlioVis database (http://gliovis.bioinfo.cnio.es/), the Wang RNA-seq dataset (FPKM format) and clinical information

were extracted from the supplemental data of the article, and the missing data were obtained with the K-nearest neighbor (KNN) method and transformed into TPM format. For the Zhao/PD1 RNA-seq dataset, we downloaded the raw data from SRA PRJNA482620 and then processed them into TPM format, and clinical information was obtained from the supplemental data of the article. The ComBat method from the 'SVA' R package was used to remove the batch effects among these different datasets (21). The basic information of all enrolled datasets is summarized in **Supplementary Table S1**.

For ICB data, RNA-seq data and clinical information from the IMvigor210 cohort, were obtained from http://research-pub.Gene.com/imvigor210corebiologies based on the Creative Commons Attribution 3.0 license. The metastatic melanoma RNA-seq data from patients treated with nivolumab were obtained from GSE78220 (22) and GSE91061 (23) datasets, and the clinical information were obtained from the supplemental data of the article, respectively.

Estimation of TME Immune Cell Infiltration

We used the ssGSEA algorithm to quantify the relative abundances of 25 infiltrating immune cells in the GBM TME. Gene sets for BMDM TAMs and MG TAMs were obtained from Bowman, R. et al. (18), and those for 23 other infiltrating immune cell types were obtained from Charoentong P. et al. (24, 25). The relative abundance of each infiltrating immune cell in each sample was represented by the enrichment score calculated by the ssGSEA algorithm. The ESTIMATE algorithm was used to assess the immune and stromal scores and tumor purity of each GBM sample.

Statistical Analysis

Spearman and distance correlations were used to calculate the correlation coefficient of 25 immune cell types. Student's t-test was used for two-group comparisons. For comparisons among more than two groups, the Kruskal-Wallis test and one-way ANOVA were used for nonparametric and parametric data. The cutoff values of each dataset (other than the TCGA dataset) were evaluated based on the association between survival time and the GTMEIscore using the "survminer" package, and the TCGA dataset was grouped according to the median GTMEIscore. The Kaplan-Meier method was used to generate survival curves for the subgroups in each dataset, and the log-rank (Mantel-Cox) test was used to determine if they were significantly different. The hazard ratios (HRs) for the univariate analyses were calculated using a univariate Cox proportional hazards regression model. Univariate prognostic analysis results were visualized using the "forestplot" R package. The specificity and sensitivity of the GTMEIscore in predicting response to anti-PD1 therapy were assessed by receiver operating characteristic (ROC) curves, and the area under the curve (AUC) was quantified using the "pROC" R package. $P>0.05$ was considered to indicate nonsignificance (ns), and $P<0.05$ was considered to indicate statistical significance (*$P<0.05$; **$P<0.01$; ***$P<0.001$, ****$P<0.0001$). All data processing with R packages was performed using R Studio (version 3.6.3).

RESULTS

Landscape of Immune Cell Infiltration and Clinicopathological Characteristics of TME Subtypes in GBM

The overview workflow of our research is shown in **Figure 1A**. First, we combined six GBM datasets (a TCGA dataset, two CGGA datasets, The Gravendeel dataset, the Wang dataset and the Zhao/PD1 dataset) with available survival data and clinical information into one meta-cohort, including 796 samples (**Supplementary Table S1**). We then performed ssGSEA and employed the ESTIMATE algorithm to quantify the abundances of immune cells in and the immune and stromal scores of GBM tumor tissues (**Supplementary Table S1**) and depicted a comprehensive landscape of TME immune cell interactions, regulatory connections and their prognostic value for patients with GBM (**Figure 1A** and **Supplementary Table S2**). We identified three independent GTMEI clusters with significant survival differences (**Figure 1B**, $P = 0.004$; **Supplementary Figure S1A** and **Table S1**). We then explored the specific differences in the abundances of immune/stromal score, tumorpurity and 25 TME-infiltrating immune cells and their intrinsic biological differences among GTMEI clusters. We found that GTMEI cluster B, which had the worst prognosis, presented significantly increased immune cell infiltration and immune and stromal scores and enrichment of both immune and stromal activation-related pathways; GTMEI cluster A, which showed survival times between those of GTMEI cluster B and GTMEI cluster C and was characterized by moderate immune cell infiltration, was prominently associated with activation of carcinogenic and stromal pathways; However, GTMEI cluster C, which was associated with a favorable prognosis and was characterized by suppression of immunity, was prominently associated with activation of the cell cycle and DNA repair pathways (**Figures 1C–F**).

Generation of the GTMEI Gene Signature and Functional Annotation

To further investigate the underlying genetic alterations and biological behavior of each GTMEI pattern, we identified 2288 GTMEI pattern phenotype-related DEGs using the "limma" package (**Supplementary Figure S1B** and **Table S3**). Further enrichment analysis of the DEGs *via* the Metascape database showed that they were significantly involved in the cell cycle, DNA repair and immune-related pathways (**Supplementary Figure S1C** and **Table S3**). Furthermore, enrichment analysis *via* PaGenBase showed that these genes were almost exclusively expressed in the blood, spleen, bone marrow, and thymus and some other tissues where peripheral immune cells gather (**Supplementary Figure S1D**). We further used the random forest algorithm for 2288 GTMEI phenotype-related DEGs to dimensionality reduction, and then extracted 135 genes with significant prognostic value ($P<0.001$) as the most representative GTMEI pattern DEGs (we call them as GTMEI phenotype signature), which were significantly enriched in immune and metabolism-related signaling pathways (**Supplementary Figure S1E** and **Supplementary Table S4**).

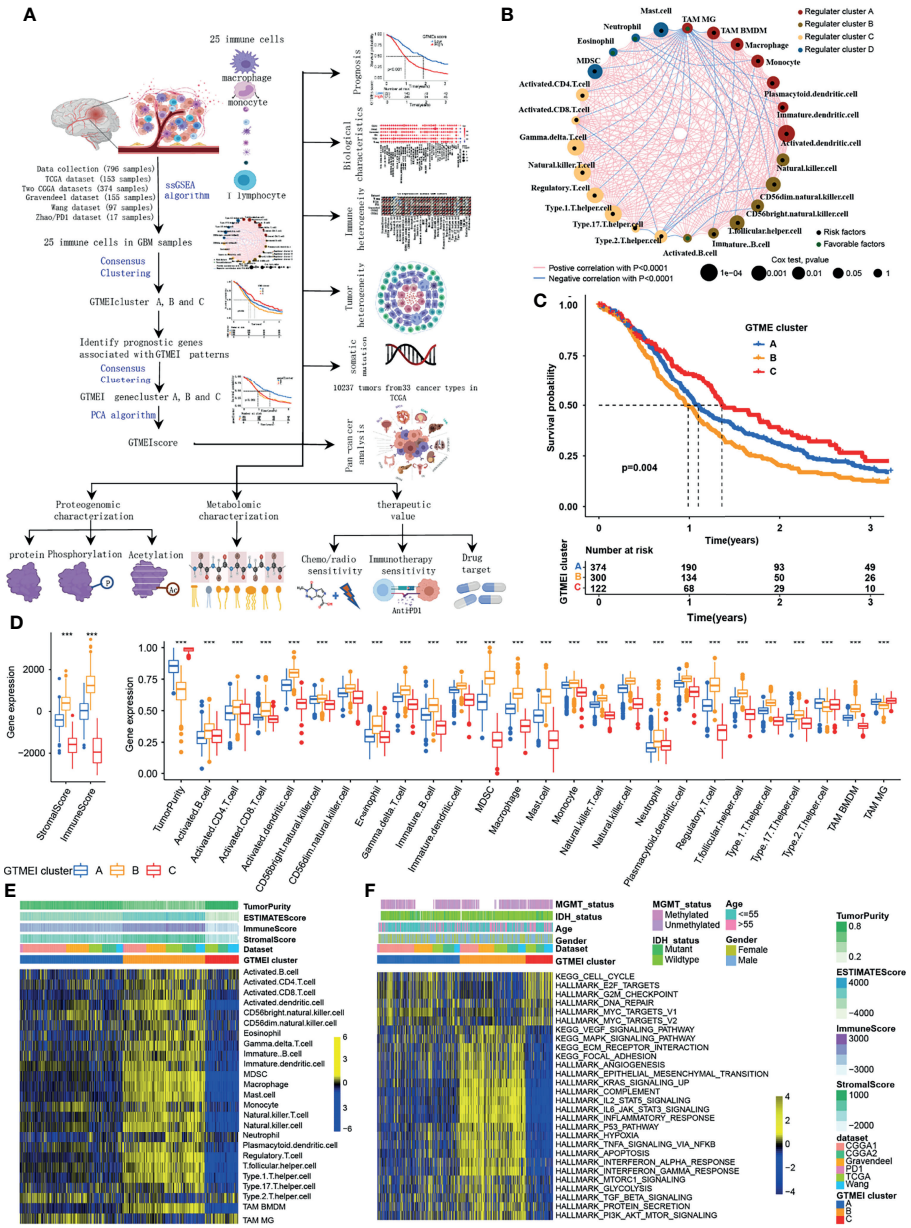

FIGURE 1 | Landscape of immune cell infiltration and clinicopathological characteristics of TME subtypes in GBM. **(A)** Overview of the workflow of our research. **(B)** Cellular interactions of 25 immune cell types in the GBM microenvironment. The size of each immune cell represents its effect on the survival of GBM patients, as calculated using a log10 formula (log-rank test P value). Green indicates that the immune cell is a protective factor for overall survival (OS), while black indicates a risk factor. The lines connecting the immune cells indicate cell-cell interactions, the thickness of which indicates the strength of the correlation estimated by Spearman correlation analysis. Positive correlations are indicated in red, and negative correlations are indicated in blue. **(C)** Kaplan-Meier curves for the OS of 796 GBM patients from 6 GBM cohorts with three GTMEI clusters. The numbers of patients in GTMEI clusters A, B and C were 374, 300 and 122, respectively, and the log-rank test showed P = 0.004. **(D)** Abundances of immune/stromal score, tumorpurity and 25 immune cell types in the three GTMEI patterns. The upper and lower ends of the boxes indicate the interquartile range of the values. The lines in the boxes represent the median values, and black dots show outliers. The significance of differences between the three clusters were determined by the Kruskal-Wallis test. *P < 0.05; **P < 0.01; ***P < 0.001. **(E)** Unsupervised clustering of 25 immune cell types in the cohort of 796 GBM patients. A heatmap was used to visualize immune cell infiltration. Yellow represents high immune cell abundance, black represents moderate immune cell abundance, and blue represents low immune cell abundance. **(F)** GSVA revealed the activation status of biological pathways in different GTMEI patterns. A heatmap was used to visualize these biological pathways. Yellow represents activated pathways, and blue represents inhibited pathways.

Consistent with the clustering groups of GTMEI patterns, unsupervised hierarchical clustering analysis also identified three distinct GTMEI pattern-related genomic phenotypes based on the expression of the GTMEI phenotype signature, and we named these three clusters as GTMEI gene clusters A-C (**Figure 2A** and **Supplementary Figures S1F, G**). Furthermore, we found that

patients in gene cluster A, who showed immune suppression, had a better prognosis, whereas patients in gene cluster B, who showed high immune cell infiltration and activation of immune, stromal and carcinogenic pathways, had the most unfavorable outcomes (**Figures 2B–D**), which was consistent with the expected outcomes of the GTMEI patterns.

Given the heterogeneity and complexity of the GTMEI patterns, we constructed a DEG-based scoring system, termed the GTMEI phenotype score (GTMEIscore), based on the GTMEI phenotype signature to quantify the GTMEI pattern of individual patients using PCA. The patients were grouped into high or low GTMEIscore groups using the cutoff value obtained with the "survminer" package, and patients with a low GTMEIscore exhibited a significant survival benefit (**Figure 2E**, $P < 0.001$). And GTMEI gene clusters B and C were linked to a higher GTMEIscore, whereas GTMEI gene cluster A exhibited a lower GTMEIscore (**Figure 2F**). Further analysis showed that both GTMEI cluster B and gene cluster B had the highest GTMEIscore (**Figure 2G**). We then tested whether the GTMEIscore could serve as an independent prognostic biomarker for GBM patients. As shown in **Figure 2H**, the robust prognostic value of the GTMEIscore was validated in six independent datasets. To further evaluate the biological relevance of the GTMEIscore system, we explored the correlation of the GTMEIscore with immune-related pathways as well as known carcinogenic signatures and found that it was positively correlated with the immune activation process, oncogenic activation and stromal activation signaling but negatively correlated with the cell cycle and DNA repair process (**Figure 2I**). A heatmap of the correlation matrix demonstrated that the GTMEIscore was markedly positively correlated with the immune and stromal scores but negatively correlated with tumor purity. Regarding immune cells, the GTMEIscore was positively correlated with most infiltrating immune cells, as well as with fibroblasts (**Figure 2J**). The expression levels of most MHC, immunostimulatory, and immunoinhibitory molecules were also positively associated with the GTMEIscore (**Figure 2K**). These results implied that the GTMEIscore can reflect immune cell infiltration and can be a reliable prognostic biomarker.

Molecular Subtypes and Tumor Somatic Mutations Associated With and Chemotherapy/Radiotherapy Prognostic Value of the GTMEIscore

To better understand the determinants of GBM tumor evolution and treatment resistance, we then evaluated the differences in GTMEIscore among TCGA molecular subtypes in the TCGA, Gravendeel and Wang datasets, in which clinical information was available. Survival analysis showed that the high GTMEIscore group in the TCGA dataset had shorter survival (**Figure 3A**, $P = 0.013$), which was further validated in the Gravendeel dataset (**Figure 3B**, $P = 0.006$) and Wang dataset (**Figure 3C**, $P = 0.006$). Samples with a higher GTMEIscore were clearly concentrated in the MES subtype, which had a poor prognosis (**Figure 3D**), and samples with the MES subtype were also mainly concentrated in the high GTMEIscore group in the TCGA dataset (**Figure 3E**); the same patterns were observed in the Gravendeel and Wang datasets (**Supplementary Figures 2A–D**).

We then analyzed the differences in the distribution of somatic mutations between the high and low GTMEIscore groups in the TCGA-GBM cohort and Wang cohort using the "maftools" package and found that the PTEN mutation rate (low: 22%, high: 35%) was significantly increased in the high GTMEIscore group compared to the low GTMEIscore group (**Figure 3F** and **Supplementary Figure 2E**). Chen et al. (26) found that PTEN deficiency in GBM increases macrophage infiltration, and the infiltrated macrophages in turn secrete SPP1 to support GBM survival *via* activating YAP1 signaling. Moreover, NF1 mutation, a MES subtype marker that drives recruitment of TAMs (27), was also remarkably more prevalent in the high GTMEIscore group (13%) than in the low GTMEIscore group (5%). In our study, we showed that there was a significant positive correlation between the GTMEIscore and macrophages, especially BMDM TAMs (hereafter also called macrophages), indicating the presence of a large group of infiltrating mononuclear-derived macrophages in the tumor tissues of GBM samples with a high GTMEIscore (**Figure 2J**). We also found a significant positive correlation between the GTMEIscore and the expression of myeloid cell-derived macrophage-restricted chemokines, representative MES genes, genes encoding ECM and immune checkpoint molecules in both the combined and independent datasets (**Figures 3G, H**). In addition, GSEA also showed that YAP1 signaling (CORDENONSI_YAP_CONSERVED_SIGNATURE) and MES signature was significantly upregulated in the high GTMEIscore group compared to the low GTMEIscore group (**Supplementary Figures S2F, G**). We next calculated the enrichment scores of individual GBM samples according to the MES gene signature (27) and found that the high MES expression group had a significantly worse prognosis than the low MES expression group (**Figure 3I**, $P < 0.001$). Further analysis revealed a significant survival advantage for patients with both a low GTMEIscore and low MES score (**Figure 3J**, $P < 0.001$). Next, we explored the relationship between the GTMEIscore and GBM chemotherapy/radiotherapy sensitivity in the CGGA dataset, for which chemotherapy/radiotherapy data were available. We further demonstrated that the prognosis of the group with a high GTMEIscore was significantly worse than that of the low GTMEIscore group (**Figure 3K**, $P = 0.010$). Further analysis showed that patients in the low GTMEIscore group and those treated with chemotherapy/radiotherapy had a significant survival advantage, while patients in the high GTMEIscore group and those not treated with chemotherapy/radiotherapy had the worst prognosis (**Figures 3L, M**).

Correlation Between the GTMEIscore and Proteomic Characteristics

Understanding the proteomic characteristics of the GTMEIscore can help us better understand the GBM TME pattern. By integrating proteomic and metabolomic data from up to 10 platforms, Wang et al. (19) identified new multi-omics

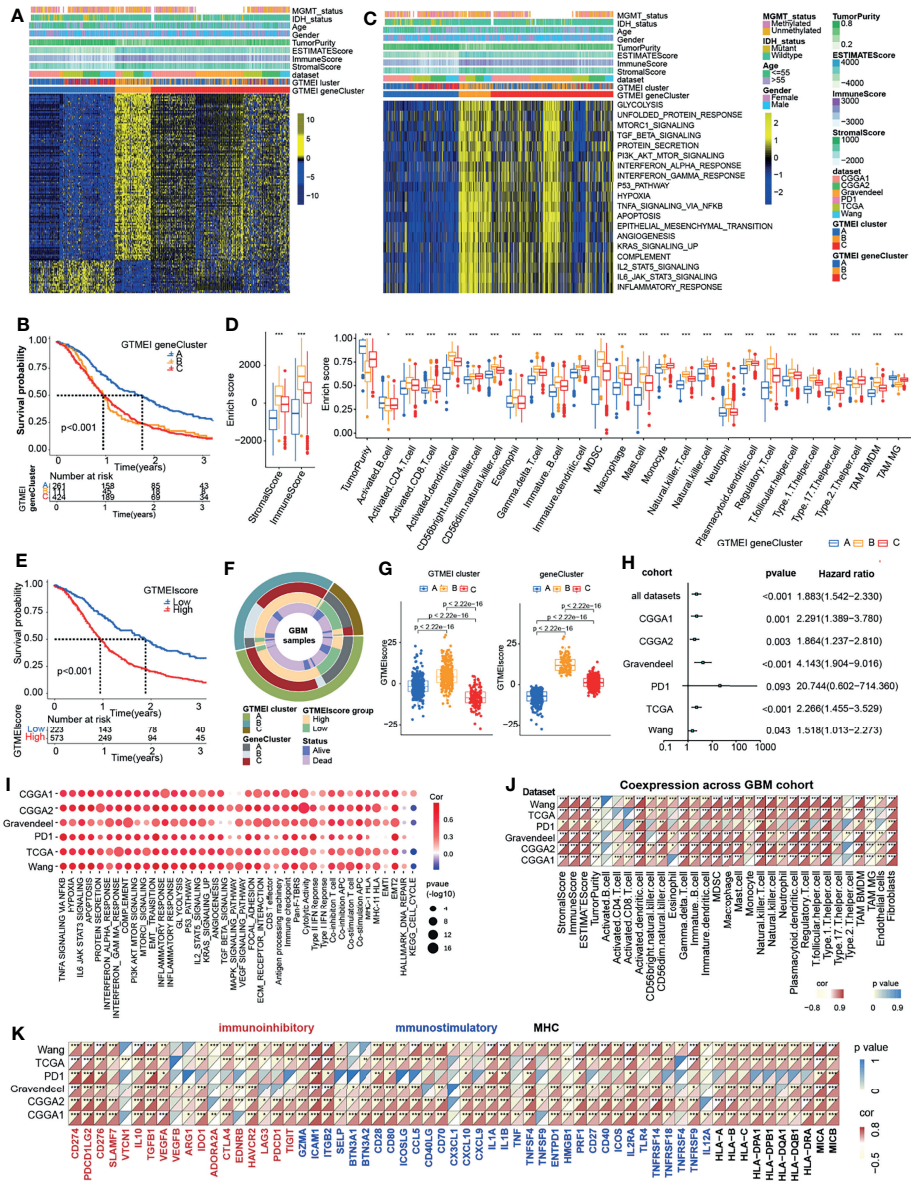

FIGURE 2 | Generation of the GTMEI gene signature and functional annotation. **(A)** Based on the expression data of 796 GBM patients, unsupervised clustering of representative DEGs associated with the GTMEI patterns was performed to classify patients into three groups, called GTMEI gene clusters A-C. A heatmap was used to visualize the gene expression. Yellow represents high expression, black represents moderate expression, and blue represents low expression. **(B)** Kaplan-Meier curves for the OS of 796 GBM patients within the three GTMEI gene clusters. The numbers of patients in GTMEI gene clusters **(A–C)** were 261, 111 and 424, respectively, and the log-rank test showed P < 0.001. C GSVA revealed the activation status of biological pathways in different GTMEI gene clusters. A heatmap was used to visualize these biological pathways. Yellow represents activated pathways, and blue represents inhibited pathways. **(D)** Abundances of immune/stromal score, tumorpurity and 25 immune cell types in the three GTMEI gene clusters. The upper and lower ends of the boxes indicate the interquartile range of values. The lines in the boxes represent the median values, and black dots show outliers. The significance of differences between the three clusters were assessed by the Kruskal-Wallis test. *P < 0.05; **P < 0.01; ***P < 0.001. **(E)** Kaplan-Meier curves for the OS of 796 GBM with a high GTMEIscore (n = 573) and a low GTMEIscore (n = 223), and the log-rank test showed P < 0.001. **(F)** CircGroup plot showing the relationships between GTMEI clusters, GTMEI gene clusters, the GTMEIscore, and survival status. **(G)** Differences in the GTMEIscore among the three (left) GTMEI clusters and (right) GTMEI gene clusters in 796 GBM patients. **(H)** Univariate Cox analysis of the prognostic value of the GTMEIscore for survival in the combined GBM cohort as well as in the independent GBM cohorts. A hazard ratio (HR) > 1.0 indicated that a high GTMEIscore was an adverse prognostic biomarker. **(I)** Spearman correlation analysis of the GTMEIscore and classical signaling pathways in independent GBM cohorts. Blue indicates negative correlations, and red indicates positive correlations. The size of the circle represents the statistical P value, with larger circles representing greater statistical significance. **(J)** Spearman analysis of the correlation of the GTMEIscore with **(J)** the abundances of 25 immune cells and **(K)** immunomodulators (immunoinhibitory, immunostimulatory and MHC molecules). Colors indicate correlation coefficients, with yellow indicating a negative correlation and red indicating a positive correlation. Asterisks indicate statistically significant P values calculated using Spearman correlation analysis. *P < 0.05; **P < 0.01; ***P < 0.001.

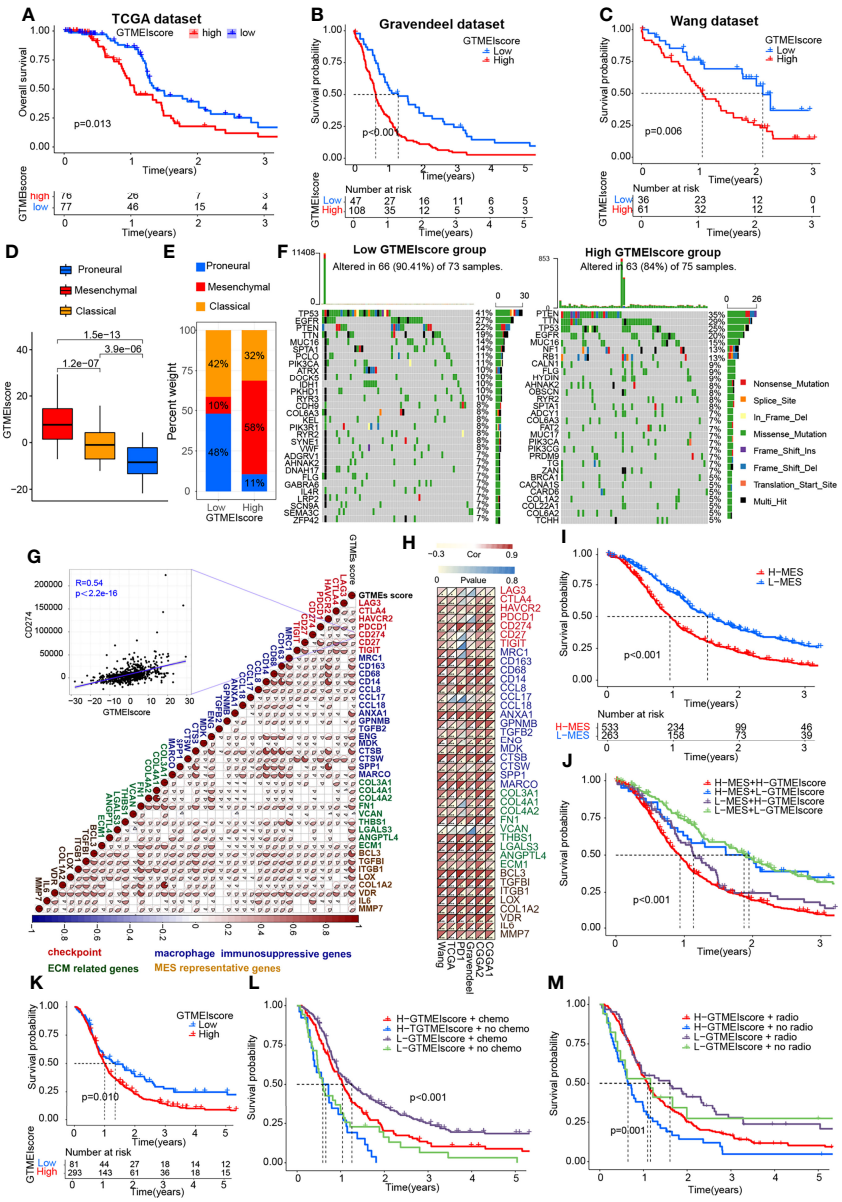

FIGURE 3 | Molecular subtypes and tumor somatic mutations associated with and the chemotherapy/radiotherapy prognostic value of the GTMEIscore. Kaplan-Meier curves showing OS for the high (red) and low (blue) GTMEIscore groups in the **(A)** TCGA dataset, **(B)** Gravendeel dataset, and **(C)** Wang dataset, and the log-rank test showed P = 0.013, P<0.001 and P=0.006, respectively. **(D)** Differences in GTMEIscore among different GBM molecular subtypes. The Kruskal-Wallis test was used to determine the significance of differences between the three GBM molecular subtypes. **(E)** Stacked bar plot of GBM molecular subtypes in the high and low GTMEIscore groups. **(F)** Waterfall plot of the tumor somatic mutation landscape in the low GTMEIscore (left) and high GTMEIscore (right) groups. Each bar represents the mutation information for an individual patient. The top bar plot shows TMB, and the numbers on the right indicate the mutation frequency of each gene. The bar plot on the right shows the proportion of each mutation type. **(G)** Spearman analysis was used to determine the correlation of the GTMEIscore with the expression of immunosuppression-related genes (checkpoint molecule genes, macrophage immunosuppressive genes, ECM-related genes and MES representative genes) in the combined GBM dataset. Colors indicate correlation coefficients, with blue indicating a negative correlation and red indicating a positive correlation. The size of the sector represents the correlation coefficient, and a larger angle means a stronger correlation. **(H)** Spearman analysis of the correlation of the GTMEIscore with the expression of immunosuppression-related genes molecules (checkpoint molecule genes, macrophage immunosuppressive genes, ECM-related genes and MES representative genes) in six independent GBM datasets. **(I)** Kaplan-Meier curves for the OS of 796 GBM patients in the high MES score (n = 533) and low MES score (n = 263) groups, and the log-rank test showed P < 0.001. **(J)** Survival analysis was performed using Kaplan-Meier curves for the subgroup of patients stratified according to GTMEIscore combined with MES score, and the log-rank test showed P < 0.001. H: High; L: Low. **(K)** Kaplan-Meier curves for the OS of the high GTMEIscore (n = 293) and low GTMEIscore (n=81) groups in 2 CGGA GBM datasets, and the log-rank test showed P = 0.010. Survival analysis was performed using Kaplan-Meier curves for subgroups of patients stratified by GTMEIscore **(L)** and treatment with adjuvant chemotherapy (chemo) (the log-rank test showed P < 0.001) by GTMEIscore **(M)** and treatment with adjuvant radiotherapy (radio) (the log-rank test showed P = 0.001).

subtypes. We then analyzed the relationship between the GTMEIscore and clinical features as well as the identified molecular subtypes and found that the high GTMEIscore group tended to have more nmf2-subtype samples (mesenchymal-like, which mainly showed enrichment of immune response and extracellular matrix organization pathways), MES-subtype samples, fewer IDH mutations, and worse pathological features (**Figure 4A**). In addition, we found that the high GTMEIscore group mainly showed enrichment of the im1 and im2 subtypes, which was characterized by high enrichment of immune cells (**Figure 4B**, P=0.001, chi-square test). To explore the underlying mechanisms that led to the different results in the low and high GTMEIscore groups, we annotated the protein data with the hallmark dataset and performed differential analysis; we found that pathways related to the cell cycle were enriched in the low GTMEIscore group, while pathways related to the immune response and ECM remodeling were enriched in the high GTMEIscore group, consistent with the RNA results (**Figure 4C**). Further GSEA also showed consistent results (**Figure 4D**). In addition, Metascape database (28) analysis revealed that genes with a significant positive association with the GTMEIscore (**Supplementary Table S5**, Pearson r > 0.3, P < 0.05) were significantly enriched in pathways related to the regulation of cell biological functions, stromal activation and immunity (**Supplementary Figure S3A** and **Table S6**). Further PaGenBase (29) enrichment analysis showed that these genes were mainly specifically expressed in peripheral immune organs such as the spleen, blood and bone marrow (**Figure 4E**). The coanalysis of proteomic and transcriptomic alterations helped us to further decipher the mechanism by which the TIME in GBM is formed. We analyzed the differences between the high and low GTMEIscore groups based on RNA-seq data and found that compared with the low GTMEIscore group, the high GTMEIscore group had 183 DEGs (FC>2 and P value<0.05) (**Supplementary Table S7**). For the protein data, we found 2758 DEGs (FC>1.2 and P value<0.05) in the high GTMEIscore group compared with the low GTMEIscore group (**Supplementary Table S8**). As shown in **Figure 4F** and **Supplementary Table S9**, *via* joint analysis of the protein and RNA-seq data, we found a moderately strong positive correlation (Pearson r = 0.2615, P value <0.001) between the differences in mRNA and protein expression levels, and all genes were divided into four main groups: 87 genes that were simultaneously upregulated (Hyper-Up), 27 genes that were simultaneously downregulated (Hypo-Down). KEGG functional enrichment analysis showed that the Hyper-Up genes were mainly enriched in some classical oncogenic pathways, metabolic pathways and immune response-related pathways (**Figure 4G**). Further enrichment analysis *via* the GO database showed that the DEGs were notably enriched in the hypoxia, immune cell migration, angiogenesis, matrix remodeling, and macrophage activation pathways (**Figure 4H**). We then performed a univariate Cox prognostic analysis of the proteins and identified 13 proteins with significant prognostic significance (**Supplementary Figure 3B**). We obtained the list of transcription factors (TFs) from the Cistrome database, and subsequently, we examined the coexpression relationships between these prognosis-related proteins and TFs. We used the criteria of Pearson |r|>0.5 and P < 0.05 to obtain the coexpressed genes. Finally, we visualized the coexpression network information using alluvial plots (**Figure 4I**). The results suggested that the expression of the proteins may be regulated by these TFs. We further analyzed the relationship between nmf2-subtype genes and the GTMEIscore. As shown in **Supplementary Figure 3C**, as the GTMEIscore increased, the protein expression levels of these genes also showed a gradual increase. Similar to results from the RNA-seq data, the results of GSEA of the protein data also showed that the MES signature was significantly enriched in the high GTMEIscore group (**Figure 4J**, FDR=0.02). Moreover, the GTMEIscore showed a remarkable positive correlation with the expression of the MES markers CD44 and CHI3L1 (YKL40) at the protein level (**Figure 4K**). Our analysis revealed that, consistent with the mRNA data, the GTMEIscore was significantly and positively correlated with the expression level of immune checkpoint proteins, myeloid cell-derived macrophage-restricted chemokines, and MES-representative and ECM-related proteins (**Figure 4L**). These results facilitate the identification of important proteins associated with the formation of GBM TME patterns.

Correlation Between the GTMEIscore and Protein Phosphorylation and Acetylation

The proteomic phosphorylation differential analysis data showed that 3811 phosphorylation sites of 1438 proteins were dramatically upregulated and 4873 phosphorylation sites of 1529 proteins were significantly downregulated in the high GTMEIscore group (**Supplementary Table S10**, FC > 1.2, P value < 0.05). KEGG enrichment analysis showed that proteins with upregulated phosphorylation were significantly enriched in oncogenic signaling pathways, stromal activation pathways and immune-related signaling pathways (**Figure 5A**). Downregulated proteins were mainly involved in the neuronal system, mitotic cell cycle processes, and so on (**Supplementary Figure S4A**). Further analysis of the combined protein quantitative data showed a significant positive correlation between phosphorylation level and protein expression levels (**Figure 5B** and **Supplementary Table S11**, Pearson r = 0.6527). Analysis of mutation distribution in the TCGA and Wang datasets showed that the PTEN and NF1 mutation rates were greatly increased in both datasets, while the BRAF mutation rate was significantly increased in the Wang dataset (**Figure 3E** and **Supplementary Figure 2C**). Next, we explored specific signaling pathways based on somatic mutations and their downstream alterations (**Figure 5C**). As shown in the heatmap, with increasing GTMEIscore, the expression levels of the tumor suppressor proteins PTEN and NF1 showed a decreasing trend, and we also observed that the phosphorylation levels of the downstream signaling pathway proteins gradually increased (**Figure 5D**). In addition, the tumor mutation distribution analysis showed that the EGFR mutation rate was slightly downregulated in the high GTMEIscore group, and the pathway enrichment analysis showed that proteins with upregulated levels

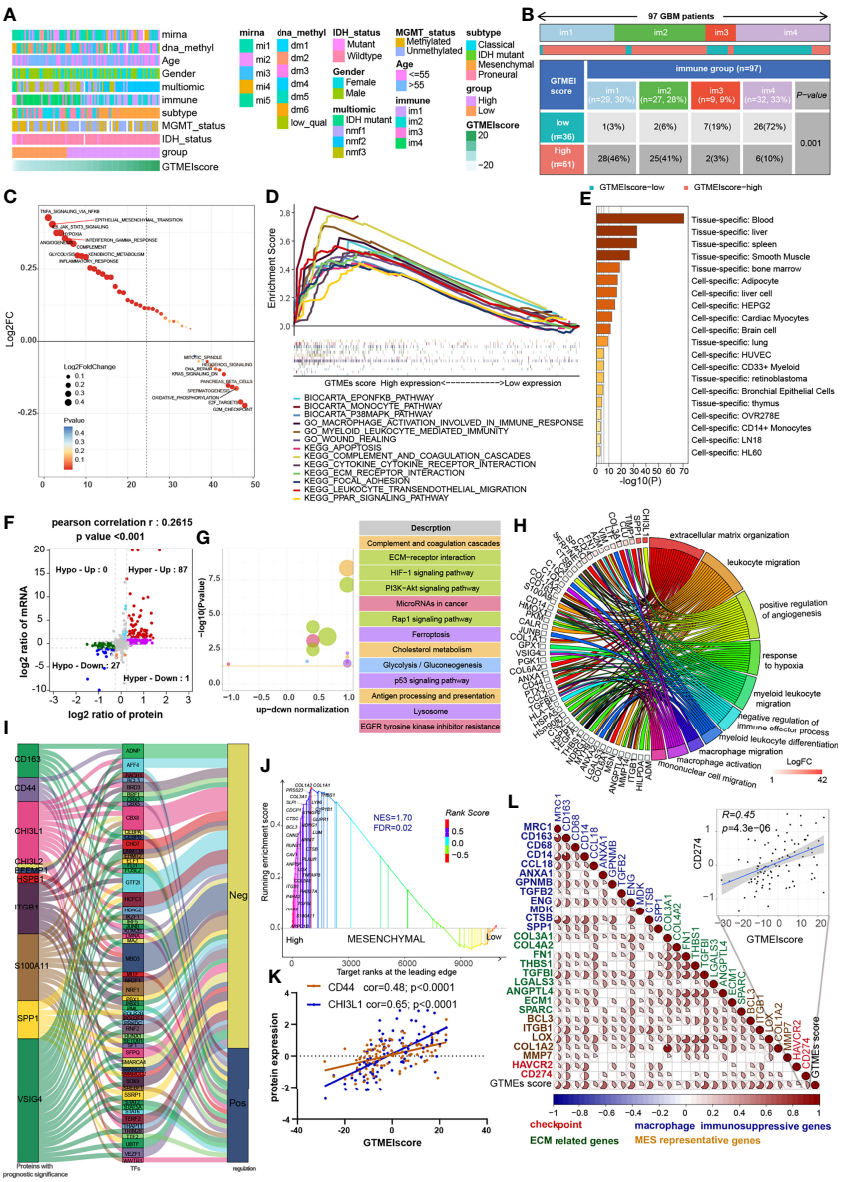

FIGURE 4 | Correlation between the GTMEIscore and proteomic characteristics. **(A)** Heatmap describing the relationship between the GTMEIscore and various clinical features in the Wang cohort. miRNA, DNA methylation, multiomics, immune cell molecular, TCGA molecular subtype, age, sex, MGMT and IDH mutation status annotations are provided as examples. **(B)** Heatmap and table of the distribution of GBM immune subtypes (im1, im2, im3 and im4) between the high and low GTMEIscore groups, chi-square test showed P = 0.001. **(C)** GSVA showing differences in hallmark biological pathways between the high and low GTMEIscore groups. Scatter plots were used to visualize these differences in pathways. The size of the circle indicates the size of the fold change (FC), and the color indicates the statistical significance of the difference. The color red indicates statistical significance, and blue indicates statistical insignificance. **(D)** GSEA showing the gene sets enriched in high GTMEIscore subgroup (P < 0.05, FDR < 0.25). **(E)** Summary enriched genes positively correlated with the GTMEIscore at the protein level in the PaGenBase database. **(F)** Dot plot of log2FC (mRNA expression) versus log2FC (protein expression) values showing a positive correlation between the overall mRNA expression and protein expression levels (Pearson's r = 0.2615; P < 0.001) and the distribution of genes with significant changes in both the mRNA (|FC| > 2, P < 0.05) and corresponding protein expression (|FC| > 1.2, P < 0.05) levels in the high GTMEIscore group compared with the low GTMEIscore group. Colored circles indicate significant changes in at least the mRNA or the protein expression of the gene. **(G)** KEGG enrichment analysis of 87 genes (Hyper-Up) and 27 genes (Hypo-Down) that were significantly differentially expressed at both the mRNA and protein levels. **(H)** GO BP enrichment analysis of 87 genes that were significantly upregulated at both the mRNA and protein levels. **(I)** Alluvial plot showing regulatory network relationships between proteins with prognostic significance and transcription factors (TFs). **(J)** GSEA of mesenchymal signatures showing that GBM samples from the high GTMEIscore group were enriched in the MES-subtype group compared to GBM samples from the low GTMEIscore group. NES, normalized enrichment score; FDR, false discovery rate. **(K)** Correlation scatter plot showing that the GTMEIscore was positively correlated with the expression of CD44 and CHI3L1, markers of the MES subtype. **(L)** Spearman analysis of the correlation between the GTMEIscore and the protein expression of immunosuppression-related genes (checkpoint molecule genes, macrophage immunosuppressive genes, ECM-related genes and MES representative genes). Colors indicate correlation coefficients, with blue indicating a negative correlation and red indicating a positive correlation. The size of the sector represents the correlation coefficient, and a larger angle means a stronger correlation.

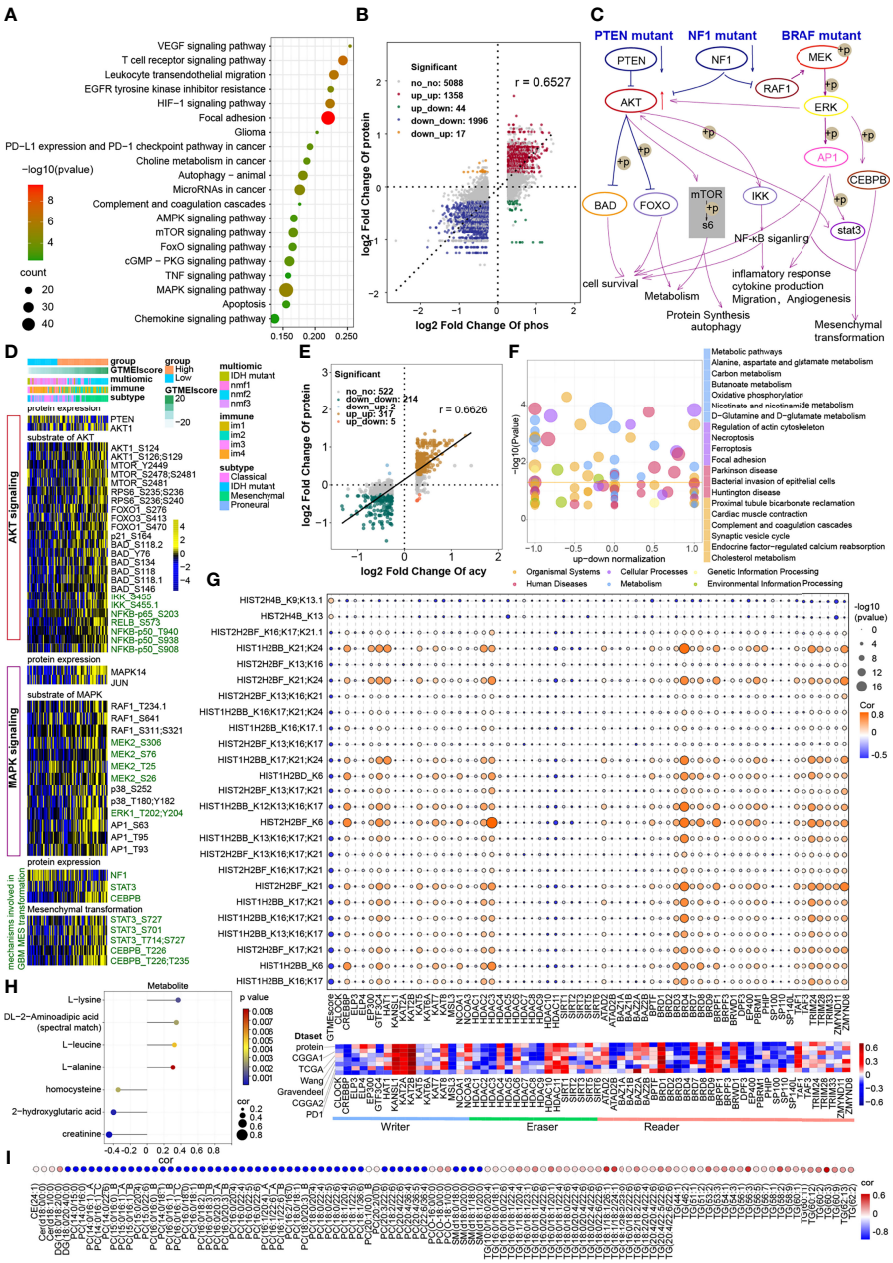

FIGURE 5 | Correlation between the GTMEIscore and protein phosphorylation and acetylation. **(A)** KEGG enrichment analysis of proteins with upregulated phosphorylation levels. **(B)** Dot plot of log2 fold change (FC) (protein phosphorylation level) versus log2FC (protein expression) values showing a positive correlation between the overall protein phosphorylation level and protein expression level (Pearson's r = 0.6527) and the distribution of genes with significant changes in both the phosphorylation level (|FC| > 1.2, P < 0.05) and corresponding protein expression (|FC| > 1.2, P < 0.05) in the high GTMEIscore group compared with the low GTMEIscore group. **(C)** Schematic diagram showing specific proteins and their downstream alterations based on somatic mutations. **(D)** Heatmap showing somatic mutation-based alterations in specific proteins and their downstream protein phosphorylation sites. **(E)** Dot plot of log2FC (protein acetylation level) versus log2FC (protein expression) values showing a positive correlation between the overall protein phosphorylation level and protein expression level (Pearson's r = 0.6527) and the distribution of genes with significant changes in both the acetylation level (|FC| > 1.2, P < 0.05) and corresponding protein expression (|FC| > 1.2, P < 0.05) in the high GTMEIscore group compared with the low GTMEIscore group. **(F)** KEGG enrichment analysis of proteins with significantly altered acetylation levels (|FC| > 1.2, P < 0.05). **(G)** (Upper) Correlation of the GTMEIscore with histone acetylation sites and histone acetyltransferase, deacetylase, and reader levels. The size of the circle represents the significance, and the color represents the correlation coefficient. (Lower) Correlation of the GTMEIscore with histone acetyltransferase, deacetylase, and reader levels; the color represents the correlation coefficient. **(H)** Lollipop chart showing metabolites with a significant correlation with the GTMEIscore (Pearson r > 0.3, P value <0.05). I Metabolites with a significant correlation with the GTMEIscore (Pearson |r| > 0.3, P value < 0.05). **(I)** Bubble plots showing significant correlations of the GTMEIscore with lipids (Pearson |r| > 0.3, P value < 0.05).

of phosphorylation were significantly enriched in the EGFR tyrosine kinase inhibitor resistance pathway (**Figure 5A**). The gene and protein expression levels of EGFR were also significantly downregulated in the high GTMEIscore group (**Supplementary Table S9**). We next analyzed the relationship between EGFR protein and phosphorylation levels and the GTMEIscore, as shown in **Supplementary Figure S4B**. The phosphorylation levels of EGFR and its downstream proteins were downregulated in the high GTMEIscore group, suggesting that EGFR activation may inhibit the infiltration of immune cells into tumor tissue and that GBM patients with a high GTMEIscore are insensitive to EGFR inhibitors. These results contribute to our understanding of the mechanisms underlying dysregulated protein expression and phosphorylation, pathway dysregulation.

The proteome differential acetylation analysis data showed that compared to the low GTMEIscore group, the high GTMEIscore group showed 459 significantly upregulated acetylation sites in 207 proteins and 605 significantly downregulated acetylation sites in 288 proteins (**Supplementary Table S12**). KEGG and GO biological process (BP) functional annotation analysis revealed that the proteins with different acetylation levels were mainly enriched in metabolism-related signaling pathways, the HIF-1 signaling pathway and immune-related signaling pathways (**Supplementary Figure S4C**). Further correlation analysis with proteomics data showed that the acetylation levels were positively correlated with the protein expression levels (Pearson r = 0.6626), with the levels of acetylation at 317 acetylation sites in 107 proteins being simultaneously upregulated with protein expression levels, the levels of acetylation at 214 acetylation sites in 106 proteins being simultaneously downregulated with protein expression levels (**Figure 5E**, **Supplementary Table S13**). Further KEGG enrichment analysis of these two fractions of altered proteins revealed that they were mainly enriched in metabolism-related and apoptosis-related signaling pathways (**Figure 5F**). Researchers detected more than 30 modified acetylation sites in histones (H1, H2A, H2B, H3.3, and H4) in GBM, and further differential analysis showed that two acetylation sites were significantly upregulated in H4 histones and 25 acetylation sites were significantly downregulated in H2B histones (**Supplementary Table S14**). Further correlation analysis showed that the GTMEIscore was significantly positively correlated with the acetylation level of H4 group proteins and negatively correlated with the acetylation level of H2 group proteins. Notably, some of the H2B acetylation modification levels were positively correlated with the protein expression of CREBBP/EP300 acetyltransferases and some proteins of the BDR family (BRD3/4) and negatively correlated with the GTMEIscore at both the RNA and protein levels; on the other hand, these modification levels were negatively correlated with the expression of the deacetylases HDAC10/11, the expression of which was positively correlated with the GTMEIscore at both the RNA and protein levels (**Figure 5G**, **Supplementary Table S15**). Further survival analysis based on the protein expression levels of these proteins revealed that CREBBP and BRD3 were protective prognostic genes in GBM, while the deacetylase HDAC10 was a prognostic risk factor (**Supplementary 4D**). These data suggest that increased levels of H2B acetylation modification may depend on the activities of CREBBP, BRD3 and HDAC10, which regulate some protective genes to inhibit the infiltration of immune cells.

Correlation Between the GTMEIscore and Metabolomic and Lipidomic Characteristics

The results of the above analysis revealed that some of the genes and proteins associated with the GTMEIscore might be involved in metabolic pathways (**Figures 4G**, **5A, F**). We thus performed a correlation analysis between the GTMEIscore and tumor metabolite abundance and identified four metabolites that were positively correlated and three metabolites that were negatively correlated with the GTMEIscore (**Figure 5H** and **Supplementary Table S16**, Pearson $|r| > 0.3$, P value <0.05). Further survival analysis showed that leucine and DL-2-aminoadipic acid (spectral match) were adverse prognostic factors for GBM patients (**Supplementary Figure 5A**), suggesting that they may play an essential role in the TIME.

Next, we analyzed the correlation of the abundances of 582 lipids with the GTMEI score in 75 GBM tumor tissues and found a large number of lipids that were correlated with the GTMEI score (**Supplementary Table S17**, Pearson $|r| > 0.3$, P value <0.05). As shown in **Figure 5I**, the triacylglycerol (TG) content showed a significant positive correlation with the GTMEIscore and a significant negative correlation with the content of most phosphatidylcholines (PCs) and sphingomyelin (SM).

To further explore the molecules mediating these metabolic changes, we performed a correlation analysis of the GTMEIscore with 29 metabolic regulatory genes previously reported to be associated with GBM prognosis (30) and further performed a survival analysis of these genes based on their protein expression levels. As shown in **Supplementary Figures S5B, C**, ALDH3A1, PSME1 and RUFY1 were adverse prognostic factors that had a significant positive correlation with the GTMEIscore. In contrast, CHD9, PON1 and PON2 were protective prognostic factors. Our results provide valuable insights into the lipid metabolic characteristics of different immune microenvironment patterns in GBM, and reveal possible metabolite targets, regulating the immune microenvironment.

Correlation of the GTMEIscore With the Efficacy of Immunotherapy and Drug Sensitivity in GBM

We further evaluated its ability to predict patient response to ICB therapy. Improved response to anti-PD-1 therapy has been found to be associated with higher TMB in tumors across multiple cancer types, including GBM (31). Survival analysis showed that patients with high TMB in the TCGA dataset had significantly better survival than those with low TMB (**Figure 6A**), and further combined GTMEIscore analysis showed that patients with a high GTMEIscore and low TMB had a significant survival disadvantage (**Figure 6B**). Touat et al. (32) recently found that mismatch repair (MMR)-deficient gliomas were characterized by poor patient survival and a low rate of response to anti-PD-1 therapy. Our data also showed that

patients with low microsatellite instability (MSI) had significantly better survival than those with high MSI (**Figure 6C**), and further combined GTMEIscore analysis showed a significant survival advantage for patients with a low GTMEIscore and low MSI (**Figure 6D**), suggesting that GTMEIscore combined with markers such as TMB and MSI significantly improved the sensitivity and accuracy, and may be a more effective way to screen the immune beneficiary GBM population. In addition, the GTMEIscore showed a significant positive correlation with immunochekpoint expression in GBM patients at both the RNA and protein levels (**Figures 3F, G**, **Figure 4L**). And survival analysis found that patients with a low GTMEIscore showed a significant clinical advantage and significantly prolonged survival (**Figure 6E**, P=0.007). Similarly, survival, as measured from the start of treatment with anti-PD1 therapy, was slightly increased in GBM patients with a low GTMEIscore (**Figure 6F**, P=0.250). Patients with a low GTMEIscore had significantly increased efficacy of ICI treatment compared to those with a high GTMEIscore (**Figure 6G**, response rate to anti-PD1 therapy: 70% vs. 43%). ROC curve analysis demonstrated good predictive capability of the GTMEIscore in predicting the effectiveness of immunotherapy in GBM patients (**Figure 6H**, AUC=0.740).

To quantify the risk assessment of individual GBM patients, we proposed a comprehensive prognostic nom model using a combination of GTMEIscore combined with other clinicopathological characteristics, an example of which is shown by the arrow (**Figure 6I**). Calibration curves and time-dependent ROC analysis of 0.5, 1 and 1.5-year OS prediction demonstrated the nomogram exhibited much more powerful capacity of survival prediction (**Figures 6J, K**).

Finally, we used the CMap database to predict potential drugs for patients with high GTMEIscore. CMap mode of action (MoA) analysis revealed a total of 38 mechanisms of action for the 54 compounds with significant enrichment (**Figure 6L** and **Supplementary Table S18**). These results provide potential drugs that can be used for patients with a high GTMEIscore.

Overview of the GTMEIscore Across Human 32 Cancers Types

We further assessed the differences in the GTMEIscore across 33 tumors, and as shown in **Figure 7A**, we found that the GTMEIscore was highest in LAML, followed by KIRP, and lowest in LIHC. Pancancer survival analysis showed that overall survival was significantly shorter in the high GTMEIscore group than in the low group (**Figure 7B**). Differences in the GTMEIscore between different immune subtypes were further investigated. Expression was significantly different between the C1 (wound healing), C2 (IFN-γ dominant, inflammatory), C3 (lymphocyte depleted), C4 (lymphocyte depletion), C5 (immunologically quiet) and C6 (TGF-β dominant) subtypes, which are characterized by differences in macrophage or lymphocyte signatures, and was higher in C2 and C6 subtypes, with poorer prognosis (**Figure 7C** and **Supplementary Figure S6A**). Additionally, Chen et al. (33) proposed three immunophenotypes, namely immune-inflamed, immune-excluded and immune-desert, which are more comparable to the subtypes we obtained (**Supplementary Figures S6B, C**). As shown in **Figure 7D**, the proportion of immune-excluded samples was almost equally distributed between the two groups, but there were more immune-inflamed samples and fewer immune-desert samples in the GTMEI-high group than in the GTMEI -low group (p = 0.001, chi-square test). Further Spearman correlation analysis showed that GTMEIscore was positively correlated with infiltrating immune cells, immune/stromal score and immunomodulatory molecules, while negatively correlated with tumor purity in most tumor types (**Figure 7E**). As shown in **Figure 7F**, we also found that GTMEIscore was positively correlated with in most tumors, indicating that the GTMEIscore is associated with enrichment scores of typical cancer hallmarks in a wide range of cancer types. The cancer-specific survival analysis also revealed a significant association between the GTMEIscore and overall survival in multiple cancer types: the GTMEIscore was a risk factor in 17 cancer types, and a protective factor in 7 cancer types (**Figure 7G** and **Supplementary Figure S7**). These results demonstrated the characteristics of the GTMEIscore in a broad range of cancer types and highlight its potential value as a predictor of immune cell infiltration and prognosis.

We further investigated the predictive power of GTMEIscore for other cancer types of ICB therapy. Thus, we used urothelial cancer cohorts of patients (IMvigor210) and two cohorts of melanoma patients who received anti-PD1 therapy (22, 23) to perform a complementary evaluation of the ability of GTMEIscore to predict the immunotherapy response. GTMEIscore was a risky factor in Urothelial Carcinoma, while was a protective factor in melanoma (**Figure 7G**). And survival analysis found that urothelial cancer patients with a low GTMEIscore showed a significant clinical advantage and significantly prolonged survival (**Figure 8A**, P=0.015), and had significantly increased efficacy of ICI treatment compared to those with a high GTMEIscore (**Figure 8B**, response rate to anti-PD1 therapy: 27% vs. 14%). However, survival analysis found that melanoma patients with a high GTMEIscore showed a significant clinical advantage and significantly prolonged survival (**Figure 8C, E, G**, P=0.015, 0.006 and 0.012, respectively), and had significantly increased efficacy of ICI treatment compared to those with a low GTMEIscore (**Figure 8D, F, H**, response rate to anti-PD1 therapy: 64% vs. 0%, 32% vs. 17% and 37% vs. 12%, respectively).

To further understand the impact of the GTMEIscore on drug response in 32 cancer types, we obtained the differential genes for each cancer type in GTMEIscore high group by grouping according to the optimal survival cut value (**Supplementary Table S19**), and further predicted the relevant compounds by inputting the most significantly up- and down-regulated 1000 genes to the cmap database. We show only the compounds found to be significantly associated with GTMEIscore in at least ten cancer types (**Figure 8I** and **Supplementary Table S20A**). Tumors with a better prognosis are sensitive to drugs with a high enrichscore and conversely tumors with a poor prognosis are sensitive to drugs with a low enrichscore. Further, we

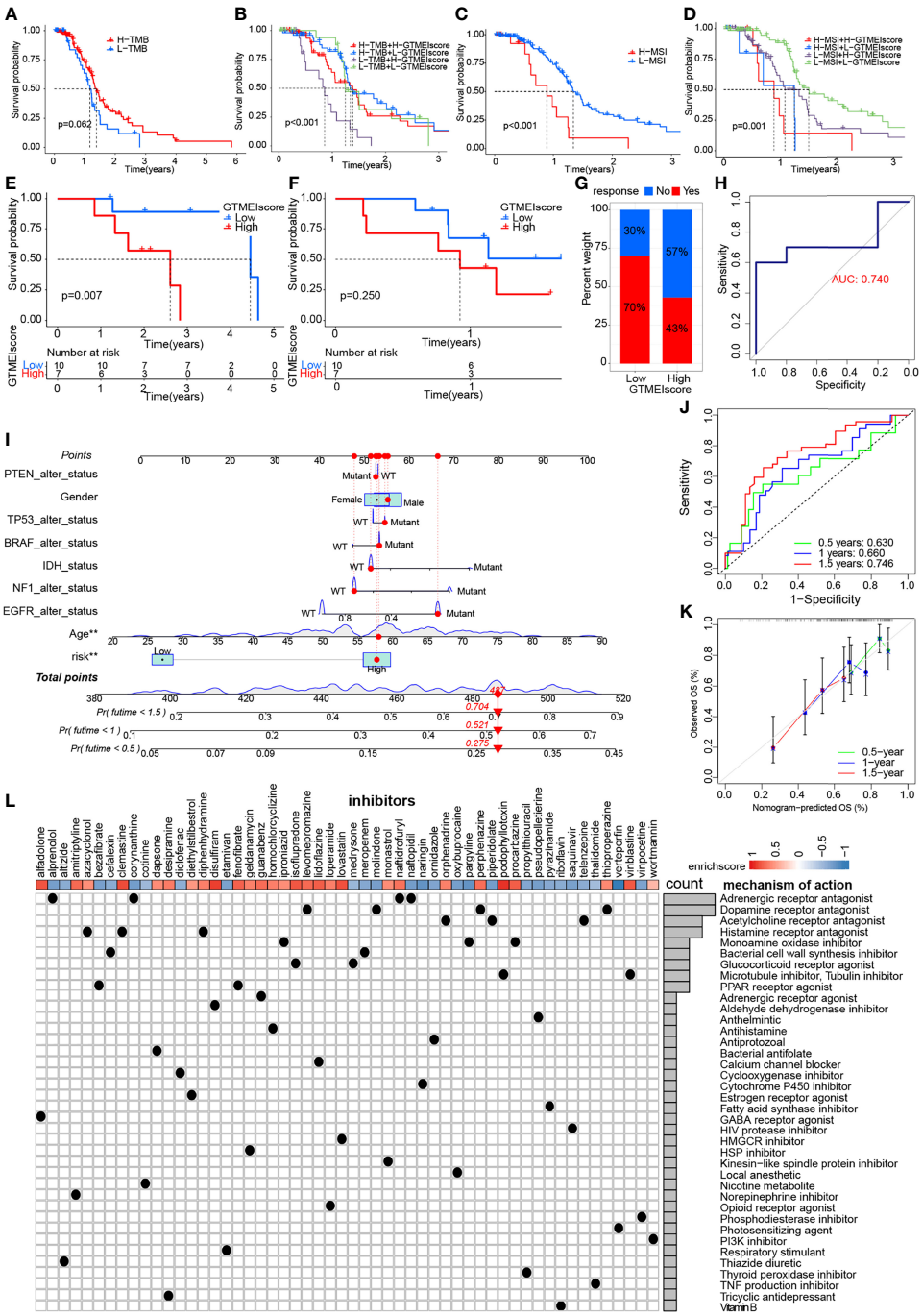

FIGURE 6 | Correlation of the GTMEIscore with the efficacy of immunotherapy and drug sensitivity in GBM. Kaplan-Meier curves for the OS of TCGA GBM patients with **(A)** TMB (log-rank test P = 0.062); **(B)** stratified by GTMEIscore and TMB (log-rank test P < 0.001); **(C)** MSI (log-rank test P < 0.001); and **(D)** GTMEIscore and MSI (log-rank test P = 0.001). Kaplan-Meier curves for **(E)** the OS of GBM patients (log-rank test P = 0.007) and **(F)** survival duration after anti-PD1 treatment (log-rank test P = 0.250 in the PD1 dataset). **(G)** Proportions of patients who responded to anti-PD1 immunotherapy in the low and high GTMEIscore groups. **(H)** ROC curve quantifying the predictive value of the GTMEIscore in GBM patients treated with anti-PD1 therapy (AUC, 0.740). **(I)** A personalized scoring nomogram was constructed to predict the OS probability for 9 parameters at 0.5, 1, and 1.5 years, an example of which is shown by the arrows. **(J)** Time-dependent ROC analysis demonstrated that the nomogram exhibited a powerful capacity for survival prediction. **(K)** Calibration curves showing that the predicted 0.5-year (green dashed line), 1-year (blue dashed line) and 1.5-year (red dashed line) OS values were close to the ideal values (45-degree line). (**L**) CMap mode of action (MoA) analysis revealed a total of 38 mechanisms of action for the 54 compounds significantly related to GTMEIscore, sorted by descending number.

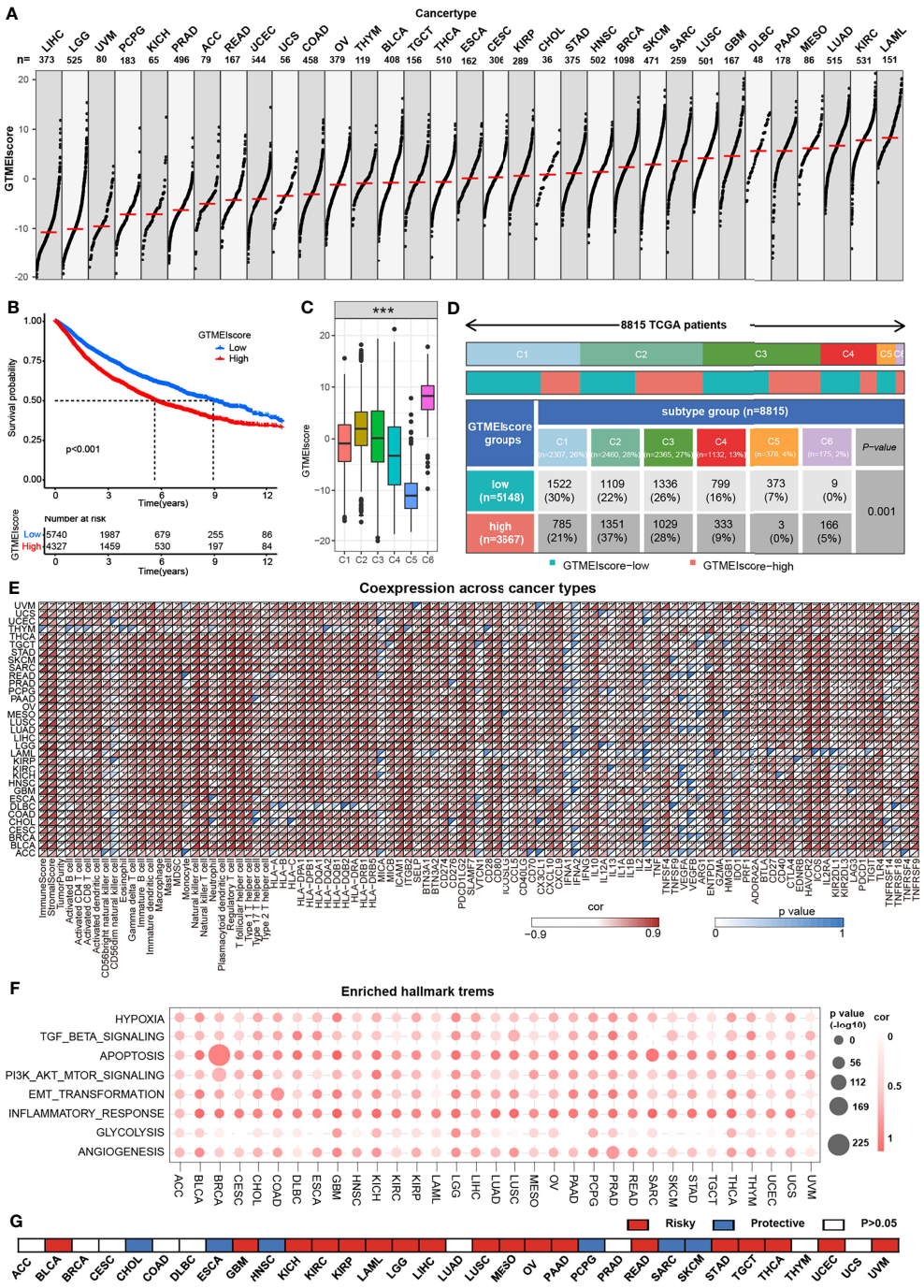

FIGURE 7 | Overview of the GTMEIscore across 32 human cancer types. **(A)** The GTMEIscore for all samples grouped by cancer type, ranked from lowest to highest. **(B)** Kaplan-Meier curves for the OS of 10067 patients with a high GTMEIscore (n = 4327) and a low GTMEIscore (n = 5740), and the log-rank test showed P < 0.001. **(C)** Differences in the GTMEIscore between six different immune molecular subtypes. The Kruskal-Wallis test was used to determine the significance of differences between the six immune molecular subtypes. **(D)** Heatmap and table of the distribution of three immune molecular subtypes between the high and low GTMEIscore groups, chi-square test showed P=0.001. **(E)** Spearman analysis of the correlation of the GTMEIscore with immunomodulators, 28 immune cell types, immune and stromal scores, and tumor purity. Colors indicate correlation coefficients, with yellow indicating a negative correlation and red indicating a positive correlation. Asterisks indicate statistically significant P values calculated using Spearman correlation analysis. *P < 0.05; **P < 0.01; ***P < 0.001. **(F)** Bubble plots showing the correlation between the GTMEIscore and classical cancer pathways. The color of the circle represented the correlation coefficient, and the size represent the p value. **(G)** Summary of the correlation between expression of GTMEIscore and 32 cancer type patients survival. Red represents a higher expression of GTMEIscore associated with worse survival, and blue represents an association with better survival. Only p values < 0.05 are shown.

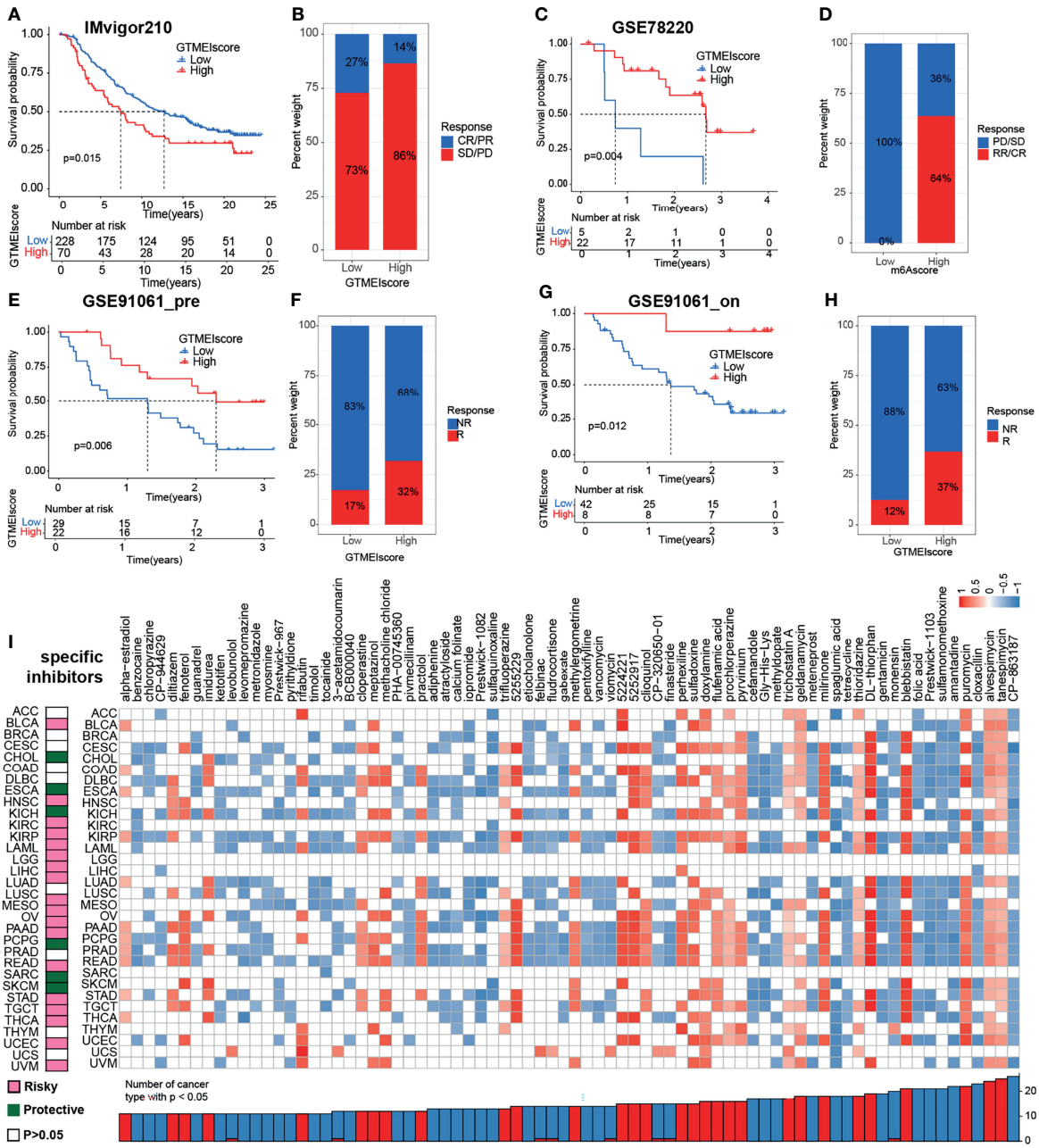

FIGURE 8 | Correlation of the GTMEIscore with the efficacy of immunotherapy and drug sensitivity in other 32 cancer types. **(A)** The Kaplan–Meier survival curves showed that GTMEIscore was a prognostic risk factor in the urothelial cancer patients in IMvigor210 dataset that received anti-PD1 therapy(log-rank test P = 0.015). **(B)** Proportions of urothelial cancer patients who responded to anti-PD1 immunotherapy in the low and high GTMEIscore groups in IMvigor210 dataset. **(C)** The Kaplan–Meier survival curves showed that GTMEIscore was a prognostic protective factor in the melanoma patients in GSE78220 dataset that received anti-PD1 therapy(log-rank test P = 0.004). **(D)** Proportions of melanoma patients who responded to anti-PD1 immunotherapy in the low and high GTMEIscore groups in GSE78220 dataset. **(E)** The Kaplan–Meier survival curves showed that GTMEIscore was a prognostic protective factor in the melanoma patients in GSE91061 dataset that had not received anti-PD1 therapy (log-rank test P = 0.006). **(F)** Proportions of melanoma patients who responded to anti-PD1 immunotherapy in the low and high GTMEIscore groups in GSE91061 dataset that had not received anti-PD1 therap. **(G)** The Kaplan–Meier survival curves showed that GTMEIscore was a prognostic protective factor in the melanoma patients in GSE91061 dataset that received anti-PD1 therapy (log-rank test P = 0.012). **(H)** Proportions of melanoma patients who responded to anti-PD1 immunotherapy in the low and high GTMEIscore groups in GSE91061 dataset received anti-PD1 therapy. **(I)** The left heatmap showing the summary of the correlation between expression of GTMEIscore and other 32 cancer type patients survival. Pink represents a higher expression of GTMEIscore associated with worse survival, and green represents an association with better survival. Only p values < 0.05 are shown. The right heatmap showing the enrichment fraction of each compound in CMap for other 32 cancer types (positive in blue, negative in red). Compounds are sorted from right to left by decreasing number of significantly enriched cancer types.

demonstrated the targeting mechanism of these drugs using MOA analysis of cmap (**Supplementary Figure S8A** and **Table S20B**). These results provide potential drugs that can be used for patients with a high GTMEIscore, offering potential therapeutic prospects for improving the prognosis of cancer patients.

DISCUSSION

Recent advances in tumor immunotherapy have created great enthusiasm and anticipation for the effective treatment of GBM (20, 34). The TME, especially the TIME, plays an important role in clinical survival and response to therapy as a key mediator of tumor progression and treatment outcome (9–11, 35). Analyzing the TIME of GBM patients may provide new insights into the development of immunotherapeutic strategies for GBM. In this study, we integrated transcriptome information from 796 GBM samples, used single sample gene-set enrichment analysis (ssGSEA) to estimate the relative abundances of 25 immune cell types, and provided a comprehensive outlook on the immune landscape within GBM tumors. We revealed three distinct GTMEI patterns with different clinical outcomes and modulated biological pathways. Moreover, we developed a scoring system to quantify the immune infiltration pattern of individual GBM sample, termed GTMEIscore. To understand the intrinsic tumor characteristics and tumor immune infiltration patterns associated with the GTMEIscore, we comprehensively analyzed the genomic characteristics, molecular subtypes and clinicopathological features as well as proteomic, phosphoproteomic, acetylomic, lipidomic and metabolomic properties associated with the GTMEIscore, revealing lots of novel dysregulated pathways and precise targets in GBM. Moreover, GTMEIscore accurately quantified the immune status of many other cancer types. Clinically, GTMEIscore was found to have significant potential therapeutic value for chemotherapy/radiotherapy, immune checkpoint inhibitor (ICI) therapy and targeted therapy. Our systematic identification and characterization of molecular subtypes of the immune microenvironment of GBM revealed many novel dysregulated signaling pathways and precise targets in GBM and provides a theoretical basis for identifying more effective predictive biomarkers and developing more effective and targeted clinical treatment strategies for GBM.

This paper highlights the important role of TME, particularly macrophages, in shaping the MES-like cellular state. Several immune microenvironment studies for other tumors display better prognosis for immune inflamed subtype which more effective immune infiltration in tumor stroma (12, 17). However, the result of immune infiltration in GBM, the GTMEI cluster C which had better prognosis did not show the increased immune infiltration and the activated immune state, which may be due to the special intracranial microenvironment. Recently, using scRNA-seq, malignant cells in GBM were classified into four potentially plastic cell states: neural progenitor cell-like (NPC-like), oligodendrocyte progenitor cell-like (OPC-like), astrocyte-like (AC-like), and mesenchymal-like (MES-like) (35). Hara et al. (36) further showed striking similarities between the MES-like state and the TCGA-MES subtype; both were rich in macrophages, and the GBM MES-like state was also associated with increased abundance and cytotoxicity of T cells. Our study showed that the characteristics of the immunoinflammatory subtypes (GTMEI clusterA) identified in our study are also highly similar to those of the previously reported MES subtypes. Whereas Ester Gangoso et al. (10) recently found that a key component of the previously reported "mesenchymal" signature is the transcriptional module acquired in GBM cells after immune attack, the observed transformation of GBM tumor subtypes can be explained by the extent to which the tumor immune microenvironment encroaches on their epigenetic landscape and alters the regulatory network of transcription factors. However, these results suggest that, at least in glioblastoma, the MES-like status of macrophages and cancer cells may also represent a therapeutic opportunity, as they are associated with high levels T cells that tend to be in a cytotoxic state, which may affect the response to immunotherapy. Thus, induction of MES-like states by safe and effective means and in combination with immunotherapeutic approaches may provide a new therapeutic option.

Genomic alterations and alterations in downstream oncogenic signaling pathways in tumors have been shown to affect antitumor immunity and TME activity (18, 20, 26). As such, we investigated the link between tumor mutations and the GTMEIscore and found that compared to the low GTMEIscore group, the GTMEIscore group had significantly higher PTEN and NF1 mutation rates (**Figure 3E** and **Supplementary Figure 2C**), and PTEN and NF1 mutations have been shown to cause increased infiltration of TAMs into tumor tissue (26, 27, 35). Single-cell sequencing studies have shown that TAMs are the most abundant component of the GBM immune microenvironment, originating from two independent sources (BMDM TAMs and MG TAMs) (9, 11), and they respond differently at different stages of tumor progression and perform different functions (37). These differences may be partly explained by the fact that the two cell populations are derived from different progenitor cells, which are selectively distributed in different locations, and employ different TFs for gene regulation (37). Numerous studies have demonstrated that the macrophage population that exerts immunosuppressive and proangiogenic effects is generally of bone marrow origin (9, 10, 26, 27), and our study found that the GTMEIscore was positively correlated with TAM BMDMs and negatively correlated with TAM MGs (**Figure 2J**). We also identified and validated a significant positive correlation between the GTMEIscore and myeloid-derived macrophage-restricted chemokines and genes encoding ECM and matricellular proteins (**Figures 2F, G**, **4L**). Our results showed that the GTMEIscore predicted GBM heterogeneity as well as the functional status of macrophages. Therefore, considering the significant differences in biological functions, TAM components and T cell abundance among GBM infiltrating immune cell subtypes, this study may provide more

ideas for the future development of subtype-specific combination immunotherapy strategies.

Proteomic analysis revealed a large number of differentially expressed proteins in GBM tumors with different immune infiltration patterns, and some tumors showed significant downregulation of cell cycle- and DNA repair-related proteins and upregulation of apoptosis-, EMT-, metabolism- and immune response-related proteins (**Figure 4**), in line with the transcriptomic analysis results (**Figure 3**). Furthermore, phosphoproteomics analysis also identified a large number of dysregulated protein phosphorylation sites in GBM tumors with different immune infiltration patterns, revealing a number of proteins associated with apoptosis, ECM, metabolism, and the immune response and further providing candidates for targeted therapy of GBM (**Figures 5A, B**). In addition, somatic mutation analysis of the high GTMEIscore group revealed significantly increased rates of PTEN, NF1 and BRAF mutation, and subsequent proteomics and phosphoproteomics analysis revealed dysregulation of downstream signaling pathway proteins and phosphorylation sites (**Figures 5C, D**). We also characterized the acetylation patterns of tumors with different immune infiltration patterns, revealing a large number of proteins with dysregulated acetylation, which were mainly involved in metabolic pathways (**Figures 5E, F**). In addition, analysis of histone modifications revealed significant downregulation of multiple acetylation site modification levels in H2B histones in the high GTMEIscore group, which may be dependent on CREBBP/EP300/BRD3/BRD4 activity (**Figure 5G**). For the first time, we employed a multilevel and multiplatform strategy to construct a multidimensional molecular map of tumors with different immune infiltration patterns. The results will help comprehensively reveal the molecular mechanisms of GBM development and immune microenvironment dysregulation, and provide an important scientific basis for improving the clinical treatment and prognosis of GBM.

In addition, we also demonstrated the immunomodulatory landscape in other 32 cancer types with a TCGA dataset and found significant correlations of the GTMEIscore with the immune status and biological functions of most tumors (**Figure 7**). We demonstrated that the GTMEIscore can be used not only as an independent prognostic biomarker for predicting survival in GBM, BLCA and SKCM patients but also for predicting the response to anti-PD1 antibody immunotherapy in these cancers. Drug sensitivity is a constant factor at the core of individualized cancer chemotherapy, we also predicted potential drugs that can be used for patients with a high GTMEIscore for 33 cancer types (**Figure 8**). TGF-beta is an important factor contributing to PD-L1/PD-1 antibody resistance by limiting T cell infiltration in the TME. Therefore, blocking TGF-beta significantly enhanced the efficacy of anti-PD-1/PD-L1. Recently, bispecific antibodies targeting TGF-Beta and PD-L1 exhibited superior antitumor activity (38–40), indicating that the combination of these drugs with ICIs, as well as antibodies targeting TGF-Beta may have better therapeutic effects for patients.

In conclusion, our systematic identification and characterization of molecular subtypes of immune microenvironments in GBM revealed many novel dysregulated signaling pathways and precise targets in GBM. Based on this multiomics data study, we found that the GTMEIscore is a reliable prognostic biomarker that can robustly predict the effect of ICIs and combination therapy with chemotherapy/radiotherapy. These findings might provide a theoretical basis for identifying more effective GBM predictive biomarkers and developing more effective and targeted clinical treatment strategies, ultimately guiding GBM clinical treatment and achieving precision medicine.

DATA AVAILABILITY STATEMENT

All data used in this work can be acquired from the Gene-Expression Omnibus (GEO; https://www.ncbi.nlm.nih.gov/geo/) under the accession numbers GSE78220 and GSE91061, CGGA (http://www.cgga.org.cn/), GlioVis database (http://gliovis.bioinfo.cnio.es/), the TCGA GDC portal (https://portal.gdc.cancer.gov/repository), https://www.ncbi.nlm.nih.gov/sra/ under the accession number PRJNA482620, and supplemental data of the Corresponding article.

AUTHOR CONTRIBUTIONS

GL and HX supervised the project. RRZ and WZP designed the research and executed all the results. BYL, SLZ, SJZ, YHQ, JWQ, ZJG, YF, QDG, WQ, SBW and QTW helped to revise the manuscript. PZ, XG, and LD provided administrative and technical support. All authors read and approved the final manuscript.

FUNDING

This work was supported by grants from the National Natural Science Foundation of China (Nos. 81874083; 82072776; 82072775; 81702468; 81802966; 81902540; 81874082; 81472353), Natural Science Foundation of Shandong Province of China (Nos. ZR2019BH057; ZR2020QH174; ZR2021LSW025), the Jinan Science and Technology Bureau of Shandong Province (2021GXRC029), Key Clinical Research Project of Clinical Research Center of Shandong University (2020SDUCRCA011) and Taishan Pandeng Scholar Program of Shandong Province (No. tspd20210322).

SUPPLEMENTARY MATERIAL

The Supplementary Material for this article can be found online at: https://www.frontiersin.org/articles/10.3389/fimmu.2022.820673/full#supplementary-material

REFERENCES

1. Tan A, Ashley D, López G, Malinzak M, Friedman H, Khasraw M. Management of Glioblastoma: State of the Art and Future Directions. *CA: Cancer J Clin* (2020) 70:299–312. doi: 10.3322/caac.21613
2. Lim M, Xia Y, Bettegowda C, Weller M. Current State of Immunotherapy for Glioblastoma. *Nat Rev Clin Oncol* (2018) 15:422–42. doi: 10.1038/s41571-018-0003-5
3. Jackson C, Choi J, Lim M. Mechanisms of Immunotherapy Resistance: Lessons From Glioblastoma. *Nat Immunol* (2019) 20:1100–9. doi: 10.1038/s41590-019-0433-y
4. Broekman M, Maas S, Abels E, Mempel T, Krichevsky A, Breakefield X. Multidimensional Communication in the Microenvirons of Glioblastoma. *Nat Rev Neurol* (2018) 14:482–95. doi: 10.1038/s41582-018-0025-8
5. Ott M, Prins R, Heimberger A. The Immune Landscape of Common CNS Malignancies: Implications for Immunotherapy. *Nat Rev Clin Oncol* (2021) 18:729–44. doi: 10.1038/s41571-021-00518-9
6. Reifenberger G, Wirsching H, Knobbe-Thomsen C, Weller M. Advances in the Molecular Genetics of Gliomas - Implications for Classification and Therapy. *Nat Rev Clin Oncol* (2017) 14:434–52. doi: 10.1038/nrclinonc.2016.204
7. Lee J, Wang J, Sa J, Ladewig E, Lee H, Lee I, et al. Spatiotemporal Genomic Architecture Informs Precision Oncology in Glioblastoma. *Nat Genet* (2017) 49:594–9. doi: 10.1038/ng.3806
8. Ringel A, Drijvers J, Baker G, Catozzi A, García-Cañaveras J, Gassaway B, et al. Obesity Shapes Metabolism in the Tumor Microenvironment to Suppress Anti-Tumor Immunity. *Cell* (2020) 183:1848–66.e26. doi: 10.1016/j.cell.2020.11.009
9. Friebel E, Kapolou K, Unger S, Núñez N, Utz S, Rushing E, et al. Single-Cell Mapping of Human Brain Cancer Reveals Tumor-Specific Instruction of Tissue-Invading Leukocytes. *Cell* (2020) 181:1626–42.e20. doi: 10.1016/j.cell.2020.04.055
10. Gangoso E, Southgate B, Bradley L, Rus S, Galvez-Cancino F, McGivern N, et al. Glioblastomas Acquire Myeloid-Affiliated Transcriptional Programs *via* Epigenetic Immunoediting to Elicit Immune Evasion. *Cell* (2021) 184:2454–70.e26. doi: 10.1016/j.cell.2021.03.023
11. Klemm F, Maas R, Bowman R, Kornete M, Soukup K, Nassiri S, et al. Interrogation of the Microenvironmental Landscape in Brain Tumors Reveals Disease-Specific Alterations of Immune Cells. *Cell* (2020) 181:1643–60.e17. doi: 10.1016/j.cell.2020.05.007
12. Bagaev A, Kotlov N, Nomie K, Svekolkin V, Gafurov A, Isaeva O, et al. Conserved Pan-Cancer Microenvironment Subtypes Predict Response to Immunotherapy. *Cancer Cell* (2021) 39:845–65.e7. doi: 10.1016/j.ccell.2021.04.014
13. Zeng D, Li M, Zhou R, Zhang J, Sun H, Shi M, et al. Tumor Microenvironment Characterization in Gastric Cancer Identifies Prognostic and Immunotherapeutically Relevant Gene Signatures. *Cancer Immunol Res* (2019) 7:737–50. doi: 10.1158/2326-6066.CIR-18-0436
14. Zeng D, Wu J, Luo H, Li Y, Xiao J, Peng J, et al. Tumor Microenvironment Evaluation Promotes Precise Checkpoint Immunotherapy of Advanced Gastric Cancer. *J Immunother Cancer* (2021) 9:e002467. doi: 10.1136/jitc-2021-002467
15. Thorsson V, Gibbs D, Brown S, Wolf D, Bortone D, Ou Yang T, et al. The Immune Landscape of Cancer. *Immunity* (2018) 48:812–30.e14. doi: 10.1016/j.immuni.2018.03.023
16. Barbie D, Tamayo P, Boehm J, Kim S, Moody S, Dunn I, et al. Systematic RNA Interference Reveals That Oncogenic KRAS-Driven Cancers Require TBK1. *Nature* (2009) 462:108–12. doi: 10.1038/nature08460
17. Zhang B, Wu Q, Li B, Wang D, Wang L, Zhou Y. mA Regulator-Mediated Methylation Modification Patterns and Tumor Microenvironment Infiltration Characterization in Gastric Cancer. *Mol Cancer* (2020) 19:53. doi: 10.1186/s12943-020-01170-0
18. Bowman R, Klemm F, Akkari L, Pyonteck S, Sevenich L, Quail D, et al. Macrophage Ontogeny Underlies Differences in Tumor-Specific Education in Brain Malignancies. *Cell Rep* (2016) 17:2445–59. doi: 10.1016/j.celrep.2016.10.052
19. Wang L, Karpova A, Gritsenko M, Kyle J, Cao S, Li Y, et al. Proteogenomic and Metabolomic Characterization of Human Glioblastoma. *Cancer Cell* (2021) 39:509–28.e20. doi: 10.1016/j.ccell.2021.01.006
20. Zhao J, Chen A, Gartrell R, Silverman A, Aparicio L, Chu T, et al. Immune and Genomic Correlates of Response to Anti-PD-1 Immunotherapy in Glioblastoma. *Nat Med* (2019) 25:462–9. doi: 10.1038/s41591-019-0349-y
21. Dai W, Li Y, Mo S, Feng Y, Zhang L, Xu Y, et al. A Robust Gene Signature for the Prediction of Early Relapse in Stage I-III Colon Cancer. *Mol Oncol* (2018) 12:463–75. doi: 10.1002/1878-0261.12175
22. Hugo W, Zaretsky J, Sun L, Song C, Moreno B, Hu-Lieskovan S, et al. Genomic and Transcriptomic Features of Response to Anti-PD-1 Therapy in Metastatic Melanoma. *Cell* (2016) 165:35–44. doi: 10.1016/j.cell.2016.02.065
23. Riaz N, Havel JJ, Makarov V, Desrichard A, Urba WJ, Sims JS, et al. Tumor and Microenvironment Evolution During Immunotherapy With Nivolumab. *Cell* (2017) 171:934–49.e16. doi: 10.1016/j.cell.2017.09.028
24. Charoentong P, Finotello F, Angelova M, Mayer C, Efremova M, Rieder D, et al. Pan-Cancer Immunogenomic Analyses Reveal Genotype-Immunophenotype Relationships and Predictors of Response to Checkpoint Blockade. *Cell Rep* (2017) 18:248–62. doi: 10.1016/j.celrep.2016.12.019
25. Jia Q, Wu W, Wang Y, Alexander P, Sun C, Gong Z, et al. Local Mutational Diversity Drives Intratumoral Immune Heterogeneity in non-Small Cell Lung Cancer. *Nat Commun* (2018) 9:5361. doi: 10.1038/s41467-018-07767-w
26. Chen P, Zhao D, Li J, Liang X, Li J, Chang A, et al. Symbiotic Macrophage-Glioma Cell Interactions Reveal Synthetic Lethality in PTEN-Null Glioma. *Cancer Cell* (2019) 35:868–84.e6. doi: 10.1016/j.ccell.2019.05.003
27. Wang Q, Hu B, Hu X, Kim H, Squatrito M, Scarpace L, et al. Tumor Evolution of Glioma-Intrinsic Gene Expression Subtypes Associates With Immunological Changes in the Microenvironment. *Cancer Cell* (2017) 32:42–56.e6. doi: 10.1016/j.ccell.2017.06.003
28. Zhou Y, Zhou B, Pache L, Chang M, Khodabakhshi A, Tanaseichuk O, et al. Metascape Provides a Biologist-Oriented Resource for the Analysis of Systems-Level Datasets. *Nat Commun* (2019) 10:1523. doi: 10.1038/s41467-019-09234-6
29. Pan J, Hu S, Shi D, Cai M, Li Y, Zou Q, et al. PaGenBase: A Pattern Gene Database for the Global and Dynamic Understanding of Gene Function. *PloS One* (2013) 8:e80747. doi: 10.1371/journal.pone.0080747
30. He Z, Wang C, Xue H, Zhao R, Li G. Identification of a Metabolism-Related Risk Signature Associated With Clinical Prognosis in Glioblastoma Using Integrated Bioinformatic Analysis. *Front Oncol* (2020) 10:1631. doi: 10.3389/fonc.2020.01631
31. Samstein R, Lee C, Shoushtari A, Hellmann M, Shen R, Janjigian Y, et al. Tumor Mutational Load Predicts Survival After Immunotherapy Across Multiple Cancer Types. *Nat Genet* (2019) 51:202–6. doi: 10.1038/s41588-018-0312-8
32. Touat M, Li Y, Boynton A, Spurr L, Iorgulescu J, Bohrson C, et al. Mechanisms and Therapeutic Implications of Hypermutation in Gliomas. *Nature* (2020) 580:517–23. doi: 10.1158/1538-7445.AM2020-5705
33. Chen D, Mellman I. Elements of Cancer Immunity and the Cancer-Immune Set Point. *Nature* (2017) 541:321–30. doi: 10.1038/nature21349
34. Cloughesy T, Mochizuki A, Orpilla J, Hugo W, Lee A, Davidson T, et al. Neoadjuvant Anti-PD-1 Immunotherapy Promotes a Survival Benefit With Intratumoral and Systemic Immune Responses in Recurrent Glioblastoma. *Nat Med* (2019) 25:477–86. doi: 10.1038/s41591-018-0337-7
35. Neftel C, Laffy J, Filbin M, Hara T, Shore M, Rahme G, et al. An Integrative Model of Cellular States, Plasticity, and Genetics for Glioblastoma. *Cell* (2019) 178:835–49.e21. doi: 10.1016/j.cell.2019.06.024
36. Hara T, Chanoch-Myers R, Mathewson ND, Myskiw C, Atta L, Bussema L, et al. Interactions Between Cancer Cells and Immune Cells Drive Transitions to Mesenchymal-Like States in Glioblastoma. *Cancer Cell* (2021) 39:779–92.e11. doi: 10.1016/j.ccell.2021.05.002
37. Shemer A, Jung S. Differential Roles of Resident Microglia and Infiltrating Monocytes in Murine CNS Autoimmunity. *Semin Immunopathol* (2015) 37:613–23. doi: 10.1007/s00281-015-0519-z
38. Yi M, Niu M, Zhang J, Li S, Zhu S, Yan Y, et al. Combine and Conquer: Manganese Synergizing Anti-TGF-β/PD-L1 Bispecific Antibody YM101 to Overcome Immunotherapy Resistance in non-Inflamed Cancers. *J Hematol Oncol* (2021) 14:146. doi: 10.1186/s13045-021-01155-6
39. Lan Y, Zhang D, Xu C, Hance KW, Marelli B, Qi J, et al. Enhanced Preclinical Antitumor Activity of M7824, a Bifunctional Fusion Protein Simultaneously Targeting PD-L1 and TGF-β. *Sci Transl Med* (2018) 10:eaan5488. doi: 10.1126/scitranslmed.aan5488

40. Yi M, Zhang J, Li A, Niu M, Yan Y, Jiao Y, et al. The Construction, Expression, and Enhanced Anti-Tumor Activity of YM101: A Bispecific Antibody Simultaneously Targeting TGF-β and PD-L1. *J Hematol Oncol* (2021) 14:27. doi: 10.1186/s13045-021-01045-x

Conflict of Interest: The authors declare that the research was conducted in the absence of any commercial or financial relationships that could be construed as a potential conflict of interest.

Publisher's Note: All claims expressed in this article are solely those of the authors and do not necessarily represent those of their affiliated organizations, or those of the publisher, the editors and the reviewers. Any product that may be evaluated in this article, or claim that may be made by its manufacturer, is not guaranteed or endorsed by the publisher.

frontiers | Frontiers in Immunology

TYPE Original Research
PUBLISHED 04 January 2023
DOI 10.3389/fimmu.2022.993444

OPEN ACCESS

EDITED BY
Yannick Simoni,
INSERM U1016 Institut Cochin, France

REVIEWED BY
Jian Bai,
Fourth Military Medical University, China
Defne Bayik,
Cleveland Clinic, United States

*CORRESPONDENCE
Jeffrey K. Harrison
jharriso@ufl.edu

†These authors have contributed equally to this work and share first authorship

SPECIALTY SECTION
This article was submitted to Cancer Immunity and Immunotherapy, a section of the journal Frontiers in Immunology

RECEIVED 13 July 2022
ACCEPTED 16 December 2022
PUBLISHED 04 January 2023

CITATION
Takacs GP, Kreiger CJ, Luo D, Tian G, Garcia JS, Deleyrolle LP, Mitchell DA and Harrison JK (2023) Glioma-derived CCL2 and CCL7 mediate migration of immune suppressive CCR2$^+$/CX3CR1$^+$ M-MDSCs into the tumor microenvironment in a redundant manner.
Front. Immunol. 13:993444.
doi: 10.3389/fimmu.2022.993444

Glioma-derived CCL2 and CCL7 mediate migration of immune suppressive CCR2$^+$/CX3CR1$^+$ M-MDSCs into the tumor microenvironment in a redundant manner

Gregory P. Takacs[1†], Christian J. Kreiger[1†], Defang Luo[1], Guimei Tian[2], Julia S. Garcia[1], Loic P. Deleyrolle[2], Duane A. Mitchell[2] and Jeffrey K. Harrison[1*]

[1]Department of Pharmacology & Therapeutics, University of Florida College of Medicine, Gainesville, FL, United States, [2]Department of Neurosurgery, University of Florida College of Medicine, Gainesville, FL, United States

Glioblastoma (GBM) is the most common and malignant primary brain tumor, resulting in poor survival despite aggressive therapies. GBM is characterized in part by a highly heterogeneous and immunosuppressive tumor microenvironment (TME) made up predominantly of infiltrating peripheral immune cells. One significant immune cell type that contributes to glioma immune evasion is a population of immunosuppressive, hematopoietic cells, termed myeloid-derived suppressor cells (MDSCs). Previous studies suggest that a potent subset of myeloid cells, expressing monocytic (M)-MDSC markers, distinguished by dual expression of chemokine receptors CCR2 and CX3CR1, utilize CCR2 to infiltrate into the TME. This study evaluated the T cell suppressive function and migratory properties of CCR2$^+$/CX3CR1$^+$ MDSCs. Bone marrow-derived CCR2$^+$/CX3CR1$^+$ cells adopt an immune suppressive cell phenotype when cultured with glioma-derived factors. Recombinant and glioma-derived CCL2 and CCL7 induce the migration of CCR2$^+$/CX3CR1$^+$ MDSCs with similar efficacy. KR158B-CCL2 and -CCL7 knockdown murine gliomas contain equivalent percentages of CCR2$^+$/CX3CR1$^+$ MDSCs compared to KR158B gliomas. Combined neutralization of CCL2 and CCL7 completely blocks CCR2-expressing cell migration to KR158B cell conditioned media. CCR2$^+$/CX3CR1$^+$ cells are also reduced within KR158B gliomas upon combination targeting of CCL2 and CCL7. High levels of CCL2 and CCL7 are also associated with negative prognostic outcomes in GBM patients. These

data provide a more comprehensive understanding of the function of CCR2$^+$/CX3CR1$^+$ MDSCs and the role of CCL2 and CCL7 in the recruitment of these immune suppressive cells and further support the significance of targeting this chemokine axis in GBM.

KEYWORDS

glioma, chemokine, chemokine receptor, migration, immune-suppression, myeloid, MDSC, bone marrow

Introduction

Glioblastoma (GBM) is a highly aggressive and recurrent primary brain tumor that continues to challenge patients and oncologists as current interventions are minimally effective (1, 2). Currently, standard of care therapy relies on surgical resection of the tumor mass followed by focal radiation and chemotherapy (temozolomide) (3–5). Foremost in GBM patients, the immune suppressive tumor microenvironment contributes to immune evasion, disease progression, and poor overall survival (6–9). Attempts at harnessing anti-tumor immune responses to overcome the immunosuppressive microenvironment have been made in cancer therapy (10–12). For example, clinically successful immunotherapy has targeted immune checkpoint systems, including the programmed cell death protein-1, i.e., PD-L1/PD-1, pathway. Unfortunately, to date targeting the PD-L1/PD-1 axis in human gliomas has not demonstrated efficacy as an adjuvant monotherapy (13, 14). While the mechanism by which gliomas are resistant to PD-1 blockade is not entirely resolved, mounting evidence suggests that infiltrating immune suppressive cells contribute significantly to the resistant phenotype (15–17).

Chief amongst the immune suppressive cells which gain access to the glioma microenvironment are a subset of myeloid cells termed myeloid-derived suppressor cells (MDSCs) (15). In humans, MDSCs represent a heterogeneous cell population that are delineated into three major classes based on phenotypic and morphological features: early-stage (e), polymorphonuclear (PMN/G)-, and monocytic (M)-MDSCs (18, 19). M-MDSCs suppress lymphocytes *via* production of free radicals and enzymes that deplete essential lymphocyte metabolites (20–23). In murine gliomas (i.e., GL261, CT-2A, 005 GSC, and KR158B), M-MDSCs characterized by lineage markers CD45$^+$, CD11b$^+$, Ly6C^{hi}, and Ly6G$^-$ (19, 24, 25), are the predominant subset present in the TME, with little to no PMN-MDSC infiltration (26–28).

We have previously reported that three populations of myeloid cells are identified in the glioma microenvironment according to their expression of chemokine receptors CCR2 and CX3CR1. One of these populations, co-expressing chemokine receptors CCR2 and CX3CR1 (denoted as CCR2$^+$/CX3CR1$^+$), express markers consistent with M-MDSCs (CD45$^+$, CD11b$^+$, Ly6C^{hi}, and Ly6G$^-$) and shows poor overlap with the mature macrophage marker F4/80 (28). Pharmacologic or genetic targeting of CCR2-expressing cells *via* a CCR2 antagonist or gene deletion limited the presence of these cells within the tumor and promoted their sequestration within the bone marrow. In combination with the immune checkpoint inhibitor, αPD-1, CCR2 antagonism unmasked an effect of PD-1 blockade in slowing the tumor progression of two immune checkpoint inhibitor-resistant murine gliomas (KR158B and 005 GSC) (28). While these previous findings established that CCR2$^+$/CX3CR1$^+$ MDSCs utilize CCR2 to traffic into the glioma microenvironment, it is unclear what chemokines drive this CCR2-dependent migration. This study investigated the T cell suppressive function and chemokine ligand dependency by which CCR2$^+$/CX3CR1$^+$ M-MDSCs traffic into the glioma microenvironment. Using a preclinical glioma model, we demonstrate that CCR2$^+$/CX3CR1$^+$ cells are sourced from the bone marrow, suppress both CD4$^+$ and CD8$^+$ T cells, migrate to CCL2 and/or CCL7 in a CCR2-dependent manner, and are reduced in the glioma microenvironment through combination targeting of CCL2 and CCL7. We also identify CCL2 and CCL7 as predictors of survival in human glioblastoma. These data establish the immune suppressive and migratory properties of CCR2$^+$/CX3CR1$^+$ myeloid cells and confirm their role as glioma-associated M-MDSCs.

Methods

Animals

Ccr2$^{RFP/WT}$/*Cx3cr1*$^{GFP/WT}$ mice were generated through the breeding of Ccr2-deficient (*Ccr2*$^{RFP/RFP}$[*B6.129(Cg)-Ccr2*$^{tm2.1Ifc}$/*J*]), and Cx3cr1-deficient (*Cx3cr1*$^{GFP/GFP}$[*B6.129P-Cx3cr1*^{tm1Litt}/*J*]) mice. Wildtype C57BL/6, Ccr2-deficient, and Cx3cr1-deficient mice were purchased from The Jackson Laboratory.

All procedures involving animal housing and surgical protocols were followed according to the guidelines of the University of Florida Institutional Animal Care and Use Committee.

Generation of chimeric mice

Chimeric mice were generated through a bone marrow transplant of *Ccr2*$^{WT/RFP}$/*Cx3cr1*$^{WT/GFP}$ donor mice into wildtype C57BL/6 recipient mice. Wildtype mice were placed under anesthesia (Xylazine 0.5mL, Ketamine 0.7mL, Saline 5.6mL) through intra peritoneal injection (100µL/20g mouse). Subsequently, wildtype mice received 900 cGy x-ray radiation (X-RAD 350 irradiator). Bone marrow was prepared from *Ccr2*$^{WT/RFP}$/*Cx3cr1*$^{WT/GFP}$ mice as described below. Cells were diluted to a final concentration of 10,000 cells/µL. After irradiation (~4hrs), whole bone marrow from *Ccr2*$^{WT/RFP}$/*Cx3cr1*$^{WT/GFP}$ donor mice was tail vein injected (100 µL) into irradiated wildtype C57BL/6 recipient mice. Seven days post-irradiation, Baytril (fluoroquinolone antibiotic) was added to the drinking water at 0.5 mg/ml for two weeks. Following recovery, chimeric mice were implanted with KR158B gliomas (see "Orthotopic Brain Tumor Model") and evaluated *via* flow cytometry (see "Flow Cytometry Analysis")

Orthotopic brain tumor model

Animals were anesthetized using isoflurane and administered analgesia prior to cell injection. While under anesthesia, the surgical site was prepared and a 2- to 3-mm incision was made at the midline of the skull. Using a stereotaxic apparatus (Stoelting), the mice were secured, and a Hamilton syringe was positioned 2-mm lateral from the bregma. KR158B, KR158B CCL2 knockdown, or KR158B CCL7 knockdown glioma cells (3.5×10^4 in a total volume of 2 µL) were injected 3-mm deep into the right cerebral hemisphere using an automated microfluidic injection system (Stoelting) at a rate of 1 µL/min; cells were suspended in a 1:1 ratio of methylcellulose to PBS. Post-injection, the needle was retracted slowly, and the surgical site was closed *via* suture and bone wax. Animals were then placed into a warm cage for postsurgical monitoring.

Tissue isolation

Mice were euthanized at experimental endpoint. Right atrium was severed, and blood was collected using an EDTA coated 1mL syringe without a needle. 200uL of blood was placed in a 1.5mL tube containing 100ul EDTA (0.5M). Transcardial perfusions, using a 10mL syringe with a 25G winged infusion set, of 20mL 0.9% saline solution were administered to remove intra-vasculature associated cells. Blood was centrifuged at 21°C 380 × *g* for 5 min, plasma was discarded. Femurs, tibiae, and humeri were harvested from the animal. Fat and muscle were removed, and the bones were subsequently cut at one end to expose bone marrow. Bones were placed in microcentrifuge tubes (2 bones per tube) with the bottoms pierced and nested in 1.5mL centrifuge tubes containing 100uL PBS. Tubes were centrifuged at 5,700 x g for 20 seconds to flush the bone marrow. Spleens were harvested and placed on a petri dish. Fat was trimmed from the tissue and spleens were injected with 1mL PBS *via* 18G needle. Spleens were minced using a razor blade and transferred to 15mL conical tubes containing 5mL PBS. Using a 5mL syringe and 18G needle, the tissue was mechanically dissociated *via* passage through the needle 20 times. Splenocytes were collected *via* centrifugation (4°C, 380 × *g*, 5 min). Bone marrow cells, blood, and splenocytes were resuspended in 1mL Ammonium-Chloride-Potassium (ACK) Lysis buffer (Gibco, Invitrogen) and placed on ice for 5 min to lyse red blood cells. Subsequently, lysis buffer was quenched with 5mL fluorescence-activated cell-sorter (FACS) washing buffer (1% FBS in PBS) and strained through a 40-µm cell strainer. Blood underwent three ACK lysis/quench cycles. Cells were collected *via* centrifugation (4°C, 380 × *g*, 5 min) and counted by trypan blue exclusion. Brains were removed and tumors were extracted and mechanically minced using a razor blade. Tumors were placed in 4°C Accumax dissociation solution (Innovative Cell Technologies) and incubated at 37° C for 5 min, followed by 5 min of agitation at room temperature. Cells were then passed through a 40-µm strainer, centrifuged (4°C, 380 × *g*, 5 min), and resuspended in 4 mL of 70% Percoll (70% Percoll and 1% PBS in RPMI-1640 cell medium). The 70% Percoll/cell solution was then carefully layered beneath 37% Percoll layer (4 mL, 37% Percoll and 1% PBS in RPMI-1640 cell medium) using an 18-gauge needle. Samples were then centrifuged for 30min at room temperature (500 x g). Cells at the interface were collected and transferred into a 1.5 mL microcentrifuge tube. Cells were washed with cold PBS and counted by trypan blue exclusion.

Flow cytometry analysis

Single cell suspensions were prepared from tissues as described above and diluted to 1 x 10^6 cells/100uL. Subsequently, cells were stained for markers of interest (Supplementary Table 1) for 30 min at 4°C. Cells were then washed twice in ice-cold PBS and stained with a viability dye. Stained samples were analyzed using single-color compensation on a Sony SP6800 spectral analyzer or Beckman Coulter CytoFLEX LX 96-well plate system and quantified using FlowJo V10.8.1 (BD Biosciences).

Cell culture

KR158B, KR158B-Luciferase, KR158B CCL2 knockdown, and KR158B CCL7 knockdown glioma cells were cultured in Dulbecco's Modified Eagle Medium (DMEM) supplemented with 1% penicillin-streptomycin and 10% fetal bovine serum (FBS). Cells were grown in a humidified incubator at 37°C with 5% CO_2. DMEM and penicillin-streptomycin were purchased through Invitrogen. FBS was purchased through Thermo Scientific.

Generation of CCL2- and CCL7-deficient glioma cells

Plasmids for knockdown of CCL2 (TRCN0000301701 and TRCN0000301702) and CCL7 (TRCN0000317599, TRCN0000068135, and TRCN0000068136) were obtained from Sigma. shRNA control plasmid (SHC002. Sigma) was used as non-targeting control. ShRNA plasmids were purified with QIAprep Spin Miniprep Kit (#27106, Qiagen) after overnight incubation with E-coli bacteria. Packaging 293T/17 cells were co-transfected with the different shRNAs and the packaging plasmids psPAX2 and pMD2.G, to generate viral particles, which were subsequently used to transduce KR158B cells. KR158B CCL2 knockdown were generated using the combination of TRCN0000301701 and TRCN0000301702. TRCN0000317599, TRCN0000068135, and TRCN0000068136 were combined to generate KR158B CCL7 knockdown. Cytokine quantification was completed using mouse CCL2 (Invitrogen# 88-7391-22) and mouse CCL7 (Invitrogen# BMS6006INST) enzyme-linked immunosorbent assay (ELISA) analysis following manufacturer protocols. KR158B, KR158B CCL2 knockdown and KR158B CCL7 knockdown glioma cell lines were cultured to 90% confluency. Cells were counted and plated in a 96-well plate at 50, 100 or 500 cells/uL in 200uL complete DMEM media. Cells were incubated at 37°C, 5% CO_2 for 24 hours. Following incubation, well contents were transferred to tubes and centrifuged as previously described. Supernatant was aliquoted and frozen at -80°C until use for ELISA as previously described (Supplementary Figure 1).

Mouse brain fixation and immunohistochemistry

Transcardial perfusions, using a 10mL syringe with a 25G winged infusion set, of 20mL 4.0% paraformaldehyde (PFA) solution were administered. Following fixative perfusion, mouse brains were removed and soaked in 4.0% PFA for 1hr. Brains were subsequently transferred to 30% sucrose solution for 24hrs and snap frozen using liquid nitrogen chilled 2-Methylbutane. Brains were embedded in optimal cutting temperature compound and mounted for cryo-sectioning (Lecia Biosystems Cryostat). 5-10µm thick sections were taken and mounted on microscope slides. Sections were dried overnight at 4°C. Tissue sections were brought to room-temperature and washed 3 times in PBS and counterstained with antifade mounting medium with DAPI (Vectashield). Brain tumor sections were imaged using an inverted Nikon TiE-PFS-A1R confocal microscope. Images were post-processed using Nikon Elements software.

Bone marrow culture

Induction of MDSCs was adapted from previously published work (Alban et al.) (26). Bone marrow-derived cells from wildtype C57BL/6 mice were prepared as previously described. Cells were then plated at a density of 400,000 cells/cm^2 and concentration of 1,000 cells/uL in media consisting of 50% complete RPMI (RPMI + 10% FBS + 2mM L-Glutamine) and 50% KR158B conditioned media. Additionally, the media was supplemented with 40ng/mL GM-CSF (R&D 415-ML) and 40ng/mL IL-6 (R&D 406-ML). On day 5, suspended cells were collected, the flask was washed in PBS and scraped using a cell scraper (Fisher), and all contents were joined together in a 50mL conical tube. Cells were collected *via* centrifugation (4°C, 380 × *g*, 5 min) and counted by trypan blue exclusion. Cells were then either subjected to flow cytometry (see "Flow Cytometry Analysis") or utilized for the T cell suppression assay (see "T cell Suppression Assay").

T cell suppression assay

Following a 5-day culture (see "Bone Marrow Culture"), MDSC enriched bone marrow cells were collected from culture as described above and subjected to M-MDSC magnetic bead isolation (Miltenyi Biotec) according to manufacturer's protocols. Additionally, fresh splenocytes were isolated as previously described and subjected to Pan-T cell magnetic bead isolation (Miltenyi Biotec) according to manufacturer's protocols. Following isolation, T cells were collected *via* centrifugation and resuspended at a density of 1 million cells/mL in PBS. T cells were incubated with 1uL CellTrace FarRed Cell Proliferation dye (ThermoFisher C34564) per 1 million cells for 20 minutes at RT. Following incubation, the dye was quenched in 5 times the present volume of complete RPMI. T cells were collected *via* centrifugation (4°C, 380 × *g*, 5 min) and resuspended in complete RPMI at 1,000 cells/uL. Dynabeads Mouse T Activator CD3/CD28 beads (Thermofisher 11452D) were washed in complete RPMI and mixed with stained T cells at a 2:1 (activating bead:T cell) ratio. T cells were retained at each step to ensure for unstained, unstimulated, and stained/unstimulated controls. 100,000 T cells were added per well in

a round-bottom 96-well plate and MDSCs were added at ratios of 1:4, 1:2 and 1:1 (MDSCs:T cells). Co-cultures were incubated at 37°C for 3 days. Following incubation, well contents, in addition to 2 subsequent PBS well washes, were transferred to centrifuge tubes. Tubes were then placed on the Dynamag-2 (Thermofisher 12321D) to remove activating beads. Cells were collected by centrifugation and stained for CD3, CD4 and CD8 (Biolegend 100234; 100510; 100708) for flow cytometry analysis. Each biologic and condition were run in triplicate. Technical triplicates were averaged prior to statistical analysis.

In vitro cell migration

Bone marrow cells were isolated from *Ccr2*$^{WT/RFP}$/*Cx3cr1*$^{WT/GFP}$ mice as described previously. Cells were diluted to a final concentration of 2,000 cells/μL in migration buffer consisting of RPMI-1640, 25mM HEPES, 1% penicillin-streptomycin, and 0.1% BSA (>98% quality). *In vitro* migration of CCR2$^{WT/RFP}$/CX3CR1$^{WT/GFP}$ cells was assessed using a transwell-96 well plate with 5μm polycarbonate membrane (Corning; product number 3388). Recombinant Mouse CCL2, CCL7, and soluble CX3CL1 chemokines were purchased from R & D Systems (product numbers 479-JE-010; 456-MC-010; 571-MF-025). Recombinant proteins were reconstituted following manufacture preparation and storage guidelines. Recombinant CCL2, CCL7, and soluble CX3CL1 ligands were diluted in migration buffer and seeded at 150μL/well in the bottom chamber. To validate a chemotaxis effect, chemokine was also placed in the top and bottom chambers at equivalent concentrations (i.e., 30ng/mL top chamber and 30ng/mL bottom chamber). Cells were plated at 150μL/well in the top chamber, and the plate was incubated at 37°C, 5% CO_2 for 2 hours. After incubation, the membrane insert was lightly shaken to detach migrated cells on the underside of the membrane and then discarded. Wells were analyzed for CCR2$^{WT/RFP}$ and CCR2$^{WT/RFP}$/CX3CR1$^{WT/GFP}$ populations using single color compensation on Beckman Coulter CytoFLEX LX 96-well plate system. 75uL/well was collected at a flow rate of 150uL/min with 3s shake time and backflush between wells. Gating strategy proceeded as follows: 1. Positive gate for myeloid population according to forward-scatter area (FSC-A) and side-scatter area (SSC-A). 2. Doublet exclusion according to FSC-A and forward-scatter height (FSC-H). 3. CCR2/CX3CR1 co-expression according to PE and FITC channels. Gating strategy was established according to analysis of raw bone marrow samples and applied constantly throughout the analysis. Final gating analysis was conducted using FCS Express software (*De Novo*) or FlowJo V10.8.1 (BD Biosciences). Control wells containing no chemokine in the bottom well were averaged and normalized as 100% migration. Sample wells are compared relative to control wells for presentation and statistical analyses.

For analysis of migration to conditioned media, KR158B or KR158B CCL2 KD cells were cultured to 90% confluency in a tissue-culture T-75 flask containing complete DMEM (see "Cell Culture" section in methods). Media was washed out and cells were plated in a 6-well plate in 6mL migration buffer at 50, 100, and 500 cells/μL overnight at 37°C, 5% CO_2. Contents from wells were extracted and centrifuged at 1,000 RPM for 5 minutes. Supernatant was collected, filtered, and aliquoted in the bottom chamber of the transwell-96 well plate. For neutralization experiments, polyclonal goat IgG antibodies (anti-CCL2, anti-CCL7, and normal goat IgG control) were purchased from R & D Systems (product number AB-479-NA, AF-456-NA, and AB-108-C) and stored following manufacture instructions. All wells that received neutralizing antibodies received equal quantities of exogenous protein (i.e., 8.25 μg/well) through supplementation of normal goat IgG control. Raw bone marrow was seeded in the top chamber as previously mentioned. Each biologic and condition were run in triplicate. Technical triplicates were averaged prior to statistical analysis.

In vivo targeting of CCL2 and CCL7

KR158B and KR158B CCL7 KD glioma cells were orthotopically implanted into *Ccr2*$^{WT/RFP}$/*Cx3cr1*$^{WT/GFP}$ mice. Polyclonal goat IgG antibodies (anti-murine CCL2 and normal goat IgG control) were purchased from R & D Systems (product number AB-479-NA and AB-108-C) and stored following manufacture instructions. Mice received a 100μg loading dose of either anti-CCL2 antibody or normal goat IgG, *via* intraperitoneal injection, 3 days post implantation of glioma cells. Subsequent maintenance doses of 50μg were administered on days: 6, 10, 13, 17, 20,2 4, 27, 31. After the last treatment, mice were euthanized and processed using flow cytometry. Tumor, peripheral blood, spleen, and bone marrow tissues were analyzed. CCR2^{+} and CX3CR1^{+} cells were gated on exclusion of viability dye, CD45, CD11b. Please see "Tissue Isolation", "Flow Cytometry Analysis", and (Supplementary Table 1) for additional information.

Survival analysis

The complete human glioblastoma multiforme (GBM) patient dataset was mined from The Cancer Genome Atlas (TCGA Research Network: cancer.gov/tcga) The Georgetown Database of Cancer (G-DOC) platform to extract gene expression and clinical parameters (29–31). G-DOC platform was accessed on February 4, 2022. Gene expression was gathered from the Affymetrix dataset (Affymetrix HT Human Genome U133a microarray platform by the Broad Institute of MIT and Harvard University cancer genomic characterization center) and RNA sequencing dataset (Illumina HiSeq 2000 RNA Sequencing

platform by the University of North Carolina TCGA genome characterization center). Patients were stratified into low or high CCL2, CCL7, and CCL2 ∩ CCL7 expressing categories (LOW<25th percentile and HIGH>75th percentile, respectively). Percentiles were generated using descriptive statistics function in GraphPad Prism version 9.3.1 for Windows, GraphPad Software, San Diego, California USA. Survival curve comparisons and numbers at risk were calculated using Log-rank (Mantel-Cox test) and graphically illustrated through GraphPad Prism version 9.3.1. P-values are reported in figures.

Statistical analysis

Multiple t-tests, Log-rank (Mantel-Cox), one-way ANOVA and two-way ANOVA analyses were performed in GraphPad Prism version 9.3.1 to determine statistically significant differences between groups. Multiple comparisons were corrected for with the recommended Dunnett multiple comparison test. A p-value <0.05 was considered significant and is indicated by symbols depicted in the figures, figure legends and text.

Results

CCR2$^+$/CX3CR1$^+$ cells in the glioma microenvironment are sourced from the bone marrow

We previously established that a glioma-associated CCR2$^+$/CX3CR1$^+$ myeloid cell population also expresses markers consistent with M-MDSCs. A CCR2$^+$/CX3CR1$^+$ myeloid cell population, expressing the same MDSC markers, is also present in bone marrow. To examine the T cell suppressive and migratory properties of these CCR2$^+$/CX3CR1$^+$ cells, dual transgenic *Ccr2*$^{WT/RFP}$/*Cx3cr1*$^{WT/GFP}$ mice were utilized in order to facilitate the direct examination of CCR2- and CX3CR1-expressing cells. Fluorescent confocal microscopy of intracranial KR158B tumors confirmed the presence of brain-resident CX3CR1$^{WT/GFP}$ microglia and revealed that CCR2$^{WT/RFP}$ and CCR2$^{WT/RFP}$/CX3CR1$^{WT/GFP}$ cells were also present within the TME as early as 5 days post-implantation of KR158B tumor cells (Figure 1A). Fluorescent imaging of naïve (non-tumor) brain tissue confirmed the absence of any RFP-expressing cells in non-tumor bearing brain tissue while RFP/GFP positive cells were present in bone marrow (Figure 1A).

To directly establish if CCR2$^+$/CX3CR1$^+$ cells present within KR158B gliomas are sourced from the bone marrow we generated chimeric mice harboring *Ccr2*$^{WT/RFP}$/*Cx3cr1*$^{WT/GFP}$ bone marrow cells. Irradiated wildtype C57BL/6 mice (recipient) received whole bone marrow isolated from *Ccr2*$^{WT/RFP}$/*Cx3cr1*$^{WT/GFP}$ mice (donor) and, following immune reconstitution, chimeric mice were orthotopically implanted with KR158B glioma cells. At experimental endpoint, bone marrow and brain tumor tissue were processed for flow cytometry. Flow cytometry analysis identified the presence of CCR2$^+$ and CCR2$^+$/CX3CR1$^+$ cells in the tumors of chimeric mice ($p<.0001$) (Figures 1B, C) which indicates that these populations were derived from the bone marrow. GFP$^+$ cells were absent from these tumors, suggesting that this population is brain-derived.

CCR2$^+$/CX3CR1$^+$ cells suppress CD8$^+$ and CD4$^+$ T cell proliferation and IFN-γ production

To investigate the functionality of CCR2$^+$/CX3CR1$^+$ cells, the impact on T cell proliferation and function was assessed. Having determined that CCR2$^+$/CX3CR1$^+$ cells are bone marrow-derived, whole bone marrow was harvested and cells were cultured in the presence of KR158B glioma-derived factors (conditioned media) containing soluble GM-CSF and IL-6 to enrich and expand the population of dual-expressing chemokine receptor cells. Following magnetic bead MDSC isolation, flow cytometry analysis confirmed the isolation of cells expressing CD45, CD11b, Ly6C, and chemokine receptors CCR2 and CX3CR1 (Figure 2A); cells were negative for Ly6G. The enriched, bone marrow-derived cells significantly suppressed the proliferation of both CD4$^+$ and CD8$^+$ T cells at ratios 1:2 and 1:1 (Figures 2B–D). In the presence of MDSCs at a 1:2 ratio, CD4$^+$ T cell proliferation decreased from 71% to 39% while CD8$^+$ T cell proliferation decreased from 82% to 50%. When co-cultured at a 1:1 ratio of MDSCs to T cells, CD4$^+$ and CD8$^+$ T cell proliferation was suppressed to 20% and 18%, respectively (Figures 2C, D). To further assess suppression within the co-culture, we analyzed the media from the suppression assay for levels of IFN-γ. Consistent with the results for proliferation, higher ratios of MDSCs:T cells also yielded lower concentrations of IFN-γ within the co-culture (Figure 2E), suggesting functional inhibition of effector T cells by the CCR2$^+$/CX3CR1$^+$ MDSCs. These results establish that bone marrow CCR2$^+$/CX3CR1$^+$ cells, when incubated in glioma-derived factors, acquire a phenotype capable of disrupting the proliferation and function of both CD4- and CD8-expressing T cells.

High CCL2 and CCL7 expression is associated with lower overall survival in human glioblastoma

Of the five known human ligands of CCR2, three are shared with mice, namely CCL2, CCL7 and CCL8. To determine the impact of these chemokines on the clinical prognosis of human

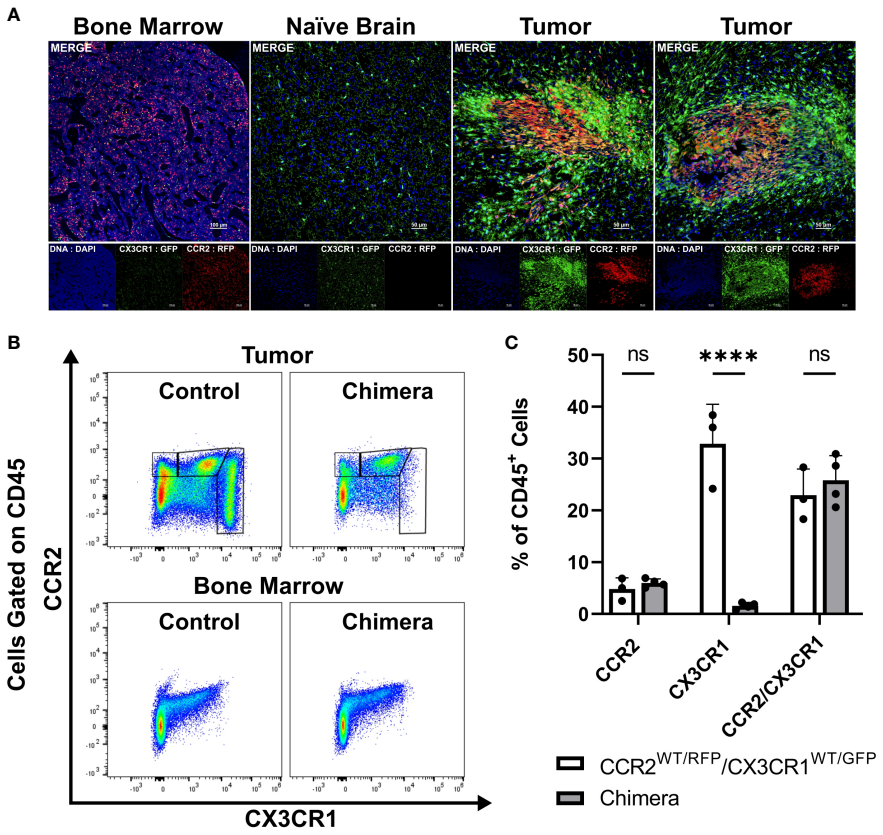

FIGURE 1
$CCR2^{+}/CX3CR1^{+}$ cells infiltrate the glioma microenvironment and are derived from the bone marrow. **(A)** Representative immunofluorescent images of bone marrow, naïve brain, and tumor-implanted brains 5 days post-implantation. Images depict the absence of $CCR2^{WT/RFP}$ cells within normal brain and presence within bone marrow and tumors 5 days post-implantation. **(B)** Representative flow cytometry plots of tumors and bone-marrow of non-irradiated control and chimeric animals at experimental endpoint. **(C)** Quantification of $CCR2^{+}$, $CX3CR1^{+}$ and $CCR2^{+}/CX3CR1^{+}$ leukocytes in control and chimeric animals (n=3). GraphPad Prism was used to conduct two-way ANOVA statistics (Dunnett's multiple comparisons test). Differences are compared to the control (0) condition. p-values: <0.0001(****). ns (not significant).

GBM, gene expression and survival data from The Cancer Genome Atlas (TCGA) GBM cohort was analyzed. Patients were stratified into "Low" and "High" expressing categories based on the lowest and highest quartiles of expression. Kaplan-Meyer survival curves, derived from Affymetrix and IlluminaHighseq datasets, were generated and Log-rank tests were utilized to compare the survival distributions. Similar to findings of Chang et al., a statistically significant decrease in survival among patients with high expression of CCL2 (MS: 11.7mo), compared to low-expressing patients (MS: 14.5mo), was evident in the Affymetrix gene expression dataset ($p<0.0005$) (Figure 3A) (32). Similar results based on high (MS: 11.7mo) and low (MS: 13.0mo) CCL7 expression was identified ($p=0.0417$) (Figure 3B). Upon grouping cohorts of high expression of CCL2 and CCL7 (MS: 11.6mo) and low expression of CCL2 and CCL7 (MS: 14.0mo) (denoted as the intersection sign "∩"), there was a statistically significant decrease in survival among the high expression cohort ($p=0.0255$) (Figure 3C). More striking results were revealed when analyzing the Illumina Highseq dataset. High CCL2 expression ($p=0.0109$) (Figure 3D) and high CCL7 ($p=0.0319$) (Figure 3E) expression among patients correlated with a statistically significant reduction in survival. This survival disadvantage was most pronounced among patients with high expression of both CCL2 and CCL7 (MS: 7.5mo) vs low expression (MS: 15.4mo) ($p=0.0018$) (Figure 3F). These results indicate that high expression of CCL2 and CCL7 is negatively correlated with survival in the context of human GBM. The Chinese Glioma Genome Atlas (CGGA) was also queried to examine survival and corroborated the TCGA analysis (Supplementary Figure 2). Expression of CCL8, the other shared CCR2 chemokine across species, was not associated with a significant survival disadvantage (Supplementary Figure 3C). CCL13 and CCL16, CCR2 ligands found only in humans, also did not show a significant survival disadvantage (Supplementary Figure 3). The CGGA was also used to

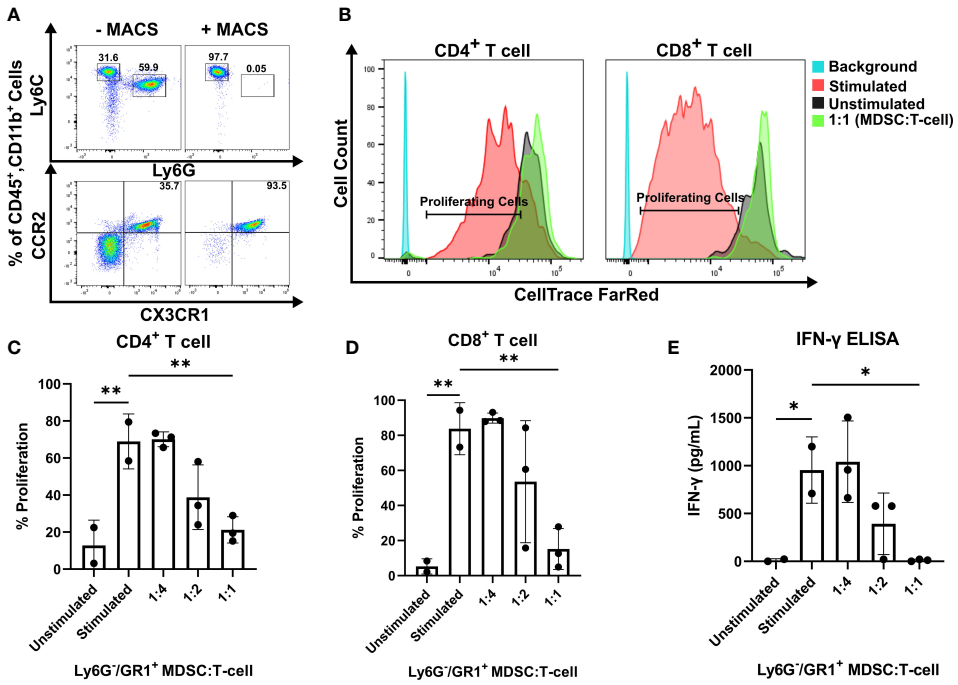

FIGURE 2
CCR2$^+$/CX3CR1$^+$ cells suppress CD8 and CD4 T cell proliferation and IFN-γ production. **(A)** Representative flow cytometry plot establishing CCR2$^+$/CX3CR1$^+$ cells are enriched using Ly6G and GR-1 magnetic-activated cell sorting (MACS). **(B)** Representative flow cytometry plot denoting CD4$^+$ and CD8$^+$ proliferating cells in the presence or absence of CCR2$^+$/CX3CR1$^+$ enriched cells. Quantification of **(C)** CD4$^+$ or **(D)** CD8$^+$ T cell proliferation in the presence and absence of CD3/CD28 activation beads (stimulated/unstimulated) and stimulated T cells co-cultured with enriched CCR2$^+$/CX3CR1$^+$ cells. Enriched CCR2$^+$/CX3CR1$^+$ cells were plated at varying ratios to dye-loaded T cells (T cell numbers were held constant). After 3 days, proliferation was assessed using flow cytometry (n=3). **(E)** Supernatant from co-culture T cell suppression assay was collected and analyzed for IFN-γ protein *via* ELISA (n=3). One-way ANOVA statistical analysis was conducted (Dunnett's multiple comparisons test). Differences are compared to the stimulated control condition. p-values: 0.0332(*), 0.0021(**).

investigate correlations between CCL2, CCL7 and markers of M-MDSCs (CD14 and CD33). Positive correlations for each comparison were found: CD14 vs CCL2 (r= 0.753) CD33 vs CCL2 (r= 0.640) CD14 vs CCL7 (r= 0.618) CD33 vs CCL7 (r= 0.481) (Supplementary Figure 5). Taken together with our previous data, we posit that this significant difference in survival between low and high expressors is due in part to an elevated level of recruitment of immunosuppressive CCR2$^+$/CX3CR1$^+$ cells into the glioma microenvironment.

CCR2$^+$/CX3CR1$^+$ cells migrate to recombinant CCL2 and CCL7 through CCR2

With evidence that CCR2$^+$/CX3CR1$^+$ cells represent a potent T cell suppressive population and CCR2 ligands (CCL2 and CCL7) confer poor survival in human GBM, we evaluated the impact of CCL2 and CCL7 on cell migration. To determine the migratory capacity of the CCR2$^+$/CX3CR1$^+$ cell population to chemokine ligands, a 96-well 5μm transwell migration assay was employed. Migration of CCR2$^+$/CX3CR1$^+$ cells was determined using flow cytometry, gating for CCR2$^{WT/RFP}$ and CX3CR1$^{WT/GFP}$ double-positive cells (Figure 4A) with results presented as percent migration relative to the control condition i.e., no recombinant chemokine in the bottom chamber.

Flow cytometry analysis revealed statistically significant migration of CCR2$^+$/CX3CR1$^+$ cells to recombinant CCL2 and CCL7 (Figure 4B). Bone marrow-derived cells from tumor-bearing animals 3-week post-implantation displayed statistically significant migration, achieving maximum migration of 500% and 334% at a plating concentration of 10ng/mL and 30ng/mL for CCL2 and CCL7 respectively ($p<0.0001$) (Figure 4B). Cells derived from naïve animals achieved a maximum percent migration to both ligands at a plating concentration of 30ng/mL ($p<0.0001$). These cells displayed a higher efficacy for CCL7 relative to CCL2, achieving a mean percent migration of 559% and 366% to CCL7 and CCL2 respectively (Figure 4C). Distinct from the naïve condition, cells from the tumor-bearing animal migrate to CCL2 with a slightly higher potency as compared to CCL7 and achieve near-maximum migration

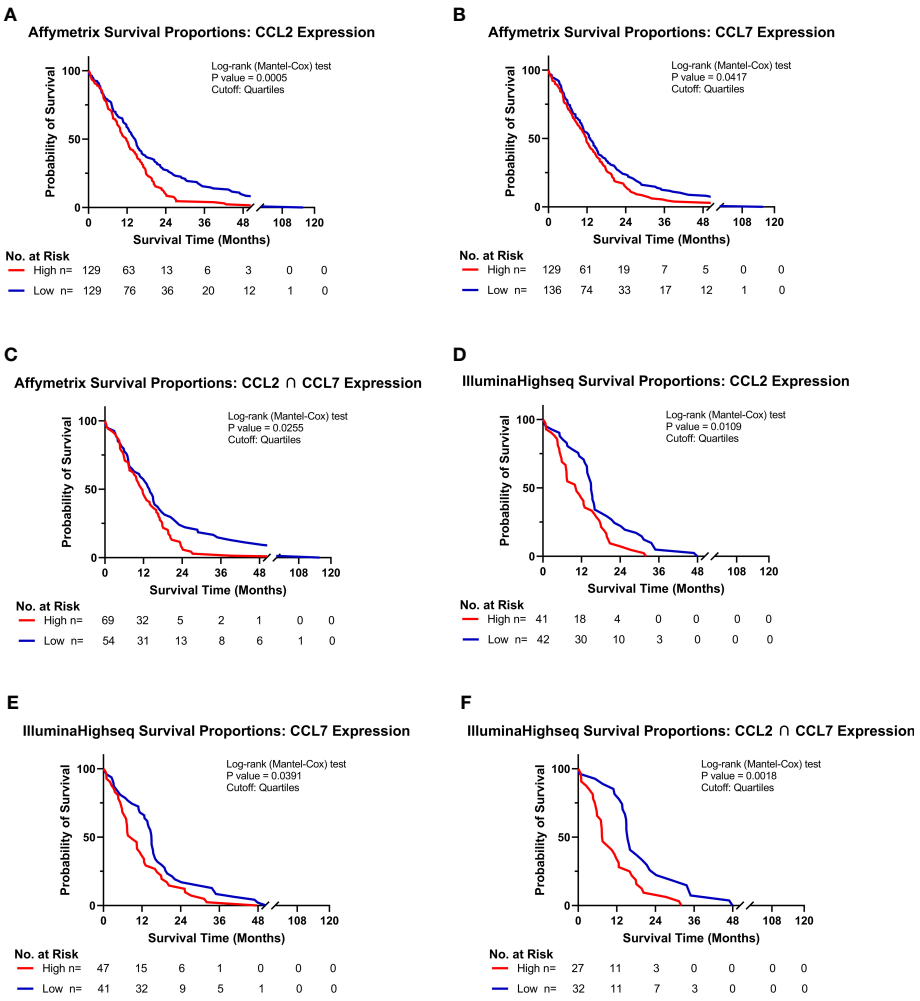

FIGURE 3
High CCL2 and CCL7 expression is associated with negative prognosis for patients with glioblastoma. **(A–C)** Kaplan-Meyer survival curves of GBM patients based on Affymetrix gene expression profiles of **(A)** CCL2 **(B)** CCL7 **(C)** intersection of CCL2 and CCL7 from TCGA database. **(D–F)** Kaplan-Meyer survival curves of GBM patients based on Illumina Highseq expression profiles of **(D)** CCL2 **(E)** CCL7 **(F)** intersection of CCL2 and CCL7 mined from TCGA database. High and low cohorts are stratified as top and bottom quartiles, respectively. Number at risk indicates surviving patients in each cohort at the respective timepoints of analysis. Log-rank (Mantel-Cox) test was conducted on high vs low expressing cohorts.

to both ligands at as low as 3ng/mL of recombinant protein plated in the bottom chamber. There was no noticeable difference in migration efficacy when comparing naïve vs tumor bearing conditions.

To establish that the effect shown through these transwell migration assays was due to chemotaxis (directed cell movement in response to a chemokine gradient) as opposed to increased chemokinetic (random cell movement) activity, recombinant chemokine was plated at equal concentrations in both chambers. Disruption of the chemokine gradient, at 30ng/mL concentrations of ligand prevented migration of bone marrow cells derived from either naïve or tumor-bearing animals (Figures 4B, C). To determine if the migration was dependent on functional CCR2, bone marrow-derived cells from tumor-bearing CCR2-deficient mice ($Ccr2^{RFP/RFP}$) were analyzed for CCL2-dependent migration. RFP-expressing cells from $Ccr2^{RFP/RFP}$ mice did not migrate to any of the CCL2 concentrations tested (Figure 4B). This indicates that CCR2-expressing cells migrate to the chemokines CCL2 and CCL7 in a CCR2-dependent mechanism. Since this cell population also expresses CX3CR1, migration of bone marrow-derived cells from tumor-bearing $Ccr2^{+/RFP}/Cx3cr1^{+/GFP}$ mice to soluble CX3CL1 was assessed. There was no statistically significant migration of $CCR2^{+}/CX3CR1^{+}$ cells to CX3CL1 (Supplementary Figure 6B). Taken together, these results suggest that bone marrow-derived $CCR2^{+}/CX3CR1^{+}$ cells from

10.3389/fimmu.2022.993444

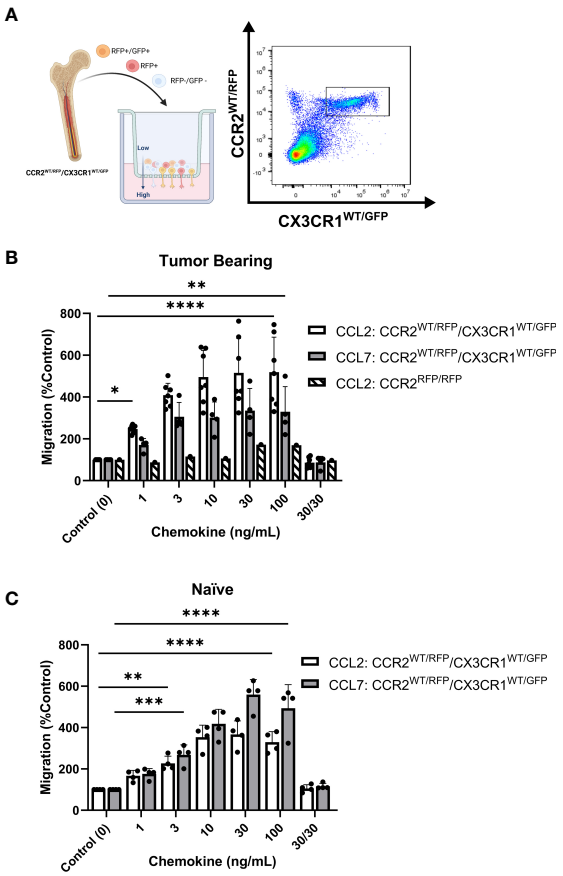

FIGURE 4
Bone marrow-derived CCR2$^+$/CX3CR1$^+$ cells migrate to recombinant CCL2 and CCL7 through CCR2. **(A)** Experimental design of transwell migration assays. Graphic (Created with BioRender.com) depicting assay preparation in which whole bone marrow is plated in the top chamber of the transwell migration plate (left). The bottom chamber contains either recombinant chemokine protein or conditioned media. Representative flow plot depicting the population of CCR2$^+$/CX3CR1$^+$ cells quantified (right). **(B)** Migration to recombinant CCL2 (n=7) and CCL7 (n=4) of CCR2$^+$/CX3CR1$^+$ cells derived from tumor-bearing animals. Graph also depicts no migration to recombinant CCL2 of bone marrow-derived RFP-expressing cells from Ccr2$^{RFP/RFP}$ animals. **(C)** Migration to recombinant CCL2 and CCL7 of CCR2/CX3CR1-expressing cells derived from naïve animals (n=4). A condition in which chemokine was also plated in the top chamber of the transwell plate (30/30) is included to validate that migration is due to chemotaxis rather than chemokinesis. Two-way ANOVA statistical analysis was conducted (Dunnett's multiple comparisons test). Differences are compared to the control (0) condition. p-values: 0.0332(*), 0.0021(**), 0.0002(***), <0.0001(****).

naïve and tumor-bearing animals migrate to CCL2 and CCL7, in a CCR2-dependent manner.

KR158B-CCL2 and -CCL7 knockdown gliomas contain equivalent percentages of CCR2$^+$/CX3CR1$^+$ MDSCs compared to KR158B gliomas

To evaluate whether KR158B tumor cells are active contributors in the recruitment of CCR2$^+$/CX3CR1$^+$ cells, we tested whether glioma cells produced and secreted CCL2 and CCL7. ELISA analysis of the conditioned media of KR158B cells determined that after 24 hours, glioma cells plated at 500 cells/uL had produced 11.1ng/mL of CCL2 and 1.9ng/mL of CCL7. Analysis of KR158B CCL2 knockdown (KR158B CCL2 KD) and KR158B CCL7 knockdown (KR158B CCL7 KD) cell lines revealed a statistically significant decrease in production of CCL2 and CCL7, measured at 2.7ng/mL and 0.8ng/mL respectively ($p<0.0001$) (Supplementary Figure 1).

KR158B, KR158B CCL2 KD or KR158B CCL7 KD glioma cell lines were implanted in *Ccr2*$^{+/RFP}$/*Cx3cr1*$^{+/GFP}$ mice, and flow cytometry analysis of tumors and bone marrow was conducted 4.5 weeks post-implantation (Supplementary Figure 7). We found no significant differences in infiltrating populations of CCR2$^+$/CX3CR1$^+$ cells, induced by KR158B CCL2 KD and KR158B CCL7 KD glioma cell lines, when compared to KR158B (Supplementary Figure 7B). We also saw no changes in the population of CCR2$^+$/CX3CR1$^+$ cells in the bone marrow of mice harboring chemokine knockdown gliomas (Supplementary Figure 7C). *In vitro* proliferation of KR158B CCL2 KD and KR158B CCL7 KD glioma cell lines showed no significant difference compared to KR158B parental cells (Supplementary Figure 7D). Survival of C57BL/6 mice orthotopically implanted with KR158B, KR158B CCL2 KD, and KR158B CCL7 KD glioma cells were also assessed. KR158B implanted mice had a median survival of 45.5 days compared to KR158B CCL2 KD (MS=53.5 days p=0.0298), and KR158B CCL7 KD (MS=48 days p=0.3323) (Supplementary Figure 7E). These results suggest that decreased production of a single CCR2 chemokine ligand by glioma cells does not impact recruitment of CCR2$^+$/CX3CR1$^+$ cells to the TME. The lack of effect observed following the implantation of individual CCL2 or CCL7 knockdown gliomas suggested a potential chemokine ligand redundant mechanism utilized by the KR158B cells to recruit CCR2$^+$/CX3CR1$^+$ cells to the TME.

10.3389/fimmu.2022.993444

CCR2$^+$/CX3CR1$^+$ cell migration to KR158B conditioned media is inhibited with CCL2 and CCL7 neutralizing antibodies

We next sought to determine whether bone marrow-derived CCR2$^+$/CX3CR1$^+$ cells migrate to KR158B conditioned media. Utilizing the same transwell migration assay and flow cytometry gating strategy as described above, conditioned media was plated as the chemoattractant, and migration was analyzed. These results indicate that CCR2$^+$/CX3CR1$^+$ cells migrate significantly to the conditioned media of both the KR158B and KR158B CCL2 KD glioma cell lines. CCR2$^+$/CX3CR1$^+$ cells migrated to the conditioned media of the KR158B cell line with a maximum percent migration of 266% relative to the migration buffer control condition (p=0.0006) (Figure 5A). Consistent with our *in vivo* results (Supplementary Figure 7B), this cell population migrated similarly to the conditioned media of the KR158B CCL2 KD cell line, achieving a maximum percent migration of 242% relative to the control (p=0.004). Of note, statistically significant migration was only achieved in conditions in which the conditioned media of KR158B or KR158B CCL2 KD cells was derived from 24-hour cultures plated at a concentration of 500cells/uL. A positive control with recombinant CCL2 at 10ng/mL as the chemoattractant confirmed the migratory potential of the cells.

Upon validating CCR2$^+$/CX3CR1$^+$ cell migration to the conditioned media of KR158B and KR158B CCL2 KD glioma cell lines, we sought to determine whether the migration was exclusively mediated by CCL2 and/or CCL7. To evaluate this question, we plated KR158B cells at 500cells/uL and collected the conditioned media after 24 hours. The impact of anti-CCL2 or anti-CCL7 neutralizing antibodies or a combination of both was evaluated on migration to the KR158B conditioned media. CCR2$^+$/CX3CR1$^+$ cells migrated significantly to conditioned media containing non-immune IgG with a percent migration of 413% (p<0.0001) (Figure 5B). Neutralizing CCL2 and CCL7 antibodies were validated by inhibiting migration in response to 10ng/mL recombinant protein (Figure 5C). There was no statistically significant difference observed between migration to conditioned media with or without non-immune IgG. In the conditions in which conditioned media was supplemented with a low concentration of neutralizing antibody (10ug/mL αCCL2 or 1ug/mL αCCL7), we observed no significant reduction in overall migration. To determine if migration could be inhibited by supplementing with a higher neutralizing antibody concentration, the conditioned media was supplemented with 50ug/mL αCCL2 or 5ug/mL αCCL7. When supplementing with 50ug/mL αCCL2, a non-significant reduction in percent migration from 413% in the control condition to 240% (p=0.087) was evident. Similarly, when supplementing the conditioned media with the high dose of αCCL7, 5ug/mL, migration was reduced from 413% to 192% (p=0.0085).

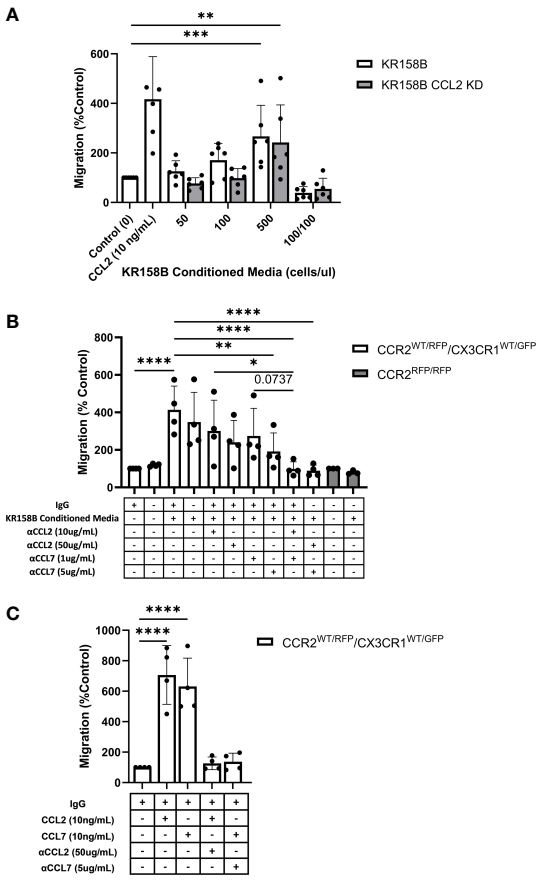

FIGURE 5
Glioma-derived CCL2 or CCL7 is necessary and sufficient for bone marrow-derived CCR2/CX3CR1 cell migration. **(A)** Graph depicting CCR2$^+$/CX3CR1$^+$ cells migrating to conditioned media of KR158B (n=6) and KR158B CCL2 knockdown (n=6) cells. A condition in which conditioned media was also plated in the top chamber of the transwell plate (100/100) is included to validate that migration is due to chemotaxis rather than chemokinesis. **(B)** Migration of CCR2$^+$/CX3CR1$^+$ cells to conditioned media in the presence or absence of chemokine-neutralizing antibodies. Migration is disrupted with the addition of high concentrations of single neutralizing antibody. Migration is completely inhibited with a combination of neutralizing antibodies at either low or high concentrations (n=4). No migration was observed to conditioned media of bone marrow-derived RFP-expressing cells from *Ccr2$^{RFP/RFP}$* animals (n=3). **(C)** Graph depicting that migration to exogenous recombinant CCL2 or CCL7 is inhibited through the addition of high concentrations of respective neutralizing antibody (n=4). Two-way ANOVA statistical analysis was conducted (Dunnett's multiple comparisons test). Differences are compared to the control condition or between cell lines. p-values: 0.0332(*), 0.0021(**), 0.0002(***), <0.0001 (****).

As CCR2$^+$/CX3CR1$^+$ cells migrate similarly to CCL2 and CCL7, we then assessed whether there was redundancy between the chemokines that would facilitate cell migration in the event that one ligand was neutralized. To evaluate this, the conditioned media was supplemented with either low combinations (10ug/

mL αCCL2 and 1ug/mL αCCL7) or high combinations (50ug/mL αCCL2 and 5ug/mL αCCL7) of neutralizing antibodies. Interestingly, supplementing with either the low or high combination of neutralizing antibodies resulted in complete inhibition of migration. In the case of the low neutralizing antibody combination, $CCR2^+/CX3CR1^+$ cells achieved 99% migration, whereas cells in the high neutralizing antibody condition reached only 89% migration compared to the migration buffer control normalized to 100% ($p<0.0001$) (Figure 5B). There was a significant reduction in migration between 10ug/mL αCCL2 condition and low combination (10ug/mL αCCL2 and 1ug/mL αCCL7) ($p=0.0215$). There was a non-significant reduction in migration from 274% to 98% between 1ug/mL αCCL7 condition and low combination (10ug/mL αCCL2 and 1ug/mL αCCL7) ($p=0.0737$) (Figure 5B). Neutralizing CCL2 and CCL7 antibodies were validated by inhibiting migration in response to 10ng/mL recombinant protein (Figure 5C). These results suggest that complete inhibition of migration is a result of combining neutralizing antibodies to CCL2 and CCL7.

To confirm that CCR2 was responsible for the migration of $CCR2^+/CX3CR1^+$ cells to KR158B conditioned media, bone marrow cells derived from a *Ccr2*-deficient mouse were utilized. Using conditioned media as the chemoattractant, no statistically significant migration of RFP-expressing cells to conditioned media, as compared to the buffer control, was seen (Figure 6B). Taken

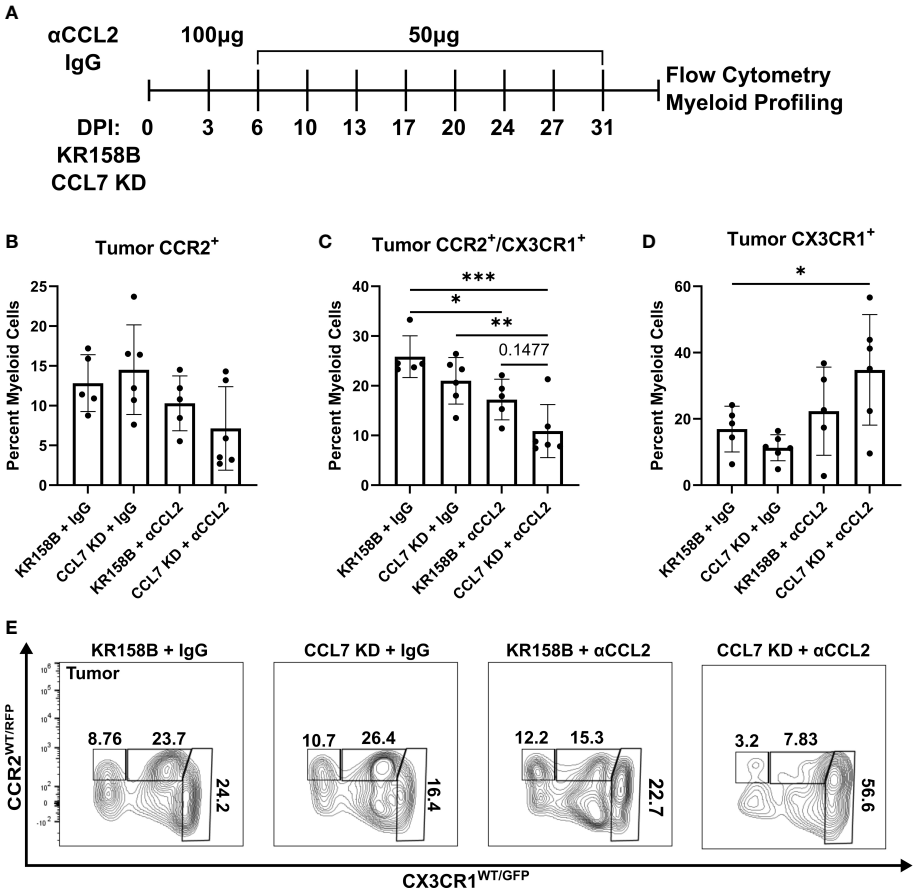

FIGURE 6
Infiltration of $CCR2^+/CX3CR1^+$ cells into the glioma is reduced upon combination targeting of CCL2 and CCL7. **(A)** Treatment schematic for targeting CCL2 and CCL7 in KR158B or KR158B CCL7 KD gliomas. Anti-CCL2 antibody loading dose of 100µg was administered 3 days post implantation (DPI). Subsequent maintenance doses of 50µg were administered twice weekly. Non-immune IgG was used as a control. A total of 4 arms were evaluated: KR158B treated with IgG control, KR158B CCL7 KD treated with IgG control, KR158B treated with anti-CCL2 antibody, and KR158B CCL7 KD treated with anti-CCL2 antibody. **(B)** Graph depicting percentage of infiltrating live, $CD45^+$, $CD11b^+$, $CCR2^+$ only cells within the tumor. **(C)** live, $CD45^+$, $CD11b^+$, $CCR2^+/CX3CR1^+$ cells within the tumor **(D)** live, $CD45^+$, $CD11b^+$, $CX3CR1^+$ only cells within the tumor. **(E)** Representative flow plot for panels B-D depicting reduction of $CCR2^+/CX3CR1^+$ population within the tumor (n=5-6 per arm). Example gating strategy can be found in Supplementary Figure 11A. Two-way ANOVA statistical analysis was conducted (Dunnett's multiple comparisons test). Differences are compared to the control condition or between cell lines. p-values: 0.0332(*), 0.0021(**), 0.0002(***).

together, these results show that CCR2$^+$/CX3CR1$^+$ cells migrate to CCL2 and CCL7 produced by KR158B cells through CCR2, and this migration can be prevented through pharmacologic or genetic disruption of this chemokine-receptor axis.

Combination targeting of CCL2 and CCL7 reduced CCR2$^+$/CX3CR1$^+$ cells in the glioma microenvironment

To test the concept that CCL2 and CCL7 drive the recruitment of CCR2$^+$/CX3CR1$^+$ cells into the glioma microenvironment, we took a combinatorial targeting approach *in vivo*. KR158B and KR158B CCL7 KD glioma cells were orthotopically implanted in *Ccr2*$^{WT/RFP}$/*Cx3cr1*$^{WT/GFP}$ mice. KR158B CCL7 KD cells were confirmed to have lower levels of secreted CCL7 measured by ELISA compared to its parental KR158B counterpart (Supplementary Figure 1). Mice were then administered either non-immune IgG (control) or anti-CCL2 antibody over 4 weeks (Figure 6A) since CCL2 neutralizing antibodies have been widely tested *in vivo* (33–35). CCR2 and CX3CR1 expressing cell populations were assessed *via* flow cytometry within the glioma microenvironment as well as non-tumor peripheral tissues: blood, spleen, and bone marrow. KR158B tumors that were administered IgG harbored a mean 12.8 percent infiltrating CCR2$^+$ only cells among the total myeloid population (live, CD45$^+$, CD11b$^+$). KR158B CCL7 KD tumors that were administered anti-CCL2 antibody displayed a non-significant (mean=7.13, p=0.1419) reduction within this CCR2$^+$ population (Figures 6B, E). Conversely, there was a significant reduction (p=0.003) from mean 25.8% to mean 10.8% glioma infiltrating CCR2$^+$/CX3CR1$^+$ cells when comparing KR158B + IgG vs. CCL7 KD + αCCL2 antibody arms (Figures 6C, E). KR158B + αCCL2 vs. CCL7 KD + αCCL2 antibody arms displayed a non-significant reduction of CCR2$^+$/CX3CR1$^+$ cells from mean 17.2% to mean 10.8% (p=0.1477) (Figures 6C, E). There was a significant increase among the CX3CR1$^+$ only population when comparing KR158B + IgG (mean=16.9) vs. CCL7 KD + αCCL2 (mean=34.8) antibody arms (p=0.048) (Figures 6D, E). There were no significant changes among these CCR2- and CX3CR1-expressing populations in the non-tumor peripheral tissues examined (Supplementary Figure 8). These results show that combination targeting the CCR2/CCL2/CCL7 axis in KR158B gliomas reduces infiltrating CCR2$^+$/CX3CR1$^+$ cells.

Discussion

Glioblastoma is a highly aggressive disease which exhibits a significant immune suppressed tumor microenvironment, lending to its poor prognosis (36–40). Although representing a diverse population in itself, infiltrating myeloid cell populations contribute to the suppressed environment and promote tumor growth (7, 8, 41–43). Our earlier studies established that CCR2$^+$/CX3CR1$^+$ myeloid cells, characterized by M-MDSC markers (CD45, CD11b, Ly6C^{hi}, and lack Ly6G), are present in the bone marrow and infiltrate into multiple murine gliomas (KR158B and 005 GSC). Moreover, genetic and pharmacologic inhibition of CCR2 reduces the presence of these CD45$^+$, CD11b$^+$, Ly6C^{hi}, Ly6G$^-$ cells in the TME, promotes sequestration of the cells in the bone marrow, and unmasks an effect of an immune checkpoint inhibitor to slow glioma progression (28). While these prior studies clearly support targeting CCR2$^+$/CX3CR1$^+$ cells as a means to treat gliomas, a greater appreciation of the immune suppressive and migratory properties of this CCR2$^+$/CX3CR1$^+$ cell population is needed. Herein, we extend our published results to better understand the functionality of these cells. The principal findings of this study are 1) glioma-associated CCR2$^+$/CX3CR1$^+$ myeloid cells are sourced from the bone marrow, 2) CCR2$^+$/CX3CR1$^+$ cells suppress both CD4$^+$ and CD8$^+$ T cells 3) CCR2$^+$/CX3CR1$^+$ cells migrate to recombinant and glioma-produced CCL2 and CCL7 in a redundant manner 4) and dual targeting CCL2 and CCL7 reduces these cells in the glioma.

Brain tumors, and particularly gliomas, contain mixed populations of myeloid cells (44–48). Our previous report provided a comprehensive analysis of the phenotypic markers expressed by myeloid cells in the glioma microenvironment of both KR158B and 005 GSC intracranial tumors. Glioma-associated myeloid cells can be distinguished by relative CD45 expression, with microglia and peripherally sourced cells expressing mid and high levels of this marker, respectively (28, 49). In addition, forward scatter properties also distinguish microglia from peripheral tumor-associated macrophages. We established that bone marrow and glioma-associated CD45^{high}, CD11b$^+$, Ly6C^{hi}/Ly6G$^-$ cells co-express CCR2 and CX3CR1. This bone marrow population expands in tumor bearing mice and pharmacological or genetic disruption of CCR2 promotes the sequestration of these cells in the bone marrow (28). Using a chimeric mouse paradigm, we formally established that the CCR2$^+$/CX3CR1$^+$ population is derived from the bone marrow. These findings suggest an involvement of CCR2, upon stimulation by its ligands, in facilitating the trafficking of CCR2$^+$/CX3CR1$^+$ cells from the bone marrow to the TME.

CCR2$^+$ M-MDSCs represent a prominent infiltrating immune suppressive cell population within murine gliomas (32, 50). Their elevated presence has shown to be correlated with negative prognosis and poor response to prospective immunotherapy approaches such as immune-checkpoint inhibitors (9, 24). Data reported here establish that CCR2$^+$/CX3CR1$^+$ M-MDSCs are directly involved in disrupting the proliferation and activated function of both CD4 and CD8-expressing T cells. CCR2$^+$/CX3CR1$^+$ M-MDSCs suppressed both T cell populations with similar potency. These ex vivo studies are consistent with our prior results where combined PD-1 and CCR2 blockade led to decreased numbers of exhausted

$CD4^+$ and $CD8^+$ T cells and increased IFN-γ expression within the gliomas. Further studies will be necessary to better understand direct and indirect mechanisms whereby $CCR2^+$/$CX3CR1^+$ M-MDSCs disrupt T cell function and dampen immune responses in the context of glioma. Nonetheless, these data provide further rationale for preventing the infiltration of these immunosuppressive cells into the TME.

CCR2 is a receptor that, among other functions, is primarily implicated in the chemotaxis of cells on which it is expressed (34, 51). A common feature amongst many chemokine receptors is the ability to be stimulated by multiple structurally similar ligands. CCR2 is no exception with five known ligands: CCL2, CCL7, CCL8, CCL13 and CCL16 (52). This feature facilitates functional redundancy in that multiple ligands may induce similar downstream cellular effects upon signaling through the same receptor. While CCL2 has previously been reported as the most potent inducer of $CCR2^+$ monocyte migration, other CCR2 ligands are likely contributing to migration in a redundant manner to respond to inflammation (53). Brait et al. reported elevated levels of CCL7, in addition to CCL2, in models of ischemia reperfusion (54). These findings suggest that CCL2 and CCL7 may function in a redundant manner to recruit CCR2-expressing cells to sites of inflammation. Additional studies have also reported that the accumulation of myeloid cells within the CNS during inflammation is dependent upon the presence of CCL2 and CCL7. In a CCL2- and CCL7-deficient mouse model, there was a significant reduction in $CD45^+$/$CD11b^+$/$Ly6C^{hi}$ cells that accumulated in the CNS; the markers that characterize this population coincide with $CCR2^+$/$CX3CR1^+$ cells in the model utilized here. This suggests that in addition to having functional CCR2, it is also necessary to maintain sufficient levels of the cognate ligands to ultimately induce accumulation of this cell population in the CNS (55). Other chemokine:chemokine receptor systems appear to have redundant roles, determined from studies in murine glioma models, including CCR1 and CCR5 and their shared ligands (56, 57). While we report redundant roles for CCL2 and CCL7, there may be spatiotemporal regulation of CCR2-expressing cells by these individual ligands. For instance, one chemokine, i.e., CCL2, might be the prominent driver of $CCR2^+$/$CX3CR1^+$ cell recruitment to the tumor, while the second, i.e., CCL7, is more important for homing to specific niches within tumor. It is known that CCL2 and CCL7 are expressed by tumor and non-tumor cells within the glioma microenvironment. For example, macrophages and microglia have been shown to express CCL2 while astrocytes are reported to produce CCL7 (32, 58). Further investigation is needed to distinguish the impact of tumor vs non-neoplastic derived chemokines in the recruitment of immune cell populations. Although soluble CX3CL1 did not stimulate migration of the MDSCs, a role for membrane attached CX3CL1 in firm adhesion of the cells to endothelium within the tumor vasculature remains a possibility (59, 60). Additional studies aimed toward determining specific CCL2-, CCL7-, and CX3CL1-expressing areas and cell types within the tumor would need to be conducted to support these concepts.

In conclusion, we determined that CCR2 and its cognate ligands are prominent regulators of the recruitment of a $CCR2^+$/$CX3CR1^+$ immune suppressive cell to gliomas. The expression and functional characterization of these chemokine receptors further defines the M-MDSC phenotype. CCL2 and CCL7 are produced, at least in part, by glioma cells and our study indicates that CCL2 and CCL7 function in a redundant manner to induce the migration of $CCR2^+$/$CX3CR1^+$ M-MDSCs into the glioma microenvironment. As such, a more effective approach to limiting this population from gaining access to the TME should involve antagonizing CCR2. However, given that high CCL2 and CCL7 expression is associated with poorer prognosis in GBM patients, consideration of the relative expression of these two chemokines may provide predictive value to a therapeutic strategy targeting this chemokine:chemokine receptor axis.

Data availability statement

The raw data supporting the conclusions of this article will be made available by the authors, without undue reservation.

Ethics statement

The animal study was reviewed and approved by The University of Florida Institutional Animal Care and Use Committee (IACUC).

Author contributions

GT and CK: Designed the study, performed experiments, data analysis, data interpretation, and wrote the manuscript. DL, JSG-performed experiments. GT: Performed experiments, data analysis. LPD-designed the study, data interpretation, and wrote the manuscript. DM: Designed the study, data interpretation, and wrote the manuscript. JH: Designed the study, data interpretation, and wrote the manuscript. All authors contributed to the article and approved the submitted version.

Funding

Research reported in this publication was supported by National Institute of Health grant RO1 NS108781 (to JKH and DAM), Florida Center for Brain Tumor Research (to JKH), as well as the National Center for Advancing Translational Sciences of the National Institutes of Health under University of Florida Clinical and Translational Science Awards TL1TR001428 and UL1TR001427 (to GPT).

Acknowledgments

We thank Joseph Flores-Toro for providing insight and technical assistance in generating chimeric mice and flow cytometry as well as members of Jeffrey Martens' lab, Department of Pharmacology & Therapeutics at the University of Florida College of Medicine, for access and training on Nikon Confocal Microscope. We gratefully acknowledge the University of Florida Interdisciplinary Center for Biotechnology Research Flow Cytometry Core and University of Florida Animal Care Service.

Conflict of interest

The authors declare that the research was conducted in the absence of any commercial or financial relationships that could be construed as a potential conflict of interest.

Publisher's note

Supplementary material

The Supplementary Material for this article can be found online at: https://www.frontiersin.org/articles/10.3389/fimmu.2022.993444/full#supplementary-material

References

1. Weller M, Cloughesy T, Perry JR, Wick W. Standards of care for treatment of recurrent glioblastoma–are we there yet? *Neuro-Oncology* (2013) 15(1):4–27. doi: 10.1093/neuonc/nos273

2. van Solinge TS, Nieland L, Chiocca EA, Broekman MLD. Advances in local therapy for glioblastoma — taking the fight to the tumour. *Nat Rev Neurol* (2022) 18(4):221–36. doi: 10.1038/s41582-022-00621-0

3. Stupp R, Mason WP, van den Bent MJ, Weller M, Fisher B, Taphoorn MJB, et al. Radiotherapy plus concomitant and adjuvant temozolomide for glioblastoma. *N Engl J Med* (2005) 352(10):987–96. doi: 10.1056/NEJMoa043330

4. Stupp R, Taillibert S, Kanner AA, Kesari S, Steinberg DM, Toms SA, et al. Maintenance therapy with tumor-treating fields plus temozolomide vs temozolomide alone for glioblastoma: A randomized clinical trial. *JAMA* (2015) 314(23):2535–43. doi: 10.1001/jama.2015.16669

5. Stupp R, Hegi ME, Mason WP, van den Bent MJ, Taphoorn MJB, Janzer RC, et al. Effects of radiotherapy with concomitant and adjuvant temozolomide versus radiotherapy alone on survival in glioblastoma in a randomised phase III study: 5-year analysis of the EORTC-NCIC trial. *Lancet Oncol* (2009) 10(5):459–66. doi: 10.1016/S1470-2045(09)70025-7

6. Ravi VM, Neidert N, Will P, Joseph K, Maier JP, Kückelhaus J, et al. T-Cell dysfunction in the glioblastoma microenvironment is mediated by myeloid cells releasing interleukin-10. *Nat Commun* (2022) 13(1):925. doi: 10.1038/s41467-022-28523-1

7. Wainwright DA, Balyasnikova IV, Chang AL, Ahmed AU, Moon KS, Auffinger B, et al. IDO expression in brain tumors increases the recruitment of regulatory T cells and negatively impacts survival. *Clin Cancer Res* (2012) 18 (22):6110–21. doi: 10.1158/1078-0432.CCR-12-2130

8. Wesolowska A, Kwiatkowska A, Slomnicki L, Dembinski M, Master A, Sliwa M, et al. Microglia-derived TGF-beta as an important regulator of glioblastoma invasion–an inhibition of TGF-beta-dependent effects by shRNA against human TGF-beta type II receptor. *Oncogene* (2008) 27(7):918–30. doi: 10.1038/sj.onc.1210683

9. Alban TJ, Alvarado AG, Sorensen MD, Bayik D, Volovetz J, Serbinowski E, et al. Global immune fingerprinting in glioblastoma patient peripheral blood reveals immune-suppression signatures associated with prognosis. *JCI Insight* (2018) 3(21):122264. doi: 10.1172/jci.insight.122264

10. Mellman I, Coukos G, Dranoff G. Cancer immunotherapy comes of age. *Nature* (2011) 480(7378):480–9. doi: 10.1038/nature10673

11. Waldman AD, Fritz JM, Lenardo MJ. A guide to cancer immunotherapy: from T cell basic science to clinical practice. *Nat Rev Immunol* (2020) 20(11):651–68. doi: 10.1038/s41577-020-0306-5

12. Gupta R, Mehta A, Wajapeyee N. Transcriptional determinants of cancer immunotherapy response and resistance. *Trends Cancer.* (2022) 8(5):404–15. doi: 10.1016/j.trecan.2022.01.008

13. *Bristol Myers Squibb Announces update on phase 3 CheckMate -548 trial evaluating patients with newly diagnosed MGMT-methylated glioblastoma multiforme* (2021). Available at: https://news.bms.com/news/details/2020/Bristol-Myers-Squibb-Announces-Update-on-Phase-3-CheckMate–548-Trial-Evaluating-Patients-with-Newly-Diagnosed-MGMT-Methylated-Glioblastoma-Multiforme/default.aspx.

14. Reardon DA, Brandes AA, Omuro A, Mulholland P, Lim M, Wick A, et al. Effect of nivolumab vs bevacizumab in patients with recurrent glioblastoma: The CheckMate 143 phase 3 randomized clinical trial. *JAMA Oncol* (2020) 6(7):1003–10. doi: 10.1001/jamaoncol.2020.1024

15. Kamran N, Kadiyala P, Saxena M, Candolfi M, Li Y, Moreno-Ayala MA, et al. Immunosuppressive myeloid cells' blockade in the glioma microenvironment enhances the efficacy of immune-stimulatory gene therapy. *Mol Ther* (2017) 25 (1):232–48. doi: 10.1016/j.ymthe.2016.10.003

16. Kamran N, Chandran M, Lowenstein PR, Castro MG. Immature myeloid cells in the tumor microenvironment: Implications for immunotherapy. *Clin Immunol* (2018) 189:34–42. doi: 10.1016/j.clim.2016.10.008

17. Kumar R, de MT, TE P, Kaptzan T, AJ J, DJ D, et al. Modulating glioma-mediated myeloid-derived suppressor cell development with sulforaphane. *PloS One* (2017) 12(6):e0179012. doi: 10.1371/journal.pone.0179012

18. Veglia F, Sanseviero E, Gabrilovich DI. Myeloid-derived suppressor cells in the era of increasing myeloid cell diversity. *Nat Rev Immunol* (2021) 1:1–14. doi: 10.1038/s41577-020-00490-y

19. Bronte V, Brandau S, Chen SH, Colombo MP, Frey AB, Greten TF, et al. Recommendations for myeloid-derived suppressor cell nomenclature and characterization standards. *Nat Commun* (2016) 7(1):1–10. doi: 10.1038/ncomms12150

20. Kwak T, Wang F, Deng H, Condamine T, Kumar V, Perego M, et al. Distinct populations of immune-suppressive macrophages differentiate from monocytic myeloid-derived suppressor cells in cancer. *Cell Rep* (2020) 33(13):108571. doi: 10.1016/j.celrep.2020.108571

21. Dorhoi A, Du Plessis N. Monocytic myeloid-derived suppressor cells in chronic infections. *Front Immunol* (2018) 8:1895. doi: 10.3389/fimmu.2017.01895

22. Yang Y, Li C, Liu T, Dai X, Bazhin AV. Myeloid-derived suppressor cells in tumors: From mechanisms to antigen specificity and microenvironmental regulation. *Front Immunol* (2020) 11:1371. doi: 10.3389/fimmu.2020.01371

23. Tcyganov EN, Hanabuchi S, Hashimoto A, Campbell D, Kar G, Slidel TW, et al. Distinct mechanisms govern populations of myeloid-derived suppressor cells in chronic viral infection and cancer. *J Clin Invest.* (2021) 131(16):145971. doi: 10.1172/JCI145971

24. Raychaudhuri B, Rayman P, Huang P, Grabowski M, Hambardzumyan D, Finke JH, et al. Myeloid derived suppressor cell infiltration of murine and human

gliomas is associated with reduction of tumor infiltrating lymphocytes. *J Neurooncol.* (2015) 122(2):293–301. doi: 10.1007/s11060-015-1720-6

25. Bergenfelz C, Leandersson K. The generation and identity of human myeloid-derived suppressor cells. *Front Oncol* (2020) 10:109. doi: 10.3389/fonc.2020.00109

26. Alban TJ, Bayik D, Otvos B, Rabljenovic A, Leng L, Jia-Shiun L, et al. Glioblastoma myeloid-derived suppressor cell subsets express differential macrophage migration inhibitory factor receptor profiles that can be targeted to reduce immune suppression. *Front Immunol* (2020) 11:1191. doi: 10.3389/fimmu.2020.01191

27. Riva M, Wouters R, Sterpin E, Giovannoni R, Boon L, Himmelreich U, et al. Radiotherapy, temozolomide, and antiprogrammed cell death protein 1 treatments modulate the immune microenvironment in experimental high-grade glioma. *Neurosurgery* (2021) 88(2):E205. doi: 10.1093/neuros/nyaa421

28. Flores-Toro JA, Luo D, Gopinath A, Sarkisian MR, Campbell JJ, Charo IF, et al. CCR2 inhibition reduces tumor myeloid cells and unmasks a checkpoint inhibitor effect to slow progression of resistant murine gliomas. *Proc Natl Acad Sci U S A.* (2020) 117(2):1129–38. doi: 10.1073/pnas.1910856117

29. Bhuvaneshwar K, Belouali A, Singh V, Johnson RM, Song L, Alaoui A, et al. G-DOC plus - an integrative bioinformatics platform for precision medicine. *BMC Bioinf* (2016) 17(1):193. doi: 10.1186/s12859-016-1010-0

30. Madhavan S, Gusev Y, Harris M, Tanenbaum DM, Gauba R, Bhuvaneshwar K, et al. G-DOC: a systems medicine platform for personalized oncology. *Neoplasia* (2011) 13(9):771–83. doi: 10.1593/neo.11806

31. Goldman MJ, Craft B, Hastie M, Repečka K, McDade F, Kamath A, et al. Visualizing and interpreting cancer genomics data *via* the xena platform. *Nat Biotechnol* (2020) 38(6):675–8. doi: 10.1038/s41587-020-0546-8

32. Chang AL, Miska J, Wainwright DA, Dey M, Rivetta CV, Yu D, et al. CCL2 produced by the glioma microenvironment is essential for the recruitment of regulatory T cells and myeloid-derived suppressor cells. *Cancer Res* (2016) 76 (19):5671–82. doi: 10.1158/0008-5472.CAN-16-0144

33. Liu C, Yang Y, Chen C, Li L, Li J, Wang X, et al. Environmental eustress modulates β-ARs/CCL2 axis to induce anti-tumor immunity and sensitize immunotherapy against liver cancer in mice. *Nat Commun* (2021) 12(1):5725. doi: 10.1038/s41467-021-25967-9

34. Gschwandtner M, Derler R, Midwood KS. More than just attractive: How CCL2 influences myeloid cell behavior beyond chemotaxis. *Front Immunol* (2019) 10:2759. doi: 10.3389/fimmu.2019.02759

35. Zhu X, Fujita M, Snyder LA, Okada H. Systemic delivery of neutralizing antibody targeting CCL2 for glioma therapy. *J Neurooncol.* (2011) 104(1):83–92. doi: 10.1007/s11060-010-0473-5

36. Hishii M, Nitta T, Ishida H, Ebato M, Kurosu A, Yagita H, et al. Human glioma-derived interleukin-10 inhibits antitumor immune responses in vitro. *Neurosurgery* (1995) 37(6):1160–6. doi: 10.1227/00006123-199512000-00016

37. Qian J, Luo F, Yang J, Liu J, Liu R, Wang L, et al. TLR2 promotes glioma immune evasion by downregulating MHC class II molecules in microglia. *Cancer Immunol Res* (2018) 6(10):1220–33. doi: 10.1158/2326-6066.CIR-18-0020

38. Ikushima H, Todo T, Ino Y, Takahashi M, Miyazawa K, Miyazono K. Autocrine TGF-beta signaling maintains tumorigenicity of glioma-initiating cells through sry-related HMG-box factors. *Cell Stem Cell* (2009) 5(5):504–14. doi: 10.1016/j.stem.2009.08.018

39. Joseph JV, Balasubramaniyan V, Walenkamp A, Kruyt FAE. TGF-β as a therapeutic target in high grade gliomas - promises and challenges. *Biochem Pharmacol* (2013) 85(4):478–85. doi: 10.1016/j.bcp.2012.11.005

40. Nduom EK, Weller M, Heimberger AB. Immunosuppressive mechanisms in glioblastoma. *Neuro Oncol* (2015) 17(Suppl 7):vii9–14. doi: 10.1093/neuonc/nov151

41. Gabrusiewicz K, Ellert-Miklaszewska A, Lipko M, Sielska M, Frankowska M, Kaminska B. Characteristics of the alternative phenotype of microglia/macrophages and its modulation in experimental gliomas. *PloS One* (2011) 6(8): e23902. doi: 10.1371/journal.pone.0023902

42. Avril T, Saikali S, Vauleon E, Jary A, Hamlat A, De Tayrac M, et al. Distinct effects of human glioblastoma immunoregulatory molecules programmed cell death ligand-1 (PDL-1) and indoleamine 2,3-dioxygenase (IDO) on tumour-specific T cell functions. *J Neuroimmunol.* (2010) 225(1–2):22–33. doi: 10.1016/j.jneuroim.2010.04.003

43. Chen Z, Hambardzumyan D. Immune microenvironment in glioblastoma subtypes. *Front Immunol* (2018) 9:1004. doi: 10.3389/fimmu.2018.01004

44. Friebel E, Kapolou K, Unger S, Núñez NG, Utz S, Rushing EJ, et al. Single-cell mapping of human brain cancer reveals tumor-specific instruction of tissue-invading leukocytes. *Cell* (2020) 181(7):1626–1642.e20. doi: 10.1016/j.cell.2020.04.055

45. Pombo Antunes AR, Scheyltjens I, Lodi F, Messiaen J, Antoranz A, Duerinck J, et al. Single-cell profiling of myeloid cells in glioblastoma across species and disease stage reveals macrophage competition and specialization. *Nat Neurosci* (2021) 24(4):595–610. doi: 10.1038/s41593-020-00789-y

46. Yuan J, Levitin HM, Frattini V, Bush EC, Boyett DM, Samanamud J, et al. Single-cell transcriptome analysis of lineage diversity in high-grade glioma. *Genome Med* (2018) 10(1):57. doi: 10.1186/s13073-018-0567-9

47. Mantovani A, Marchesi F, Jaillon S, Garlanda C, Allavena P. Tumor-associated myeloid cells: diversity and therapeutic targeting. *Cell Mol Immunol* (2021) 18(3):566–78. doi: 10.1038/s41423-020-00613-4

48. Klemm F, Maas RR, Bowman RL, Kornete M, Soukup K, Nassiri S, et al. Interrogation of the microenvironmental landscape in brain tumors reveals disease-specific alterations of immune cells. *Cell* (2020) 181(7):1643–60. doi: 10.1016/j.cell.2020.05.007

49. Chen Z, Feng X, Herting CJ, Garcia VA, Nie K, Pong WW, et al. Cellular and molecular identity of tumor-associated macrophages in glioblastoma. *Cancer Res* (2017) 77(9):2266–78. doi: 10.1158/0008-5472.CAN-16-2310

50. Alghamri MS, Banerjee K, Mujeeb AA, Mauser A, Taher A, Thalla R, et al. Systemic delivery of an adjuvant CXCR4–CXCL12 signaling inhibitor encapsulated in synthetic protein nanoparticles for glioma immunotherapy. *ACS Nano.* (2022) 16(6):8729–50. doi: 10.1021/acsnano.1c07492

51. Takacs GP, Flores-Toro JA, Harrison JK. Modulation of the chemokine/chemokine receptor axis as a novel approach for glioma therapy. *Pharmacol Ther* (2021) 222:107790. doi: 10.1016/j.pharmthera.2020.107790

52. Proudfoot AEI. Chemokine receptors: multifaceted therapeutic targets. *Nat Rev Immunol* (2002) 2(2):106–15. doi: 10.1038/nri722

53. Chu HX, Arumugam TV, Gelderblom M, Magnus T, Drummond GR, Sobey CG. Role of CCR2 in inflammatory conditions of the central nervous system. *J Cereb Blood Flow Metab* (2014) 34(9):1425–9. doi: 10.1038/jcbfm.2014.120

54. Brait VH, Rivera J, Broughton BRS, Lee S, Drummond GR, Sobey CG. Chemokine-related gene expression in the brain following ischemic stroke: No role for CXCR2 in outcome. *Brain Res* (2011) 1372:169–79. doi: 10.1016/j.brainres.2010.11.087

55. Bardina SV, Michlmayr D, Hoffman KW, Obara CJ, Sum J, Charo IF, et al. Differential roles of chemokines CCL2 and CCL7 in monocytosis and leukocyte migration during West Nile virus infection. *J Immunol* (2015) 195(9):4306–18. doi: 10.4049/jimmunol.1500352

56. Pham K, Luo D, Liu C, Harrison JK. CCL5, CCR1 and CCR5 in murine glioblastoma: immune cell infiltration and survival rates are not dependent on individual expression of either CCR1 or CCR5. *J Neuroimmunol.* (2012) 246(1–2):10–7. doi: 10.1016/j.jneuroim.2012.02.009

57. Dyer DP. Understanding the mechanisms that facilitate specificity, not redundancy, of chemokine-mediated leukocyte recruitment. *Immunology* (2020) 160(4):336–44. doi: 10.1111/imm.13200

58. Rath BH, Fair JM, Jamal M, Camphausen K, Tofilon PJ. Astrocytes enhance the invasion potential of glioblastoma stem-like cells. *PloS One* (2013) 8(1):e54752. doi: 10.1371/journal.pone.0054752

59. Umehara H, Goda S, Imai T, Nagano Y, Minami Y, Tanaka Y, et al. Fractalkine, a CX3C-chemokine, functions predominantly as an adhesion molecule in monocytic cell line THP-1. *Immunol Cell Biol* (2001) 79(3):298–302. doi: 10.1046/j.1440-1711.2001.01004.x

60. Ostuni MA, Hermand P, Saindoy E, Guillou N, Guellec J, Coens A, et al. CX3CL1 homo-oligomerization drives cell-to-cell adherence. *Sci Rep* (2020) 10 (1):9069. doi: 10.1038/s41598-020-65988-w

frontiers | Frontiers in Immunology

TYPE Review
PUBLISHED 04 September 2023
DOI 10.3389/fimmu.2023.1238233

OPEN ACCESS

EDITED BY
Riccardo Dolcetti,
Peter MacCallum Cancer Centre, Australia

REVIEWED BY
Dalia Haydar,
Children's National Hospital, United States
Theo Mantamadiotis,
The University of Melbourne, Australia

*CORRESPONDENCE
Gao Zhang
gaozhang@hku.hk
Shiyou Wei
weishiyouscu@163.com

RECEIVED 11 June 2023
ACCEPTED 21 August 2023
PUBLISHED 04 September 2023

CITATION
Zhang L, Jiang Y, Zhang G and Wei S (2023) The diversity and dynamics of tumor-associated macrophages in recurrent glioblastoma.
Front. Immunol. 14:1238233.
doi: 10.3389/fimmu.2023.1238233

The diversity and dynamics of tumor-associated macrophages in recurrent glioblastoma

Lingyun Zhang[1,2], Yu Jiang[3], Gao Zhang[4]* and Shiyou Wei[1]*

[1]Institute of Thoracic Oncology and Department of Thoracic Surgery, West China Hospital, Sichuan University, Chengdu, China, [2]School of Biomedical Sciences, The Chinese University of Hong Kong, Hong Kong, Hong Kong SAR, China, [3]Department of Neurosurgery, West China Hospital, Sichuan University, Chengdu, China, [4]Faculty of Dentistry, The University of Hong Kong, Sai Ying Pun, Hong Kong, Hong Kong SAR, China

Despite tremendous efforts to exploit effective therapeutic strategies, most glioblastoma (GBM) inevitably relapse and become resistant to therapies, including radiotherapy and immunotherapy. The tumor microenvironment (TME) of recurrent GBM (rGBM) is highly immunosuppressive, dominated by tumor-associated macrophages (TAMs). TAMs consist of tissue-resident microglia and monocyte-derived macrophages (MDMs), which are essential for favoring tumor growth, invasion, angiogenesis, immune suppression, and therapeutic resistance; however, restricted by the absence of potent methods, the heterogeneity and plasticity of TAMs in rGBM remain incompletely investigated. Recent application of single-cell technologies, such as single-cell RNA-sequencing has enabled us to decipher the unforeseen diversity and dynamics of TAMs and to identify new subsets of TAMs which regulate anti-tumor immunity. Here, we first review hallmarks of the TME, progress and challenges of immunotherapy, and the biology of TAMs in the context of rGBM, including their origins, categories, and functions. Next, from a single-cell perspective, we highlight recent findings regarding the distinctions between tissue-resident microglia and MDMs, the identification and characterization of specific TAM subsets, and the dynamic alterations of TAMs during tumor progression and treatment. Last, we briefly discuss the potential of TAM-targeted strategies for combination immunotherapy in rGBM. We anticipate the comprehensive understanding of the diversity and dynamics of TAMs in rGBM will shed light on further improvement of immunotherapeutic efficacy in rGBM.

KEYWORDS

recurrent glioblastoma, tumor microenvironment, immunotherapy, microglia, monocyte-derived macrophages, single-cell

1 Introduction

Glioblastoma (GBM) is the most prevalent and malignant type of brain tumors. Nearly 90% of GBM relapse despite the standard of care involving surgery, radiotherapy, and chemotherapy (1). Recurrent GBM (rGBM) generally differs from primary GBM in their molecular and histological characteristics, intra-tumor heterogeneity, immune microenvironment, and biological behaviors due to the therapeutic pressure and clonal selection, which contributes to the aggressiveness and therapeutic resistance of rGBM (2). Therefore, patients with GBM rapidly succumb to this disease, with a median overall survival of 12-15 months after initial diagnosis and a 5-year survival rate of less than 10% (3, 4); however, due to the lack of abundant high-quality rGBM samples, most current studies focus on primary GBM, while the biology of rGBM remains largely unknown, and practical therapeutic approaches against rGBM are lacking. Therefore, it is instrumental to understand the biology of rGBM for developing effective therapeutic strategies and improving the clinical outcome of patients with GBM.

Recently, emerging immunotherapies, including immune checkpoint blockade (ICB), vaccine, and chimeric antigen receptor (CAR) T-cell therapy, have revolutionized the therapeutic landscape of multiple types of cancers (5); however, several clinical trials have revealed disappointing therapeutic efficacy of immunotherapy in rGBM, and the underlying mechanisms remain incompletely elucidated (6–8). The tumor microenvironment (TME) is pivotal in orchestrating immune activity and modulating response to immunotherapy. GBM is a typically "cold tumor" with an immunosuppressive TME featured by the paucity of cytotoxic T cells (CTLs) and the abundance of immunosuppressive cells such as myeloid cells (8–11). Tumor-associated macrophages (TAMs) are the most predominant non-malignant cells infiltrating GBM, which consist of tissue-resident microglia and monocyte-derived macrophages (MDMs). Growing evidence has suggested pro-tumor functions of TAMs in GBM include aggravating tumor growth and metastasis, angiogenesis, immunosuppression, treatment resistance, *etc* (12–14). Besides, the level of TAMs is markedly increased in rGBM, which in turn is associated with poor prognosis of patients (8, 15).

TAMs are incredibly plastic and heterogeneous, exhibiting diverse phenotypes and functions when responding to the environment-specific stimuli. Recently, high-resolution methodologies [e.g., single-cell RNA-sequencing (scRNA-seq)] have been instrumental in identifying and characterizing various subsets of TAMs with distinct functions in GBM (13, 16). Interestingly, emerging evidence has revealed the dynamic alterations of TAMs during disease progression and therapeutic resistance in rGBM. Meanwhile, different TAM-targeted therapeutic approaches have been developed, showing promising potential in multiple types of cancers, including rGBM (17, 18). Therefore, an elaborated understanding of the complexity of TAMs and molecular mechanisms underlying the tumor-promoting roles of TAMs in rGBM is vital to facilitating TAM-modulating treatment in order to overcome resistance of rGBM to immunotherapy.

In this review, we first provide a concise overview of characteristics of TME and immunotherapy for patients with rGBM. We then describe the biology of TAMs in rGBM, including their origins, categories and functions. In particular, we review recent advances regarding the phenotypic and functional diversity of TAMs in rGBM at the single-cell resolution, and focus on distinctions between tissue-resident microglia and MDMs, the characterization of specific subsets, and the dynamic changes of TAMs during tumor evolution and treatment in GBM. Finally, we highlight the potential of therapeutically targeting TAM as the basis for combination immunotherapy for patients with rGBM.

2 TME and immunotherapy in rGBM

2.1 TME of rGBM

In the context of cancer, various types of immune cells enter the central nervous system (CNS) by disrupting the blood-brain barrier. The TME of GBM is dominated by immunosuppressive cells, including TAMs, myeloid-derived suppressor cells (MDSC), and regulatory T cells (Treg) (9, 10). Besides, genetic alterations are associated with the immune status of GBM, and diverse immune landscapes in four molecular subtypes of GBM [neural, pro-neural (PN), classical (CL), and mesenchymal (MES)] have been documented (19, 20). For example, tumor-infiltrating CTLs were scarce in the CL subtype but abundant in the MES subtype (21). Also, a preponderance of TAMs was identified in the MES subtype (22). In addition, the *IDH-1* mutation, which frequently occurrs in the PN subtype, is correlated with reduced Tregs and monocyte signatures, PD-L1 expression, and a favorable prognosis (23–25). Thus, the heterogeneity of TME that is associated with cancer genetics provides a foundation for tailoring therapies for patients with GBM.

Crucially, the TME altered by the treatment results in a unique TME for rGBM that differs from that of primary GBM. For instance, 82% of rGBM lost the expression of *epidermal growth factor receptor variant III* (*EGFRvIII*). *EGFRvIII* is an immunogenic mutation widely detected and constitutively activated in primary GBM, indicating that immunologic escape occured after a period of progression-free survival in rGBM (26). Recently, it was reported that $CD103^+$ Tregs with upregulated lipid metabolism accumulated in response to ICB therapy and concurrent radiotherapy, which hindered the cytotoxic activity of CTLs in GBM (27). Additionally, rGBM exhibited an increase in the infiltration of $CD68^+$ macrophages following anti-angiogenic therapy, suggestive of the potential role of TAMs in controlling therapeutic resistance and tumor relapse (15). More dynamic changes of TAMs during tumor progression and treatment will be reviewed in the following sessions. Taken together, the highly heterogeneous, dynamic and immunosuppressive TME is a key player contributing to anti-tumor immune evasion in rGBM.

2.2 Progress and challenges of immunotherapy in rGBM

ICB therapy could inhibit the immune checkpoint pathways such as programmed death-1/programmed death-ligand 1 (PD-1/PD-L1) signaling, thus alleviating T cell exhaustion and enhancing CTLs-mediated tumor killing (28). Despite the therapeutic success of anti-PD-1/PD-L1 treatment in multiple types of cancers, the phase III clinical trial Checkmate 143 reported that anti-PD-1 antibody nivolumab failed to achieve survival benefits compared with bevacizumab in rGBM patients (6, 29–31). In contrast, another clinical trial conducted by Cloughesy et al. demonstrated that OS in rGBM patients treated with neoadjuvant anti-PD-1 therapy (surgery following pembrolizumab) was improved compared with adjuvant-only treatment, which was accompanied by increases in the expression levels of genes related to T cells and interferon (IFN)-γ within the tumor (32). Besides, several studies have suggested the promising anti-tumor effects of ICB-based combination therapy in pre-clinical GBM mouse models, but clinical trials are needed to determine the clinical efficacy (33–36). Overall, current evidence hints that a single ICB treatment might be insufficient to revert the immunosuppressive TME of rGBM and elicit satisfactory efficacy. Therefore, it is worth investigating an ICB-based combination treatment against rGBM.

The tumor-specific peptide vaccination provides a promising approach to trigger specific immune responses by targeting tumor-associated antigens (TAAs). rGBM possesses a broad spectrum of TAAs, including CD133, gp100, EGFRvIII, IL-13Rα2, Wilms' tumor 1 (WT1), HER2, *etc* (37–40). Several clinical trials have demonstrated the survival benefit of GBM-specific peptide vaccination, but the therapeutic response was hampered by pre-treatment lymphopenia, which highlighted the necessity of more rigorous selection criteria for patient enrollment (41). On the other hand, given the crucial role of dendritic cells (DCs) in antigen presentation and activation of CTLs, DC vaccination therapy has also exhibited an encouraging effect in treating patients with rGBM (42–45); however, it is incredibly time-consuming to isolate and purify autologous DCs, making it challenging to exploit DCs-based immunotherapy for rapidly progressing rGBM.

Recently, CAR-T cell immunotherapy has presented an attractive anti-tumor method and succeeded in treatment of hematological malignancies (46–48). Several studies have demonstrated the safety and feasibility of IL-13Rα2-specific and HER2-specific CAR T cells in patients with rGBM (49–52); however, researchers reported the limited efficacy of EGFRvIII-specific CAR-T cell therapy in patients with rGBM (7). EGFRvIII was highly expressed in primary GBM but exhibited a specific loss or decreased expression in tumors resected after CAR-T cell therapy (7, 53, 54). Apart from EGFRvIII antigen escape, the adaptive immunosuppressive response was observed in the TME upon CAR-T therapy, suggested by the upregulated expression of inhibitory molecules, including PD-L1, TGF-β, IDO, and IL-10 and infiltration of Tregs (7). Currently, the durable clinical efficacy of CAT-T cell therapy in rGBM is hindered by the short lifespan of CAR-T cells, the poor infiltration of T cells in tumor tissues, tumor heterogeneity, and antigen escape, which needs to be addressed in the future (55).

Despite the recent breakthrough of immunotherapy in a subset of patients with rGBM, there are still many obstacles in the practical application. More efforts should be made to solve the issues regarding the optimum approach, treatment timing, patient selection, and combination modalities to augment the efficacy of immunotherapies for patients with rGBM.

3 Origin, classification, and roles of TAMs in rGBM

3.1 Origin and recruitment of TAMs in rGBM

Microglia are the brain-resident macrophages originating from yolk sac-derived embryogenetic precursors. Under normal physiological conditions, microglia comprise 10% of the adult brain cell populations, represent the main component of brain macrophages, and play an essential role in maintaining the immune homeostasis of CNS (16, 56). Upon inflammatory stimulation, such as infection and cancer, bone marrow-derived monocytes in the peripheral blood are recruited to the tumor site and then differentiate into macrophages. Various recruitment signals have been recognized, including colony-stimulating factor-1 (CSF-1), monocyte chemoattractant protein-1 (MCP-1), and stromal-derived factor (SDF)-1α derived from tumor cells and other cells in the TME (12, 57–60).

The term TAMs in GBM include both tissue-resident microglia and MDMs. It is challenging to distinguish or separate microglia from MDMs using conventional approaches (e.g., flow cytometry) due to the lack of specific markers (61); however, growing evidence has demonstrated the dramatic distinctions in preferential localizations and functions between these two subpopulations. For example, Chen et al. found that MDMs accounted for most TAMs in GBM and were mainly located in perivascular areas. Inversely, microglia only represented a minor TAM population, usually appearing in the peritumoral zones (58). Moreover, microglia-derived TAMs are predominant in primary GBM but are outnumbered by MDMs following recurrence, especially under hypoxia (62). Phenotypically, MDMs upregulate immunosuppressive cytokines and show an altered metabolism compared to microglial TAMs (63). More studies are needed to dissect the exact origin and specific roles of TAM populations in GBM.

3.2 Classification of TAMs in rGBM

Based on the polarization status and regulatory functions under inflammation, macrophages are divided into classically activated macrophages (M1, pro-inflammatory) and alternatively activated macrophages (M2, anti-inflammatory) (64). M1 macrophages can be induced by lipopolysaccharide (LPS), IFN-γ, granulocyte–

macrophage colony-stimulating factor (GM-CSF) or Toll-like receptor signaling pathway. M1 macrophages spur inflammation by releasing cytokines such as IL-1α, IL-1β, IL-6, IL-12, and tumor necrosis factor (TNF)-α. On the other hand, M2 macrophages are stimulated by IL-4, IL-10, IL-13, and glucocorticoid. M2 macrophages express PD-L1 and exert immunosuppressive functions by secreting IL-10, arginase-1, TGF-β, *etc* (64, 65). Generally, M1 macrophages exert an anti-tumor role, whereas M2 macrophages play a pro-tumor role. Several markers distinguish the M1 from the M2 phenotype, e.g., CD80, CD86, and MHC-II for M1, CD163 and CD206 for M2, although they are not absolutely specific (66, 67). CSF-1, TGF-β1, macrophage inhibitory cytokine 1 (MIC-1), osteopontin (OPN), and Periostin produced by GBM cells recruit and polarize macrophages to a tumor-supporting M2-like phenotype (68–71). CD163 and CD206 are highly expressed in perivascular macrophages in the brain tumor cores and are associated with an immunosuppressive TME (72).

M1/M2 nomenclature is proposed mainly based on *in vitro* data when macrophages were stimulated with type 1 or 2 cytokines. This nomenclature remains oversimplified, albeit widely used (66). Indeed, macrophages are highly plastic and heterogeneous, with the capacity of being reprogrammed into distinct phenotypes by different microenvironmental stimuli. Besides, canonical M1 and M2 markers are co-expressed in individual cells, implying that macrophages could possess a mixed M1/M2 phenotype (63). Beyond M1/M2, the more complicated phenotypic and functional diversity of TAMs in GBM has been recently appreciated (73–75). Next, we will review the diverse roles of TAMs in regulating progression of GBM, and summarize recent advances that reveal the complexity of TAMs in GBM based on single-cell omics approaches.

3.3 Functions of TAMs in GBM

TAMs are involved in tumor development and progression via releasing various factors and interacting with other cells in multiple malignancies (17, 76). In GBM, the pro-tumor roles of TAMs are well documented that implicate the importance of TAMs as a therapeutic vulnerability in GBM, involving tumor growth, invasion, angiogenesis, immunosuppression, and treatment resistance (Figure 1) (12, 18).

3.3.1 TAMs aggravate tumor growth and invasion

The molecular interaction between TAMs and tumor cells is critical for regulating tumor growth and invasion. For instance, TAMs secrete TGF-β1 to recruit $CD133^+$ cancer stem-like cells (CSCs) (77). Pleiotrophin (PTN) derived from $CD163^+$ M2 macrophages binds to its receptor protein tyrosine phosphatase receptor type Z1 (PTPRZ1) on the surface of CSCs. The binding of PTN and PTPRZ1 contributes to the stemness maintenance and tumorigenic capacity of CSCs, thus accelerating the growth of GBM

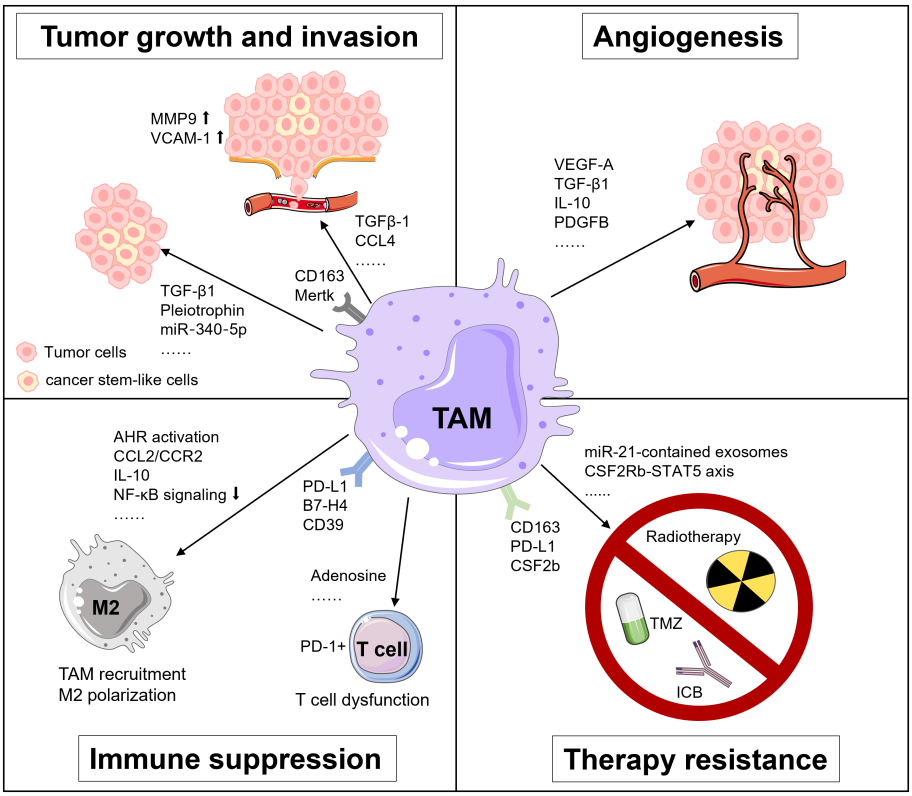

FIGURE 1
Tumor-supportive functions of TAMs in GBM. TAMs foster tumor growth and invasion, angiogenesis, immunosuppression and treatment resistance in GBM via multiple pathways.

(78). Besides, TAMs upregulate the expression of metalloproteinase 9 (MMP-9) of CSCs via TGF-β1 and CCL4-CCR5 signaling to enhance the GBM invasiveness (79). Also, the vascular cell adhesion molecule-1 (VCAM-1)-mediated interaction between macrophages and GBM cells reinforces GBM invasion (80). Additionally, Liu et al. unveiled that a miR-340-5p-macrophage feedback loop regulated tumor progression and was related to a poor prognosis for patients with GBM (81). Moreover, TAMs expressing myeloid-epithelial-reproductive tyrosine kinase (MerTK), a critical tyrosine kinase for phagocytosis function, are associated with tumor growth (82).

3.3.2 TAMs promote angiogenesis

The rapid proliferation of tumor cells accelerates the consumption of oxygen and nutrients in the TME, rendering a highly hypoxic environment for GBM, especially in its core region (83). Under the hypoxic condition, TAMs produce angiogenesis-promoting cytokines, chemokines, and growth factors, like vascular endothelial growth factor A (VEGF-A), a well-known factor for vascularization and immunosuppression in multiple cancers, including GBM (83–85). Besides, Cui et al. found that GBM-induced M2-like macrophages secreted more TGF-β1 and IL-10. These anti-inflammatory cytokines facilitated endothelial capillary proliferation and angiogenic sprouting through integrin (αvβ3) receptors and Src-PI3K-YAP signaling. Hence, dual blockade of integrin (αvβ3) and cytokine receptor (TGFβ-R1) could suppress the neovascularization of GBM induced by the TAM-endothelial interaction (86). Moreover, a recent study by Zhu et al. suggested that the expression of cat eye syndrome critical region protein 1 (CECR1) was upregulated in M2 macrophages and correlated with microvascular density in GBM. Mechanistically, CECR1 mediated the crosstalk between macrophages and vascular mural cells via the PDGFB-PDGFRβ signaling axis, leading to recruitment of pericytes, migration, and tumor angiogenesis (87). Collectively, TAMs exert potent pro-angiogenic properties in GBM, implying that therapeutically targeting TAMs may present an attractive way against rGBM.

3.3.3 TAMs orchestrate immune suppression

The highly immunosuppressive TME represents a hallmark of GBM, which is primarily attributed to TAMs via multiple mechanisms. For instance, decreased IKBKB expression and NF-κB signaling in TAMs support M2 polarization and correlate with defective expression of immune/inflammatory genes, resulting in immune suppression in GBM (88). Accordingly, NF-κB-targeted therapy could reverse M2 polarization, induce tumor regression and improve survival of a GBM mouse model in T cell-dependent manner (89). Besides, Takenaka and colleagues recently uncovered mechanisms by which TME controlled TAMs and T cells in GBM. Kynurenine produced by GBM cells elicited the activation of aryl hydrocarbon receptor (AHR) in TAMs, which further increased the expression of *CCR2* and boosted TAM recruitment via the CCL2/CCR2 axis. Aside from that, AHR drove the expression of ectonucleotidase CD39 in TAMs and led to the dysfunction of CTLs via adenosine accumulation. Moreover, elevated expression of AHR was associated with glioma grade and unfavorable prognosis in patients with GBM (90).

Immune checkpoint molecules are critical inducers of immunosuppressive TME. Reportedly, GBM could upregulate PD-L1 expression in circulating monocytes and TAMs through the IL-10 signaling axis in an autocrine/paracrine manner. *In vitro*, macrophages stimulated by IL-10 induced T cell apoptosis, which could be attenuated by inhibiting IL-10 and its receptor (91). Besides, Yao et al. unveiled that $CD133^+$ CSCs activated the expression of B7-H4 in TAMs via the IL6/JAK/STAT3 pathway. Such B7-H4-mediated crosstalk between glioma-initiating cells and TAMs was associated with a bleak prognosis of human GBM (92).

3.3.4 TAMs mediate therapeutic resistance

TAMs are involved in therapuetic resistance of GBM to temozolomide (TMZ), radiotherapy, and immunotherapy. For example, TAMs release oncomiR-21-contained exosomes, which upregulate the production of PDCD4, SOX2, STAT3, IL-6, and TGF-1 in GBM cells, rendering resistance of GBM to TMZ. Pacritinib, a STAT3 inhibitor, could overcome resistance to TMZ by decreasing miR-21-enriched exosomes from TAMs (93). Besides, Miyazaki et al. revealed that TMZ-resistant GBM cells produced M2-related cytokines including IL-10, IL-4, IL-13, and CSF-1, and PD-L1 expression. Upon *in vivo* anti-PD-L1 antibody administration, TMZ-resistant GBM tumor tissues showed abundant infiltration of $CD163^+$ M2 macrophages. Expectedly, remarkable anti-tumor efficacy was achieved using a combination therapy of anti-PD-L1 antibody plus IPI-549, a PI3Kγ inhibitor that could skew M2 macrophages to M1 macrophages (94). Moreover, dynamic transcriptional alterations of TAMs in the irradiated and recurrent tumors have been observed in mouse and human GBM, and CSF-1R inhibition could overcome resistance of pre-clinical models to radiotherapy (95).

As for the significance of TAMs in mediating resistance of GBM to immunotherapy, Simonds et al. previously discovered the association between $PD\text{-}L1^+$ TAMs and resistance to ICB by comparing the TME of human ICB-refractory GBM and ICB-responsive tumors using cytometry by time-of-flight (CyTOF) (96). Additionally, through integrated analyses of multi-dimensional data, Lee et al. demonstrated that neoadjuvant anti-PD-1 blockade induced conventional type 1 DC (cDC1) and activation of T cells but failed to eliminate immunosuppressive TAMs in rGBM (97). Interestingly, in the mouse model of brain metastases, pro-inflammatory activation of TAM which was mediated by the compensatory CSF2Rb–STAT5 signaling axis fostered tumor recurrence after CSF1R inhibition. Furthermore, blockade of CSF1R combined with STAT5 signaling inhibitor could sustain tumor control and rectify adaptive resistance to CSF1R inhibition (98). All of these findings highlight the potential benefit of TAM-targeted therapeutic intervention for overcoming treatment resistance in rGBM and metastatic brain tumors.

4 Emerging diversity of TAMs in GBM at the single-cell resolution

As mentioned before, owing to the plastic and heterogenous nature of TAMs, the linear M1/M2 activation theory is insufficient to explain the *in vivo* complexity of TAMs in GBM (66). On the other hand, despite the well-documented anti-tumor functions of M1 macrophages and pro-tumoral functions of M2 macrophages, the prognostic value of $CD163^+$ and $CD206^+$ M2 macrophages was controversial in different cohorts of patients with GBM, emphasizing an unmet need to decipher the exact function of specific TAM subtypes in GBM (20, 99); however, limited by conventional approaches, hurdles exist to distinguish and characterize TAM subpopulations in GBM. In the past years, the application of high-dimensional and high-resolution techniques has enabled us to decipher unprecedented macrophage subclusters in the brain under homeostasis and disease, and moved us beyond the binary M1/M2 polarization paradigm. Herein, we will review recent advances in the phenotypic and functional diversity of TAMs in GBM and provide insights into the therapeutic potential of TAM-based strategies for patients with rGBM.

4.1 Distinctions between tissue-resident and monocyte-derived macroohages in GBM

Microglia and MDMs are different in the spatial distribution, enrichment extent, phenotypic and functional characteristics during disease progression in GBM (Figure 2). A study by Darmanis et al. suggested that the majority of myeloid cells within the tumor center preferentially exhibited gene signatures of macrophages, whereas microglia-related genes were mainly expressed in myeloid cells located in the surrounding space in human GBM (100). Similarly, by analyzing RNA-seq data from the human GBM cohort, Kim et al. recently confirmed that microglial genes (*CX3CR1*, *TMEM119*, and *P2RY12*) were mainly expressed in the periphery, while activated macrophage genes (*TNF*, *CCL2*, *LYZ*, *CCR2*, *CXCR4*, and *SIGLEC1*) were predominantly detected within the core tumor regions (74). Besides, Muller's group has reported that differing from microglia, MDMs were usually enriched in perivascular and necrotic areas in human glioma (63).

Several studies have attempted to dissect longitudinal changes of TAM composition throughout tumor evolution and recurrence in GBM. For instance, Yeo et al. reported a progression of TME from M1-like proinflammatory microglia towards an M2-like pro-tumorigenic infiltrating macrophages during tumor growth in the mouse model of GBM. Notably, a similar transition was observed in tumor biopsies derived from patients with low-grade glioma and GBM (101). Besides, Pombo Antunes et al. profiled myeloid cells in mouse and human GBM at new diagnosis and recurrence by employing scRNA-seq and cellular indexing of transcriptomes and epitopes by sequencing (CITE-seq) technical platforms. The researchers found that microglia-derived TAMs were predominant in initial tumors but were outnumbered by MDMs in recurrent tumors, especially under hypoxic conditions. Although microglia and MDMs exhibited functional specialization to some extent, both of them showed a convergent angiogenic and T-cell suppressive capacity (62).

Emerging evidence has suggested additional phenotypic and functional differences between microglia and MDMs. By performing scRNA-seq of *IDH*-mutant human gliomas, Venteicher et al. unmasked a continuous rather than a bimodal distribution of transcriptional signatures of microglia/macrophages, underscoring the plasticity of cellular states of TAMs. Besides, the macrophage signature, but not the microglia signature, was associated with clinical grade and increased vascularity in gliomas (102). Additionally, Ochocka et al. identified distinct transcriptional programs of microglia and monocytes/macrophages in mice bearing GBM via scRNA-seq analysis. The transcriptional responses of macrophages were associated with the activation of immunosuppressive genes such as *Cd274* encoding PD-L1, while microglia had higher expression levels of major histocompatibility complex II (MHC-II) genes in a sex-specific manner (103). Consistently, Muller et al. determined that MDMs tended to express immunosuppressive cytokines and to undergo metabolic

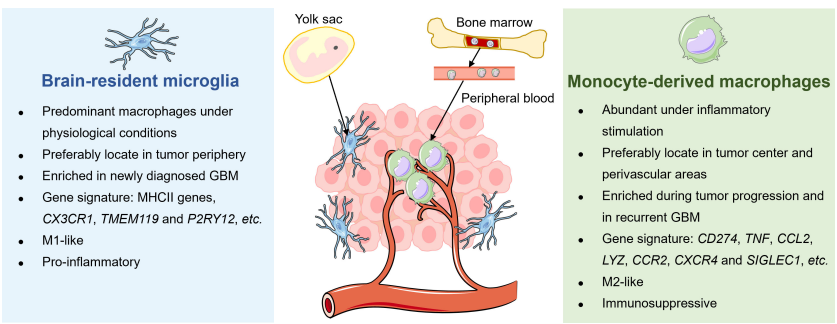

FIGURE 2
Distinctions between tissue-resident microglia and monocyte-derived macrophages in GBM. The tissue-resident microglia originate from the yolk sac and represent the primary macrophages in the brain under physiological conditions to maintain immune homeostasis. Under malignant conditions, microglia preferably locate in the periphery of newly diagnosed GBM, exhibiting a pro-inflammatory M1-like phenotype. Meanwhile, bone marrow-derived monocytes in circulation are recruited into the brain and differentiate into macrophages. Unlike microglia, MDMs are enriched during tumor progression, particularly in tumor core and perivascular regions of rGBM, and present immunosuppressive M2-like properties.

reprogramming compared with microglia in human gliomas (63). Collectively, these results shed light on the dynamic alterations of TAMs with different origins in response to disease status and microenvironment stimulation in GBM.

4.2 Identification and characterization of specific subsets of TAMs in GBM

Substantial efforts have been made to identify specific subsets of TAMs with the most promising therapeutic potential in GBM (Table 1). For instance, by integrating analyses of scRNA-seq and CyTOF data, Sankowski et al. mapped microglial states in the human brain under healthy and malignant conditions, and uncovered a disease-associated transcriptional signature in TAMs from patients with GBM. These TAMs exhibited down-regulation of the microglia core signature and concomitant up-regulation of inflammatory, metabolic, and hypoxia-related genes, including *SPP1*, and several type I interferon genes, *APOE*, and *CD163*. Furthermore, the top differentially expressed proteins, including HLA-DR, TREM2, APOE, CD163, and GPR56, could be detected in a TAM subset via CyTOF, providing a possibility for therapeutically targeting specific TAM states in GBM (75).

Using similar approaches, Goswami et al. determined the persistence of a unique population of $CD73^+$ macrophages in patients with GBM upon anti-PD-1 treatment. They further demonstrated the critical function of $CD73^+$ macrophages in conferring resistance to ICB, which was mediated by the modulation of macrophage polarization and T cell infiltration. Compared with wild-type mice, the authors detected a decrease of immunosuppressive $CD206^+Arg1^+VISTA^+PD\text{-}1^+CD115^+$ myeloid cluster and an increase of $iNOS^+$ myeloid cells in CD73-deficient mice. Upon the treatment of CD73-knockout mice with the combination with anti-CTLA-4 plus anti-PD-1, the tumor burden was significantly alleviated and survival was improved, along with the elevated ratio of the granzyme B^+ effector CD8 T cells to the $CD206^+$ macrophages in the TME. The study indicated that CD73 was a promising immunotherapeutic target to augment anti-tumor immune responses to the combination immunotherapy in GBM (104).

Recently, through multi-regional and -dimensional analyses at the single-cell level, Abdelfattah et al. sought to discover immune modulatory targets in GBM. scRNA-seq analysis identified that *S100A4* was highly expressed in innate and adaptive immunosuppressive cells, including Tregs, exhausted T cells, and three subsets of pro-tumorigenic myeloid cells. The immunofluorescence staining confirmed the expression of S100A4 in immunosuppressive $CD163^+$, $CD206^+$ macrophages, and $FOXP3^+$ T cells in human glioma. Moreover, a higher expression of S100A4 was markedly associated with a worse survival and was recognized as an independent prognostic indicator for patients with GBM. Subsequent animal experiments and functional analyses demonstrated the roles of S100A4 in impeding immune response, including phagocytic activity of macrophages, production of IFN-γ and activation of T cells, thus favoring the growth of glioma, supporting S100A4 as a promising immunotherapeutic target (105).

Additionally, Chen et al. integrated analyses of newly generated and published single-cell RNA-seq data, which identified a tumor-

TABLE 1 Specific TAM subsets in GBM identified through single-cell omics technologies.

Species	Marker/Signature	Function/enriched pathway	Technique	Dataset
Human	*SPP1*, *HLA-DR*, *TREM2*, *APOE*, *CD163*, *GPR56*	↓: Microglia core signature. ↑: Inflammatory, metabolic and hypoxia-associated molecules.	scRNA-seq and CyTOF	GSE135437 (75)
Human	$CD73^+$	Immunosuppression. Modulate macrophage polarization and T cell infiltration.	scRNA-seq and CyTOF	PRJNA588461 (104)
Human	$S100A4^+$	Impede immune response, including phagocytic activity of macrophages, production of IFN-γ and activation of T cells, thus favoring glioma growth	scRNA-seq	GSE182109 (105)
Human	$MACRO^+$	Anti-inflammatory. Loss of pro-inflammatory pathways (interferon response, allograft rejection, TNFα signaling via NFKB) and antigen presentation.	scRNA-seq	GSE141383 (106)
Human	↑: *CX3CR1*, *NLRP1*, *IL1B*, *APOE*, *PDGFRA*, *SOX2*. ↓: *P2RY12*, *TMEM119*.	Pro-inflammatory and proliferative. Promoting tumor progression through IL-1β secretion.	scRNA-seq	PRJNA669369 (107)
Human	$HMOX1^+$	Mediate T cell dysfunction via IL-10 release.	scRNA-seq and spatial transcriptomics	https://osf.io/4q32e/ (108)
Human	$CD14^+ERO1A^+$	Hypoxia-response signatures. Associated with tumor angiogenesis, invasion, and poor prognosis	scRNA-seq	GSE135045 (109)
Human	MPO^+	Less interactions with endothelial cells, enhanced cytotoxic functions.	Imaging mass cytometry	Available upon request (73)
Mouse	$CD169^+$	Pro-inflammatory and anti-tumor. Induce T cells and NK cells infiltration.	scRNA-seq	GSE201559 and GSE200533 (74)

↑ Upregulation; ↓ Downregulation.

supportive subcluster of TAMs characterized by the scavenger receptor MARCO, almost exclusively expressed in *IDH1*-wild-type (*IDH*-WT) GBM. Moreover, MACRO was reportedly detrimental in melanoma and non-small cell lung cancer. The expression of *MARCO* in bulk tumors was also associated with a disappointing prognosis and mesenchymal subtype in the GBM cohort. Further analysis observed the loss of pro-inflammatory pathways (interferon response, allograft rejection, and TNFα signaling via NFKB) and antigen presentation in $MACRO^+$ TAMs, supporting its anti-inflammatory phenotype. Altogether, the study revealed a novel TAM subpopulation driving the progression of GBM and implied a potential strategy for $MACRO^+$ TAM-targeted therapy (106).

Increasing evidence has also elucidated how TAMs orchestrate the immunosuppressive TME through various crosstalk with their neighboring components. Through scRNA-seq analysis of human GBM, Liu et al. identified a unique pro-inflammatory and proliferative subpopulation of microglia, marked by upregulated expression of *CX3CR1, NLRP1, IL1B, APOE, PDGFRA*, and *SOX2*. The microglia were activated by TGF-β1 derived from *SETD2*-mut/*IDH*-WT tumor cells, and accelerated tumor progression via secreting IL-1β. Notably, depletion of TGF-β1/TGF-β RI successfully reduced the pro-inflammatory and proliferative microglia and restrained tumor growth (107). Through integrative analysis of single-cell and spatial transcriptomics data of human GBM, Ravi et al. revealed that a subset of $HMOX1^+$ microglia and macrophages released IL-10 and mediated T cell dysfunction, thus fostering an immunosuppressive TME (108). Additionally, a specific $CD14^+ERO1A^+$ TAM cluster with detrimental prognostic value in human primary GBM has been identified, which showed a gene signature enriched in hypoxia-response, invasion and extracellular matrix organization. The $CD14^+ERO1A^+$ TAM cluster, together with two hypoxia-dependent MES-like tumor cells expressed VEGFA, indicating their contribution to the induction of angiogenesis in GBM via interacting with endothelial cells (109).

Contrary to the well-known tumor-supportive functions of TAMs, studies also showed that several subsets of macrophages favor anti-tumor immunity against GBM. For example, through the analysis of scRNA-seq data, Kim et al. unraveled that $CD169^+$ TAMs were IFN-responsive macrophages, which produced pro-inflammatory chemokines, hence inducing the infiltration of T cells and NK cells in human and mouse gliomas. Mechanistically, $CD169^+$ TAMs originated from $CCR2^+$ blood monocytes, and IFN-γ derived from NK cells was critical for recruiting $CD169^+$ macrophages into gliomas. CD169 boosted the phagocytosis capacity of macrophages through ligands of apoptotic tumor cells and ignited antigen-specific T cell responses. Moreover, the clearance of $CD169^+$ TAMs impaired anti-tumor responses mediated by T cells and shortened the survival of mice bearing glioma (74). Recently, Karimi et al. characterized the immune landscape of primary and metastatic human brain tumors at the single-cell level by applying imaging mass cytometry. Specifically, they identified a unique subpopulation of myeloperoxidase (MPO)-positive neutrophil-like macrophages, which was related to reduced interactions with endothelial cells, enhanced cytotoxic functions and survival benefit for patients with GBM (73).

The remarkably distinct and even inverse roles of TAMs in orchestrating GBM progression reflect their plasticity and heterogeneity. Therefore, it is necessary to identify specific targets and mechanisms for tailoring TAMs-modulating therapy regimens. Still, the vast diversity of TAMs in GBM remains incompletely illustrated, highlighting an urgent demand for more investigations that utilize high-dimension and high-resolution approaches and platforms.

4.3 The dynamic alterations of TAMs during disease progression and treatment

Several studies have investigated alterations of TAMs during tumor evolution in GBM at the single-cell level (Table 2). For instance, Rajendran et al. not only revealed an immune-activated feature displayed by TAM clusters in low-grade murine glioma but also demonstrated an immunosuppressive property in murine high-grade murine glioma, accompanied by the restriction of T cell trafficking and activation. They further identified high expression of CD74 and its binding partner, macrophage migration inhibition factor (MIF) in distinct TAM populations, which was subsequently validated in human samples and supported the CD74-MIF axis as a potential target for TAMs (11). As mentioned above, the preponderance of TAMs underwent a transition from M1-like proinflammatory microglia to M2-like pro-tumorigenic macrophages during GBM progression, which was conserved in human and mouse. The transition was concurrent with a disruption of the blood-brain barrier and an explosive growth of malignant cells (101).

Hoogstrate et al. conducted a large-scale transcriptome analysis of paired primary-recurrent GBM resections of patients following standard therapy and suggested that rGBM preferentially progressed to MES-like subtype (110). Macrophages are known to be recruited by GBM stem cells and induce the MES-like state of GBM cells (110, 114, 115). Consistently, Hoogstrate et al.'s study identified significant increase of TAM infiltration in MES-like rGBM, which was inversely correlated with tumor purity, supporting the essential role of TAMs in favoring MES-like GBM progression at recurrence (110).

As mentioned above, Pombo Antunes et al. compared the immune landscape of newly diagnosed (ND) GBM versus rGBM following surgery, adjuvant radiotherapy and chemotherapy through scRNA-seq and CITE-seq analyses. The TME of ND GBM mainly consisted of TAMs (82–97%), followed by T cells (2–20%), while rGBM displayed a more diverse immune compartment including increased T cells, NK, B cells and monocytes. Microglia formed the major TAM fraction in ND GBM, but MDMs outcompeted microglia in rGBM, especially in the hypoxic tumor niche. TAMs in recurrent versus ND GBM displayed higher expression of genes related to monocyte chemotaxis, IFN signaling, and phagocytosis (62). Additionally, a single-cell multi-omics analysis conducted by Wang et al.

TABLE 2 The dynamic alterations of TAMs during disease progression and treatment in GBM at the single-cell resolution.

Species	Therapy	Alterations of TAMs	Technique	Transcriptome datasets
High-grade vs. low-grade glioma				
Mouse (validated in human via IF and RNA-seq analysis)	N/A	TAM clusters displayed an immune-activated feature in low-grade glioma but adopted an immunosuppressive property in high-grade glioma, accompanied by restriction of T cell trafficking and activation.	scRNA-seq	GSE221440 (11)
During tumor growth of GBM				
Mouse (validated in human via flow cytometry)	N/A	The predominance of TAMs switched from M1-like proinflammatory microglia towards M2-like protumorigenic macrophage during GBM progression.	scRNA-seq	GSE195848 (101)
Recurrent vs. primary GBM				
Human	Radiotherapy and chemotherapy	TAM infiltration increased in MES-like rGBM and was inversely correlated with tumor purity	snRNA-seq and RNA-seq	EGAD00001009871; EGAD00001009964 (110)
Human and mouse	Surgical resection, adjuvant radiotherapy and chemotherapy	Microglia were predominant in ND tumors, but were outnumbered by MDMs following recurrence, especially in hypoxic niche. Notable genes that were enriched in recurrent versus ND TAMs were related to monocyte chemotaxis, IFN signaling and phagocytosis.	scRNA-seq and CITE-seq	EGAS00001004871 (human); GSE163120 (mouse) (62)
Human	TMZ, IR and surgical resection	Bone marrow-derived monocytic lineage cells increased and microglia reduced in all tumor-associated innate immune cells at recurrence. Although both subsets had more activated M1 and M2 cells at recurrence, most of them were remained M0 state.	snRNA, scATAC-seq, spatial transcriptomic/ proteomic assays, exome-seq	EGAS00001004909 (111)
Mouse (validated in human via RNA-seq and IF staining)	Radiotherapy	The abundance of MDMs increased relative to microglia in rGBM. MDMs and microglia converged upon a common phenotype at recurrence, which is potentially regulated by SMAD and RBPJ.	RNA-seq of isolated MG and MDMs	GSE99537 (95)
Human	Surgical resection followed by radiotherapy and chemotherapy	Microglial population prominently decreased in rGBM.	scRNA-seq	HRA003075 (112)
Human	Mainly chemotherapy and radiotherapy	MDMs were enriched in rGBM, while microglia were enriched in primary GBM.	snRNA and spatial transcriptomics	GSE228500 (113)
Human	Neoadjuvant PD-1 blockade therapy	Myeloid populations sustainedly expressed T-cell-suppressive checkpoints, including TIGIT and CTLA-4, and displayed reinforced interactions between T cells upon PD-1 blockade therapy	scRNA-seq and CyTOF	GSE154795 (97)
Human	Anti-PD-1 treatment	*MACRO* expression decreased in post-treatment tumors compared with pre-treatment tumors in responders rather than non-responders in anti-PD-1-treated rGBM patients.	scRNA-seq	GSE141383 (106)

N/A, Not applicable.

demonstrated an increase of bone marrow-derived monocytic lineage cells and a reduction of microglia in all tumor-associated innate immune cells at recurrence upon standard-of-care therapy including TMZ, IR and surgical resection. Although both subsets had more activated M1 and M2 macrohages at recurrence, most of them were classified as M0 state without expressing either program above. It may be attributed to the oversimplification of M1/M2 paradigm, and a continuous modal for macrophage classification is demanded (111).

In another study, by analysing RNA-seq data of isolated microglia and MDMs in pre- and post-treatment murine gliomas, Akkari and colleagues identified stage-dependent transcriptional reprogramming of these two TAM subpopulations in irradiated murine glioma. In line with previous studies, the results confirmed the increased abundance of MDMs relative to microglia in rGBM compared with primary GBM (62, 111–113). MDMs and microglia maintained their ontogeny-based identities and converged upon a common phenotype at recurrence, which is potentially regulated by

SMAD and RBPJ. Notably, recurrence-specific transcriptional changes of TAMs were also observed in human rGBM. Inhibition of CSF1-R could counteract the recurrence-induced gene signature alterations in TAMs, enhance the efficacy of radiation therapy and delay tumor regrowth in pre-clinical mouse models (95). Collectively, the findings disclosed the dynamics and plasticity of individual TAM populations during radiation treatment and provided novel insight into improving the treatment landscape in GBM.

Additionally, a study by Lee et al. also mapped the landscape of infiltrating immune cells in GBM, with a particular focus on alterations in TME following neoadjuvant PD-1 blockade therapy. By exploiting high-dimensional proteomics, scRNA-seq and quantitative multiplex immunofluorescence (mIF), the authors determined increased activation and infiltration of T cells and cDC1 after ICB treatment; however, TAMs and monocytes maintained the dominance of tumor-infiltrating immune cells upon anti-PD-1 therapy. Although the interferon-mediated T-cell chemotactic factors (such as CXCL9, CXCL10, and CXCL11) were secreted in myeloid populations after PD-1 blockade, these cells sustainedly expressed T cell-suppressive checkpoints, including TIGIT and CTLA-4. Furthermore, the analysis of scRNA-seq data recognized reinforced interactions between T cells and myeloid cells through TIGIT- and CTLA-4-related signaling after PD-1 blockade therapy, which could impede optimal and durable activation of CTLs. Therefore, additional strategies targeting TIGIT and/or CTLA-4 may enhance the strength and durability of CTL-mediated anti-tumor response of GBM to immunotherapy (97).

Besides, in the above-described study, decreased expression of *MACRO* was observed in post-treatment tumors compared with pre-treatment tumors in responders rather than non-responders in a longitudinal cohort of patients with rGBM treated with anti-PD-1. However, there were no apparent changes in expression of *MARCO* after treatment in another longitudinal cohort of patients of GBM with standard therapy. These findings suggested that *MACRO* was altered upon treatment in an immunotherapy-specific and response-dependent manner (106).

More investigations are required to delineate the dynamics and plasticity of TAMs during treatment and determine the mechanisms by which TAMs modulate therapy outcomes, thus providing translational relevance for enhancing therapeutic efficacy in GBM.

5 Targeting TAMs for boosting immunotherapy against rGBM

The strong tumor-promoting activity of TAMs has highlighted its promising potential as a therapeutic target against rGBM. Multiple TAM-targeted approaches have been explored in preclinical and clinical settings for patients with rGBM, mainly including: i). reduction of the recruitment of TAMs into tumors; ii). elimination of TAMs within tumors; iii). reprogramming of TAMs. Since these strategies have been reviewed recently, we provide a concise summary here (13, 14, 17, 18, 116).

5.1 Reduction of TAM recruitment

The inhibition of TAM infiltration could be realized by directly blocking signalings between chemokines and their receptors. For example, CCL2 derived from tumor cells recruit $CCR2^+$ myeloid cells; hence CCR2 antagonist could directly reduce TAM infiltration and improve the efficacy of ICB in murine GBM (117). As mentioned above, kynurenine produced by GBM cells led to AHR activation, further promoting CCR2 expression and enhancing TAM recruitment. In this case, AHR antagonist effectively suppressed GBM growth via reducing CCL2/CCR2-mediated TAM infiltration (90). Besides CCL2/CCR2 axis, other chemoattractant-receptor interactions have also shown therapeutic potential in GBM, such as lysyl oxidase (LOX)/β1 integrin, OPN/αvβ5 integrin, and slit guidance ligand 2 (SLIT2)/Roundabout 1 and 2 (ROBO1/2) (71, 118, 119).

5.2 Elimination of TAMs

CSF-1R is expressed on macrophages and critical for regulating the survival, proliferation, differentiation, and polarization of TAMs by binding with its ligands CSF-1 and IL-34 (120, 121). Targeting CSF-1R using antibodies or small molecule inhibitors has represent a powerful strategy to deplete TAMs and induce TAM repolarization in various types of cancers, including GBM (122–124). It is worth noting that monotherapy of targeting CSF-1R was insufficient to elicit satisfactory efficacy, and combination therapy with immunotherapy or radiation demonstrated better clinical outcome, which highlight the necessity of combination strategy in clinical exploration (125, 126). Besides, along with our extended understanding of the complexity of TME and the heterogeneity of TAM subpopulations, we should realize that the unbiased depletion of the whole TAM cluster may not be an optimal option, because it is likely to eliminate beneficial TAM subpopulations and influence other TME components. Therefore, more efforts should be made to identify specific tumor-supporting subtypes of TAMs (e.g., $CD73^+$, $MACRO^+$, and $HMOX1^+$ TAMs) and develop targeted therapy across ravious scenarios.

5.3 Reprogramming of TAMs

In spite of the detrimental function of TAM subsets, macrophage play an essential role in phagocytosis and antigen presentation, which is beneficial for the activation of anti-tumor immunity (127). Therefore, rather than macrophage clearance and recruitment inhibition, another attractive strategy is to reprogram/re-deucate TAMs, i.e., reprogram immunosuppressive TAMs to immune-supportive TAMs by restoring their phagocytic and antigen presenting capacities (76). To achieve reprogramming of TAMs in GBM, multiple approaches have been developed. For instance, the blockade of phagocytosis checkpoint pairs, e.g., CD47/SIRPα, CD24/Siglec-10 could augment the phagocytic ability of TAMs (128–132). To unleash the immune-stimulatory capacity of

TAMs, blockade of CSF1/CSF1R, stimulation of CD40/CD40L, as well as inhibition of PI3Kγ, IL-6, SLIT2, monoacylglycerol lipase (MAGL) have shown promising targetable potential and are worth further investigation (94, 119, 124, 133–135).

Notably, no single TAM-targeted agent has been successful in clinical trials for patients with GBM. Given the complexity of the TME and the close interplay between TAMs, tumor cells, and other non-malignant cells, combination therapy emerges as an attractive option. For instance, in a mouse model of GBM, the SDF-1α inhibitor in combination with VEGF blockade was more efficient in suppressing TAM recruitment, reducing tumor vasculature and improving survival compared with monotherapy of VEGF blockade (136). As discussed in the above, CSF1-R blockade in combination with radiotherapy substantially inhibited tumor growth and prolonged survival by reversing transcriptional changes of TAM induced by radiation in pre-clinical glioma models, thus overcoming resistance to radiotherapy (95). Similarly, a triple combination of oncolytic virus expressing IL-12, and anti-PD-1 plus anti-CTLA-4 antibodies synergistically cured pre-clinical murine GBM via increasing M1-like polarization and the ratio of effector T cells to Tregs (137). Further investigation regarding combination therapy regimens in the clinical setting is dispensable for strengthening the efficacy of immunotherapies for patients with rGBM.

6 Conclusions and perspectives

rGBM has been characterized by a highly immunosuppressive TME and an extremely low response to immunotherapy. TAMs, originating from microglia and peripheral monocytes, represent the dominant non-malignant cells in the TME of rGBM. TAMs exert various tumor-supportive functions, contributing to tumor growth and invasion, angiogenesis, immune evasion, and treatment resistance. More importantly, TAMs are plastic and heterogeneous, displaying more complicated phenotypes beyond the binary M1/M2 polarization. Recently, single-cell omics methodologies have enabled us to characterize the dynamics and diversity of TAMs in the TME of GBM at the single-cell resolution. Microglia and MDMs show different spatial distribution and exhibit distinctive transcriptional alterations across disease stages. Besides, specific subsets of TAMs with different functions have been determined in the context of rGBM, e.g., the pro-tumor MACRO$^+$, CD73$^+$, HMOX1$^+$, and S100A4$^+$ macrophages, and anti-tumor CD169$^+$ and MPO$^+$ macrophages, further underscoring the complexity of TAMs. Moreover, several studies have interrogated the dynamic changes of TAMs responding to treatment and microenvironmental stimulation, providing novel insights into how TAMs modulate therapeutic response and resistance. Therefore, harnessing TAMs via different approaches may be feasible in treating rGBM, and TAM-based combination therapy regimens have started to show a promising potential.

Still, dynamics and diversities of TAMs in the context of rGBM, and underlying molecular mechanisms remain incompletely clarified, which warrants further investigations and integrated analyses of high-dimensional and high-resolution data, such as spatial scRNA-seq, single-cell proteomics, and single-cell sequencing assay for transposase-accessible chromatin (scATAC-seq). More studies in the near future should focus on i). distinguishing microglia from MDMs; ii). identifying specific tumor-supportive and tumor-suppressive TAM subclusters; iii). delineating the stage- and therapy-specific reprogramming of TAMs in longitudinal cohorts; iv). dissecting the cellular crosstalk between TAMs and other cells; v). exploring rationale-based combination therapy modalities in clinical trials targeting TAMs. Ultimately, comprehensively understanding TAMs and their interplay with other cells will be instrumental for optimal immunomodulation and enhanced immunotherapeutic efficacy for patients with rGBM.

Author contributions

GZ and SW conceived and designed the study. LZ wrote the original draft. YJ, GZ and SW revised the manuscript. All authors contributed to the article and approved the submitted version.

Funding

This research is supported by grants from China Postdoctoral Science Foundation (No. 2022M720103), Postdoctoral Program of Sichuan Province (No. TB2022018), and the Fundamental Research Funds for the Central Universities (No. 2023SCU12052).

Acknowledgments

The authors thank all subjects for their participation in the research.

Conflict of interest

The authors declare that the research was conducted in the absence of any commercial or financial relationships that could be construed as a potential conflict of interest.

Publisher's note

References

1. Tan AC, Ashley DM, Lopez GY, Malinzak M, Friedman HS, Khasraw M. Management of glioblastoma: State of the art and future directions. *CA Cancer J Clin* (2020) 70:299–312. doi: 10.3322/caac.21613

2. Campos B, Olsen LR, Urup T, Poulsen HS. A comprehensive profile of recurrent glioblastoma. *Oncogene* (2016) 35:5819–25. doi: 10.1038/onc.2016.85

3. Stupp R, Mason WP, van den Bent MJ, Weller M, Fisher B, Taphoorn MJ, et al. Radiotherapy plus concomitant and adjuvant temozolomide for glioblastoma. *N Engl J Med* (2005) 352:987–96. doi: 10.1056/NEJMoa043330

4. Stupp R, Hegi ME, Mason WP, van den Bent MJ, Taphoorn MJ, Janzer RC, et al. Effects of radiotherapy with concomitant and adjuvant temozolomide versus radiotherapy alone on survival in glioblastoma in a randomised phase III study: 5-year analysis of the EORTC-NCIC trial. *Lancet Oncol* (2009) 10:459–66. doi: 10.1016/S1470-2045(09)70025-7

5. Zhang Y, Zhang Z. The history and advances in cancer immunotherapy: understanding the characteristics of tumor-infiltrating immune cells and their therapeutic implications. *Cell Mol Immunol* (2020) 17:807–21. doi: 10.1038/s41423-020-0488-6

6. Reardon DA, Brandes AA, Omuro A, Mulholland P, Lim M, Wick A, et al. Effect of nivolumab vs bevacizumab in patients with recurrent glioblastoma: the checkMate 143 phase 3 randomized clinical trial. *JAMA Oncol* (2020) 6:1003–10. doi: 10.1001/jamaoncol.2020.1024

7. O'Rourke DM, Nasrallah MP, Desai A, Melenhorst JJ, Mansfield K, Morrissette JJD, et al. A single dose of peripherally infused EGFRvIII-directed CAR T cells mediates antigen loss and induces adaptive resistance in patients with recurrent glioblastoma. *Sci Transl Med* (2017) 9:eaaa0984. doi: 10.1126/scitranslmed.aaa0984

8. de Groot J, Penas-Prado M, Alfaro-Munoz K, Hunter K, Pei BL, O'Brien B, et al. Window-of-opportunity clinical trial of pembrolizumab in patients with recurrent glioblastoma reveals predominance of immune-suppressive macrophages. *Neuro Oncol* (2020) 22:539–49. doi: 10.1093/neuonc/noz185

9. Tomaszewski W, Sanchez-Perez L, Gajewski TF, Sampson JH. Brain tumor microenvironment and host state: implications for immunotherapy. *Clin Cancer Res* (2019) 25:4202–10. doi: 10.1158/1078-0432.CCR-18-1627

10. Quail DF, Joyce JA. The microenvironmental landscape of brain tumors. *Cancer Cell* (2017) 31:326–41. doi: 10.1016/j.ccell.2017.02.009

11. Rajendran S, Hu Y, Canella A, Peterson C, Gross A, Cam M, et al. Single-cell RNA sequencing reveals immunosuppressive myeloid cell diversity during Malignant progression in a murine model of glioma. *Cell Rep* (2023) 42:112197. doi: 10.1016/j.celrep.2023.112197

12. Hambardzumyan D, Gutmann DH, Kettenmann H. The role of microglia and macrophages in glioma maintenance and progression. *Nat Neurosci* (2016) 19:20–7. doi: 10.1038/nn.4185

13. Khan F, Pang L, Dunterman M, Lesniak MS, Heimberger AB, Chen P. Macrophages and microglia in glioblastoma: heterogeneity, plasticity, and therapy. *J Clin Invest.* (2023) 133:e163446. doi: 10.1172/JCI163446

14. Wu M, Shi Y, Zhu L, Chen L, Zhao X, Xu C. Macrophages in glioblastoma development and therapy: A double-edged sword. *Life (Basel).* (2022) 12:1225. doi: 10.3390/life12081225

15. Lu-Emerson C, Snuderl M, Kirkpatrick ND, Goveia J, Davidson C, Huang Y, et al. Increase in tumor-associated macrophages after antiangiogenic therapy is associated with poor survival among patients with recurrent glioblastoma. *Neuro Oncol* (2013) 15:1079–87. doi: 10.1093/neuonc/not082

16. Ochocka N, Kaminska B. Microglia diversity in healthy and diseased brain: insights from single-cell omics. *Int J Mol Sci* (2021) 22:3027. doi: 10.3390/ijms22063027

17. Mantovani A, Allavena P, Marchesi F, Garlanda C. Macrophages as tools and targets in cancer therapy. *Nat Rev Drug Discovery* (2022) 21:799–820. doi: 10.1038/s41573-022-00520-5

18. Andersen JK, Miletic H, Hossain JA. Tumor-associated macrophages in gliomas-basic insights and treatment opportunities. *Cancers (Basel).* (2022) 14:1319. doi: 10.3390/cancers14051319

19. Verhaak RG, Hoadley KA, Purdom E, Wang V, Qi Y, Wilkerson MD, et al. Integrated genomic analysis identifies clinically relevant subtypes of glioblastoma characterized by abnorMalities in PDGFRA, IDH1, EGFR, and NF1. *Cancer Cell* (2010) 17:98–110. doi: 10.1016/j.ccr.2009.12.020

20. Martinez-Lage M, Lynch TM, Bi Y, Cocito C, Way GP, Pal S, et al. Immune landscapes associated with different glioblastoma molecular subtypes. *Acta Neuropathol Commun* (2019) 7:203. doi: 10.1186/s40478-019-0803-6

21. Rutledge WC, Kong J, Gao J, Gutman DA, Cooper LA, Appin C, et al. Tumor-infiltrating lymphocytes in glioblastoma are associated with specific genomic alterations and related to transcriptional class. *Clin Cancer Res* (2013) 19:4951–60. doi: 10.1158/1078-0432.CCR-13-0551

22. Neftel C, Laffy J, Filbin MG, Hara T, Shore ME, Rahme GJ, et al. An integrative model of cellular states, plasticity, and genetics for glioblastoma. *Cell* (2019) 178:835–49 e21. doi: 10.1016/j.cell.2019.06.024

23. Rahman M, Kresak J, Yang C, Huang J, Hiser W, Kubilis P, et al. Analysis of immunobiologic markers in primary and recurrent glioblastoma. *J Neurooncol.* (2018) 137:249–57. doi: 10.1007/s11060-017-2732-1

24. Berghoff AS, Kiesel B, Widhalm G, Wilhelm D, Rajky O, Kurscheid S, et al. Correlation of immune phenotype with IDH mutation in diffuse glioma. *Neuro Oncol* (2017) 19:1460–8. doi: 10.1093/neuonc/nox054

25. Myung JK, Cho HJ, Park CK, Kim SK, Phi JH, Park SH. IDH1 mutation of gliomas with long-term survival analysis. *Oncol Rep* (2012) 28:1639–44. doi: 10.3892/or.2012.1994

26. Sampson JH, Heimberger AB, Archer GE, Aldape KD, Friedman AH, Friedman HS, et al. Immunologic escape after prolonged progression-free survival with epidermal growth factor receptor variant III peptide vaccination in patients with newly diagnosed glioblastoma. *J Clin Oncol* (2010) 28:4722–9. doi: 10.1200/JCO.2010.28.6963

27. van Hooren L, Handgraaf SM, Kloosterman DJ, Karimi E, van Mil L, Gassama AA, et al. CD103(+) regulatory T cells underlie resistance to radio-immunotherapy and impair CD8(+) T cell activation in glioblastoma. *Nat Cancer* (2023) 4:665–671. doi: 10.1038/s43018-023-00547-6

28. Pauken KE, Wherry EJ. Overcoming T cell exhaustion in infection and cancer. *Trends Immunol* (2015) 36:265–76. doi: 10.1016/j.it.2015.02.008

29. Reck M, Rodriguez-Abreu D, Robinson AG, Hui R, Csoszi T, Fulop A, et al. Pembrolizumab versus chemotherapy for PD-L1-positive non-small-cell lung cancer. *N Engl J Med* (2016) 375:1823–33. doi: 10.1056/NEJMoa1606774

30. Hamid O, Robert C, Daud A, Hodi FS, Hwu WJ, Kefford R, et al. Safety and tumor responses with lambrolizumab (anti-PD-1) in melanoma. *N Engl J Med* (2013) 369:134–44. doi: 10.1056/NEJMoa1305133

31. Ansell SM, Lesokhin AM, Borrello I, Halwani A, Scott EC, Gutierrez M, et al. PD-1 blockade with nivolumab in relapsed or refractory Hodgkin's lymphoma. *N Engl J Med* (2015) 372:311–9. doi: 10.1056/NEJMoa1411087

32. Cloughesy TF, Mochizuki AY, Orpilla JR, Hugo W, Lee AH, Davidson TB, et al. Neoadjuvant anti-PD-1 immunotherapy promotes a survival benefit with intratumoral and systemic immune responses in recurrent glioblastoma. *Nat Med* (2019) 25:477–86. doi: 10.1038/s41591-018-0337-7

33. Puigdelloses M, Garcia-Moure M, Labiano S, Laspidea V, Gonzalez-Huarriz M, Zalacain M, et al. CD137 and PD-L1 targeting with immunovirotherapy induces a potent and durable antitumor immune response in glioblastoma models. *J Immunother Cancer.* (2021) 9:1. doi: 10.1136/jitc-2021-002644

34. Wainwright DA, Chang AL, Dey M, Balyasnikova IV, Kim CK, Tobias A, et al. Durable therapeutic efficacy utilizing combinatorial blockade against IDO, CTLA-4, and PD-L1 in mice with brain tumors. *Clin Cancer Res* (2014) 20:5290–301. doi: 10.1158/1078-0432.CCR-14-0514

35. Reardon DA, Gokhale PC, Klein SR, Ligon KL, Rodig SJ, Ramkissoon SH, et al. Glioblastoma eradication following immune checkpoint blockade in an orthotopic, immunocompetent model. *Cancer Immunol Res* (2016) 4:124–35. doi: 10.1158/2326-6066.CIR-15-0151

36. Maghrouni A, Givari M, Jalili-Nik M, Mollazadeh H, Bibak B, Sadeghi MM, et al. Targeting the PD-1/PD-L1 pathway in glioblastoma multiforme: Preclinical evidence and clinical interventions. *Int Immunopharmacol.* (2021) 93:107403. doi: 10.1016/j.intimp.2021.107403

37. Saikali S, Avril T, Collet B, Hamlat A, Bansard JY, Drenou B, et al. Expression of nine tumour antigens in a series of human glioblastoma multiforme: interest of EGFRvIII, IL-13Ralpha2, gp100 and TRP-2 for immunotherapy. *J Neurooncol.* (2007) 81:139–48. doi: 10.1007/s11060-006-9220-3

38. Zhu X, Prasad S, Gaedicke S, Hettich M, Firat E, Niedermann G. Patient-derived glioblastoma stem cells are killed by CD133-specific CAR T cells but induce the T cell aging marker CD57. *Oncotarget* (2015) 6:171–84. doi: 10.18632/oncotarget.2767

39. Ahmed N, Salsman VS, Kew Y, Shaffer D, Powell S, Zhang YJ, et al. HER2-specific T cells target primary glioblastoma stem cells and induce regression of autologous experimental tumors. *Clin Cancer Res* (2010) 16:474–85. doi: 10.1158/1078-0432.CCR-09-1322

40. Izumoto S, Tsuboi A, Oka Y, Suzuki T, Hashiba T, Kagawa N, et al. Phase II clinical trial of Wilms tumor 1 peptide vaccination for patients with recurrent glioblastoma multiforme. *J Neurosurg* (2008) 108:963–71. doi: 10.3171/JNS/2008/108/5/0963

41. Bloch O, Crane CA, Fuks Y, Kaur R, Aghi MK, Berger MS, et al. Heat-shock protein peptide complex-96 vaccination for recurrent glioblastoma: a phase II, single-arm trial. *Neuro Oncol* (2014) 16:274–9. doi: 10.1093/neuonc/not203

42. Sakai K, Shimodaira S, Maejima S, Udagawa N, Sano K, Higuchi Y, et al. Dendritic cell-based immunotherapy targeting Wilms' tumor 1 in patients with recurrent Malignant glioma. *J Neurosurg* (2015) 123:989–97. doi: 10.3171/2015.1.JNS141554

43. De Vleeschouwer S, Fieuws S, Rutkowski S, Van Calenbergh F, Van Loon J, Goffin J, et al. Postoperative adjuvant dendritic cell-based immunotherapy in patients with relapsed glioblastoma multiforme. *Clin Cancer Res* (2008) 14:3098–104. doi: 10.1158/1078-0432.CCR-07-4875

44. Shah AH, Bregy A, Heros DO, Komotar RJ, Goldberg J. Dendritic cell vaccine for recurrent high-grade gliomas in pediatric and adult subjects: clinical trial protocol. *Neurosurgery* (2013) 73:863–7. doi: 10.1227/NEU.0000000000000107

45. Okada H, Kalinski P, Ueda R, Hoji A, Kohanbash G, Donegan TE, et al. Induction of CD8+ T-cell responses against novel glioma-associated antigen peptides and clinical activity by vaccinations with alpha-type 1 polarized dendritic cells and polyinosinic-polycytidylic acid stabilized by lysine and carboxymethylcellulose in patients with recurrent Malignant glioma. *J Clin Oncol* (2011) 29:330–6. doi: 10.1200/JCO.2010.30.7744

46. Grupp SA, Kalos M, Barrett D, Aplenc R, Porter DL, Rheingold SR, et al. Chimeric antigen receptor-modified T cells for acute lymphoid leukemia. *N Engl J Med* (2013) 368:1509–18. doi: 10.1056/NEJMoa1215134

47. Maude SL, Frey N, Shaw PA, Aplenc R, Barrett DM, Bunin NJ, et al. Chimeric antigen receptor T cells for sustained remissions in leukemia. *N Engl J Med* (2014) 371:1507–17. doi: 10.1056/NEJMoa1407222

48. Almasbak H, Aarvak T, Vemuri MC. CAR T cell therapy: A game changer in cancer treatment. *J Immunol Res* (2016) 2016:5474602. doi: 10.1155/2016/5474602

49. Brown CE, Badie B, Barish ME, Weng L, Ostberg JR, Chang WC, et al. Bioactivity and safety of IL13Ralpha2-redirected chimeric antigen receptor CD8+ T cells in patients with recurrent glioblastoma. *Clin Cancer Res* (2015) 21:4062–72. doi: 10.1158/1078-0432.CCR-15-0428

50. Ahmed N, Brawley V, Hegde M, Bielamowicz K, Kalra M, Landi D, et al. HER2-specific chimeric antigen receptor-modified virus-specific T cells for progressive glioblastoma: A phase 1 dose-escalation trial. *JAMA Oncol* (2017) 3:1094–101. doi: 10.1001/jamaoncol.2017.0184

51. Brown CE, Rodriguez A, Palmer J, Ostberg JR, Naranjo A, Wagner JR, et al. Off-the-shelf, steroid-resistant, IL13Ralpha2-specific CAR T cells for treatment of glioblastoma. *Neuro Oncol* (2022) 24:1318–30. doi: 10.1093/neuonc/noac024

52. Migliorini D, Dietrich PY, Stupp R, Linette GP, Posey AD Jr., June CH. CAR T-cell therapies in glioblastoma: A first look. *Clin Cancer Res* (2018) 24:535–40. doi: 10.1158/1078-0432.CCR-17-2871

53. Gan HK, Kaye AH, Luwor RB. The EGFRvIII variant in glioblastoma multiforme. *J Clin Neurosci* (2009) 16:748–54. doi: 10.1016/j.jocn.2008.12.005

54. van den Bent MJ, Gao Y, Kerkhof M, Kros JM, Gorlia T, van Zwieten K, et al. Changes in the EGFR amplification and EGFRvIII expression between paired primary and recurrent glioblastomas. *Neuro Oncol* (2015) 17:935–41. doi: 10.1093/neuonc/nov013

55. Wang X, Lu J, Guo G, Yu J. Immunotherapy for recurrent glioblastoma: practical insights and challenging prospects. *Cell Death Dis* (2021) 12:299. doi: 10.1038/s41419-021-03568-0

56. Alliot F, Godin I, Pessac B. Microglia derive from progenitors, originating from the yolk sac, and which proliferate in the brain. *Brain Res Dev Brain Res* (1999) 117:145–52. doi: 10.1016/s0165-3806(99)00113-3

57. Platten M, Kretz A, Naumann U, Aulwurm S, Egashira K, Isenmann S, et al. Monocyte chemoattractant protein-1 increases microglial infiltration and aggressiveness of gliomas. *Ann Neurol* (2003) 54:388–92. doi: 10.1002/ana.10679

58. Chen Z, Feng X, Herting CJ, Garcia VA, Nie K, Pong WW, et al. Cellular and molecular identity of tumor-associated macrophages in glioblastoma. *Cancer Res* (2017) 77:2266–78. doi: 10.1158/0008-5472.CAN-16-2310

59. Wang SC, Hong JH, Hsueh C, Chiang CS. Tumor-secreted SDF-1 promotes glioma invasiveness and TAM tropism toward hypoxia in a murine astrocytoma model. *Lab Invest.* (2012) 92:151–62. doi: 10.1038/labinvest.2011.128

60. Stafford JH, Hirai T, Deng L, Chernikova SB, Urata K, West BL, et al. Colony stimulating factor 1 receptor inhibition delays recurrence of glioblastoma after radiation by altering myeloid cell recruitment and polarization. *Neuro Oncol* (2016) 18:797–806. doi: 10.1093/neuonc/nov272

61. Muller A, Brandenburg S, Turkowski K, Muller S, Vajkoczy P. Resident microglia, and not peripheral macrophages, are the main source of brain tumor mononuclear cells. *Int J Cancer.* (2015) 137:278–88. doi: 10.1002/ijc.29379

62. Pombo Antunes AR, Scheyltjens I, Lodi F, Messiaen J, Antoranz A, Duerinck J, et al. Single-cell profiling of myeloid cells in glioblastoma across species and disease stage reveals macrophage competition and specialization. *Nat Neurosci* (2021) 24:595–610. doi: 10.1038/s41593-020-00789-y

63. Muller S, Kohanbash G, Liu SJ, Alvarado B, Carrera D, Bhaduri A, et al. Single-cell profiling of human gliomas reveals macrophage ontogeny as a basis for regional differences in macrophage activation in the tumor microenvironment. *Genome Biol* (2017) 18:234. doi: 10.1186/s13059-017-1362-4

64. Liu YC, Zou XB, Chai YF, Yao YM. Macrophage polarization in inflammatory diseases. *Int J Biol Sci* (2014) 10:520–9. doi: 10.7150/ijbs.8879

65. Lawrence T, Natoli G. Transcriptional regulation of macrophage polarization: enabling diversity with identity. *Nat Rev Immunol* (2011) 11:750–61. doi: 10.1038/nri3088

66. Martinez FO, Gordon S. The M1 and M2 paradigm of macrophage activation: time for reassessment. *F1000Prime Rep* (2014) 6:13. doi: 10.12703/P6-13

67. Murray PJ, Allen JE, Biswas SK, Fisher EA, Gilroy DW, Goerdt S, et al. Macrophage activation and polarization: nomenclature and experimental guidelines. *Immunity* (2014) 41:14–20. doi: 10.1016/j.immuni.2014.06.008

68. Alterman RL, Stanley ER. Colony stimulating factor-1 expression in human glioma. *Mol Chem Neuropathol.* (1994) 21:177–88. doi: 10.1007/BF02815350

69. Zhou W, Ke SQ, Huang Z, Flavahan W, Fang X, Paul J, et al. Periostin secreted by glioblastoma stem cells recruits M2 tumour-associated macrophages and promotes Malignant growth. *Nat Cell Biol* (2015) 17:170–82. doi: 10.1038/ncb3090

70. Wu A, Wei J, Kong LY, Wang Y, Priebe W, Qiao W, et al. Glioma cancer stem cells induce immunosuppressive macrophages/microglia. *Neuro Oncol* (2010) 12:1113–25. doi: 10.1093/neuonc/noq082

71. Wei J, Marisetty A, Schrand B, Gabrusiewicz K, Hashimoto Y, Ott M, et al. Osteopontin mediates glioblastoma-associated macrophage infiltration and is a potential therapeutic target. *J Clin Invest.* (2019) 129:137–49. doi: 10.1172/JCI121266

72. Noorani I, Sidlauskas K, Pellow S, Savage R, Norman JL, Chatelet DS, et al. Clinical impact of anti-inflammatory microglia and macrophage phenotypes at glioblastoma margins. *Brain Commun* (2023) 5:fcad176. doi: 10.1093/braincomms/fcad176

73. Karimi E, Yu MW, Maritan SM, Perus LJM, Rezanejad M, Sorin M, et al. Single-cell spatial immune landscapes of primary and metastatic brain tumours. *Nature* (2023) 614:555–63. doi: 10.1038/s41586-022-05680-3

74. Kim HJ, Park JH, Kim HC, Kim CW, Kang I, Lee HK. Blood monocyte-derived CD169(+) macrophages contribute to antitumor immunity against glioblastoma. *Nat Commun* (2022) 13:6211. doi: 10.1038/s41467-022-34001-5

75. Sankowski R, Bottcher C, Masuda T, Geirsdottir L, Sagar, Sindram E, et al. Mapping microglia states in the human brain through the integration of high-dimensional techniques. *Nat Neurosci* (2019) 22:2098–110. doi: 10.1038/s41593-019-0532-y

76. Duan Z, Luo Y. Targeting macrophages in cancer immunotherapy. *Signal Transduct Target Ther* (2021) 6:127. doi: 10.1038/s41392-021-00506-6

77. Ye XZ, Xu SL, Xin YH, Yu SC, Ping YF, Chen L, et al. Tumor-associated microglia/macrophages enhance the invasion of glioma stem-like cells via TGF-beta1 signaling pathway. *J Immunol* (2012) 189:444–53. doi: 10.4049/jimmunol.1103248

78. Shi Y, Ping YF, Zhou W, He ZC, Chen C, Bian BS, et al. Tumour-associated macrophages secrete pleiotrophin to promote PTPRZ1 signalling in glioblastoma stem cells for tumour growth. *Nat Commun* (2017) 8:15080. doi: 10.1038/ncomms15080

79. Wang Y, Liu T, Yang N, Xu S, Li X, Wang D. Hypoxia and macrophages promote glioblastoma invasion by the CCL4-CCR5 axis. *Oncol Rep* (2016) 36:3522–8. doi: 10.3892/or.2016.5171

80. Zheng Y, Yang W, Aldape K, He J, Lu Z. Epidermal growth factor (EGF)-enhanced vascular cell adhesion molecule-1 (VCAM-1) expression promotes macrophage and glioblastoma cell interaction and tumor cell invasion. *J Biol Chem* (2013) 288:31488–95. doi: 10.1074/jbc.M113.499020

81. Liu Y, Li X, Zhang Y, Wang H, Rong X, Peng J, et al. An miR-340-5p-macrophage feedback loop modulates the progression and tumor microenvironment of glioblastoma multiforme. *Oncogene* (2019) 38:7399–415. doi: 10.1038/s41388-019-0952-x

82. Wu J, Frady LN, Bash RE, Cohen SM, Schorzman AN, Su YT, et al. MerTK as a therapeutic target in glioblastoma. *Neuro Oncol* (2018) 20:92–102. doi: 10.1093/neuonc/nox111

83. Tamura R, Ohara K, Sasaki H, Morimoto Y, Kosugi K, Yoshida K, et al. Difference in immunosuppressive cells between peritumoral area and tumor core in glioblastoma. *World Neurosurg* (2018) 120:e601–e10. doi: 10.1016/j.wneu.2018.08.133

84. Riabov V, Gudima A, Wang N, Mickley A, Orekhov A, Kzhyshkowska J. Role of tumor associated macrophages in tumor angiogenesis and lymphangiogenesis. *Front Physiol* (2014) 5:75. doi: 10.3389/fphys.2014.00075

85. Tamura R, Tanaka T, Akasaki Y, Murayama Y, Yoshida K, Sasaki H. The role of vascular endothelial growth factor in the hypoxic and immunosuppressive tumor microenvironment: perspectives for therapeutic implications. *Med Oncol* (2019) 37:2. doi: 10.1007/s12032-019-1329-2

86. Cui X, Morales RT, Qian W, Wang H, Gagner JP, Dolgalev I, et al. Hacking macrophage-associated immunosuppression for regulating glioblastoma angiogenesis. *Biomaterials* (2018) 161:164–78. doi: 10.1016/j.biomaterials.2018.01.053

87. Zhu C, Chrifi I, Mustafa D, van der Weiden M, Leenen PJM, Duncker DJ, et al. CECR1-mediated cross talk between macrophages and vascular mural cells promotes neovascularization in Malignant glioma. *Oncogene* (2017) 36:5356–68. doi: 10.1038/onc.2017.145

88. Mieczkowski J, Kocyk M, Nauman P, Gabrusiewicz K, Sielska M, Przanowski P, et al. Down-regulation of IKKbeta expression in glioma-infiltrating microglia/macrophages is associated with defective inflammatory/immune gene responses in glioblastoma. *Oncotarget* (2015) 6:33077–90. doi: 10.18632/oncotarget.5310

89. Barberi T, Martin A, Suresh R, Barakat DJ, Harris-Bookman S, Drake CG, et al. Absence of host NF-kappaB p50 induces murine glioblastoma tumor regression, increases survival, and decreases T-cell induction of tumor-associated macrophage M2 polarization. *Cancer Immunol Immunother.* (2018) 67:1491–503. doi: 10.1007/s00262-018-2184-2

90. Takenaka MC, Gabriely G, Rothhammer V, Mascanfroni ID, Wheeler MA, Chao CC, et al. Control of tumor-associated macrophages and T cells in glioblastoma via AHR and CD39. *Nat Neurosci* (2019) 22:729–40. doi: 10.1038/s41593-019-0370-y

91. Bloch O, Crane CA, Kaur R, Safaee M, Rutkowski MJ, Parsa AT. Gliomas promote immunosuppression through induction of B7-H1 expression in tumor-associated macrophages. *Clin Cancer Res* (2013) 19:3165–75. doi: 10.1158/1078-0432.CCR-12-3314

92. Yao Y, Ye H, Qi Z, Mo L, Yue Q, Baral A, et al. B7-H4(B7x)-Mediated Cross-talk between Glioma-Initiating Cells and Macrophages via the IL6/JAK/STAT3 Pathway Lead to Poor Prognosis in Glioma Patients. *Clin Cancer Res* (2016) 22:2778–90. doi: 10.1158/1078-0432.CCR-15-0858

93. Chuang HY, Su YK, Liu HW, Chen CH, Chiu SC, Cho DY, et al. Preclinical Evidence of STAT3 Inhibitor Pacritinib Overcoming Temozolomide Resistance via Downregulating miR-21-Enriched Exosomes from M2 Glioblastoma-Associated Macrophages. *J Clin Med* (2019) 8:959. doi: 10.3390/jcm8070959

94. Miyazaki T, Ishikawa E, Matsuda M, Sugii N, Kohzuki H, Akutsu H, et al. Infiltration of CD163-positive macrophages in glioma tissues after treatment with anti-PD-L1 antibody and role of PI3Kgamma inhibitor as a combination therapy with anti-PD-L1 antibody in *in vivo* model using temozolomide-resistant murine glioma-initiating cells. *Brain Tumor Pathol* (2020) 37:41–9. doi: 10.1007/s10014-020-00357-z

95. Akkari L, Bowman RL, Tessier J, Klemm F, Handgraaf SM, de Groot M, et al. Dynamic changes in glioma macrophage populations after radiotherapy reveal CSF-1R inhibition as a strategy to overcome resistance. *Sci Transl Med* (2020) 12:552. doi: 10.1126/scitranslmed.aaw7843

96. Simonds EF, Lu ED, Badillo O, Karimi S, Liu EV, Tamaki W, et al. Deep immune profiling reveals targetable mechanisms of immune evasion in immune checkpoint inhibitor-refractory glioblastoma. *J Immunother Cancer*. (2021) 9:e002181. doi: 10.1136/jitc-2020-002181

97. Lee AH, Sun L, Mochizuki AY, Reynoso JG, Orpilla J, Chow F, et al. Neoadjuvant PD-1 blockade induces T cell and cDC1 activation but fails to overcome the immunosuppressive tumor associated macrophages in recurrent glioblastoma. *Nat Commun* (2021) 12:6938. doi: 10.1038/s41467-021-26940-2

98. Klemm F, Mockl A, Salamero-Boix A, Alekseeva T, Schaffer A, Schulz M, et al. Compensatory CSF2-driven macrophage activation promotes adaptive resistance to CSF1R inhibition in breast-to-brain metastasis. *Nat Cancer*. (2021) 2:1086–101. doi: 10.1038/s43018-021-00254-0

99. Zeiner PS, Preusse C, Golebiewska A, Zinke J, Iriondo A, Muller A, et al. Distribution and prognostic impact of microglia/macrophage subpopulations in gliomas. *Brain Pathol* (2019) 29:513–29. doi: 10.1111/bpa.12690

100. Darmanis S, Sloan SA, Croote D, Mignardi M, Chernikova S, Samghababi P, et al. Single-cell RNA-seq analysis of infiltrating neoplastic cells at the migrating front of human glioblastoma. *Cell Rep* (2017) 21:1399–410. doi: 10.1016/j.celrep.2017.10.030

101. Yeo AT, Rawal S, Delcuze B, Christofides A, Atayde A, Strauss L, et al. Single-cell RNA sequencing reveals evolution of immune landscape during glioblastoma progression. *Nat Immunol* (2022) 23:971–84. doi: 10.1038/s41590-022-01215-0

102. Venteicher AS, Tirosh I, Hebert C, Yizhak K, Neftel C, Filbin MG, et al. Decoupling genetics, lineages, and microenvironment in IDH-mutant gliomas by single-cell RNA-seq. *Science* (2017) 355:eaai8478. doi: 10.1126/science.aai8478

103. Ochocka N, Segit P, Walentynowicz KA, Wojnicki K, Cyranowski S, Swatler J, et al. Single-cell RNA sequencing reveals functional heterogeneity of glioma-associated brain macrophages. *Nat Commun* (2021) 12:1151. doi: 10.1038/s41467-021-21407-w

104. Goswami S, Walle T, Cornish AE, Basu S, Anandhan S, Fernandez I, et al. Immune profiling of human tumors identifies CD73 as a combinatorial target in glioblastoma. *Nat Med* (2020) 26:39–46. doi: 10.1038/s41591-019-0694-x

105. Abdelfattah N, Kumar P, Wang C, Leu JS, Flynn WF, Gao R, et al. Single-cell analysis of human glioma and immune cells identifies S100A4 as an immunotherapy target. *Nat Commun* (2022) 13:767. doi: 10.1038/s41467-022-28372-y

106. Chen AX, Gartrell RD, Zhao J, Upadhyayula PS, Zhao W, Yuan J, et al. Single-cell characterization of macrophages in glioblastoma reveals MARCO as a mesenchymal pro-tumor marker. *Genome Med* (2021) 13:88. doi: 10.1186/s13073-021-00906-x

107. Liu H, Sun Y, Zhang Q, Jin W, Gordon RE, Zhang Y, et al. Pro-inflammatory and proliferative microglia drive progression of glioblastoma. *Cell Rep* (2021) 36:109718. doi: 10.1016/j.celrep.2021.109718

108. Ravi VM, Neidert N, Will P, Joseph K, Maier JP, Kuckelhaus J, et al. T-cell dysfunction in the glioblastoma microenvironment is mediated by myeloid cells releasing interleukin-10. *Nat Commun* (2022) 13:925. doi: 10.1038/s41467-022-28523-1

109. Xiao Y, Wang Z, Zhao M, Deng Y, Yang M, Su G, et al. Single-cell transcriptomics revealed subtype-specific tumor immune microenvironments in human glioblastomas. *Front Immunol* (2022) 13:914236. doi: 10.3389/fimmu.2022.914236

110. Hoogstrate Y, Draaisma K, Ghisai SA, van Hijfte L, Barin N, de Heer I, et al. Transcriptome analysis reveals tumor microenvironment changes in glioblastoma. *Cancer Cell* (2023) 41:678–92 e7. doi: 10.1016/j.ccell.2023.02.019

111. Wang L, Jung J, Babikir H, Shamardani K, Jain S, Feng X, et al. A single-cell atlas of glioblastoma evolution under therapy reveals cell-intrinsic and cell-extrinsic therapeutic targets. *Nat Cancer*. (2022) 3:1534–52. doi: 10.1038/s43018-022-00475-x

112. Wu H, Guo C, Wang C, Xu J, Zheng S, Duan J, et al. Single-cell RNA sequencing reveals tumor heterogeneity, microenvironment, and drug-resistance mechanisms of recurrent glioblastoma. *Cancer Sci* (2023) 114:2609–21. doi: 10.1111/cas.15773

113. Al-Dalahmah O, Argenziano MG, Kannan A, Mahajan A, Furnari J, Paryani F, et al. Re-convolving the compositional landscape of primary and recurrent glioblastoma reveals prognostic and targetable tissue states. *Nat Commun* (2023) 14:2586. doi: 10.1038/s41467-023-38186-1

114. Hara T, Chanoch-Myers R, Mathewson ND, Myskiw C, Atta L, Bussema L, et al. Interactions between cancer cells and immune cells drive transitions to mesenchymal-like states in glioblastoma. *Cancer Cell* (2021) 39:779–92 e11. doi: 10.1016/j.ccell.2021.05.002

115. Buonfiglioli A, Hambardzumyan D. Macrophages and microglia: the cerberus of glioblastoma. *Acta Neuropathol Commun* (2021) 9:54. doi: 10.1186/s40478-021-01156-z

116. Wang G, Zhong K, Wang Z, Zhang Z, Tang X, Tong A, et al. Tumor-associated microglia and macrophages in glioblastoma: From basic insights to therapeutic opportunities. *Front Immunol* (2022) 13:964898. doi: 10.3389/fimmu.2022.964898

117. Flores-Toro JA, Luo D, Gopinath A, Sarkisian MR, Campbell JJ, Charo IF, et al. CCR2 inhibition reduces tumor myeloid cells and unmasks a checkpoint inhibitor effect to slow progression of resistant murine gliomas. *Proc Natl Acad Sci U S A*. (2020) 117:1129–38. doi: 10.1073/pnas.1910856117

118. Chen P, Zhao D, Li J, Liang X, Li J, Chang A, et al. Symbiotic macrophage-glioma cell interactions reveal synthetic lethality in PTEN-null glioma. *Cancer Cell* (2019) 35:868–84 e6. doi: 10.1016/j.ccell.2019.05.003

119. Geraldo LH, Xu Y, Jacob L, Pibouin-Fragner L, Rao R, Maissa N, et al. SLIT2/ROBO signaling in tumor-associated microglia and macrophages drives glioblastoma immunosuppression and vascular dysmorphia. *J Clin Invest*. (2021) 131:e141083. doi: 10.1172/JCI141083

120. Stanley ER, Chitu V. CSF-1 receptor signaling in myeloid cells. *Cold Spring Harb Perspect Biol* (2014) 6:a021857. doi: 10.1101/cshperspect.a021857

121. Achkova D, Maher J. Role of the colony-stimulating factor (CSF)/CSF-1 receptor axis in cancer. *Biochem Soc Trans* (2016) 44:333–41. doi: 10.1042/BST20150245

122. Laoui D, Van Overmeire E, De Baetselier P, Van Ginderachter JA, Raes G. Functional relationship between tumor-associated macrophages and macrophage colony-stimulating factor as contributors to cancer progression. *Front Immunol* (2014) 5:489. doi: 10.3389/fimmu.2014.00489

123. Barca C, Foray C, Hermann S, Herrlinger U, Remory I, Laoui D, et al. The colony stimulating factor-1 receptor (CSF-1R)-mediated regulation of microglia/macrophages as a target for neurological disorders (Glioma, stroke). *Front Immunol* (2021) 12:787307. doi: 10.3389/fimmu.2021.787307

124. Yan D, Kowal J, Akkari L, Schuhmacher AJ, Huse JT, West BL, et al. Inhibition of colony stimulating factor-1 receptor abrogates microenvironment-mediated therapeutic resistance in gliomas. *Oncogene* (2017) 36:6049–58. doi: 10.1038/onc.2017.261

125. Butowski N, Colman H, De Groot JF, Omuro AM, Nayak L, Wen PY, et al. Orally administered colony stimulating factor 1 receptor inhibitor PLX3397 in recurrent glioblastoma: an Ivy Foundation Early Phase Clinical Trials Consortium phase II study. *Neuro Oncol* (2016) 18:557–64. doi: 10.1093/neuonc/nov245

126. Przystal JM, Becker H, Canjuga D, Tsiami F, Anderle N, Keller AL, et al. Targeting CSF1R alone or in combination with PD1 in experimental glioma. *Cancers (Basel)*. (2021) 13:2400. doi: 10.3390/cancers13102400

127. DeNardo DG, Ruffell B. Macrophages as regulators of tumour immunity and immunotherapy. *Nat Rev Immunol* (2019) 19:369–82. doi: 10.1038/s41577-019-0127-6

128. Liu Y, Wang Y, Yang Y, Weng L, Wu Q, Zhang J, et al. Emerging phagocytosis checkpoints in cancer immunotherapy. *Signal Transduct Target Ther* (2023) 8:104. doi: 10.1038/s41392-023-01365-z

129. Logtenberg MEW, Scheeren FA, Schumacher TN. The CD47-SIRPalpha immune checkpoint. *Immunity* (2020) 52:742–52. doi: 10.1016/j.immuni.2020.04.011

130. Li F, Lv B, Liu Y, Hua T, Han J, Sun C, et al. Blocking the CD47-SIRPalpha axis by delivery of anti-CD47 antibody induces antitumor effects in glioma and glioma stem cells. *Oncoimmunology* (2018) 7:e1391973. doi: 10.1080/2162402X.2017.1391973

131. Barkal AA, Brewer RE, Markovic M, Kowarsky M, Barkal SA, Zaro BW, et al. CD24 signalling through macrophage Siglec-10 is a target for cancer immunotherapy. *Nature* (2019) 572:392–6. doi: 10.1038/s41586-019-1456-0

132. Wu H, Liu J, Wang Z, Yuan W, Chen L. Prospects of antibodies targeting CD47 or CD24 in the treatment of glioblastoma. *CNS Neurosci Ther* (2021) 27:1105–17. doi: 10.1111/cns.13714

133. Chonan M, Saito R, Shoji T, Shibahara I, Kanamori M, Sonoda Y, et al. CD40/CD40L expression correlates with the survival of patients with glioblastomas and an augmentation in CD40 signaling enhances the efficacy of vaccinations against glioma models. *Neuro Oncol* (2015) 17:1453–62. doi: 10.1093/neuonc/nov090

134. Yang F, He Z, Duan H, Zhang D, Li J, Yang H, et al. Synergistic immunotherapy of glioblastoma by dual targeting of IL-6 and CD40. *Nat Commun* (2021) 12:3424. doi: 10.1038/s41467-021-23832-3

135. Yin J, Kim SS, Choi E, Oh YT, Lin W, Kim TH, et al. ARS2/MAGL signaling in glioblastoma stem cells promotes self-renewal and M2-like polarization of tumor-associated macrophages. *Nat Commun* (2020) 11:2978. doi: 10.1038/s41467-020-16789-2

136. Deng L, Stafford JH, Liu SC, Chernikova SB, Merchant M, Recht L, et al. SDF-1 blockade enhances anti-VEGF therapy of glioblastoma and can be monitored by MRI. *Neoplasia* (2017) 19:1–7. doi: 10.1016/j.neo.2016.11.010

137. Saha D, Martuza RL, Rabkin SD. Macrophage polarization contributes to glioblastoma eradication by combination immunovirotherapy and immune checkpoint blockade. *Cancer Cell* (2017) 32:253–67 e5. doi: 10.1016/j.ccell.2017.07.006

frontiers | Frontiers in Immunology

TYPE Review
PUBLISHED 20 October 2023
DOI 10.3389/fimmu.2023.1273986

OPEN ACCESS

EDITED BY
Stephanie E.B. McArdle,
Nottingham Trent University,
United Kingdom

REVIEWED BY
Fanen Yuan,
University of Pittsburgh, United States
Prashant Sharma,
University of Arizona, United States

*CORRESPONDENCE
Heung Kyu Lee
heungkyu.lee@kaist.ac.kr

RECEIVED 07 August 2023
ACCEPTED 09 October 2023
PUBLISHED 20 October 2023

CITATION
Kang I, Kim Y and Lee HK (2023)
γδ T cells as a potential therapeutic
agent for glioblastoma.
Front. Immunol. 14:1273986.
doi: 10.3389/fimmu.2023.1273986

γδ T cells as a potential therapeutic agent for glioblastoma

In Kang[1], Yumin Kim[2] and Heung Kyu Lee[1,2]*

[1]Graduate School of Medical Science and Engineering, Korea Advanced Institute of Science and Technology (KAIST), Daejeon, Republic of Korea, [2]Department of Biological Sciences, KAIST, Daejeon, Republic of Korea

Although γδ T cells comprise a small population of T cells, they perform important roles in protecting against infection and suppressing tumors. With their distinct tissue-localizing properties, combined with their various target recognition mechanisms, γδ T cells have the potential to become an effective solution for tumors that do not respond to current therapeutic procedures. One such tumor, glioblastoma (GBM), is a malignant brain tumor with the highest World Health Organization grade and therefore the worst prognosis. The immune-suppressive tumor microenvironment (TME) and immune-evasive glioma stem cells are major factors in GBM immunotherapy failure. Currently, encouraged by the strong anti-tumoral function of γδ T cells revealed at the preclinical and clinical levels, several research groups have shown progression of γδ T cell–based GBM treatment. However, several limitations still exist that block effective GBM treatment using γδ T cells. Therefore, understanding the distinct roles of γδ T cells in anti-tumor immune responses and the suppression mechanism of the GBM TME are critical for successful γδ T cell–mediated GBM therapy. In this review, we summarize the effector functions of γδ T cells in tumor immunity and discuss current advances and limitations of γδ T cell–based GBM immunotherapy. Additionally, we suggest future directions to overcome the limitations of γδ T cell–based GBM immunotherapy to achieve successful treatment of GBM.

KEYWORDS

glioblastoma, tumor microenvironment, γδ T cells, immunotherapy, engineering

1 Introduction

γδ T cells, named after their distinctive γδ T cell receptor (TCR) usage, comprise approximately 5% of all T lymphocytes (1). Similar to conventional αβ T cells, γδ T cells recognize targets and exert direct cytotoxic effector functions by secreting granzymes or perforin (2, 3) and inducing immune responses of other cells by secreting cytokines (4), thereby participating in host protection against various pathogens or tumors. Unlike αβ T cells, which recognize peptides on the major histocompatibility complex (MHC) (5), γδ T cells recognize other surface molecules (6). In humans, Vδ2$^+$ T cells recognize the

butyrophilin family 2A1 and 3A1 complex (BTN2A1–BTN3A1 complex) linked by phosphoantigens (7), and Vδ1$^+$ T cells recognize MHC class I chain-related molecule A (8). Because these surface molecules are upregulated in the presence of infection or cellular damage (9, 10), γδTCR-mediated target recognition of γδ T cells resembles that of pattern recognition receptors. Therefore, γδ T cells function as linkers between innate and adaptive immune responses (11) and act as the first-line defense system of the body during early infection.

In addition to infection, γδ T cells have demonstrated their importance in immune responses related to tumors (12, 13). γδ T cells not only localize in peripheral organs (14) but also circulate through blood and lymphatics (15). Therefore, they play critical roles in tumor immune responses in solid cancers, such as lung (16) or colorectal cancer (17), as well as in hematopoietic malignancies (18). Particularly for solid cancers, high infiltration of γδ T cells represents a good prognosis marker (19). Therefore, many research groups have investigated γδ T cell–based immunotherapeutic procedures for cancer treatment (20, 21). Based on their diverse target recognition mechanism, a strong tendency toward activation via various types of stimulation, subsequent cytotoxic effector functions (22, 23), and MHC-independent target recognition mechanism (6), the possibility exists that γδ T cells can be effective immunotherapeutic agents that can target tumors that do not respond to current therapeutic procedures (24–26). Therefore, several research groups are investigating γδ T cell–based cancer therapy targeting various tumor models.

Glioblastoma (GBM) is a malignant tumor that occurs in the brain and is the most common yet lethal malignancy among central nervous system (CNS) tumors (27). A lack of distinctive risk factors (28) combined with nonspecific symptoms (29) make GBM difficult to diagnose in the early phase, thereby decreasing the survival rate. Many research groups have performed extensive investigations to identify an effective treatment for GBM. As a result, various mechanical (30, 31), chemical (32), and immunological (33) treatment approaches have been developed for GBM. Although some treatments have shown meaningful increases in patient survival rates (34, 35), many of those procedures did not show substantial results (26, 36, 37). Therefore, identification of novel therapeutic procedures is critical for effective treatment of GBM.

In this review, we will summarize the immunologic signatures of γδ T cells, focusing on their roles in anti-tumoral immune responses. Then, we will discuss current immunotherapeutic approaches in GBM treatment and challenges arising from the tumor microenvironment (TME) of GBM. Additionally, we will discuss current approaches to target GBM using γδ T cells and the limitations of γδ T cell–based treatments. Finally, we will suggest possible solutions to overcome those challenges in γδ T cell–based GBM immunotherapy.

2 γδ T cells

γδ T cells are a small subset of T cells that express the γδTCR instead of the conventional αβTCR. Even though they comprise a small population of circulating lymphocytes (38), γδ T cells localize in peripheral organs and barrier sites such as the skin, mucosal tract of the intestine or reproductive organs, and pulmonary tract (39) and comprise 15–30% of intraepithelial lymphocytes in the human gut (40). γδ T cells are further subdivided into various subsets according to their Vγ (mouse) or Vδ (human) usage, and Vγ or Vδ utilization determines their localization. In mice, γδ T cells expressing Vγ1 or Vγ4 (Tonegawa nomenclature) circulate through the bloodstream, Vγ5 is localized in the skin, Vγ6 is localized in the dermis and meninges, and Vγ7 is localized in the gut (39). In humans, Vδ2$^+$ γδ T cells circulate in the blood, whereas Vδ1$^+$ and Vδ3$^+$ γδ T cells have resident features (13). Even though they make up a small portion of the T cell population (1), their various effector functions and distinct tissue localization make γδ T cells a first-line immune system defense mechanism by directly suppressing pathogenic infection and working as both innate and adaptive immune cells.

γδ T cells recognize various types of surface molecules, unlike conventional αβ T cells that recognize peptides loaded on the MHC. For example, human Vδ1$^+$ γδ T cells recognize the CD1d molecule (41), Vγ8Vδ3$^+$ T cells recognize stress-induced annexin A2 (42), and Vγ9Vδ1$^+$ T cells recognize ephrin type-A receptor 2 induction by AMP-activated protein kinase (43). In addition to these tissue-localizing human γδ T cells, Vγ9Vδ2$^+$ T cells circulating in the peripheral blood recognize the BTN2A1-BTN3A1 complex in the presence of phosphoantigens (7, 44). Because γδTCRs recognize stress-induced molecules expressed on the target cell surface, recognition of γδTCRs resembles that of pattern recognition receptors (45). Therefore, γδ T cells possess invariant or semi-variant signatures, unlike αβ T cells, which have to recognize various peptides; therefore, TCR diversity is critical (46). In addition to the γδTCR, γδ T cells recognize a broad spectrum of surface molecules via NK receptors (NKRs) and exert effector functions synergistically with γδTCR ligation (47). In addition to γδTCR and NKR-mediated target recognition and effector function, γδ T cells may exert a cytolytic function via death ligands (Fas-ligand or TRAIL) (48, 49). With these multi-faceted target recognition mechanisms, γδ T cells play important roles in the first-line protection of various tissues (50, 51).

γδ T cells exert multiple effector functions and share those effector functions with conventional αβ T cells. For example, γδ T cells lyse target cells by granzyme and perforin production (52), similar to cytotoxic CD8$^+$ T cells. Additionally, γδ T cells secrete various cytokines, including IFNγ and TNFα, demonstrating that γδ T cells can modulate the immune system through cytokine production (53). Furthermore, similar to effector CD4$^+$ T cells, γδ T cells polarize into distinct subtypes and concomitantly produce cytokines that affect the surrounding immune microenvironment. Among murine γδ T cells, IL-17-producing γδ T cells and IFN-γ-producing γδ T cells differentially develop in the thymus (54) and perform distinct roles (55, 56). In contrast, human Vγ9Vδ2$^+$ T cells show functional plasticity (57, 58) according to their exposure to cytokines during TCR stimulation. This functional plasticity of γδ T cells makes them multi-faceted effectors that exert both protective and damaging effects in disease conditions, including cancers (1).

2.1 Roles of γδ T cells in tumor suppression

Among the multi-faceted roles of γδ T cells in tumor conditions, tumor-suppressive roles of γδ T cells have been extensively studied by many research groups because of their high cytotoxicity, multipotent effector function, and unique tissue localization, along with the fact that their presence is a positive prognostic marker for all types of solid tumors (19). In a mouse model of prostate cancer, Liu et al. showed that knockout of γδ T cells resulted in extensive tumor growth, and adoptive transfer of γδ T cells significantly reduced tumor burden (59). Moreover, γδ T cells showed superior tumor control compared with the same number of conventional αβ T cells, demonstrating that γδ T cells have better tumor suppression and target-lysing abilities than conventional T cells without tumor specificity. Similarly, in the colorectal cancer model induced by azoxymethane, mice lacking γδ T cells had a higher tumor incidence than those lacking αβ T cells, demonstrating that γδ T cells can act as a primary tumor suppressor (60). Also, in chemically induced skin cancer, knockout of γδ T cells significantly increased tumor growth, whereas depletion of αβ T cells did not affect tumor formation and growth. Therefore, γδ T cells act as tumor suppressors in various organs, including the skin and colon.

In addition to the anti-tumor functional studies of mouse γδ T cells, human γδ T cells have demonstrated anti-tumor function. Figure 1 summarizes the anti-tumoral effector functions of γδ T cells. In case of human Vδ2$^+$ γδ T cells, which bind to BTN2A1-BTN3A1 complex in the presence of phosphoantigens, can exert anti-tumoral functions (61). In addition to γδTCR-mediated cytotoxicity, Vδ2$^+$ γδ T cells also exert cytolytic function via NKG2D-mediated target recognition (62). Furthermore, human Vδ2$^+$ γδ T cells-but not Vδ1$^+$ γδ T cells-can eliminate tumor cells by antibody-dependent cell-mediated cytotoxicity, and the cytotoxicity was proportionate to CD16 upregulation (63).

γδ T cells regulate not only tumor growth via cytotoxic effector function but also other immune cells. Unlike αβ T cells, activated γδ T cells upregulate MHC-II and other co-stimulatory molecules (CD40, CD80, and CD86) and can activate conventional T cells (64). In addition to their high cytotoxicity, γδ T cells can kill tumor cells and present the tumor antigen to conventional T cells, thereby facilitating systemic immune response against tumor cells. Moreover, γδ T cells can augment the functionality of dendritic cells, thereby facilitating antigen presentation and priming of conventional T cells (65). In summary, γδ T cells can efficiently lyse tumor cells, spread the tumor antigen, and facilitate adaptive and systemic immune responses against tumors. Therefore, γδ T cells can be a promising solution to improve current anti-tumor immunotherapy. Thus, many research groups have expanded the utilization of γδ T cells by investigating their roles and effector functions in various types of cancers and have attempted to treat

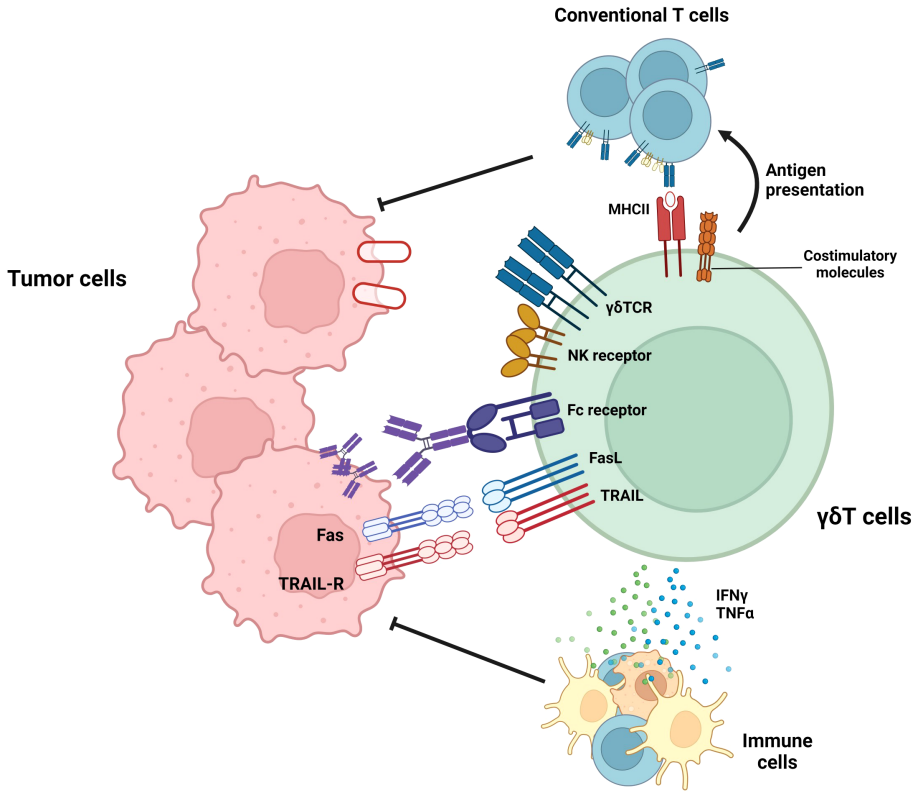

FIGURE 1
Roles of γδ T cells in tumor suppression. γδ T cells exert anti-tumoral immune responses by diverse mechanisms. By recognizing target molecules via γδTCR and NKG2D, γδ T cells can lyse tumor cells. In addition, Vδ2+ γδ T cells can eliminate tumor cells by antibody-dependent cell-mediated cytotoxicity (ADCC) in a CD16-dependent manner. Furthermore, γδ T cells can suppress tumor cells by death ligands, such as TRAIL or Fas ligands. In addition to these direct killings, γδ T cells can indirectly suppress tumor cells by activating T cells via working as antigen-presenting cells (APCs) or facilitating other immune cells via pro-inflammatory cytokine secretion.

cancers that do not respond to current therapeutic procedures such as immune checkpoint inhibitors (24, 25, 66, 67). One example of these cancer types is GBM, a malignant brain cancer that shows limited therapeutic responses to immune checkpoint inhibitors (26). Recently, several research groups demonstrated the importance of γδ T cells in glioma suppression (68, 69). Therefore, γδ T cells have the potential to become an effective therapeutic agent for GBM. However, several limitations exist that suppress the optimal effector function of γδ T cells in the GBM TME (68, 70–72). Therefore, the general background and current therapeutic procedures targeting GBM will subsequently be discussed. Furthermore, current advances and limitations in γδ T cell–mediated GBM treatment will be investigated. Finally, we will suggest several methodologies to overcome the limitations of γδ T cells in GBM immunotherapy.

3 GBM: Epidemiology and classification

GBM is a malignant brain tumor that is classified as WHO grade IV. Annually, approximately 10 out of every 100,000 people are diagnosed with GBM (73). Though the overall incidence is relatively low compared with other types of cancers, GBM is the most common malignant tumor occurring in the CNS (74) and has one of the worst prognoses of all cancer types. GBM patients survive less than 1 year without treatment, and the 5-year survival rate is less than 10% even with intensive care (34). GBM typically occurs in old adults, but it can also occur in children (75). GBM more commonly occurs in male patients than in female patients (76), and female GBM patients have better responses to standard treatment (radiotherapy + temozolomide) (77). Several studies of the risk factors of GBM have revealed that high-dose ionizing radiation (78–80) and rare genetic disorders, such as neurofibromatosis (81), increase GBM incidence. However, other risk factors, including smoking, alcohol uptake, and exposure to pesticides or steroidal hormones were not correlated with GBM onset (28). Common symptoms of GBM are headache, seizures, and cognitive and behavioral impairment (29). Because these symptoms are nonspecific, patients usually miss the opportunity for early therapeutic intervention.

Recent research revealed that GBM starts in the subventricular zone of the brain and spreads to the cortex (82). GBM originates from three cell types: neural stem cells (NSCs), NSC-derived astrocytes, and oligodendrocyte precursor cells. Among these, NSC and NSC-derived astrocytes are the more frequent cells of origin that induce GBM (83). Moreover, GBM consists of glioma stem cells (GSCs), which develop into a heterogenous cell population responsible for increasing GBM tumor burden (84). GSCs contribute to GBM's resistance to chemoradiotherapy and high recurrence rate (85).

Current studies on molecular and genetic signatures have enabled researchers to classify GBM into various subtypes. According to the WHO classification, IDH-wildtype GBM is characterized by *TERT* promoter mutation, epidermal growth factor receptor (*EGFR*) amplification, and a combination of chromosome 7 duplication and chromosome 10 loss (86). Using gene expression patterns, researchers further classified GBM into four different subtypes: proneural, neural, mesenchymal, and classical (87, 88). Not only do these subtypes express different morphological signatures and distinct genes (89), but they also show different susceptibility toward therapeutics. Classical subtypes, which possess a TP53 mutation, show susceptibility to radiotherapy and concurrent chemotherapy with temozolomide (90). By contrast, the mesenchymal GBM subtype shows resistance to radiotherapy and chemotherapy (91, 92). Although GBM cells are classified into various subtypes, the subtypes are not stable because transitions between subtypes frequently occur, most commonly to the mesenchymal subtype from other subtypes. Ionizing radiation (91, 93) from radiotherapy and hypoxic stress (94) that arises during tumor progression instigate this transition to the mesenchymal subtype. In addition to the four subtype-based GBM classifications, epigenetic signatures can differentiate GBM types. The methylation status of the O (6)-methylguanine-DNA methyltransferase (MGMT) promoter can be used to categorize GBM tumor cells as *MGMT* promoter methylated or unmethylated. The classification by *MGMT* promoter methylation is important for GBM patient prognosis because MGMT-expressing GBM cells are more resistant to DNA alkylating agents, such as temozolomide. Therefore, those patients with *MGMT* promoter methylation in GBM tumor cells respond better to temozolomide treatment and live longer (95).

4 Therapeutic procedures targeting GBM

Currently, the Stupp protocol is the standard care for GBM. The protocol reduces tumor burden by resecting GBM to the extent feasible followed by radiotherapy and concomitant chemotherapy using temozolomide, a DNA alkylating agent administered orally or intravenously (96). Although this therapeutic approach improved overall survival, GBM still has a poor prognosis due to the recurrence of tumors after treatment, which leads to a lower survival rate. This high recurrence rate is a result of the intrinsic characteristics of GBM, the unique anatomical and immunological features of the brain, and the limitations of the current treatment procedures. First, GBM cancer cells undergo a mesenchymal transition during tumor progression or due to radiation therapy. This mesenchymal transition is driven by hypoxia-inducible factors (97), and the high hypoxic signature of GBM can promote mesenchymal transition. Cancer cells exhibiting a mesenchymal signature can invade through the surrounding normal brain tissue (98), which makes it difficult to determine the boundary of the GBM and renders complete resection of the tumor impossible. Furthermore, GSCs in brain tumors undergo self-renewal and differentiation (99), thereby contributing to tumor recurrence if not completely removed (100). In addition, the brain is protected by the blood–brain barrier (BBB), which hinders active involvement of the external immune system (101). As a result, brain tumors are classified as immunologically cold cancers with limited infiltration of lymphoid cells, particularly T cells (102). These characteristics lead to the ineffectiveness of various therapeutic

procedures in the context of GBM treatment (26), even though those procedures have proven effective in other types of cancers (103). Moreover, brain-residing microglia (104) and neurons (105) maintain an anti-inflammatory immune environment, which hinders a robust tumor-suppressive immune response even when immune cells infiltrate the GBM. Lastly, the standard of care for GBM patients does not use target-specific therapeutic agents and may lead to off-target toxicity in the surrounding normal cells. GBM surgical resection leads to the loss of normal tissues surrounding the tumor, and radiation therapy can deplete brain immune cells or trigger mutations in normal brain tissue, potentially leading to the initiation of new tumor foci. It can also promote the mesenchymal transition of existing cancer cells, increasing resistance to drugs and radiation therapy (106). Temozolomide can affect normal cells as well, including immune cells. Most importantly, brain tumors with an unmethylated *MGMT* promoter exhibit resistance to temozolomide (107). In 2014, it was discovered that the addition of anti–vascular endothelial growth factor therapy, which inhibits angiogenesis, had a synergistic effect with conventional treatment methods in recurrent gliomas. However, the improvement in patient survival resulting from this combination therapy was found to be modest (108). Similarly, although the utilization of a novel treatment method, called tumor-treating fields (35), has led to a meaningful improvement in overall survival in brain tumor patients, overall patient survival rates remain low (109). To overcome the current limitations of brain tumor therapy, it is crucial to devise novel therapeutic approaches that not only effectively remove tumors but also facilitate the involvement of the immune system to prevent tumor recurrence. Consequently, research has emphasized the necessity of immunotherapy, a treatment modality that focuses on enhancing the immune response against brain tumors.

4.1 Immunotherapeutic approaches targeting GBM

The brain has historically been considered an immunologically privileged site, where immune activation is suppressed by the presence of the BBB and the immunosuppressive microenvironment (110). However, it has been revealed that the brain, like other organs, also possesses draining lymph nodes (111). Additionally, brain tumors with a higher infiltration of T cells are associated with better patient survival (112). This discovery suggests that immune surveillance also occurs in the brain, underscoring the significance of immune cell involvement in brain tumor therapy. Because various immunotherapies have proven effective in treating various types of cancers, there have been efforts to apply these immune-based treatments to GBM as well. These endeavors can be broadly categorized into four main approaches: immune checkpoint inhibitors, oncolytic viruses, vaccination, and cell-based therapies. Despite their success in clinical trials for several types of tumors (113–115), these immunotherapies have not achieved meaningful success in GBM patients (26, 36, 116). Hence, it is crucial for future advancements in brain tumor therapy to investigate why conventional immunotherapies have not been effective in GBM treatment and propose treatment strategies to overcome these limitations.

4.2 Challenges in using current immunotherapies to treat GBM

The lack of efficacy of conventional immunotherapies for GBM is attributed to both the characteristics of the brain and the unique features of GBM. Figure 2 represents the characteristics of the brain and GBM TME that participate in the suppression of GBM immunotherapy. First, the brain is not directly connected to the bloodstream due to the presence of the BBB (Figure 2A). Although the BBB plays a protective role by distinguishing the brain from the periphery under normal conditions, it can hinder drug delivery and immune cell infiltration in pathological conditions, such as GBM. In cases of neuroinflammation, such as experimental autoimmune encephalomyelitis, the glial limitans of the BBB become leaky, which allows peripheral immune cells to reach the brain parenchyma (117). In the context of GBM, the influx of immune cells is inhibited due to high levels of anti-inflammatory cytokines, which suppress the migration of peripheral immune cells to the brain parenchyma (70). Indeed, reports have indicated that the BBB remains intact even in the presence of brain tumors (118), which suggests that the BBB may limit the effectiveness of immunotherapy in GBM. The production of anti-inflammatory cytokines by normal brain tissue (71) suppresses not only immune cell infiltration but also the effector function of infiltrated immune cells (Figure 2B). Infiltration of lymphocytes is reduced in GBM, whereas myeloid cells, especially bone marrow-derived macrophages and monocytes, are highly abundant (119). In GBM, bone marrow-derived macrophages are polarized toward an M2 phenotype in response to the anti-inflammatory brain microenvironment. These M2 macrophages play a critical role in establishing and sustaining the anti-inflammatory microenvironment of GBM, leading to the suppression of immune cell function and ultimately contributing to a decrease in patient survival rates (120). In the GBM anti-inflammatory immune environment, regulatory T cells (Tregs) are well known for their ability to suppress the functions of effector T cells and antigen-presenting cells (121). Recurrent GBM patients have a higher proportion of Tregs among their immune cells, and this elevated Treg ratio is associated with lower patient survival rates (122). Not only immune cells but also microglia (104) and neurons (105), which reside in brain parenchyma from the homeostatic condition, participate in the formation of the anti-inflammatory immune environment of the brain (Figure 2B). In normal conditions, that immunosuppression is protective for brain homeostasis, but in tumor conditions, that immunosuppression hinders a robust tumor-suppressive immune response against the GBM. In addition to the anti-inflammatory immune environment, the inherent characteristics of GBM cancer cells also contribute to resistance to immunotherapies. GSCs downregulate major histocompatibility complex-I (MHC-I) and antigen-processing machinery via activation of the Wnt/β-catenin pathway, thereby leading to evasion from T cell-mediated immunosurveillance (123) (Figure 2C). In addition, GBM shows high intra-tumoral heterogeneity (124, 125); therefore, single target–based chimeric antigen receptor (CAR)-T cell therapy or vaccination cannot eliminate tumor cells that do not express the target antigen or

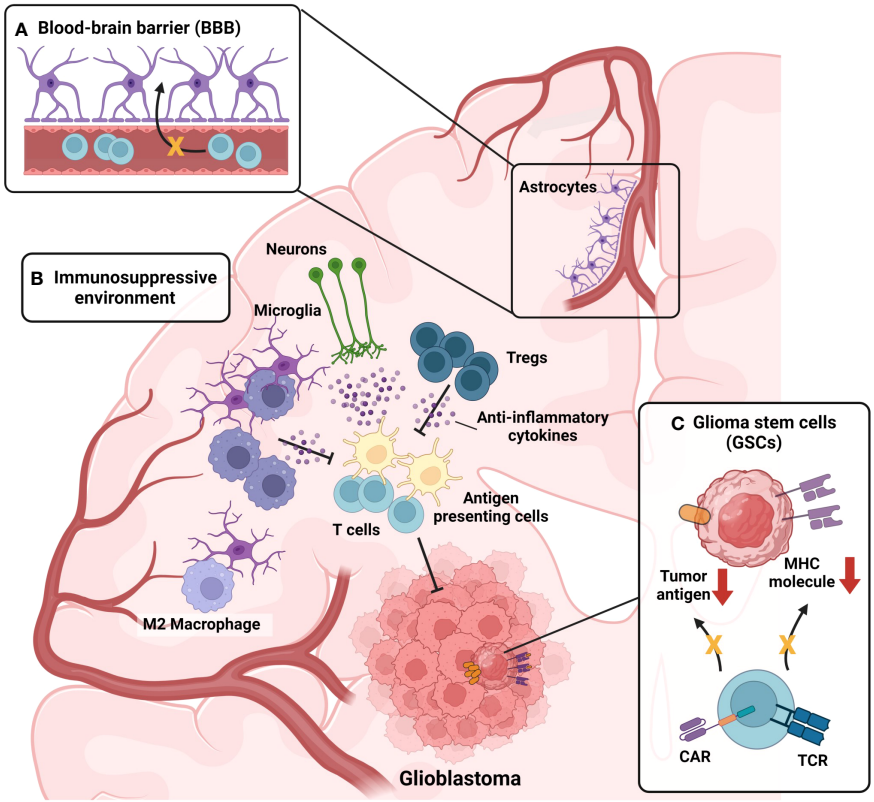

FIGURE 2
Challenges in current immunotherapy for GBM. **(A)** Presence of the Blood-brain barrier (BBB) act as a limiting factor for GBM immunotherapy. BBB hinders the infiltration of drugs and immune cells into brain parenchyma. High levels of anti-inflammatory cytokines present in brain parenchyma under GBM condition further suppress the breach of immune cells through the glial limitans of BBB. **(B)** Immunosuppressive microenvironment of GBM suppresses tumor-suppressive immune responses of infiltrated immune cells. Monocytes infiltrated into the GBM tumor microenvironment (TME) are skewed toward anti-inflammatory M2 phenotype, becoming M2-polarized bone-marrow-derived macrophages (BMDMs). M2-polarized BMDMs further strengthen anti-inflammatory TME by secreting anti-inflammatory cytokines. Not only myeloid cells but also, lymphoid cells, sustain the anti-inflammatory TME of GBM. Regulatory T cells (Tregs) are present in GBM TME, participating in the formation of immunosuppressive TME. In addition, microglia and neurons also participate in the formation of the anti-inflammatory immune environment of the brain, by secreting anti-inflammatory cytokines. **(C)** Intrinsic characteristics of glioma stem cells (GSCs) also contribute to the resistance of immunotherapies. By activation of the Wnt-β-catenin pathway, GSCs downregulate the expression of MHC-I expression, evading T cell immunosurveillance. Also, GSCs can evade chimeric-antigen receptors (CAR)-mediated immunosurveillance in the case of CAR-T treatment by downregulating the antigen targeted by CAR.

peptides (Figure 2C). Because numerous factors act as obstacles to the effectiveness of current immunotherapeutic procedures, novel therapeutic approaches are required to overcome these hurdles, and γδ T cell-mediated immunotherapy can be the solution. From now on, we will focus on the GBM immunotherapy utilizing γδ T cells, on their advances and facing limitations. Then, we will suggest several methodologies to overcome the limitations.

5 γδ T cells in GBM immunotherapy

5.1 Current advances in γδ T cell-mediated GBM immunotherapy

Encouraged by their strong anti-tumor function in preclinical and clinical research, the functionality of γδ T cells in GBM has been studied at both the preclinical and clinical levels. Park et al. demonstrated that enrichment of γδ T cells is a positive prognostic marker for survival in both mice and humans. However, γδ T cell functions in the TME are suppressed by severe hypoxia. As a result, γδ T cells downregulate NKG2D expression, which suppresses their target recognition and effector functions. Therefore, resolving tumor hypoxia through metformin treatment restored γδ T cell functionality (68). Lee et al. revealed that Vγ9Jγ2-Vδ2 T cells preferentially infiltrate the GBM TME, suggesting that human γδ T cells mediate tumor suppression *in-vivo* (69). In an *in-vitro* cytotoxicity model, human peripheral blood mononuclear cell (PBMC)-derived γδ T cells showed higher cytotoxicity on the U251MG human glioma cell line compared with αβ T cells. In addition, human PBMC-derived γδ T cells did not show cytotoxicity to non-tumor cells, such as primary human astrocytes (126). The effectiveness of γδ T cells in GBM therapy is also revealed by their ability to suppress GSCs, which are responsible for tumor initiation, maintenance, metastasis, and resistance to standard therapy (127). GSCs evade immune surveillance via MHC class I downregulation and antigen-processing machinery, thereby evading the CD8 T cell-mediated immune response (123). Despite this, γδ T cells can target GSCs.

Jarry et al. injected primary GBM cells rich in GSCs (~25%) into the brains of immunocompetent (NSG) mice. Then, they injected bromohydrin pyrophosphate–activated human Vγ9Vδ2$^+$ T cells into the tumor site, which successfully controlled tumor growth in combination with zoledronate (128). The superior targeting ability of γδ T cells also originated from their low activation threshold. CD8 T cells cannot be activated by NKG2D alone and require TCR signaling (129), whereas γδ T cells can be activated by NKG2D alone (23). Therefore, γδ T cells are more readily activated in the absence of TCR engagement, making it difficult for tumor cells to evade the surveillance of γδ T cells. Encouraged by those effector functions, Choi et al. showed that intra-tumoral transfer of human Vγ9Vδ2$^+$ T cells significantly improved survival in mice that were injected with the U87 human glioma cell line. When analyzed by co-culturing γδ T cells with a human glioma patient-derived sample, Vγ9Vδ2$^+$ T cells showed DNAM1-mediated cytotoxicity, suggesting the possible mechanism of the γδ T cell–mediated tumoricidal effector function against GBM (130).

However, clinical studies using γδ T cells have shown disappointing results in various tumor settings, and only one currently recruiting clinical trial was designed to target GBM with γδ T cells (ClinicalTrials.gov Identifier: NCT04165941). γδ T cells did not cause severe toxicity after *in-vitro* expansion and subsequent adoptive transfer (131, 132), but their therapeutic effect was moderate (21). Even though γδ T cells are promising immunotherapy to treat cancers, including GBM, several obstacles must be overcome to fully utilize γδ T cells in the clinical setting.

5.2 Limitations of γδ T cells in GBM immunotherapy

Several limitations may explain the modest effect of γδ T cells on tumor control in clinical settings, including GBM (Figure 3). Regarding *in-vivo* zoledronate administration, because Vδ2$^+$ γδ T cells are significantly reduced in the peripheral blood of GBM patients (133), γδ T cell expansion does not produce the expected amount of cells (Figure 3A). Therefore, the number of expanded γδ T cells *in-vivo* is not sufficient to fully control the tumor, even after expansion by zoledronic acid treatment (133). Next, the GBM TME can suppress the effector function of γδ T cells (Figure 3B) (68, 72). As demonstrated by Park et al., a hypoxic TME not only induces γδ T cell exhaustion but can also make γδ T cells ineffective at targeting tumor cells (68). Therefore, γδ T cells may not target tumor cells *in-vivo* even though they could lyse tumor cells *in-vitro*. Also, the TME can have deleterious effects on γδ T cells. GBM expresses PD-L1, and PD-L1 expression is negatively correlated with patient survival (72). Because T cells upregulate PD-1 upon TCR stimulation (134), γδ T cells that have infiltrated the brain and sensed tumor cells may also express high levels of PD-1. Therefore, γδ T cells may be functionally impaired and cannot exert cytotoxic effector functions even though they expanded and infiltrated the GBM TME (Figure 3B). The GBM TME impairs γδ T cell function and may facilitate the transition of γδ T cells into a pro-tumoral signature (Figure 3C) (58, 135). Though Vγ9Vδ2$^+$ γδ T cells are known for their cytotoxic effector function and secretion of tumor-suppressive IFN-γ, they show functional plasticity in the presence of different cytokines. IL-12, IL-18, and type-I IFN induce Th1-like functionality (57, 136), whereas the addition of IL-15 with TGF-β induces Treg-like functionality (58). Furthermore, the combination of IL-6, IL-23, IL-1β, and TGF-β skews Vγ9Vδ2$^+$ T cells to Th17-like cells (135). Due to this plasticity, GBM-infiltrated Vγ9Vδ2$^+$ T cells may promote rather than suppress tumor growth (Figure 3C). TGF-β not only skews Vγ9Vδ2$^+$ T cells toward pro-tumoral subtype, but they also dampen the effector function of anti-tumoral functionality of γδ T cells. Rafia et al. showed that after TGF-β treatment, the target-lysing ability of γδ T cells was diminished due to the downregulation of NKG2D and granzyme/perforin expression on γδ T cells (137). In addition, a lymphocyte-depleted TME dampens the antigen-presenting effectiveness of γδ T cells (Figure 3D). Although γδ T cells phagocytose and present tumor antigens, there may not be enough CD4 or CD8 T cells in the TME that are primed and activated by this antigen presentation. In addition, TCR stimulation upregulates CXCR6 while downregulating CXCR4, which is required for T cell egress and subsequent localization in the lymphatic organs (138) (Figure 3E). γδ T cells in the TME not only phagocytose tumor antigens but are also activated by TCR stimulation, leading to their retention in the tumor. Consequently, γδ T cells cannot spread tumor antigens by egressing out from the tumor and localizing in the lymphatic organs (138).

6 Future directions to overcome the limitation of γδ T cells

For successful GBM therapy using γδ T cells, the current limitations of γδ T cells must be addressed and novel therapeutic procedures that fully utilize the benefits of γδ T cells must be devised (Figure 4). Rather than expanding patient γδ T cells by zoledronic acid, allogeneic γδ T cell transfer from a healthy donor to the patient is gaining interest (139) (Figure 4A). γδ T cells have already proven their safety in allograft transfers, with low risk of graft-versus-host diseases and rejection (131) (Figure 4A). With an allograft transfer, global suppression of γδ T cells induced by GBM and chemotherapy will be reduced. In addition to allograft transfers, further engineering of allogeneic γδ T cells can lead to synergistic effects (Figures 4B-D). CAR-T cell-based GBM treatment currently shows a modest effect (140), possibly due to the low persistence of CAR-T cells in peripheral blood. It is known that a weak-not high-level of tonic signaling is required for better *in-vivo* persistence and superior antitumor function (141). Anti-EGFRviii CAR-T cells were used for GBM treatment, although this target is not expressed in peripheral blood and cannot provide tonic signaling to T cells (Figure 4B). However, the issues caused by the lack of tonic signaling can be resolved by expressing the CAR in human Vγ9Vδ2$^+$ γδ T cells, which can receive tonic signaling by γδTCR and have endogenous butyrophilin expression (Figure 4B). Introduction of the CAR to γδ T cells provides an additional route by which γδ T cells can target tumor cells, which prevents tumor cells from escaping immune surveillance by antigen loss. In conventional CAR-T cells, which introduce CAR molecules to conventional T cells, tumor cells may escape CAR-T cell surveillance by

10.3389/fimmu.2023.1273986

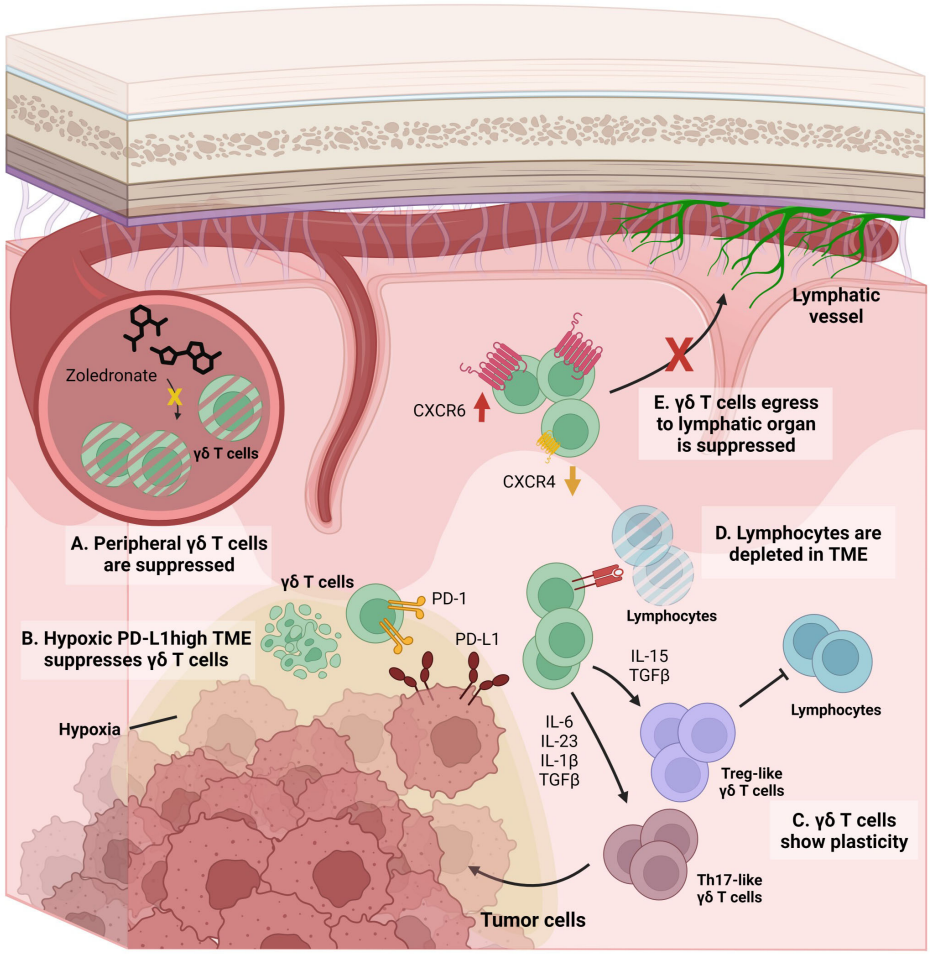

FIGURE 3
Limiting factors on γδ T cell-based GBM immunotherapy. **(A)** In the peripheral blood of GBM patients, γδ T cells are significantly decreased. Therefore, expansion of γδ T cells via *in-vivo* administration of zoledronates does not fit for GBM treatment. **(B)** Immune-suppressive microenvironment of GBM suppresses the optimal function of γδ T cells. For example, hypoxia present in GBM TME suppresses the tumoricidal function of γδ T cells by downregulating NKG2D expression on γδ T cells. In addition, PD-L1-enriched GBM TME suppresses γδ T cells by ligation with PD-1 expressed on γδ T cells. γδ T cells target GBM tumor cells in a TCR-dependent manner and express PD-1. In this condition, PD-L1-enriched GBM TME is detrimental to the optimal activation and function of γδ T cells. **(C)** Plasticity of γδ T cells can act as a detrimental factor for anti-tumoral functionality of γδ T cells. In the presence of IL-15 and TGF-β, γδ T cells skew toward the Treg-like population, thereby conspiring with other anti-inflammatory immune cells and suppressing tumoricidal functionality. Likewise, in the presence of IL-6, IL-23, IL-1β and TGF-β, γδ T cells can act as Th17-like cells, thereby facilitating tumor growth. **(D)** Lymphocyte-depleted signature of GBM TME also dampens the optimal functionality of γδ T cells. Even though γδ T cells can activate T cells by their antigen-presenting functionality, they cannot initiate T cell-mediated anti-tumoral responses due to the scarcity of lymphocytes in GBM TME. **(E)** Even though γδ T cells can phagocytose and act as antigen-presenting cells (APCs), they cannot migrate and work in draining lymph nodes, due to downregulation of CXCR4 and concomitant CXCR6 upregulation induced by TCR stimulation.

downregulating the target of the CAR. However, if the CAR is introduced to human $V\gamma9V\delta2^+$ γδ T cells, tumor cells cannot evade surveillance even after antigen downregulation because γδ T cells can target tumor cells via TCR and other NK receptors. By reducing the chance of tumor cell immune escape, CAR–γδ T cells may represent an improvement over conventional CAR-T cell (Figure 4B).

The introduction of engineering expands the opportunities of γδ T cell-based therapy beyond the CAR (Figures 4C, D). For example, γδ T cells can be engineered to overcome the immune-suppressive GBM environment. Liu et al. suggested engineering a novel switch receptor that switches the immune-suppressive PD-1 signaling into immune-activating CD28 signaling (142) (Figure 4C). Introducing the receptor augmented the anti-tumor immune response of CAR-T cells. In GBM that express PD-L1 (72), engineering γδ T cells by introducing the switch receptor can overcome immunosuppression and may even exploit the suppressive microenvironment. A similar approach to the switch receptor mediation can also be applied to TGF-β to overcome immunosuppression (Figure 4C). It is well known that TGF-β is highly expressed in GBM (143), and TGF-β signaling reduces the γδ T cell anti-tumoral immune response by making these cells anti-inflammatory (58). The introduction of a switch receptor that changes the TGF-β signal into other pro-inflammatory signals may help γδ T cells overcome TGF-β-induced immunosuppression. Noh et al. recently introduced a TGF-β-targeting switch receptor that can change TGF-β signaling into IL-

10.3389/fimmu.2023.1273986

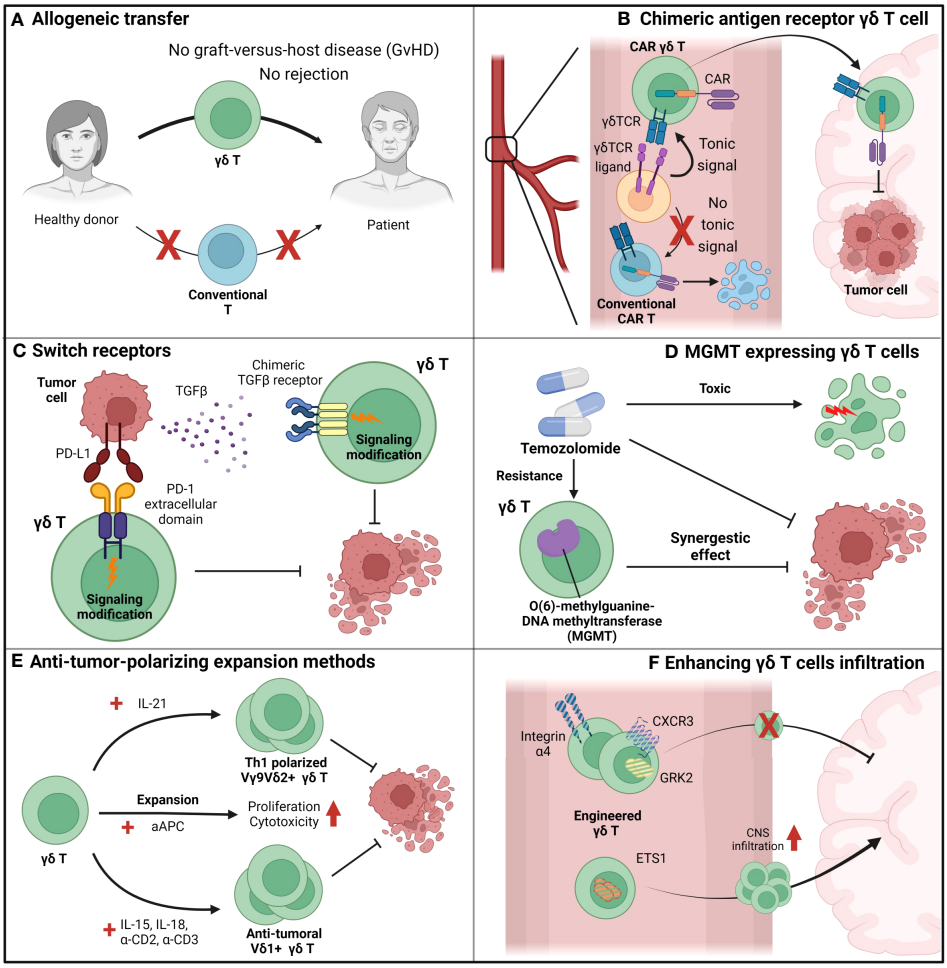

FIGURE 4
Suggestions to overcome the limiting factors of γδ T cells. **(A)** Allogeneic adoptive cell transfer (ACT) can be beneficial for γδ T cell-based immunotherapy since γδ T cells do not show graft-versus-host diseases (GvHD), in contrast to conventional T cells. By allogeneic ACT of γδ T cells, problems induced by the scarcity of γδ T cells in peripheral blood can be overcome. **(B)** Chimeric-antigen-receptors (CAR)-augmented γδ T cells can be an effective therapeutic option for GBM since they can overcome various issues that arose in conventional T cell-based CAR-T therapy. First, in contrast to conventional T cell-based CAR-T cells, γδ T cell-based CAR-T cells can receive tonic signaling in the peripheral blood, which is critical for CAR-T cell persistence. Next, γδ T cells can lyse GBM tumor cells by its intrinsic γδ TCR, while conventional T cells cannot. Therefore, in contrast to conventional T cell-based CAR-T cells which only target tumor cells by their CARs, γδ T cell-based CAR-T cells can target tumor cells by multiple receptors and block the chance of tumor cells' evasion of immunosurveillance. **(C)** γδ T cells augmented to express switch-receptors that can exchange the immunosuppressive signaling cues into immune-progressive signaling can overcome the immunosuppressive TME. For example, PD-L1 and TGF- β, well-known anti-inflammatory environmental cues, can be utilized as targets for switch receptors, and γδ T cells expressing switch receptors targeting those factors can sustain their functionality. **(D)** γδ T cells engineered to synergize with other therapy can even increase the therapeutic potential than just a mere combination of two distinct therapy. For example, temozolomide, which suppresses tumor growth but also exerts toxic side-effect on normal immune function, is normally considered a detrimental factor for immunotherapy. However, MGMT-overexpressed γδ T cells, which can overcome the temozolomide-mediated suppression, can synergize with temozolomide, and it is expected that the combination of temozolomide and temozolomide-overcoming γδ T cells can be more effective than just a sum of two single treatment. **(E)** Blocking the plasticity of γδ T cells and polarizing them toward an anti-tumoral population can prevent the skewing of γδ T cells into a pro-tumoral population in the TME. Addition of IL-21 polarizes human $V\gamma9V\delta2^+$ T cells toward a Th1-like population, and Th1-skewed $V\gamma9V\delta2^+$ T cells produce pro-inflammatory cytokines and exhibit enhanced cytotoxic roles. If IL-21 mediated polarization could be combined with another expansion protocol with greater expansion efficiency, such as artificial antigen-presenting cell (aAPC)-based methods, the synergistic effect would be dramatic. In addition to $V\gamma9V\delta2^+$ T cell expansion, another procedure to expand human $V\delta1^+$ T cells using IL-15, IL-18, anti-CD2 antibody, and anti-CD3 antibody can efficiently expand and polarize these cells toward an anti-tumoral population. Therefore, with these various procedures to expand and polarize γδ T cells into tumoricidal effectors, γδ T cells could overcome the TME and retain anti-tumoral functionality. **(F)** Augmentation of γδ T cells so that they can cross the BBB can be an effective strategy to transport γδ T cells to the tumor site and increase the number of γδ T cells in the TME. By engineering integrins (e.g., integrin α4), chemokine receptors (e.g., CXCR3 and GRK2), and transcription factors (e.g., ETS1), trafficking of γδ T cells to the central nervous system (CNS) can be modulated.

7 signaling, and expression of the receptor improved tumor control in the CAR-T-based B-cell lymphoma suppression model (144). Therefore, similar concepts can be applied when designing γδ T cell-based GBM treatment.

Engineered γδ T cells can have synergistic effects when combined with other treatments. Recently, novel genetically engineered human $V\gamma9V\delta2^+$ γδ T cells were used in a GBM clinical trial (Figure 4D). The current standard care therapy for

GBM includes temozolomide; however, this treatment affects immune cells, which may lose functionality, because temozolomide does not specifically target tumor cells. In this situation, γδ T cells engineered to express MGMT retain their functionality under temozolomide treatment (145). A clinical trial for GBM treatment using adoptive transfer of human γδ T cells expressing MGMT (ClinicalTrials.gov Identifier: NCT04165941) in combination with temozolomide is currently in progress. In summary, although γδ T cell therapy alone cannot control GBM, it still has therapeutic potential. γδ T cells can overcome current limitations with engineering and combination therapy and may become an effective therapeutic agent for GBM treatment.

Developing novel expansion methods to block the skewing of γδ T cells toward the pro-tumoral population can be an effective and plausible solution for γδ T cell adoptive transfer (Figure 4E). Several studies have previously demonstrated procedures to skew γδ T cells toward anti-tumoral populations. For example, the addition of IL-21 helps human $V\gamma9V\delta2^+$ γδ T cells to produce pro-inflammatory cytokines and exert increased cytotoxicity by irreversibly polarizing $V\gamma9V\delta2^+$ γδ T cells to express Th1-like signatures (146). This Th1-polarizing condition may show strong synergy with another expansion protocol devised by Choi et al., which uses artificial antigen-presenting cells to expand human $V\gamma9V\delta2^+$ T cells (147). The expansion strategy proposed by Harmon et al. also showed that addition of IL-15, IL-18, anti-CD2 antibody, and anti-CD3 antibody effectively expanded human $V\delta1^+$ T cells and polarized them toward an anti-tumoral population (148). Because the plasticity of γδ T cells in the TME is a major issue that hinders γδ T cell therapy, development of an improved expansion protocol to block this plasticity is crucial for effective γδ T cell therapy.

Engineering γδ T cells to cross the BBB is another effective strategy to increase the infiltration of γδ T cells into GBM (Figure 4F). Recent findings from Kendirli et al. show that various factors, ranging from transcription factors to chemokine receptors, regulate T cell migration to the CNS (104). Using genome-wide CRISPR screening, the authors found that knockout of integrin α4, CXCR3, and GRK2 significantly reduced T cell trafficking to the CNS, while ETS1 knockout significantly upregulated T cell trafficking to the CNS. Therefore, modulation of molecules related to T cell trafficking to the CNS in γδ T cells can facilitate infiltration of these cells into GBM.

7 Closing remarks

γδ T cells, with their versatile effector functions, have the potential to be a promising therapeutic agent to target tumors. Their ability to target tumor cells via various mechanisms, including γδTCRs, NK receptors, Fc receptors, and death receptors, decreases the possibility of tumor cells evading surveillance. Their ability to produce pro-inflammatory cytokines and spread antigens via direct antigen presentation to the adaptive immune system helps γδ T cells overcome the immunosuppression of the TME and induce optimal anti-tumoral immune responses. Additionally, because they do not recognize MHC molecules and do not risk inducing graft-versus-host disease when transferred from donors to MHC-mismatched patients, γδ T cells can possibly be used in allogeneic adoptive transfer therapy. Therefore, γδ T cells have the potential to be a novel therapeutic agent for GBM, a malignant brain tumor with the highest WHO grade and therefore the worst prognosis. Understanding the immunological signatures of the GBM TME is critical for optimal function of γδ T cells in the GBM TME and subsequent tumor suppression. The immunosuppressive microenvironment, BBB, and MHC-deficient GSCs are the major factors that suppress effective immunotherapy. Although γδ T cells have the potential to overcome some of these limitations, several obstacles still exist, hindering effective therapy and the achievement of successful treatment for GBM. Therefore, for successful γδ T cell–based immunotherapy, it is critical to devise strategies to overcome those limitations. With further studies to determine the signatures of the GBM TME and γδ T cells themselves, in combination with the augmentation of their abilities and improvement of current limitations, γδ T cells can become an innovative therapeutic agent for GBM.

Author contributions

IK: Conceptualization, Writing – original draft, Writing – review & editing. YK: Conceptualization, Writing – original draft. HL: Conceptualization, Funding acquisition, Supervision, Writing – original draft, Writing – review & editing.

Funding

The author(s) declare financial support was received for the research, authorship, and/or publication of this article. This work was supported by the National Research Foundation of Korea (NRF-2021M3A9H3015688 and NRF-2021M3A9D3026428) funded by the Ministry of Science and ICT of Korea. This work was also supported by the Samsung Science and Technology Foundation (SSTF-BA1902-05), Republic of Korea.

Acknowledgments

The authors thank the members of the laboratory of Host Defenses for their helpful discussions. Figures were created with BioRender.com.

Conflict of interest

The authors declare that the research was conducted in the absence of any commercial or financial relationships that could be construed as a potential conflict of interest.

Publisher's note

References

1. Zhao Y, Niu C, Cui J. Gamma-delta (gammadelta) T cells: friend or foe in cancer development? *J Transl Med* (2018) 16(1):3. doi: 10.1186/s12967-017-1378-2

2. Pastar I, O'Neill K, Padula L, Head CR, Burgess JL, Chen V, et al. Staphylococcus epidermidis boosts innate immune response by activation of gamma delta T cells and induction of perforin-2 in human skin. *Front Immunol* (2020) 11:550946. doi: 10.3389/fimmu.2020.550946

3. Zakeri N, Hall A, Swadling L, Pallett LJ, Schmidt NM, Diniz MO, et al. Characterisation and induction of tissue-resident gamma delta T cells to target hepatocellular carcinoma. *Nat Commun* (2022) 13(1):1372. doi: 10.1038/s41467-022-29012-1

4. Wo J, Zhang F, Li Z, Sun C, Zhang W, Sun G. The role of gamma-delta T cells in diseases of the central nervous system. *Front Immunol* (2020) 11:580304. doi: 10.3389/fimmu.2020.580304

5. Szeto C, Lobos CA, Nguyen AT, Gras S. TCR recognition of peptide-MHC-I: rule makers and breakers. *Int J Mol Sci* (2020) 22(1):68. doi: 10.3390/ijms22010068

6. Willcox BE, Willcox CR. gammadelta TCR ligands: the quest to solve a 500-million-year-old mystery. *Nat Immunol* (2019) 20(2):121–8. doi: 10.1038/s41590-018-0304-y

7. Mamedov MR, Vedova S, Freimer JW, Sahu AD, Ramesh A, Arce MM, et al. CRISPR screens decode cancer cell pathways that trigger gammadelta T cell detection. *Nature* (2023) 621(7977):188–95. doi: 10.1038/s41586-023-06482-x

8. Li J, Cui L, He W. Distinct pattern of human Vdelta1 gammadelta T cells recognizing MICA. *Cell Mol Immunol* (2005) 2(4):253–8.

9. Bonneville M, Scotet E. Human Vgamma9Vdelta2 T cells: promising new leads for immunotherapy of infections and tumors. *Curr Opin Immunol* (2006) 18(5):539–46. doi: 10.1016/j.coi.2006.07.002

10. Yamamoto K, Fujiyama Y, Andoh A, Bamba T, Okabe H. Oxidative stress increases MICA and MICB gene expression in the human colon carcinoma cell line (CaCo-2). *Biochim Biophys Acta* (2001) 1526(1):10–2. doi: 10.1016/S0304-4165(01)00099-X

11. Holtmeier W, Kabelitz D. gammadelta T cells link innate and adaptive immune responses. *Chem Immunol Allergy* (2005) 86:151–83. doi: 10.1159/000086659

12. Mensurado S, Blanco-Dominguez R, Silva-Santos B. The emerging roles of gammadelta T cells in cancer immunotherapy. *Nat Rev Clin Oncol* (2023) 20(3):178–91. doi: 10.1038/s41571-022-00722-1

13. Park JH, Lee HK. Function of gammadelta T cells in tumor immunology and their application to cancer therapy. *Exp Mol Med* (2021) 53(3):318–27. doi: 10.1038/s12276-021-00576-0

14. Qu G, Wang S, Zhou Z, Jiang D, Liao A, Luo J. Comparing mouse and human tissue-resident gammadelta T cells. *Front Immunol* (2022) 13:891687. doi: 10.3389/fimmu.2022.891687

15. Fonseca S, Pereira V, Lau C, Teixeira MDA, Bini-Antunes M, Lima M. Human peripheral blood gamma delta T cells: report on a series of healthy caucasian Portuguese adults and comprehensive review of the literature. *Cells* (2020) 9(3):729. doi: 10.3390/cells9030729

16. Wu Y, Biswas D, Usaite I, Angelova M, Boeing S, Karasaki T, et al. A local human Vdelta1 T cell population is associated with survival in nonsmall-cell lung cancer. *Nat Cancer* (2022) 3(6):696–709. doi: 10.1038/s43018-022-00376-z

17. Ma R, Yuan D, Guo Y, Yan R, Li K. Immune effects of gammadelta T cells in colorectal cancer: A review. *Front Immunol* (2020) 11:1600. doi: 10.3389/fimmu.2020.01600

18. Barros MS, de Araujo ND, Magalhaes-Gama F, Pereira Ribeiro TL, Alves Hanna FS, Tarrago AM, et al. gammadelta T cells for leukemia immunotherapy: new and expanding trends. *Front Immunol* (2021) 12:729085. doi: 10.3389/fimmu.2021.729085

19. Gentles AJ, Newman AM, Liu CL, Bratman SV, Feng W, Kim D, et al. The prognostic landscape of genes and infiltrating immune cells across human cancers. *Nat Med* (2015) 21(8):938–45. doi: 10.1038/nm.3909

20. Lee D, Rosenthal CJ, Penn NE, Dunn ZS, Zhou Y, Yang L. Human gammadelta T cell subsets and their clinical applications for cancer immunotherapy. *Cancers (Basel)* (2022) 14(12):3005. doi: 10.3390/cancers14123005

21. Saura-Esteller J, de Jong M, King LA, Ensing E, Winograd B, de Gruijl TD, et al. Gamma delta T cell based cancer immunotherapy: past-present-future. *Front Immunol* (2022) 13:915837. doi: 10.3389/fimmu.2022.915837

22. Yazdanifar M, Barbarito G, Bertaina A, Airoldi I. gammadelta T cells: the ideal tool for cancer immunotherapy. *Cells* (2020) 9(5):1305. doi: 10.3390/cells9051305

23. Rincon-Orozco B, Kunzmann V, Wrobel P, Kabelitz D, Steinle A, Herrmann T. Activation of V gamma 9V delta 2 T cells by NKG2D. *J Immunol* (2005) 175(4):2144–51. doi: 10.4049/jimmunol.175.4.2144

24. Li HB, Yang ZH, Guo QQ. Immune checkpoint inhibition for pancreatic ductal adenocarcinoma: limitations and prospects: a systematic review. *Cell Commun Signal* (2021) 19(1):117. doi: 10.1186/s12964-021-00789-w

25. Venkatachalam S, McFarland TR, Agarwal N, Swami U. Immune checkpoint inhibitors in prostate cancer. *Cancers (Basel)* (2021) 13(9):2187. doi: 10.3390/cancers13092187

26. Reardon DA, Brandes AA, Omuro A, Mulholland P, Lim M, Wick A, et al. Effect of nivolumab vs bevacizumab in patients with recurrent glioblastoma: the checkMate 143 phase 3 randomized clinical trial. *JAMA Oncol* (2020) 6(7):1003–10. doi: 10.1001/jamaoncol.2020.1024

27. Tamimi AF, Juweid M. Epidemiology and outcome of glioblastoma. In: De Vleeschouwer S, editor. *Glioblastoma*. Brisbane (AU): Codon Publications (2017).

28. Hanif F, Muzaffar K, Perveen K, Malhi SM, Simjee Sh U. Glioblastoma Multiforme: A Review of its Epidemiology and Pathogenesis through Clinical Presentation and Treatment. *Asian Pac J Cancer Prev* (2017) 18(1):3–9. doi: 10.22034/APJCP.2017.18.1.3

29. Schaff LR, Mellinghoff IK. Glioblastoma and other primary brain Malignancies in adults: A review. *JAMA* (2023) 329(7):574–87. doi: 10.1001/jama.2023.0023

30. Barani IJ, Larson DA. Radiation therapy of glioblastoma. *Cancer Treat Res* (2015) 163:49–73. doi: 10.1007/978-3-319-12048-5_4

31. Rominiyi O, Vanderlinden A, Clenton SJ, Bridgewater C, Al-Tamimi Y, Collis SJ. Tumour treating fields therapy for glioblastoma: current advances and future directions. *Br J Cancer* (2021) 124(4):697–709. doi: 10.1038/s41416-020-01136-5

32. Pajak B. Looking for the holy grail-drug candidates for glioblastoma multiforme chemotherapy. *Biomedicines* (2022) 10(5):1001. doi: 10.3390/biomedicines10051001

33. Rocha Pinheiro SL, Lemos FFB, Marques HS, Silva Luz M, de Oliveira Silva LG, Faria Souza Mendes Dos Santos C, et al. Immunotherapy in glioblastoma treatment: Current state and future prospects. *World J Clin Oncol* (2023) 14(4):138–59. doi: 10.5306/wjco.v14.i4.138

34. Stupp R, Hegi ME, Mason WP, van den Bent MJ, Taphoorn MJ, Janzer RC, et al. Effects of radiotherapy with concomitant and adjuvant temozolomide versus radiotherapy alone on survival in glioblastoma in a randomised phase III study: 5-year analysis of the EORTC-NCIC trial. *Lancet Oncol* (2009) 10(5):459–66. doi: 10.1016/S1470-2045(09)70025-7

35. Davies AM, Weinberg U, Palti Y. Tumor treating fields: a new frontier in cancer therapy. *Ann N Y Acad Sci* (2013) 1291:86–95. doi: 10.1111/nyas.12112

36. Weller M, Butowski N, Tran DD, Recht LD, Lim M, Hirte H, et al. Rindopepimut with temozolomide for patients with newly diagnosed, EGFRvIII-expressing glioblastoma (ACT IV): a randomised, double-blind, international phase 3 trial. *Lancet Oncol* (2017) 18(10):1373–85. doi: 10.1016/S1470-2045(17)30517-X

37. Omuro A, Brandes AA, Carpentier AF, Idbaih A, Reardon DA, Cloughesy T, et al. Radiotherapy combined with nivolumab or temozolomide for newly diagnosed glioblastoma with unmethylated MGMT promoter: An international randomized phase III trial. *Neuro Oncol* (2023) 25(1):123–34. doi: 10.1093/neuonc/noac099

38. Carding SR, Egan PJ. Gammadelta T cells: functional plasticity and heterogeneity. *Nat Rev Immunol* (2002) 2(5):336–45. doi: 10.1038/nri797

39. Ribot JC, Lopes N, Silva-Santos B. gammadelta T cells in tissue physiology and surveillance. *Nat Rev Immunol* (2021) 21(4):221–32. doi: 10.1038/s41577-020-00452-4

40. Mayassi T, Jabri B. Human intraepithelial lymphocytes. *Mucosal Immunol* (2018) 11(5):1281–9. doi: 10.1038/s41385-018-0016-5

41. Russano AM, Agea E, Corazzi L, Postle AD, De Libero G, Porcelli S, et al. Recognition of pollen-derived phosphatidyl-ethanolamine by human CD1d-restricted gamma delta T cells. *J Allergy Clin Immunol* (2006) 117(5):1178–84. doi: 10.1016/j.jaci.2006.01.001

42. Marlin R, Pappalardo A, Kaminski H, Willcox CR, Pitard V, Netzer S, et al. Sensing of cell stress by human gammadelta TCR-dependent recognition of annexin A2. *Proc Natl Acad Sci U.S.A.* (2017) 114(12):3163–8. doi: 10.1073/pnas.1621052114

43. Harly C, Joyce SP, Domblides C, Bachelet T, Pitard V, Mannat C, et al. Human gammadelta T cell sensing of AMPK-dependent metabolic tumor reprogramming through TCR recognition of EphA2. *Sci Immunol* (2021) 6(61):eaba9010. doi: 10.1126/sciimmunol.aba9010

44. Willcox CR, Salim M, Begley CR, Karunakaran MM, Easton EJ, von Klopotek C, et al. Phosphoantigen sensing combines TCR-dependent recognition of the BTN3A IgV domain and germline interaction with BTN2A1. *Cell Rep* (2023) 42(4):112321. doi: 10.1016/j.celrep.2023.112321

45. Deseke M, Prinz I. Ligand recognition by the gammadelta TCR and discrimination between homeostasis and stress conditions. *Cell Mol Immunol* (2020) 17(9):914–24. doi: 10.1038/s41423-020-0503-y

46. Willcox CR, Mohammed F, Willcox BE. The distinct MHC-unrestricted immunobiology of innate-like and adaptive-like human gammadelta T cell subsets-Nature's CAR-T cells. *Immunol Rev* (2020) 298(1):25–46. doi: 10.1111/imr.12928

47. Yin S, Zhang J, Mao Y, Hu Y, Cui L, Kang N, et al. Vav1-phospholipase C-gamma1 (Vav1-PLC-gamma1) pathway initiated by T cell antigen receptor (TCRgammadelta) activation is required to overcome inhibition by ubiquitin ligase Cbl-b during gammadeltaT cell cytotoxicity. *J Biol Chem* (2013) 288(37):26448–62. doi: 10.1074/jbc.M113.484600

48. Dalton JE, Howell G, Pearson J, Scott P, Carding SR. Fas-Fas ligand interactions are essential for the binding to and killing of activated macrophages by gamma delta T cells. *J Immunol* (2004) 173(6):3660–7. doi: 10.4049/jimmunol.173.6.3660

49. Tawfik D, Groth C, Gundlach JP, Peipp M, Kabelitz D, Becker T, et al. TRAIL-receptor 4 modulates gammadelta T cell-cytotoxicity toward cancer cells. *Front Immunol* (2019) 10:2044. doi: 10.3389/fimmu.2019.02044

50. Hu W, Shang R, Yang J, Chen C, Liu Z, Liang G, et al. Skin gammadelta T cells and their function in wound healing. *Front Immunol* (2022) 13:875076. doi: 10.3389/fimmu.2022.875076

51. McCarthy NE, Eberl M. Human gammadelta T cell control of mucosal immunity and inflammation. *Front Immunol* (2018) 9:985. doi: 10.3389/fimmu.2018.00985

52. Niu C, Jin H, Li M, Xu J, Xu D, Hu J, et al. *In vitro* analysis of the proliferative capacity and cytotoxic effects of ex vivo induced natural killer cells, cytokine-induced killer cells, and gamma-delta T cells. *BMC Immunol* (2015) 16:61. doi: 10.1186/s12865-015-0124-x

53. Ramstead AG, Jutila MA. Complex role of gammadelta T cell-derived cytokines and growth factors in cancer. *J Interferon Cytokine Res* (2012) 32(12):563–9. doi: 10.1089/jir.2012.0073

54. Shibata K, Yamada H, Nakamura M, Hatano S, Katsuragi Y, Kominami R, et al. IFN-gamma-producing and IL-17-producing gammadelta T cells differentiate at distinct developmental stages in murine fetal thymus. *J Immunol* (2014) 192(5):2210–8. doi: 10.4049/jimmunol.1302145

55. Gao Y, Yang W, Pan M, Scully E, Girardi M, Augenlicht LH, et al. Gamma delta T cells provide an early source of interferon gamma in tumor immunity. *J Exp Med* (2003) 198(3):433–42. doi: 10.1084/jem.20030584

56. Wakita D, Sumida K, Iwakura Y, Nishikawa H, Ohkuri T, Chamoto K, et al. Tumor-infiltrating IL-17-producing gammadelta T cells support the progression of tumor by promoting angiogenesis. *Eur J Immunol* (2010) 40(7):1927–37. doi: 10.1002/eji.200940157

57. Wesch D, Glatzel A, Kabelitz D. Differentiation of resting human peripheral blood gamma delta T cells toward Th1- or Th2-phenotype. *Cell Immunol* (2001) 212(2):110–7. doi: 10.1006/cimm.2001.1850

58. Casetti R, Agrati C, Wallace M, Sacchi A, Martini F, Martino A, et al. Cutting edge: TGF-beta1 and IL-15 Induce FOXP3+ gammadelta regulatory T cells in the presence of antigen stimulation. *J Immunol* (2009) 183(6):3574–7. doi: 10.4049/jimmunol.0901334

59. Liu Z, Eltoum IE, Guo B, Beck BH, Cloud GA, Lopez RD. Protective immunosurveillance and therapeutic antitumor activity of gammadelta T cells demonstrated in a mouse model of prostate cancer. *J Immunol* (2008) 180(9):6044–53. doi: 10.4049/jimmunol.180.9.6044

60. Matsuda S, Kudoh S, Katayama S. Enhanced formation of azoxymethane-induced colorectal adenocarcinoma in gammadelta T lymphocyte-deficient mice. *Jpn J Cancer Res* (2001) 92(8):880–5. doi: 10.1111/j.1349-7006.2001.tb01176.x

61. Kunzmann V, Bauer E, Feurle J, Weissinger F, Tony HP, Wilhelm M. Stimulation of gammadelta T cells by aminobisphosphonates and induction of antiplasma cell activity in multiple myeloma. *Blood* (2000) 96(2):384–92. doi: 10.1182/blood.V96.2.384.013k07_384_392

62. Viey E, Fromont G, Escudier B, Morel Y, Da Rocha S, Chouaib S, et al. Phosphostim-activated gamma delta T cells kill autologous metastatic renal cell carcinoma. *J Immunol* (2005) 174(3):1338–47. doi: 10.4049/jimmunol.174.3.1338

63. Fisher JP, Yan M, Heuijerjans J, Carter L, Abolhassani A, Frosch J, et al. Neuroblastoma killing properties of Vdelta2 and Vdelta2-negative gammadeltaT cells following expansion by artificial antigen-presenting cells. *Clin Cancer Res* (2014) 20(22):5720–32. doi: 10.1158/1078-0432.CCR-13-3464

64. Brandes M, Willimann K, Moser B. Professional antigen-presentation function by human gammadelta T Cells. *Science* (2005) 309(5732):264–8. doi: 10.1126/science.1110267

65. Van Acker HH, Anguille S, Van Tendeloo VF, Lion E. Empowering gamma delta T cells with antitumor immunity by dendritic cell-based immunotherapy. *Oncoimmunology* (2015) 4(8):e1021538. doi: 10.1080/2162402X.2015.1021538

66. Nezhad Shamohammadi F, Yazdanifar M, Oraei M, Kazemi MH, Roohi A, Mahya Shariat Razavi S, et al. Controversial role of gammadelta T cells in pancreatic cancer. *Int Immunopharmacol* (2022) 108:108895. doi: 10.1016/j.intimp.2022.108895

67. Naoe M, Ogawa Y, Takeshita K, Morita J, Shichijo T, Fuji K, et al. Zoledronate stimulates gamma delta T cells in prostate cancer patients. *Oncol Res* (2010) 18(10):493–501. doi: 10.3727/096504010x12671222663638

68. Park JH, Kim HJ, Kim CW, Kim HC, Jung Y, Lee HS, et al. Tumor hypoxia represses gammadelta T cell-mediated antitumor immunity against brain tumors. *Nat Immunol* (2021) 22(3):336–46. doi: 10.1038/s41590-020-00860-7

69. Lee M, Park C, Woo J, Kim J, Kho I, Nam DH, et al. Preferential infiltration of unique vgamma9Jgamma2-vdelta2 T cells into glioblastoma multiforme. *Front Immunol* (2019) 10:555. doi: 10.3389/fimmu.2019.00555

70. Razavi SM, Lee KE, Jin BE, Aujla PS, Gholamin S, Li G. Immune evasion strategies of glioblastoma. *Front Surg* (2016) 3:11. doi: 10.3389/fsurg.2016.00011

71. Vitkovic L, Maeda S, Sternberg E. Anti-inflammatory cytokines: expression and action in the brain. *Neuroimmunomodulation* (2001) 9(6):295–312. doi: 10.1159/000059387

72. Hao C, Chen G, Zhao H, Li Y, Chen J, Zhang H, et al. PD-L1 expression in glioblastoma, the clinical and prognostic significance: A systematic literature review and meta-analysis. *Front Oncol* (2020) 10:1015. doi: 10.3389/fonc.2020.01015

73. Thakkar JP, Dolecek TA, Horbinski C, Ostrom QT, Lightner DD, Barnholtz-Sloan JS, et al. Epidemiologic and molecular prognostic review of glioblastoma. *Cancer Epidemiol Biomarkers Prev* (2014) 23(10):1985–96. doi: 10.1158/1055-9965.EPI-14-0275

74. Low JT, Ostrom QT, Cioffi G, Neff C, Waite KA, Kruchko C, et al. Primary brain and other central nervous system tumors in the United States (2014-2018): A summary of the CBTRUS statistical report for clinicians. *Neurooncol Pract* (2022) 9(3):165–82. doi: 10.1093/nop/npac015

75. Ostrom QT, Gittleman H, Liao P, Rouse C, Chen Y, Dowling J, et al. CBTRUS statistical report: primary brain and central nervous system tumors diagnosed in the United States in 2007-2011. *Neuro Oncol* (2014) 16 Suppl 4(Suppl 4):iv1–63. doi: 10.1093/neuonc/nou223

76. Carrano A, Juarez JJ, Incontri D, Ibarra A, Guerrero Cazares H. Sex-specific differences in glioblastoma. *Cells* (2021) 10(7):1783. doi: 10.3390/cells10071783

77. Yang W, Warrington NM, Taylor SJ, Whitmire P, Carrasco E, Singleton KW, et al. Sex differences in GBM revealed by analysis of patient imaging, transcriptome, and survival data. *Sci Transl Med* (2019) 11(473):eaao5253. doi: 10.1126/scitranslmed.aao5253

78. Inskip PD. Frequent radiation exposures and frequency-dependent effects: the eyes have it. *Epidemiology* (2001) 12(1):1–4. doi: 10.1097/00001648-200101000-00001

79. Bondy ML, Scheurer ME, Malmer B, Barnholtz-Sloan JS, Davis FG, Il'yasova D, et al. Brain tumor epidemiology: consensus from the Brain Tumor Epidemiology Consortium. *Cancer* (2008) 113(7 Suppl):1953–68. doi: 10.1002/cncr.23741

80. Ohgaki H. Epidemiology of brain tumors. *Methods Mol Biol* (2009) 472:323–42. doi: 10.1007/978-1-60327-492-0_14

81. Iacob G, Dinca EB. Current data and strategy in glioblastoma multiforme. *J Med Life* (2009) 2(4):386–93.

82. Lee JH, Lee JE, Kahng JY, Kim SH, Park JS, Yoon SJ, et al. Human glioblastoma arises from subventricular zone cells with low-level driver mutations. *Nature* (2018) 560(7717):243–7. doi: 10.1038/s41586-018-0389-3

83. Zong H, Parada LF, Baker SJ. Cell of origin for Malignant gliomas and its implication in therapeutic development. *Cold Spring Harb Perspect Biol* (2015) 7(5):a020610. doi: 10.1101/cshperspect.a020610

84. Piper K, DePledge L, Karsy M, Cobbs C. Glioma stem cells as immunotherapeutic targets: advancements and challenges. *Front Oncol* (2021) 11:615704. doi: 10.3389/fonc.2021.615704

85. Alves ALV, Gomes INF, Carloni AC, Rosa MN, da Silva LS, Evangelista AF, et al. Role of glioblastoma stem cells in cancer therapeutic resistance: a perspective on antineoplastic agents from natural sources and chemical derivatives. *Stem Cell Res Ther* (2021) 12(1):206. doi: 10.1186/s13287-021-02231-x

86. Louis DN, Perry A, Wesseling P, Brat DJ, Cree IA, Figarella-Branger D, et al. The 2021 WHO classification of tumors of the central nervous system: a summary. *Neuro Oncol* (2021) 23(8):1231–51. doi: 10.1093/neuonc/noab106

87. Verhaak RG, Hoadley KA, Purdom E, Wang V, Qi Y, Wilkerson MD, et al. Integrated genomic analysis identifies clinically relevant subtypes of glioblastoma characterized by abnormalities in PDGFRA, IDH1, EGFR, and NF1. *Cancer Cell* (2010) 17(1):98–110. doi: 10.1016/j.ccr.2009.12.020

88. Neftel C, Laffy J, Filbin MG, Hara T, Shore ME, Rahme GJ, et al. An integrative model of cellular states, plasticity, and genetics for glioblastoma. *Cell* (2019) 178(4):835–49 e21. doi: 10.1016/j.cell.2019.06.024

89. Soomro SH, Ting LR, Qing YY, Ren M. Molecular biology of glioblastoma: Classification and mutational locations. *J Pak Med Assoc* (2017) 67(9):1410–4.

90. Verdugo E, Puerto I, Medina MA. An update on the molecular biology of glioblastoma, with clinical implications and progress in its treatment. *Cancer Commun (Lond)* (2022) 42(11):1083–111. doi: 10.1002/cac2.12361

91. Bhat KPL, Balasubramaniyan V, Vaillant B, Ezhilarasan R, Hummelink K, Hollingsworth F, et al. Mesenchymal differentiation mediated by NF-kappaB

promotes radiation resistance in glioblastoma. *Cancer Cell* (2013) 24(3):331–46. doi: 10.1016/j.ccr.2013.08.001

92. Liu T, Ma W, Xu H, Huang M, Zhang D, He Z, et al. PDGF-mediated mesenchymal transformation renders endothelial resistance to anti-VEGF treatment in glioblastoma. *Nat Commun* (2018) 9(1):3439. doi: 10.1038/s41467-018-05982-z

93. Halliday J, Helmy K, Pattwell SS, Pitter KL, LaPlant Q, Ozawa T, et al. *In vivo* radiation response of proneural glioma characterized by protective p53 transcriptional program and proneural-mesenchymal shift. *Proc Natl Acad Sci U.S.A.* (2014) 111 (14):5248–53. doi: 10.1073/pnas.1321014111

94. Joseph JV, Conroy S, Pavlov K, Sontakke P, Tomar T, Eggens-Meijer E, et al. Hypoxia enhances migration and invasion in glioblastoma by promoting a mesenchymal shift mediated by the HIF1alpha-ZEB1 axis. *Cancer Lett* (2015) 359 (1):107–16. doi: 10.1016/j.canlet.2015.01.010

95. Weller M, Stupp R, Reifenberger G, Brandes AA, van den Bent MJ, Wick W, et al. MGMT promoter methylation in Malignant gliomas: ready for personalized medicine? *Nat Rev Neurol* (2010) 6(1):39–51. doi: 10.1038/nrneurol.2009.197

96. Stupp R, Mason WP, van den Bent MJ, Weller M, Fisher B, Taphoorn MJ, et al. Radiotherapy plus concomitant and adjuvant temozolomide for glioblastoma. *N Engl J Med* (2005) 352(10):987–96. doi: 10.1056/NEJMoa043330

97. Tam SY, Wu VWC, Law HKW. Hypoxia-induced epithelial-mesenchymal transition in cancers: HIF-1alpha and beyond. *Front Oncol* (2020) 10:486. doi: 10.3389/fonc.2020.00486

98. Mikheeva SA, Mikheev AM, Petit A, Beyer R, Oxford RG, Khorasani L, et al. TWIST1 promotes invasion through mesenchymal change in human glioblastoma. *Mol Cancer* (2010) 9:194. doi: 10.1186/1476-4598-9-194

99. Liebelt BD, Shingu T, Zhou X, Ren J, Shin SA, Hu J. Glioma stem cells: signaling, microenvironment, and therapy. *Stem Cells Int* (2016) 2016:7849890. doi: 10.1155/2016/7849890

100. Jackson M, Hassiotou F, Nowak A. Glioblastoma stem-like cells: at the root of tumor recurrence and a therapeutic target. *Carcinogenesis* (2015) 36(2):177–85. doi: 10.1093/carcin/bgu243

101. Larochelle C, Alvarez JI, Prat A. How do immune cells overcome the blood-brain barrier in multiple sclerosis? *FEBS Lett* (2011) 585(23):3770–80. doi: 10.1016/j.febslet.2011.04.066

102. Thorsson V, Gibbs DL, Brown SD, Wolf D, Bortone DS, Ou Yang TH, et al. The immune landscape of cancer. *Immunity* (2018) 48(4):812–30 e14. doi: 10.1016/j.immuni.2018.03.023

103. Larkin J, Chiarion-Sileni V, Gonzalez R, Grob JJ, Rutkowski P, Lao CD, et al. Five-year survival with combined nivolumab and ipilimumab in advanced melanoma. *N Engl J Med* (2019) 381(16):1535–46. doi: 10.1056/NEJMoa1910836

104. Abellanas MA, Zamarbide M, Basurco L, Luquin E, Garcia-Granero M, Clavero P, et al. Midbrain microglia mediate a specific immunosuppressive response under inflammatory conditions. *J Neuroinflamm* (2019) 16(1):233. doi: 10.1186/s12974-019-1628-8

105. Tomaszewski WH, Waibl-Polania J, Chakraborty M, Perera J, Ratiu J, Miggelbrink A, et al. Neuronal CaMKK2 promotes immunosuppression and checkpoint blockade resistance in glioblastoma. *Nat Commun* (2022) 13(1):6483. doi: 10.1038/s41467-022-34175-y

106. Braganza MZ, Kitahara CM, Berrington de Gonzalez A, Inskip PD, Johnson KJ, Rajaraman P. Ionizing radiation and the risk of brain and central nervous system tumors: a systematic review. *Neuro Oncol* (2012) 14(11):1316–24. doi: 10.1093/neuonc/nos208

107. Alnahhas I, Alsawas M, Rayi A, Palmer JD, Raval R, Ong S, et al. Characterizing benefit from temozolomide in MGMT promoter unmethylated and methylated glioblastoma: a systematic review and meta-analysis. *Neurooncol Adv* (2020) 2(1): vdaa082. doi: 10.1093/noajnl/vdaa082

108. Fu M, Zhou Z, Huang X, Chen Z, Zhang L, Zhang J, et al. Use of Bevacizumab in recurrent glioblastoma: a scoping review and evidence map. *BMC Cancer* (2023) 23 (1):544. doi: 10.1186/s12885-023-11043-6

109. Stupp R, Taillibert S, Kanner A, Read W, Steinberg D, Lhermitte B, et al. Effect of tumor-treating fields plus maintenance temozolomide vs maintenance temozolomide alone on survival in patients with glioblastoma: A randomized clinical trial. *JAMA* (2017) 318(23):2306–16. doi: 10.1001/jama.2017.18718

110. Jackson CM, Lim M, Drake CG. Immunotherapy for brain cancer: recent progress and future promise. *Clin Cancer Res* (2014) 20(14):3651–9. doi: 10.1158/1078-0432.CCR-13-2057

111. Louveau A, Smirnov I, Keyes TJ, Eccles JD, Rouhani SJ, Peske JD, et al. Structural and functional features of central nervous system lymphatic vessels. *Nature* (2015) 523(7560):337–41. doi: 10.1038/nature14432

112. Yang I, Tihan T, Han SJ, Wrensch MR, Wiencke J, Sughrue ME, et al. CD8+ T cell infiltrate in newly diagnosed glioblastoma is associated with long-term survival. *J Clin Neurosci* (2010) 17(11):1381–5. doi: 10.1016/j.jocn.2010.03.031

113. Ferris RL, Blumenschein G Jr., Fayette J, Guigay J, Colevas AD, Licitra L, et al. Nivolumab for recurrent squamous-cell carcinoma of the head and neck. *N Engl J Med* (2016) 375(19):1856–67. doi: 10.1056/NEJMoa1602252

114. DeMaria PJ, Bilusic M. Cancer vaccines. *Hematol Oncol Clin North Am* (2019) 33(2):199–214. doi: 10.1016/j.hoc.2018.12.001

115. Nemunaitis J. GVAX (GMCSF gene modified tumor vaccine) in advanced stage non small cell lung cancer. *J Control Release* (2003) 91(1-2):225–31. doi: 10.1016/S0168-3659(03)00210-4

116. Brown CE, Alizadeh D, Starr R, Weng L, Wagner JR, Naranjo A, et al. Regression of glioblastoma after chimeric antigen receptor T cell therapy. *N Engl J Med* (2016) 375(26):2561–9. doi: 10.1056/NEJMoa1610497

117. Marchetti L, Engelhardt B. Immune cell trafficking across the blood-brain barrier in the absence and presence of neuroinflammation. *Vasc Biol* (2020) 2(1):H1–H18. doi: 10.1530/VB-19-0033

118. Luo H, Shusta EV. Blood-brain barrier modulation to improve glioma drug delivery. *Pharmaceutics* (2020) 12(11):1085. doi: 10.3390/pharmaceutics12111085

119. Hambardzumyan D, Gutmann DH, Kettenmann H. The role of microglia and macrophages in glioma maintenance and progression. *Nat Neurosci* (2016) 19(1):20–7. doi: 10.1038/nn.4185

120. Vidyarthi A, Agnihotri T, Khan N, Singh S, Tewari MK, Radotra BD, et al. Predominance of M2 macrophages in gliomas leads to the suppression of local and systemic immunity. *Cancer Immunol Immunother* (2019) 68(12):1995–2004. doi: 10.1007/s00262-019-02423-8

121. Strepkos D, Markouli M, Klonou A, Piperi C, Papavassiliou AG. Insights in the immunobiology of glioblastoma. *J Mol Med (Berl)* (2020) 98(1):1–10. doi: 10.1007/s00109-019-01835-4

122. Sayour EJ, McLendon P, McLendon R, De Leon G, Reynolds R, Kresak J, et al. Increased proportion of FoxP3+ regulatory T cells in tumor infiltrating lymphocytes is associated with tumor recurrence and reduced survival in patients with glioblastoma. *Cancer Immunol Immunother* (2015) 64(4):419–27. doi: 10.1007/s00262-014-1651-7

123. Yang W, Li Y, Gao R, Xiu Z, Sun T. MHC class I dysfunction of glioma stem cells escapes from CTL-mediated immune response *via* activation of Wnt/beta-catenin signaling pathway. *Oncogene* (2020) 39(5):1098–111. doi: 10.1038/s41388-019-1045-6

124. Sottoriva A, Spiteri I, Piccirillo SG, Touloumis A, Collins VP, Marioni JC, et al. Intratumor heterogeneity in human glioblastoma reflects cancer evolutionary dynamics. *Proc Natl Acad Sci U.S.A.* (2013) 110(10):4009–14. doi: 10.1073/pnas.1219747110

125. Patel AP, Tirosh I, Trombetta JJ, Shalek AK, Gillespie SM, Wakimoto H, et al. Single-cell RNA-seq highlights intratumoral heterogeneity in primary glioblastoma. *Science* (2014) 344(6190):1396–401. doi: 10.1126/science.1254257

126. Bryant NL, Suarez-Cuervo C, Gillespie GY, Markert JM, Nabors LB, Meleth S, et al. Characterization and immunotherapeutic potential of gammadelta T cells in patients with glioblastoma. *Neuro Oncol* (2009) 11(4):357–67. doi: 10.1215/15228517-2008-111

127. Bradshaw A, Wickremesekera A, Brasch HD, Chibnall AM, Davis PF, Tan ST, et al. Cancer stem cells in glioblastoma multiforme. *Front Surg* (2016) 3:48. doi: 10.3389/fsurg.2016.00048

128. Jarry U, Chauvin C, Joalland N, Leger A, Minault S, Robard M, et al. Stereotaxic administrations of allogeneic human Vgamma9Vdelta2 T cells efficiently control the development of human glioblastoma brain tumors. *Oncoimmunology* (2016) 5(6): e1168554. doi: 10.1080/2162402X.2016.1168554

129. Jamieson AM, Diefenbach A, McMahon CW, Xiong N, Carlyle JR, Raulet DH. The role of the NKG2D immunoreceptor in immune cell activation and natural killing. *Immunity* (2002) 17(1):19–29. doi: 10.1016/S1074-7613(02)00333-3

130. Choi H, Lee Y, Park SA, Lee JH, Park J, Park JH, et al. Human allogenic gammadelta T cells kill patient-derived glioblastoma cells expressing high levels of DNAM-1 ligands. *Oncoimmunology* (2022) 11(1):2138152. doi: 10.1080/2162402X.2022.2138152

131. Xu Y, Xiang Z, Alnaggar M, Kouakanou L, Li J, He J, et al. Allogeneic Vgamma9Vdelta2 T cell immunotherapy exhibits promising clinical safety and prolongs the survival of patients with late-stage lung or liver cancer. *Cell Mol Immunol* (2021) 18(2):427–39. doi: 10.1038/s41423-020-0515-7

132. Lin M, Zhang X, Liang S, Luo H, Alnaggar M, Liu A, et al. Irreversible electroporation plus allogenic Vgamma9Vdelta2 T cells enhances antitumor effect for locally advanced pancreatic cancer patients. *Signal Transduct Target Ther* (2020) 5 (1):215. doi: 10.1038/s41392-020-00260-1

133. Chitadze G, Fluh C, Quabius ES, Freitag-Wolf S, Peters C, Lettau M, et al. In-depth immunophenotyping of patients with glioblastoma multiforme: Impact of steroid treatment. *Oncoimmunology* (2017) 6(11):e1358839. doi: 10.1080/2162402X.2017.1358839

134. Ahn E, Araki K, Hashimoto M, Li W, Riley JL, Cheung J, et al. Role of PD-1 during effector CD8 T cell differentiation. *Proc Natl Acad Sci U.S.A.* (2018) 115 (18):4749–54. doi: 10.1073/pnas.1718217115

135. Qin G, Liu Y, Zheng J, Ng IH, Xiang Z, Lam KT, et al. Type 1 responses of human Vgamma9Vdelta2 T cells to influenza A viruses. *J Virol* (2011) 85(19):10109–16. doi: 10.1128/JVI.05341-11

136. Devilder MC, Allain S, Dousset C, Bonneville M, Scotet E. Early triggering of exclusive IFN-gamma responses of human Vgamma9Vdelta2 T cells by TLR-activated myeloid and plasmacytoid dendritic cells. *J Immunol* (2009) 183(6):3625–33. doi: 10.4049/jimmunol.0901571

137. Rafia C, Loizeau C, Renoult O, Harly C, Pecqueur C, Joalland N, et al. The antitumor activity of human Vgamma9Vdelta2 T cells is impaired by TGF-beta

through significant phenotype, transcriptomic and metabolic changes. *Front Immunol* (2022) 13:1066336. doi: 10.3389/fimmu.2022.1066336

138. Steele MM, Jaiswal A, Delclaux I, Dryg ID, Murugan D, Femel J, et al. T cell egress *via* lymphatic vessels is tuned by antigen encounter and limits tumor control. *Nat Immunol* (2023) 24(4):664–75. doi: 10.1038/s41590-023-01443-y

139. Jhita N, Raikar SS. Allogeneic gamma delta T cells as adoptive cellular therapy for hematologic Malignancies. *Explor Immunol* (2022) 2(3):334–50. doi: 10.37349/ei.2022.00054

140. O'Rourke DM, Nasrallah MP, Desai A, Melenhorst JJ, Mansfield K, Morrissette JJD, et al. A single dose of peripherally infused EGFRvIII-directed CAR T cells mediates antigen loss and induces adaptive resistance in patients with recurrent glioblastoma. *Sci Transl Med* (2017) 9(399):eaaa0984. doi: 10.1126/scitranslmed.aaa0984

141. Chen J, Qiu S, Li W, Wang K, Zhang Y, Yang H, et al. Tuning charge density of chimeric antigen receptor optimizes tonic signaling and CAR-T cell fitness. *Cell Res* (2023) 33(5):341–54. doi: 10.1038/s41422-023-00789-0

142. Liu X, Ranganathan R, Jiang S, Fang C, Sun J, Kim S, et al. A chimeric switch-receptor targeting PD1 augments the efficacy of second-generation CAR T cells in advanced solid tumors. *Cancer Res* (2016) 76(6):1578–90. doi: 10.1158/0008-5472.CAN-15-2524

143. Maxwell M, Galanopoulos T, Neville-Golden J, Antoniades HN. Effect of the expression of transforming growth factor-beta 2 in primary human glioblastomas on immunosuppression and loss of immune surveillance. *J Neurosurg* (1992) 76(5):799–804. doi: 10.3171/jns.1992.76.5.0799

144. Noh KE, Lee JH, Choi SY, Jung NC, Nam JH, Oh JS, et al. TGF-beta/IL-7 chimeric switch receptor-expressing CAR-T cells inhibit recurrence of CD19-positive B cell lymphoma. *Int J Mol Sci* (2021) 22(16):8706. doi: 10.3390/ijms22168706

145. Lamb LS Jr., Bowersock J, Dasgupta A, Gillespie GY, Su Y, Johnson A, et al. Engineered drug resistant gammadelta T cells kill glioblastoma cell lines during a chemotherapy challenge: a strategy for combining chemo- and immunotherapy. *PloS One* (2013) 8(1):e51805. doi: 10.1371/journal.pone.0051805

146. Thedrez A, Harly C, Morice A, Salot S, Bonneville M, Scotet E. IL-21-mediated potentiation of antitumor cytolytic and proinflammatory responses of human V gamma 9V delta 2 T cells for adoptive immunotherapy. *J Immunol* (2009) 182 (6):3423–31. doi: 10.4049/jimmunol.0803068

147. Choi H, Lee Y, Hur G, Lee SE, Cho HI, Sohn HJ, et al. gammadelta T cells cultured with artificial antigen-presenting cells and IL-2 show long-term proliferation and enhanced effector functions compared with gammadelta T cells cultured with only IL-2 after stimulation with zoledronic acid. *Cytotherapy* (2021) 23(10):908–17. doi: 10.1016/j.jcyt.2021.06.002

148. Harmon C, Zaborowski A, Moore H, St Louis P, Slattery K, Duquette D, et al. gammadelta T cell dichotomy with opposing cytotoxic and wound healing functions in human solid tumors. *Nat Cancer* (2023) 4(8):1122–37. doi: 10.1038/s43018-023-00589-w

frontiers | Frontiers in Immunology

TYPE Original Research
PUBLISHED 28 December 2023
DOI 10.3389/fimmu.2023.1297932

OPEN ACCESS

EDITED BY
Divya Nagarajan,
Uppsala University, Sweden

REVIEWED BY
Ichwaku Rastogi,
University of Wisconsin-Madison, United States
Michal Amit Rahat,
Technion-Israel Institute of Technology, Israel

*CORRESPONDENCE
David A. Reardon
david_reardon@dfci.harvard.edu
Catherine J. Wu
cwu@partners.org

†PRESENT ADDRESS
J. Bryan Iorgulescu,
Molecular Diagnostics Laboratory, Department of Hematopathology, Division of Pathology and Laboratory Medicine, The University of Texas MD Anderson Cancer Center, Houston, TX, United States

‡These authors have contributed equally to this work and share second authorship

§These authors have contributed equally to this work and share last authorship

RECEIVED 20 September 2023
ACCEPTED 11 December 2023
PUBLISHED 28 December 2023

CITATION
Iorgulescu JB, Ruthen N, Ahn R, Panagioti E, Gokhale PC, Neagu M, Speranza MC, Eschle BK, Soroko KM, Piranlioglu R, Datta M, Krishnan S, Yates KB, Baker GJ, Jain RK, Suvà ML, Neuberg D, White FM, Chiocca EA, Freeman GJ, Sharpe AH, Wu CJ and Reardon DA (2023) Antigen presentation deficiency, mesenchymal differentiation, and resistance to immunotherapy in the murine syngeneic CT2A tumor model. *Front. Immunol.* 14:1297932. doi: 10.3389/fimmu.2023.1297932

Antigen presentation deficiency, mesenchymal differentiation, and resistance to immunotherapy in the murine syngeneic CT2A tumor model

J. Bryan Iorgulescu[1,2,3†], Neil Ruthen[1‡], Ryuhjin Ahn[4,5‡], Eleni Panagioti[6‡], Prafulla C. Gokhale[7‡], Martha Neagu[8], Maria C. Speranza[1], Benjamin K. Eschle[7], Kara M. Soroko[7], Raziye Piranlioglu[6], Meenal Datta[9,10], Shanmugarajan Krishnan[9], Kathleen B. Yates[3,11], Gregory J. Baker[12,13], Rakesh K. Jain[9], Mario L. Suvà[3,11,14], Donna Neuberg[1], Forest M. White[4,5], E. Antonio Chiocca[6], Gordon J. Freeman[1], Arlene H. Sharpe[2,3,8], Catherine J. Wu[1,3*§] and David A. Reardon[1*§]

[1]Department of Medical Oncology, Dana-Farber Cancer Institute, Boston, MA, United States, [2]Department of Pathology, Brigham and Women's Hospital, Harvard Medical School, Boston, MA, United States, [3]The Eli and Edythe L. Broad Institute of MIT and Harvard, Cambridge, MA, United States, [4]Department of Biological Engineering, Massachusetts Institute of Technology, Cambridge, MA, United States, [5]Koch Institute for Integrative Cancer Research, Massachusetts Institute of Technology, Cambridge, MA, United States, [6]Department of Neurosurgery, Brigham and Women's Hospital and Harvard Medical School, Boston, MA, United States, [7]Experimental Therapeutics Core and Belfer Center for Applied Cancer Science, Dana-Farber Cancer Institute, Boston, MA, United States, [8]Department of Immunology, Blavatnik Institute, Harvard Medical School, Boston, MA, United States, [9]Edwin L. Steele Laboratories for Tumor Biology, Massachusetts General Hospital, Harvard Medical School, Boston, MA, United States, [10]Department of Aerospace and Mechanical Engineering, University of Notre Dame, Notre Dame, IN, United States, [11]Center for Cancer Research, Massachusetts General Hospital, Boston, MA, United States, [12]Laboratory of Systems Pharmacology, Program in Therapeutic Science, Harvard Medical School, Boston, MA, United States, [13]Ludwig Center for Cancer Research at Harvard, Harvard Medical School, Boston, MA, United States, [14]Department of Pathology, Massachusetts General Hospital, Harvard Medical School, Boston, MA, United States

Background: The GL261 and CT2A syngeneic tumor lines are frequently used as immunocompetent orthotopic mouse models of human glioblastoma (huGBM) but demonstrate distinct differences in their responses to immunotherapy.

Methods: To decipher the cell-intrinsic mechanisms that drive immunotherapy resistance in CT2A-luc and to define the aspects of human cancer biology that these lines can best model, we systematically compared their characteristics using whole exome and transcriptome sequencing, and protein analysis through immunohistochemistry, Western blot, flow cytometry, immunopeptidomics, and phosphopeptidomics.

10.3389/fimmu.2023.1297932

Results: The transcriptional profiles of GL261-luc2 and CT2A-luc tumors resembled those of some huGBMs, despite neither line sharing the essential genetic or histologic features of huGBM. Both models exhibited striking hypermutation, with clonal hotspot mutations in RAS genes (*Kras* p.G12C in GL261-luc2 and *Nras* p.Q61L in CT2A-luc). CT2A-luc distinctly displayed mesenchymal differentiation, upregulated angiogenesis, and multiple defects in antigen presentation machinery (e.g. *Tap1* p.Y488C and *Psmb8* p.A275P mutations) and interferon response pathways (e.g. copy number losses of loci including IFN genes and reduced phosphorylation of JAK/STAT pathway members). The defect in MHC class I expression could be overcome in CT2A-luc by interferon-γ treatment, which may underlie the modest efficacy of some immunotherapy combinations. Additionally, CT2A-luc demonstrated substantial baseline secretion of the CCL-2, CCL-5, and CCL-22 chemokines, which play important roles as myeloid chemoattractants.

Conclusion: Although the clinical contexts that can be modeled by GL261 and CT2A for huGBM are limited, CT2A may be an informative model of immunotherapy resistance due to its deficits in antigen presentation machinery and interferon response pathways.

KEYWORDS

immunotherapy, resistance, mouse model, cancer, antigen presentation machinery, glioblastoma, mesenchymal

Introduction

Therapeutic blockade of inhibitory immune checkpoint pathways (*e.g.*, PD-1/PD-L1 and CTLA-4) has transformed the care of patients across multiple cancer types, including many formerly intractable advanced cancers (1). However, for human IDH-wildtype glioblastoma (huGBM)—a common and aggressive brain cancer typified by a median survival of just 14-22 months depending on *MGMT* promoter methylation status (2, 3)—the near-uniform negative results of single-agent immune checkpoint blockade (ICB) clinical trials have been disappointing (4–6). The intracranial location of huGBM and the blood brain barrier by themselves do not appear to preclude effective anti-tumoral immunity, since ICB has been successful in treating brain metastases from a variety of primary cancers (7, 8). In contrast to many brain metastasis types, however, huGBM is characterized by a 'cold' (i.e., a paucity of T cells) immune microenvironment. This immuno-resistance has been also ascribed to other multifaceted sources, including: 1) a dominance of suppressive myeloid cells; 2) a low tumor mutational burden; 3) limited PD-L1 expression; 4) T cell sequestration in the bone marrow; and 5) immunosuppression mediated by the frequent need for high-dose corticosteroids to treat symptomatic cerebral edema (9–12). In an effort to overcome these barriers, numerous immunotherapeutic approaches are currently under clinical investigation for huGBM, including immunomodulatory agents (e.g. NCT04547777), peptide vaccination (e.g. NCT02287428), oncolytic virotherapy (e.g. NCT03152318), adoptive cell therapy (e.g. NCT05660369), and next-generation immune checkpoint modulators (e.g. NCT04826393) – which have been extensively reviewed elsewhere (10).

A valuable cornerstone of preclinical oncology research is the use of syngeneic orthotopic murine cancer lines as immunocompetent models of cancer. For huGBM, the two frequently used lines are GL261 and CT2A, both of which were generated by injecting the carcinogen methylcholanthrene into the brains of mice (13–15). As with other methylcholanthrene-derived cancers, both GL261 and CT2A exhibit a striking degree of hypermutation, which contrasts with the low tumor mutational burden typically observed in huGBM (16, 17). However, whereas GL261 is readily responsive to several immunotherapies, we and others have previously demonstrated the broad resistance of the syngeneic CT2A mouse model to diverse single-agent immunotherapies, including PD-1/PD-L1 pathway inhibition, vaccine therapy, and oncolytic virotherapy (12, 17–21) – a phenotype that is observed even in CT2A lines that express the immunogenic luciferase protein (12, 19). Given the urgent need to devise better therapeutics for huGBM, our specific aim was to decipher the cell-intrinsic mechanisms driving the broad immuno-resistance in CT2A and to define the aspects of human cancer biology that these lines can best model for further preclinical research. To achieve this aim, we systematically characterized these lines using multi-modal profiling, including genomic,

transcriptomic, protein, immuno-peptidomic, and phospho-peptidomic analyses.

Materials and methods

All animal experiments were approved by the Dana-Farber Cancer Institute and Harvard Medical School Animal Care and Use Committees.

Cell culture

Luciferase-transduced GL261 cells (GL261-luc2; RRID: CVCL_X986) were obtained from PerkinElmer (Waltham, MA). CT2A cells were obtained from Thomas Seyfried (Boston College; RRID: CVCL_ZJ44) and transduced using firefly luciferase lentiviral particles (CT2A-luc; Kerafast Inc., Boston, MA). Cell lines were expanded and frozen at the same generation. For experiments, cells were thawed and cultured at 37°C in a humidified incubator with 5% CO_2 using Dulbecco's Modified Eagle Medium supplemented with 10% heat-inactivated fetal calf serum and 100 µg/mL G418 (for GL261-luc2) or 2 µg/mL puromycin (for CT2A-luc). Cultures were regularly tested as negative for mycoplasma. Luciferase was used to enable bioluminescent imaging and ensure that tumors' engraftments were comparable prior to extraction or therapeutic experiments.

For the second set of experiments (Cohort B), a truncated human *CD19* reporter gene was introduced into GL261-luc2 and CT2A-luc as previously described (22). The purity of hCD19-positive tumor cells was confirmed by flow cytometry following sorting, using isotype controls for comparison. Unless otherwise noted, all cell lines were grown as adherent cultures. Neurospheres were cultured as previously described (23). All cell lines were fingerprinted using their DNA/RNA sequencing data.

Intracranial tumor cell inoculation

Thawed cells were cultured for up to three passages prior to intracranial implantation. 1×10^5 GL261-luc2 cells or 0.25×10^5 CT2A-luc cells were suspended in phosphate-buffered saline (PBS) and stereotactically injected into the right striatum of anesthetized, female 7-10 week-old, albino C57BL/6 mice (Jackson Laboratory; Bar Harbor, ME). For GL261-hCD19-luc2 and CT2A-hCD19-luc, 2×10^5 cells were implanted.

Survival experiments

For checkpoint immunotherapy, all antibodies were injected intraperitoneally as previously described (12, 18). The 332.8H3 mouse anti-mouse PD-1 monoclonal antibody (IgG1; generated in Gordon Freeman's laboratory; with MOPC21 isotype control [BioXCell, West Lebanon, NH]) and/or CTLA-4 antibody (clone 9D9, BioXCell) were administered as a loading dose (500 µg) on day 6 after tumor implantation, followed by 250 µg injections every 3 days for 7 additional doses. The OX40 antibody (clone OX-86, BioXCell; with rat IgG1 clone HRPN isotype control) was administered as 100 µg weekly, either for 2 doses starting on day 6 for GL261-luc2 or 3 doses starting on day 3 for CT2A-luc. All monoclonal antibodies contained <2 EU/mg endotoxin. Bioluminescent imaging (BLI) was used to identify mice with growing tumor burden for randomization into experimental cohorts, which included 8 mice per experimental arm. Bioluminescence imaging involved subcutaneous injection of D-luciferin and imaging with the IVIS imaging system approximately once each week across experiments, as previously described (18). Mice were euthanized for signs of morbidity or after ≥100 days if healthy appearing.

Bulk whole exome sequencing (WES) and RNA sequencing (RNAseq)

In vitro GL261-luc2 and CT2A-luc cells, and GL261-luc2 and CT2A-luc *ex vivo* bulk tumors (harvested 22-24 days after implantation) were prepared for DNA and RNA extractions, library preparations, and sequencing that were performed at GENEWIZ (South Plainfield, NJ). For *in vitro* GL261-luc2 and CT2A-luc cells, and GL261-luc2 and CT2A-luc *ex vivo* bulk tumors, DNA was extracted using the PureLink Genomic DNA Mini Kit (Thermo Fisher Scientific, Waltham, MA) and the sequencing libraries were prepared using the SureSelectXT Mouse All Exon Kit (Agilent, Santa Clara, CA). Fragmented DNAs were cleaned up, end repaired, and adenylated at the 3'ends. Adapters were ligated to the DNA fragments, which were then enriched with limited cycle PCR. 200 ng adapter-ligated DNA fragments were hybridized with biotinylated RNA baits at 65°C for 24 hours. The hybrid DNAs were captured by streptavidin-coated magnetic beads, extensively washed, and then amplified and indexed with Illumina indexing primers.

Total RNA was extracted using RNeasy Plus Mini kit (Qiagen, Hilden, Germany) and sequencing libraries were prepared using the NEBNext Ultra II RNA Library Prep Kit for Illumina (New England Biolabs, Ipswich, MA). mRNAs were enriched with Oligod(T) beads and fragmented for 15 minutes at 94°C. First-strand and second-strand cDNA were synthesized, end repaired, adenylated at 3'ends, and ligated to universal adapters; followed by index addition and library enrichment by PCR with limited cycles.

For GL261-hCD19-luc2 and CT2A-hCD19-luc, tumor cells were first isolated from dissociated *ex vivo* tumors by bead-based positive magnetic selection for hCD19 (Miltenyi). RNA was isolated using the RNeasy Mini kit. First-strand Illumina-barcoded libraries were generated using the NEB RNA Ultra Directional kit, including 12 cycles of PCR enrichment. Libraries were subsequently sequenced on an Illumina NextSeq500 instrument using paired-end 37 bp reads. The DNA and RNA sequencing libraries were validated on the TapeStation (Agilent Technologies, Palo Alto, CA), multiplexed, and clustered onto flow cells for sequencing using a 2x150 bp Paired End configuration on the Illumina HiSeq. Raw sequence data were converted into fastq files and de-multiplexed using Illumina bcl2fastq 2.17 software. One mis-match was allowed for index sequence identification.

WES and RNAseq analysis

Default settings were used for all WES and bulk RNAseq analysis tools. For all samples, WES data were aligned to the mm10 reference genome using bwaMem (v0.7.15), then deduplicated and recalibrated with the Picard tools MarkDuplicates, BaseRecalibrator, and ApplyBQSR packaged in GATK (v4.1.8.1). SNVs were identified by consensus calling with Mutect2 (packaged in GATK 4.1.8.1) and Strelka2 (v2.9.3). InDels were identified by consensus calling with Mutect2 and Manta (v1.5.0) packaged with Strelka2. Variants were annotated using Ensembl VEP (v102). Contiguous copy ratio segments were identified with CollectReadCounts, DenoiseReadCounts, and ModelSegments packaged in GATK (v4.1.8.1). Recurrent CNVs were subsequently identified from these segmentation files with GISTIC2.0. All calls were tested against a panel of normals comprising three C57BL/6 tail samples. Tumor mutational burden was estimated based on the SureSelectXT Mouse All Exon Kit's 49.6 MB capture.

Transcript abundances were estimated from RNA sequencing data directly using Salmon (v1.4.0) with the mm10 reference transcriptome. Differential expression analysis was performed using DESeq2 (v1.30.1), including genes with normalized transcript counts >10. Gene set enrichment analysis with the fgsea R package (v1.20.0) was performed across all genes pre-ranked by $\log_{10}$(p-value) * -(sign of the LFC). Additionally, the sequencing data were aligned to the mm10 reference transcriptome with STAR (v2.7.7a) and expression metrics for each gene were computed using RSEM (v1.3.3). Neoantigens were predicted from the aggregated results of the WES and bulk RNAseq analyses using the pVACseq pipeline (pVACtools v2.0.2) and vatools (v4.1.0). MHC I binding predictions were performed using a consensus of NetMHCpan, NetMHC, and PickPocket algorithms. RNA expression between samples was visualized using a heatmap, in which DESeq2 normalization was applied to the matrix of transcript counts, bounded to 1 if normalized value > 1 and to -1 if normalized value < -1, and then scaled to a range of 0 to 1 (by adding 1 to all counts and dividing by 2). Immune cell abundances were estimated from the RNA sequencing of bulk tumors using the murine Microenvironment Cell Population (mMCP) tool, according to default settings (24).

Immunoprecipitation of MHC class I-bound peptides

Peptide-bound MHC and phosphopeptide samples were analyzed as previously described (25). GL261-luc2 and CT2A-luc tumors were flash-frozen 22-24 days after implantation. Following homogenization and clearing by centrifugation, 1.5 mg of lysate per sample was immunoprecipitated overnight at 4°C with 0.1 mg of anti-H2-K^b (clone Y3, BioXCell) and 0.1 mg of anti-H2-D^b (clone 28-14-8S; hybridoma from ATCC) bound to 20 µL FastFlow Protein A sepharose beads (GE Healthcare). Beads were washed with TBS and water and then peptide-bound MHCs were eluted with 10% acetic acid. Peptides were separated from antibody and MHC via 10K molecular weight cut-off filters (PALL life sciences), lyophilized, and stored in -80°C before labeling. For multiplexing, lyophilized peptide-bound MHCs were resuspended in 33 µL of labeling buffer (50% ethanol, 150 mM TEAB) and mixed with 40 µg of pre-aliquoted TMTpro 16plex Label Reagent (Thermo Fisher Scientific) resuspended in 10 µL of anhydrous acetonitrile. Labeling reaction occurred on a shaker for 4.5 hours at room temperature and quenched with 0.3% hydroxylamine. Samples were pooled and dried in SpeedVac centrifuge prior to cleaning up with SP3 protocol as previously described (25).

Phosphopeptide enrichment

Tandem mass tag (TMT)-labeled samples were resuspended in IP buffer (1% Nonidet P-40, 100 mM Tris-HCl, pH 7.4) with protein G agarose beads conjugated to 24 µg of 4G10 V312 IgG and 6 µg PT-66 (Sigma) overnight at 4°C. Beads were washed with 100 mM Tris-HCl (pH 7.4), and eluted twice with 0.2% trifluoroacetic acid for 10 minute at room temperature followed by the enrichment of phosphopeptides using High-Select Fe-NTA enrichment kit (Pierce) with modification to the elution step (20 µL of elution buffer into a 1.7 mL microcentrifuge tube). Eluates were dried and resuspended in 10 µL of 3% acetonitrile in 0.1% formic acid for direct loading onto an in-house packed analytical capillary column (50 µm ID x 10 cm x 5 µm C18 beads; YMC gel). Supernatant from pTyr enrichment was used for fractionation as previously described into 10 fractions using high pH reverse-phase chromatography on a ZORBAX C18 column. One tenth of each fraction was used for global proteomics analysis and the rest subjected to phosphopeptide enrichment using Fe-NTA enrichment kit for global phosphoproteomic analysis (25).

Liquid chromatography tandem mass spectrometry

Peptide-bound MHC samples were analyzed using an Exploris 480 Hybrid Quadrupole-Orbitrap mass spectrometer (Thermo Fisher Scientific) coupled to an Agilent 1260 LC system. TMT-labeled peptides were resuspended in 3% acetonitrile/0.1% formic acid and loaded on a precolumn (100 um ID x 10 cm packed in-house with 10 µm C18 beads; YMC gel) connected in tandem to an in-house packed analytical column (50 µm ID × 15 cm and 1.9 µM C18 beads, ReproSil-Pur). Peptides were eluted using a gradient with 70% acetonitrile in 0.2 M acetic acid at the flow rate of 0.2 mL/min and a pre-column split of 2000:1. Standard mass spectrometry parameters were: spray voltage, 2.0 kV, no sheath or auxiliary gas flow, and heated capillary temperature of 275°C. The Exploris was operated in data dependent acquisition mode with the following MS1 parameters: scan range of 350-1200 m/z; resolution of 60,000; normalized AGC target of 300%; automatic IT; and dynamic exclusion (exclude precursors from selection for 30 seconds once fragmented twice within 20 second). Collection of MS2 spectra was performed under the following parameters: 60,000 resolution; isolation width of 0.4 m/z; maximum injection time (maxIT) of 250 ms; 100% normalized

AGC target fragmented by HCD with 33% collision energy; 3 second cycle time; and exclusion of charge state <2 and >4.

Enriched tyrosine phosphopeptides were direct-loaded onto the analytical column as above, and were analyzed using an Exploris 480 Hybrid Quadrupole-Orbitrap mass spectrometer (Thermo Fisher Scientific) coupled to an Agilent 1260 LC system. Fractionated serine and threonine phosphopeptides were loaded onto in-house packed precolumn connected in tandem to an in-house packed analytical column, as described above. Peptides were separated using a 145 min gradient (11% for 10 min, 11-32% for 105 min, 32-60% for 10 min, 60-100% for 10 min, hold for 3 min, 100% to 0% for 7 min) with 70% acetonitrile in 0.2M acetic acid at flow rate of 0.2 mL/min with approximate pre-column split of 2000:1. Exploris was operated in data-dependent acquisition for MS1 scans with 350-2000 m/z scan range, 60,000 resolution, normalized AGC target of 300%, maxIT of 50 ms. For every full scan, MS2 spectra were collected with an isolation width of 0.4 m/z, maxIT of 250 ms, standard AGC target, fragmentation by HCD with 33% collision energy, resolution of 60,000, 3 second cycle time and dynamic exclusion (exclude for 45 sec if precursor occurs twice within 30 sec).

Mass spectrometry data analysis

Mass spectra were analyzed using Proteome Discoverer (v2.5, Thermo Fisher Scientific) and searched using Mascot (v2.4) against the mouse Swiss-Prot database (v2021_03). For peptide-bound MHC, peptides were searched with no enzyme and variable methionine oxidation. Peptide spectrum matches were filtered by an ion score ≥15, length 8-11, search engine rank of 1, and aggregated across unique peptides. GibbsCluster 2.0 was used for motif analysis (26). For phosphoproteomic data, peptide spectrum matches were filtered by an ion score ≥20 for pTyr data and ≥25 for pSer/pThr data and search engine rank of 1. Missing values were converted to 1000 for downstream analysis. Data were processed in R studio (v4.1.0). Volcano plots were plotted with EnhancedVolcano and heatmaps were plotted with ComplexHeatmapR package. Global phosphoproteome data were subjected to PTM Signature Enrichment Analysis (27). KinMap was used for plotting kinases that were differentially phosphorylated (28). Protein expression between samples was visualized using a heatmap, in which Z-score normalization was applied to the matrix of protein MS expression values, bounded to 1 if normalized value > 1 and to -1 if normalized value < -1, and then scaled to a range of 0 to 1 (by adding 1 to all counts and dividing by 2).

Immunohistochemical staining

GL261-hCD19-luc2 and CT2A-hCD19-luc tumor-bearing brains were harvested and fixed in 4% paraformaldehyde for 24 hours, paraffin-embedded, sectioned, and stained using standard hematoxylin & eosin stain and immunohistochemical methods, as previously described (29). Slides were scanned in brightfield on a Zeiss AxioScan.Z1 using a 20x objective. Antibodies are detailed in the Supplemental Antibodies Table.

Immunofluorescent staining

Formalin-fixed paraffin-embedded tissue sections of brains implanted with GL261-luc2 or CT2A-luc tumors were counterstained and immunolabeled using a 1:5000 dilution of Hoechst dye (10 mg/ml stock) in Odyssey Blocking Buffer to which anti-vimentin (AF594-conjugated, clone: D21H3; Cell Signaling #7675S) and anti-Ki67 (AF488-conjugated, clone: D3B5; Cell Signaling #11882S) primary antibodies were added at 1:25 dilutions. Tissue sections were incubated with the resulting counterstain/antibody solution for 1 hour in the dark at room temperature, rinsed in opaque Coplin jars containing fresh 1X PBS for 10 minutes in triplicate, and cover slipped in a 50% v/v glycerol solution diluted in 1X PBS immediately prior to imaging. Image tiles were acquired using a CyteFinder slide-scanning fluorescence microscope (RareCyte Inc.) at 20x magnification with 2x2 binning then stitched, registered, and flatfield-corrected using the MCMICRO image processing pipeline to generate whole-slide mosaic images. Tissue sections were also stained with hematoxylin and eosin for histological evaluation.

Western blot

GL261-luc2 and CT2A-luc cells were seeded at 500,000 cells/well in 6-well plates and cultured for 48 hours with or without 50 ng/mL of recombinant murine IFNγ (#315-05, Peprotech) at 37°C in a humidified incubator with 5% CO2, and then lysed in RIPA buffer (#89900, Thermo Fisher Scientific) containing protease and phosphatase inhibitors (#11836153001, #524624; Sigma-Aldrich). SDS polyacrylamide gel electrophoresis was performed using 10 µg of each lysate boiled for 10 minutes in Laemmli sample buffer. Proteins were transferred onto a PVDF membrane using a wet Trans-Blot transfer system (Bio-Rad Laboratories), blocked with TBS buffer containing 3% milk for 1 hour at room temperature, incubated with primary antibody overnight at 4 °C, washed, and then incubated with rabbit secondary antibody (# NA934, GE Healthcare). Primary and secondary antibody dilutions were prepared with a TBS buffer containing 0.1% Tween20 and 3% milk. Staining was detected using Supersignal West Pico or Femto Chemiluminescent Substrate (Thermo Fisher Scientific) and Biorad ChemiDoc MP imaging system. Antibodies are detailed in the Supplemental Antibodies Table. Band densities were normalized to the sample's corresponding B-actin band signal, averaged across experimental replicates, and compared between experimental conditions using AzureSpot Pro 1.4.

Secreted protein and MHC expression analysis

GL261-luc2 and CT2A-luc were seeded at 1×10^6 cells/well in 6-well plates with their respective media conditions, and treated with either none or 50 ng/mL of recombinant murine IFN-γ (BioLegend #575304) at 37°C in triplicate. The manufacturer-reported specific activity of the IFN-γ was $1\text{-}4\times10^6$ units/mg. After 24 hours, the conditioned media were aspirated and frozen

for storage. Wells were rinsed with PBS and the cells were detached by incubation with 0.5 mM EDTA in PBS. Cells were suspended in media, pelleted, and washed with media. Cells were then stained for 15 minutes with the Zombie Aqua Fixable Viability Kit (BioLegend) for live/dead discrimination. Samples were then washed, blocked with anti-mouse CD16/32 for 10 minutes and stained with fluorophore-conjugated antibodies (either H2-K^b with I-A/I-E, or H2-D^b alone) or respective isotype controls for 20 minutes on ice. PBS with 2% fetal bovine serum was used for antibody staining and washing. All antibodies were used at 1:100 dilution and detailed in the Supplemental Antibodies Table. Concurrently, splenocytes from a naïve mouse were dissociated, lysed with ACK buffer, and used as additional positive controls. Samples were washed and analyzed with a BD LSR Fortessa. Data were collected using FACSDiva (BD Biosciences) and then compensated and analyzed using FlowJo (v10, BD Biosciences).

For assessment of cytokine and chemokine signatures, the conditioned media were thawed, centrifuged at 3000 x *g* for 5 min to remove debris, and processed using the LEGENDplex bead-based immunoassay with cytokine and chemokine analyte panels (BioLegend #740446 Mouse Inflammation Panel and #740451 Mouse Proinflammatory Chemokine Panel) following the manufacturer's instructions. Samples were acquired with FACSymphony A3 cell analyzer (BD Biosciences) and analyzed using the LEGENDplex Data Analysis Software Suite.

Comparison of RNA sequencing from murine tumor and human tumor samples

Scaled TPM matrices across TCGA human cancer cohorts were obtained from the Broad GDAC Firehose (Firehose 2016_01_28 run) and multiplied by 1,000,000 to generate standard TPM values. The TPM matrices were previously created by aggregating RSEM gene-level outputs generated from bulk RNAseq data. Because the original read counts were unavailable, the TPM values were rounded to the nearest integers in order to simulate count data for use with DESeq2 (30). Using the same method, TPM matrices were generated from the GL261 and CT2A bulk RNAseq data. For comparability between human and mouse data, the orthologous genes shared by both species were identified from Ensembl Project's "Multiple Species Comparison" function (Ensembl 102) and analyzed. Principal component analysis (PCA) and differential expression using DESeq2 were performed using default parameters. The top 500 differentially expressed genes (FDR-adjusted $p < 0.05$) were excluded from the PCA analysis to minimize species-specific differences and batch effects. As a metric for the overall transcriptomic similarity of the mouse models to each of the human cancers, the Euclidean distances in PCA-space were computed from the center of the mouse cohorts to the center of each human cohort. To visualize individual sample-to-sample differences and orthogonally confirm PCA clustering, clustered heatmaps were generated with the pheatmap package (v1.0.12) in R 4.1.1 (31). Representative histological images of human tumors were acquired from the Cancer Digital Slide Archive in cBioPortal (32, 33).

Statistical analysis

Overall survival was measured from tumor implantation, estimated using Kaplan-Meier techniques and analyzed using logrank test with Bonferroni correction. Continuous variables were assessed using one-way ANOVA with the Holm-Šídák method to adjust for multiple comparisons. False discovery rates were calculated using Benjamini-Hochberg method. Analyses were performed with R, GraphPad Prism (v9.3.1), and Stata (v17.1).

Results

GL261-luc2 and CT2A-luc exhibit distinct biologic behavior, histology, and transcriptional profiles

To identify the intrinsic mechanisms of immunotherapy response and resistance in the GL261 and CT2A murine models, respectively, we systematically compared their proteogenomic profiles. Unless otherwise specified, all experiments were conducted on *ex vivo* tumor samples. The tumor lines were transduced with firefly luciferase to permit the tracking of intracranial tumor growth *in vivo* (Cohort A, Figure 1A). We further extended our analysis of tumor cell-specific attributes through the evaluation of a second set of experiments, in which the immunologically inert human *CD19* was ectopically expressed in the GL261-luc2 and CT2A-luc lines to provide a tumor-specific marker that facilitated cell sorting and characterization of the tumor cells (Cohort B, Figure 1A).

As expected, we confirmed the sensitivity of GL261-luc to single-agent anti-PD-1 and single-agent anti-OX40, as well as enhanced benefit for anti-PD-1 plus anti-CTLA-4 or anti-OX40 combinatorial therapy in Cohort A mice (all $p_{adjusted} \leq 0.01$ compared to IgG control; Figure 1B). In contrast, CT2A-luc demonstrated relative resistance with minimal benefit to single-agent immune checkpoint therapy (all $p_{adjusted} \geq 0.12$ compared to IgG controls) and improved survival was only seen with anti-PD-1 plus anti-CTLA-4 therapy ($p_{adjusted} < 0.001$ compared to IgG control). The corresponding tumor growth plots are displayed in Supplementary Figure 1.

GL261-luc2 tumors were histopathologically characterized by polymorphic, poorly-differentiated cells with marked pleomorphism and sporadic giant cell features (Figure 1C, Supplementary Figure 2A). By contrast, CT2A-luc tumors displayed a spindled cellular morphology and fascicular architecture that were consistent with mesenchymal differentiation. Although both models had occasional foci of necrosis, neither displayed the diffuse infiltrative patterns or microvascular proliferation that are diagnostic for huGBM. Furthermore, glial fibrillary acidic protein (GFAP) – an intermediate filament expressed by astrocytic lineages, including a majority of huGBM – was only focally expressed in both tumor models (Supplementary Figure 2B).

We investigated the transcriptional differences between CT2A-luc and GL261-luc2 *ex vivo* tumors in Cohorts A and B and found that many genes were differentially expressed between the models (Cohort

10.3389/fimmu.2023.1297932

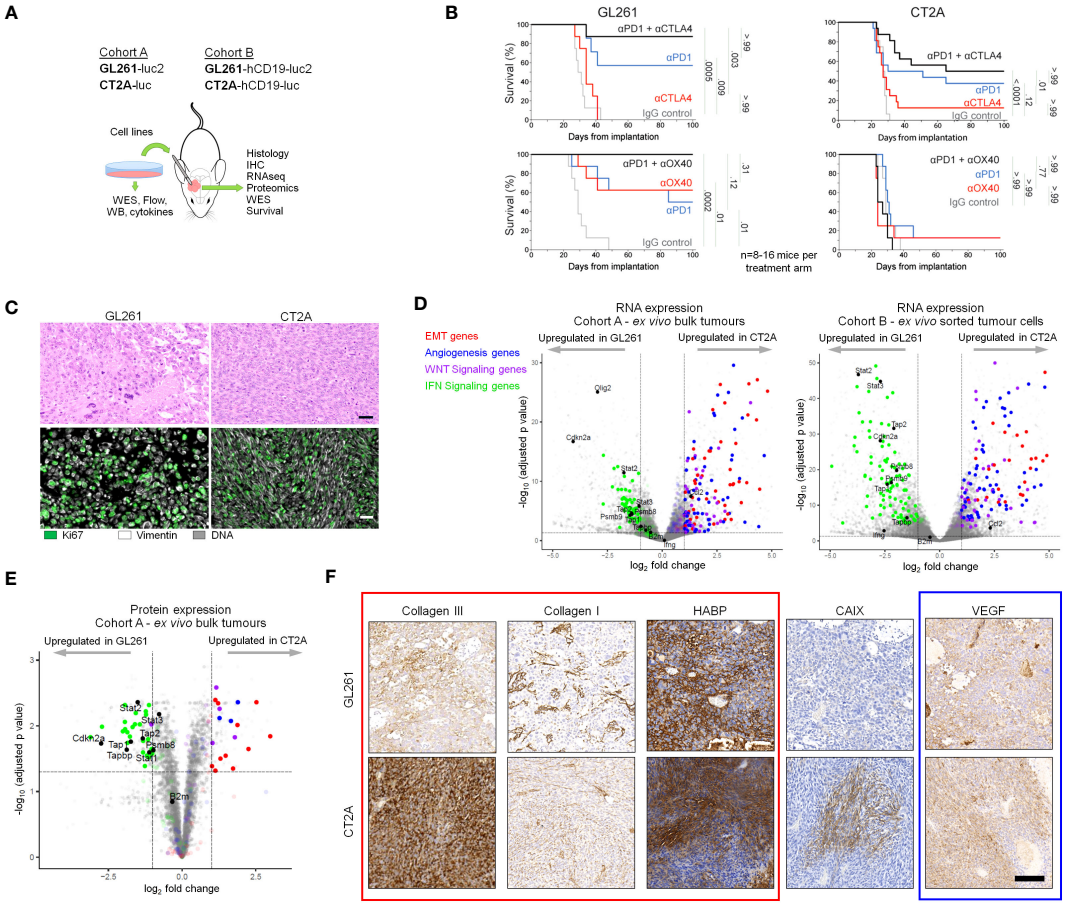

FIGURE 1
GL261-luc2 and CT2A-luc exhibit distinct biologic behaviors, histologies, and transcriptional profiles. **(A)** Schematic of the experimental analyses. Cohort A consisted of *in vitro* and bulk *ex vivo* samples of GL261-luc2 and CT2A-luc. Cohort B consisted of GL261-hCD19-luc2 and CT2A-hCD19-luc, in which human CD19 expression permitted the *ex vivo* sorting of hCD19-positive tumor cells. WES, whole exome sequencing; WB, Western Blot; Flow, flow cytometry; IHC, immunohistochemistry. **(B)** Kaplan-Meier overall survival curves associated with checkpoint immunotherapy in intracranial GL261-luc2 (*left*) and CT2A-luc (*right*) tumor-bearing mice. *Top:* anti-PD-1 and/or anti-CTLA-4 treatment experiments. *Bottom:* anti-PD-1 and/or anti-OX40 treatment experiments. (n=8-16 mice per experimental arm). One mouse in the single-agent anti-PD-1 GL261-luc2 group from the anti-CTLA-4 experiment was excluded due to tumor-unrelated death (day 9) prior to completing treatment. Adjusted p values are displayed from pairwise logrank tests, using Bonferroni correction for the 5 comparisons in each experiment. A two-sided adjusted $p<0.05$ for each experiment was considered significant. Checkpoint immunotherapy and IgG control dosing are detailed in the Methods. **(C)** Representative hematoxylin & eosin histological (*top*) and immunofluorescent (*bottom*) staining of *ex vivo* GL261-luc2 and CT2A-luc tumors. Scale bars = 50 μm. **(D)** *Left:* Volcano plot displaying the genes that were differentially expressed in *ex vivo* CT2A-luc bulk tumors, as compared to GL261-luc2 (n=4 mice each). *Right:* Volcano plot displaying the genes that were differentially expressed in *ex vivo* CT2A-hCD19-luc sorted tumor cells, as compared to GL261-hCD19-luc2 (n=3-5 mice each). Cutoffs included $|\log_2 FoldChange| > 1$ and Benjamini-Hochberg FDR-adjusted $p<0.05$. **(E)** Volcano plot displaying the proteins that were differentially expressed in *ex vivo* CT2A-luc bulk tumors, as compared to GL261-luc2 (n=3 mice each). Cutoffs included $|\log_2 FoldChange| > 1$ and Benjamini-Hochberg FDR-adjusted $p<0.05$. **(F)** Representative immunohistochemical staining of collagen III, collagen I, hyaluronan-binding protein (HABP), vascular endothelial growth factor (VEGF), and carbonic anhydrase IX (CAIX) in *ex vivo* GL261-hCD19-luc2 (*top*) and CT2A-hCD19-luc (*bottom*) tumors. Scale bar = 100 μm.

A: 24.9% of detected genes, Cohort B: 46.4% of detected genes; FDR-adjusted $p<0.05$; Figure 1D; Supplementary Figure 3A; Supplementary Tables 1, 2). Among these genes, gene sets associated with epithelial-to-mesenchymal transformation (EMT), angiogenesis, and WNT signaling were notably enriched in CT2A tumors in both Cohorts, whereas interferon γ and α response pathways were enriched in GL261 tumors (FDR-adjusted $p<0.1$) – findings which were also reflected at the protein expression level (Figure 1E; Supplementary Tables 3, 4). Because previous studies suggested that cell lines grown as neurospheres might better model huGBM (13, 23, 34), we also evaluated neurosphere-derived tumors and again found enrichment of EMT and WNT signaling gene sets in CT2A-hCD19-luc and inflammatory response-related gene sets enriched in GL261-hCD19-luc (Supplementary Figure 3B). EMT-related signaling pathways (e.g., TGF-β) were also enriched in CT2A-luc tumors. Because EMT is associated with marked remodeling of the extracellular matrix, we examined the extracellular matrix of *ex vivo* tumors using immunohistochemistry and qualitatively observed elevated deposition of collagen III and collagen I in the microenvironment of CT2A-luc tumors (Figure 1F; Supplementary Figures 2C–E). Additionally, gene sets associated with hypoxia were also enriched in the CT2A-luc tumors, which corresponded with a focally increased expression of carbonic anhydrase IX by immunohistochemistry (Figure 1F; Supplementary Figures 2F, G).

10.3389/fimmu.2023.1297932

Genomic profiles of GL261-luc2 and CT2A-luc

To investigate the potential genetic correlates to the histologic and transcriptional profiles that were observed in CT2A-luc, we performed whole-exome sequencing (WES) of both lines. Both models exhibited the canonical C>A/G>T transversion signature and CAG>CTG peak profile associated with a methylcholanthrene-induced etiology, which most closely resembles smoking carcinogen-related COSMIC Signature 4 in humans (35). GL261-luc2 also exhibited more C>T and A>G variants than CT2A-luc (Figure 2A) (36). Although CT2A-luc had less than half of the tumor mutational burden of GL261-luc2, both models were markedly hypermutated (approximately 79 and 176 mutations/MB, respectively), and both exhibited a predominance of missense single nucleotide variants and limited insertion/deletion burden (Figure 2B). Similar WES results were observed in non-luciferized GL261 and CT2A lines (data not shown). Excluding somatic variants with subclonal variant allele frequencies (VAF) <20%, among the 2,803 genes with variants in GL261-luc2 and 2,381 in CT2A-luc, 571 (12.4%) of altered genes were shared between the lines, but none of these involved known cancer drivers (Figures 2C, D; Supplementary Table 5). The copy number profiles of the models were clearly distinct. GL261-luc2 exhibited multiple whole chromosomal gains (e.g., chromosomes 5, 10, 11, 15) and losses (e.g., chromosomes 8, 12, 14,16) – among

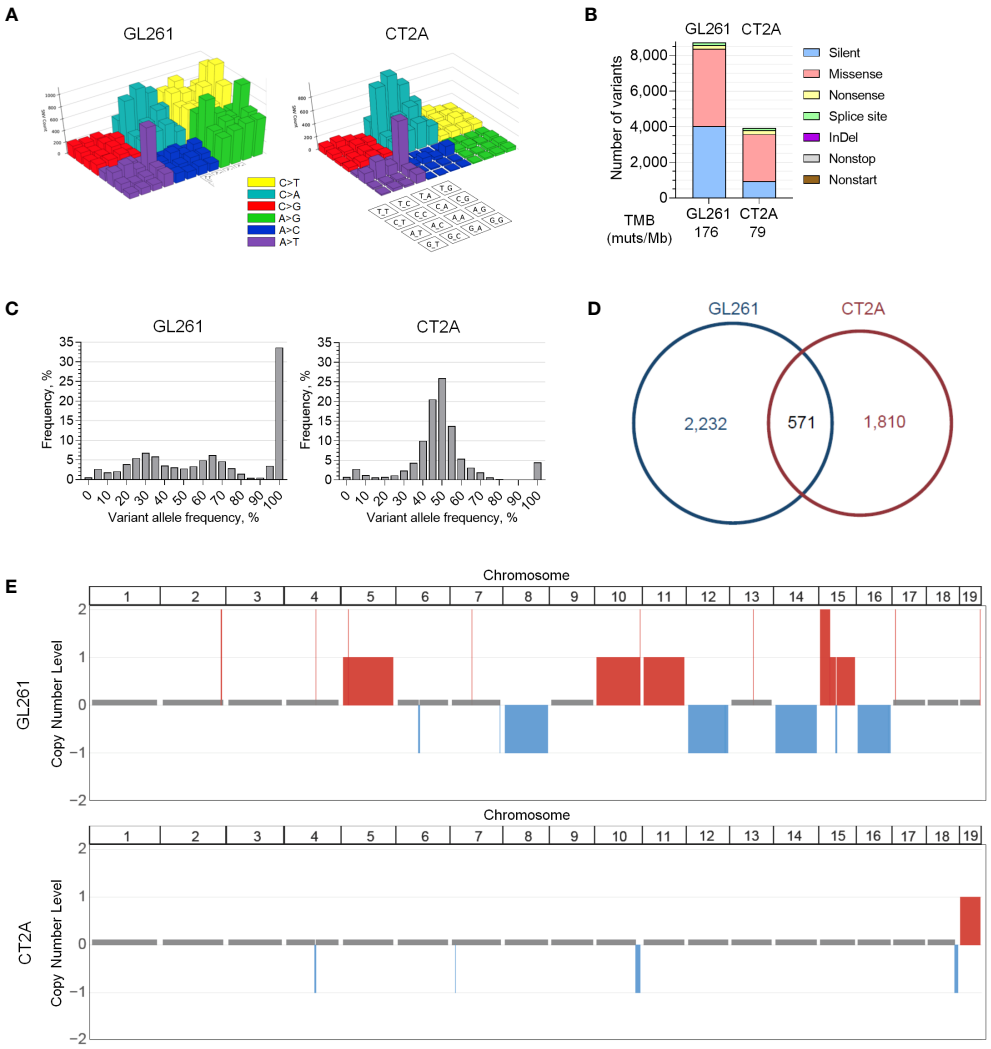

FIGURE 2
Genomic profiles of GL261-luc2 and CT2A-luc. **(A)** Lego plots visualizing the patterns of all types of transversion and transition mutations detected in whole exome sequencing of *in vitro* GL261-luc2 and CT2A-luc cells. Both models exhibited the C>A/G>T and CAG>CTG/GTC>GAC mutations that have been associated with a methylcholanthrene-induced etiology. GL261-luc2 additionally showed high levels of A>G/T>C and C>T/G>A transitions. **(B)** Frequency of small somatic sequence variants (*i.e.*, single nucleotide variants and small insertions/deletions [InDel]) by mutation type from whole exome sequencing of *in vitro* GL261-luc2 and CT2A-luc cells, with corresponding estimated tumor mutational burden (TMB). **(C)** Frequency of variants by variant allele fraction (VAF) from whole exome sequencing of *in vitro* GL261-luc2 and CT2A-luc cells. GL261-luc2 demonstrated an increased frequency of variants at 100% VAF (*i.e.*, likely homozygous). **(D)** Pie chart depicting the overlap of genes that have sequence variants (VAF ≥ 20%) between *in vitro* GL261-luc2 and CT2A-luc cells. **(E)** Copy number analysis of *in vitro* GL261-luc2 (n=5) and CT2A-luc (n=2) samples displaying somatic chromosomal segments that were significantly gained (*red*) or lost (*blue*) as compared to diploid reference (GISTIC2.0 FDR-adjusted p<0.05).

other segmental alterations – whereas CT2A-luc exhibited losses of chromosomal segments involving 4qC4, 7qA1, 10qD2-10qD3, and 18qE4 (all FDR-adjusted p<0.05; Figure 2E; Supplementary Table 6). In CT2A-luc, the 4qC4 loss included single-copy loss of *Cdkn2a/b*. GL261-luc2 distinctly harbored a *Kras* p.G12C clonal mutation whereas CT2A-luc had an *Nras* p.Q61L clonal mutation (Supplementary Figure 3C). *Nf1* and *Trp53* alterations were present in both models, but neither model exhibited *Idh1/2*, *Atrx*, *Braf*, *H3f3a* mutations nor copy number alterations of *Pten*, *Egfr*, *Nf1*, or *Rb1*, all of which are commonly associated with huGBM and astrocytoma.

Multifactorial defects in antigen processing and presentation machinery in CT2A-luc

The availability of high-quality MHC class I neoantigen candidates did not appear to differ between the two lines, as they both demonstrated similar proportions of highly-expressed strong predicted HLA class I binders (Figure 3A). On the other hand, CT2A-luc uniquely contained multiple mutations in antigen presentation machinery genes that were computationally predicted to have deleterious biologic effects, including a clonal p.A275P missense mutation in *Psmb8* (a subunit of the immunoproteasome, which degrades proteins into peptides for loading onto MHC class I) and a clonal p.Y488C missense mutation in *Tap1* (which transports peptides into the endoplasmic reticulum for loading onto MHC class I) (Figure 3B). Based on these results and the critical role that MHC molecules play in mediating immune responses, we next experimentally examined the expression of antigen processing and presentation machinery components in CT2A-luc.

Although RNA sequencing of *ex vivo* bulk tumor and sorted tumor cells showed similar expression of the MHC class I α (*H2-D1* and *H2-K1*) and β (*B2m*) chains between CT2A-luc and GL261-luc2, CT2A-luc displayed lower expression of genes associated with the immunoproteasome complex (*Psmb8*, *Psmb9*) and peptide transporter/loading complex (*Tap1*, *Tap2*, *Tapbp*) (differential expression analysis, all FDR-adjusted p<0.05; Figure 3C; Supplementary Figure 4A). Both GL261-luc2 and CT2A-luc lines exhibited minimal basal levels of antigen presentation and processing machinery protein expression by Western blot analyses of *in vitro* cultured cells (Figure 3D; Supplementary Figure 4B). Proteomic analysis of *ex vivo* bulk tumors further confirmed that Tap1, Tap2, Tapbp, and Psmb8 protein expression was reduced in CT2A-luc tumors (all FDR-adjusted p<0.05, Figure 3E; Supplementary Table 7).

Deficiency in the peptide loading complex may limit the peptides available for binding to MHC class I, and accordingly, the successful assembly of MHC class I molecules for surface expression (37). Indeed, flow cytometric analysis confirmed considerably less MHC class I (H2-D^b) surface expression on CT2A-luc *in vitro* ($p_{adjusted}$=0.006; Figure 3F) compared to GL261-luc2. Without IFN-γ stimulation, GL261-luc2 cells displayed surface expression of H2-D^b ($p_{adjusted}$ = 0.008 compared to isotype control), but not H2-K^b ($p_{adjusted}$ > 0.99 compared to isotype control); whereas neither H2-D^b nor H2-K^b cell surface expression were detected on CT2A-luc cells at baseline (both $p_{adjusted} \geq 0.94$ compared to isotype control; Figure 3F). Furthermore, of 644 MHC class I-bound peptides immunoprecipitated from *ex vivo* tumors, 64 (9.9%) peptides were more likely to be presented by GL261-luc2, whereas 16 (2.5%) peptides were more likely to be presented by CT2A-luc – although this analysis was complicated by the presence of infiltrating non-neoplastic cells with MHC expression (Figure 3G; Supplementary Figure 4C, Supplementary Table 8). Beyond MHC class I, both cell lines had low expression of β2m and minimal expression of MHC class II *in vitro* (all $p_{adjusted}$>0.05 compared to isotype control; Supplementary Figures 4D, E), with CT2A-luc exhibiting minimal MHC class II expression ($p_{adjusted}$ = 0.04). Taken together, these data suggest a marked, multi-factorial defect in antigen presentation by CT2A-luc tumors; whereas GL261-luc2 tumors exhibited intact antigen presentation machinery.

CT2A-luc is deficient in interferon response and signaling

Although multiple pathways were enriched in CT2A-luc tumors, only two gene sets were consistently downregulated in CT2A-luc in both Cohorts: interferon (IFN)-α and IFN-γ response via both RNA and protein expression analyses (Figure 4A). To determine if there was a genomic basis for this altered circuitry, we evaluated the multiple arm-level chromosomal copy number alterations that were detected in each cell line through analysis of WES data. CT2A-luc uniquely exhibited a single-copy loss of a chromosomal segment involving 4qC4 (FDR-adjusted p=0.04), which encompassed multiple type I IFN genes, as well as a single-copy loss of 10qD2-10qD3 (FDR-adjusted p=0.04), which contained *Stat2*, *Stat6*, and *Ifng* (Figures 2E; 4B, Supplementary Table 6).

Consistent with our observation of down-regulated IFN response pathways in CT2A-luc, phosphoproteomic analysis revealed decreased phosphorylation of several members of the JAK/STAT pathway in *ex vivo* CT2A-luc tumors, including Ptpn11 (i.e., Shp2), Il13ra1, and Stat3 – together suggesting reduced JAK/STAT signaling (Figure 4C; Supplementary Figure 5A, Supplementary Table 9). CT2A-luc tumors were further distinguished by phosphorylation of the Pik3 regulatory subunit 1 (Pik3r1) and enrichment of downstream mTOR signaling, consistent with a parallel activation of the Pi3k/Akt/mTOR pathway (Figures 4C, D; Supplementary Table 10). CT2A-luc also displayed elevated phosphorylation of cell cycle (Cdk1) and decreased phosphorylation of Prkca pathways, which are involved in diverse cellular signaling pathways (Figure 4D; Supplementary Figures 5B, C).

During immune responses, IFN-γ strongly upregulates the antigen processing and presentation components in cells (38) – which we hypothesized might be impaired in CT2A-luc. IFN-γ treatment boosted the expression of antigen processing and presentation proteins (e.g., Tap1, Tapbp, Psmb9, β2m) in both cell lines *in vitro*, although notably to a lesser degree in CT2A-luc

10.3389/fimmu.2023.1297932

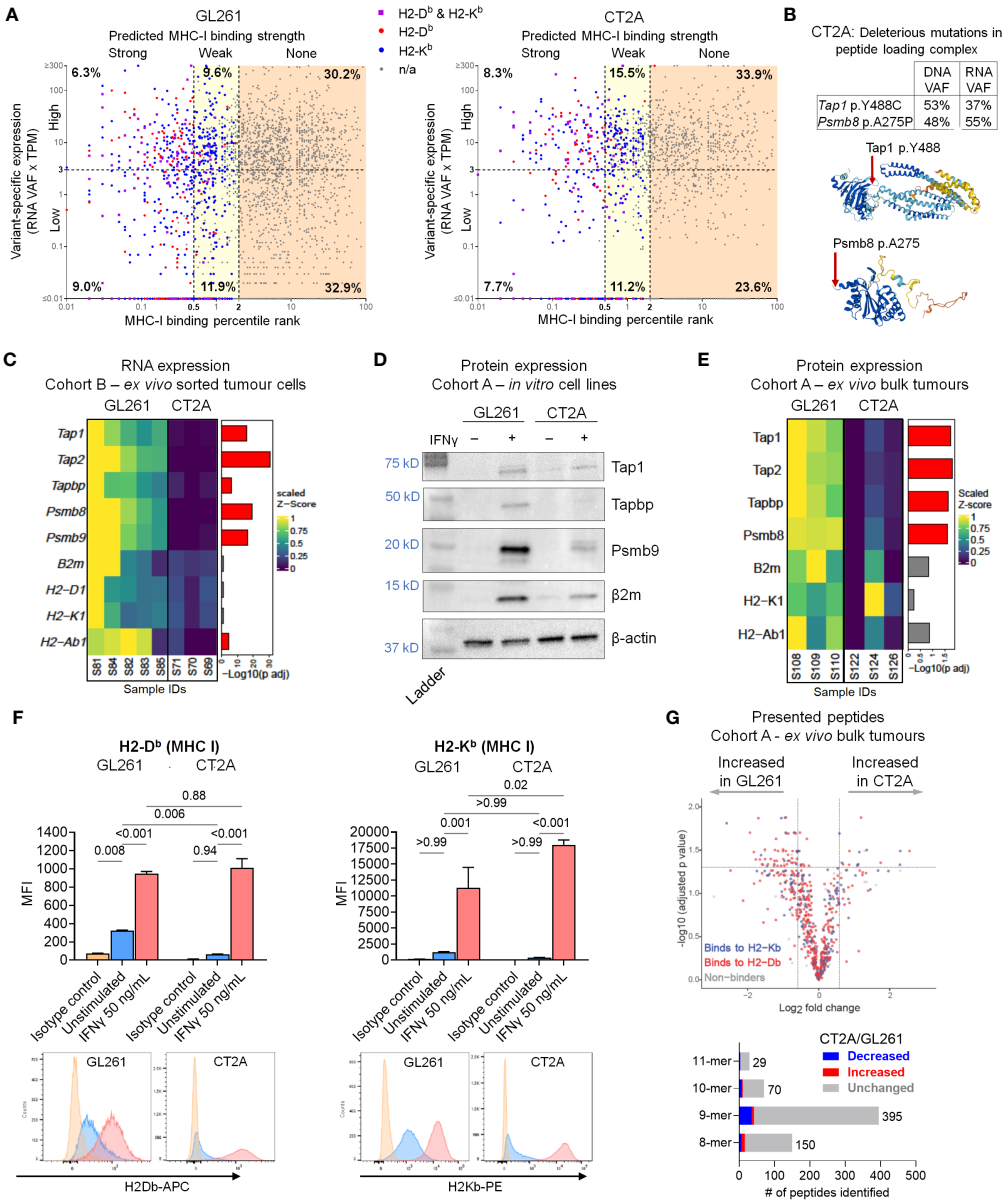

FIGURE 3
Multifactorial defects in antigen processing and presentation machinery in CT2A-luc. **(A)** Scatter plot displaying the predicted MHC class I binding strength (binding percentile rank) by variant-specific RNA expression (RNA variant allele frequencies [VAF] x TPM of gene's expression) for each variant detected in the whole exome sequencing of GL261-luc2 (*left*) and CT2A-luc (*right*) tumors, colored by which MHC class I allele(s) the variant was predicted to bind. Axes are in $\log_{10}$ scale. Variant-specific expression was dichotomized into high and low using a cutoff of 3 TPM. MHC class I binding strength was categorized as strong (percentile rank < 0.5), weak (0.5 ≤ percentile rank < 2.0), or none (percentile rank ≥ 2.0). The corresponding percent of total variants found in each cell is displayed. TPM = transcripts per million. **(B)** *Top*: The VAF of antigen presentation machinery gene mutations detected in the whole exome sequencing of *in vitro* CT2A-luc and RNA sequencing of CT2A-luc tumors. *Bottom*: The predicted 3-D structure of Tap1 (Y488 residue highlighted) and Psmb8 (A275 residue highlighted) from AlphaFold. **(C)** Heatmap depicting the differential RNA expression of antigen processing and presentation machinery genes in *ex vivo* sorted GL261-hCD19-luc2 (n=5 mice) and CT2A-hCD19-luc (n=3 mice) tumor cells, with the corresponding FDR-adjusted p value. Expression values were row normalized, Z-scored, bounded, and scaled. Red = FDR-adjusted p value<0.05. **(D)** Western blot displaying the antigen presentation and processing machinery protein expression in *in vitro* GL261-luc2 and CT2A-luc cell lines, with or without 50 ng/mL IFN-γ stimulation. β-actin was evaluated as a loading control. Displaying one representative of two replicate experiments (replicates shown in Supplementary File). Corresponding band densitometry quantification is shown in Supplementary Figure 4B. **(E)** Heatmap depicting the differential protein expression of antigen processing and presentation machinery genes in *ex vivo* bulk GL261-luc2 and CT2A-luc tumors (n=3 mice each), with the corresponding FDR-adjusted p value. Expression values were row normalized, Z-scored, bounded, and scaled. Red = FDR-adjusted p value<0.05. **(F)** *Top*: MHC class I surface expression median fluorescence intensity (MFI) detected by flow cytometric analysis on *in vitro* GL261-luc2 and CT2A-luc cells that were either stimulated with 50 ng/mL IFN-γ or unstimulated for 24 hours, compared to isotype controls. Expression was analyzed using one-way ANOVA, with two-sided pairwise p values adjusted for multiple testing using the Holm-Šídák method. The experiment was conducted in triplicate, bars = mean ± standard error. *Bottom*: Representative histograms of MHC expression. **(G)** *Top:* Volcano plot displaying the differential presentation of peptides between *ex vivo* GL261-luc2 and CT2A-luc bulk tumors (n=3 mice each), colored by MHC class I allele. *Bottom:* the proportions of presented peptides that were significantly decreased (blue) or increased (red) in *ex vivo* CT2A-luc bulk tumors as compared to GL261-luc2.

10.3389/fimmu.2023.1297932

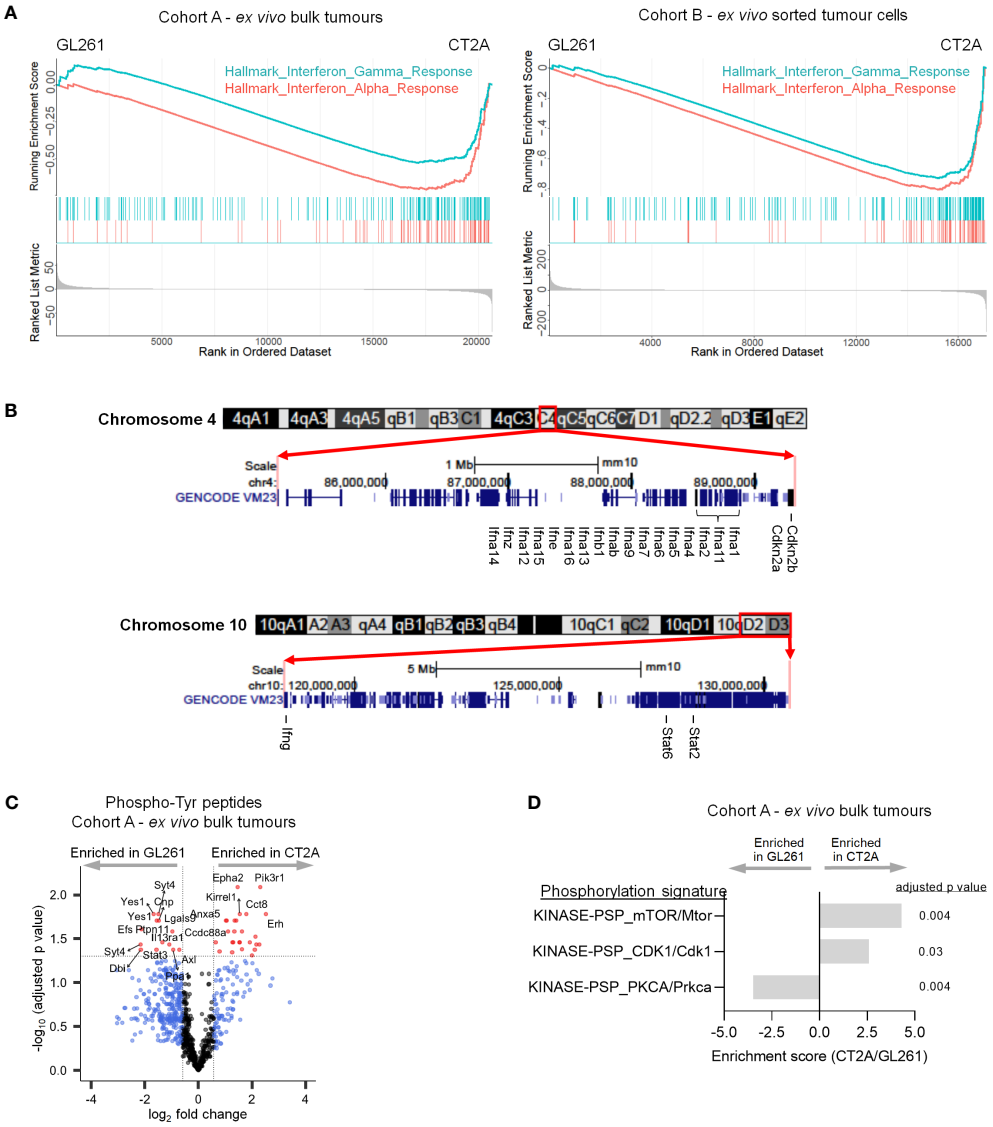

FIGURE 4
CT2A-luc is deficient in interferon response and signaling. **(A)** Gene set enrichment plots derived from the differential expression analyses in Figure 1E, displaying hallmark interferon response gene sets that were significantly depleted in CT2A-luc as compared to GL261-luc2, for *ex vivo* bulk tumors (*left*) and sorted hCD19+ tumor cells (*right*). n=3-5 mice each. **(B)** Chromosomal ideograms with GENCODE VM23 tracks for the chromosomal segments involving 4qC4 (*top*) and 10qD2-10qD3 (*bottom*) that were lost in CT2A-luc tumors, from the UCSC Genome Browser (http://genome.ucsc.edu). Select genes are highlighted. **(C)** Volcano plot displaying differential phosphorylation of tyrosine residues between *ex vivo* GL261-luc2 and CT2A-luc bulk tumors (n=856 total phosphotyrosine [pTyr] peptides). Cutoffs included $|\log_2\text{FoldChange}| > \log_2(1.5)$ and Benjamini-Hochberg FDR-adjusted p<0.05. n=3 mice each. **(D)** Post-translational modification Signature Enrichment Analysis (PTM-SEA) of the differentially expressed phosphoserine and phosphothreonine peptides between *ex vivo* GL261-luc2 and CT2A-luc bulk tumors. FDR-adjusted p<0.05. n=3 mice each.

(Figure 3D; Supplementary Figure 4B). However, MHC class I surface expression was strongly upregulated by IFN-γ treatment in both lines (all $p_{adjusted} \leq 0.001$; Figure 3F; Supplementary Figure 4D), potentially suggesting that the Tap1 mutational defect and impaired antigen presentation machinery in CT2A could be – at least partially – overcome by exposure to exogenous IFN-γ. Analysis of the RNA sequencing data revealed that *ex vivo* purified CT2A-hCD19-luc tumors retained IFN-γ receptor expression (*Ifngr1* $\log_2$FoldChange 0.39, FDR-adjusted p=0.02; *Ifngr2* $\log_2$FoldChange 1.41, FDR-adjusted p = 5.38E-10) compared to GL261-hCD19-luc2 tumors (Supplementary Table 2).

Secreted immunomodulatory proteins distinguish GL261-luc2 and CT2A-luc

To assess how GL261-luc2 and CT2A-luc interact with the immune microenvironment, we profiled their secretion of 12 cytokines and 13 chemokines that are known to have important immunomodulatory roles. Unstimulated GL261-luc2 secreted the pro-inflammatory IL-6 and IFN-β cytokines, which were further increased following IFN-γ stimulation (Figure 5A). By contrast, unstimulated CT2A-luc only minimally secreted IL-6 and IFN-β; and these were unchanged upon IFN-γ stimulation, again

suggesting impaired response to IFN-γ in CT2A-luc. Both lines lacked detectable IFN-γ, IL-17A, and GM-CSF secretion, and showed limited secretion of IL-10, IL-1β, and TNF-α (Supplementary Figures 6A, B). CT2A-luc demonstrated substantial baseline secretion of the CCL-2, CCL-5, and CCL-22 chemokines, all of which are known to play important roles as myeloid chemoattractants (Figure 5B), in marked contrast to GL261-luc2. Analysis of the *ex vivo* RNA sequencing data from Cohort A tumors also found increased *Ccl22* chemokine expression among CT2A-luc tumors (Supplementary Figure 6C).

Additionally, whereas the chemokines CCL4 (a natural killer cell and monocyte chemoattractant), CXCL10 (a broad immune cell population chemoattractant), CXCL9 (activated T cell chemoattractant), and CXCL1 (neutrophil chemoattractant) were secreted at low-to-negligible baseline levels in both models, their secretion was increased following IFN-γ treatment in GL261-luc2 (all $p_{adjusted} < 0.05$; Figure 5B; Supplementary Figure 6B). Neither line had detectable secretion of CCL3, CCL11, CCL17, CXCL5, or CXCL13 chemokines, including after IFN-γ stimulation (Supplementary Figure 6B). Chemokine gradients strongly influence the immune cell composition of the TME and prior studies have identified a myeloid cell predominance in CT2A tumors (17, 40). The murine Microenvironment Cell Population (mMCP) tool (24) was used to estimate the immune cell abundances from the RNA sequencing data from Cohort A *ex vivo* bulk tumors, and found a greater proportion of monocytes in CT2A-luc tumors as compared to GL261-luc2 tumors (log_2FoldChange 1.03, p=0.03; Supplementary Table 11). In addition to secreted immunomodulatory proteins, RNA sequencing analysis of the *ex vivo* purified tumors showed that CT2A-hCD19-luc expressed less *Cd274* (i.e. PD-L1; log_2FoldChange -2.27, FDR-adjusted p = 5.44E-13), but not *Pdcd1lg2* (i.e. PD-L2; log_2FoldChange -0.48, FDR-adjusted p = 0.46) than GL261-hCD19-luc2 (Supplementary Table 2).

The relationship of GL261-luc2 and CT2A-luc models to human cancer contexts

To investigate to what extent these murine tumor lines might transcriptionally model huGBM, we performed unsupervised principal component analysis that included huGBM (166 samples) as well as all other cancer types available in TCGA. We thereby attempted to assess the expression of all genes shared by both human and mouse transcriptomes (n=15,457 genes) (Figure 5C). The top 500 differentially expressed genes between mouse tumors and human tumors were excluded from the analysis to help account for species-specific transcriptional bias (as well as without exclusion in Supplementary Figure 7A). Both GL261-luc2 and CT2A-luc *ex vivo* samples occupied the transcriptional space between human gliomas (including glioblastoma and low-grade glioma) and other human cancer types (including cutaneous melanomas and sarcomas) in the first principal component of principal component analysis.

We assessed whether CT2A-luc may model a distinct human cancer context as compared to GL261-luc2 by evaluating the murine tumors against human cancers that commonly exhibit similar features to those that we observed in our GL261-luc2 and CT2A-luc characterizations, including RAS driver mutations (e.g., pancreatic adenocarcinoma and colorectal adenocarcinoma), carcinogen-induced mutation signatures (lung adenocarcinoma), and mesenchymal differentiation (renal cell carcinoma) – in addition to huGBM. Because CT2A-luc was characterized by notable dysregulation of epithelial-mesenchymal transition, angiogenesis, WNT signaling, and IFN-α/γ response hallmark gene sets, we repeated the unsupervised hierarchical clustering analyses using only the member genes of those hallmark gene sets (Supplementary Tables 12, 13; Supplementary Figures 7B–D). From this analysis, all CT2A-luc samples clustered together and were more similar to seven (of 166) huGBM and two (of 534) kidney renal cell carcinoma samples, rather than to GL261-luc2. Review of the pathology reports and histological images from TCGA database for these huGBMs revealed that all indeed displayed mesenchymal differentiation (e.g., gliosarcomatous or spindle cell morphology) (Supplementary Figure 7B). Additionally, six of these seven huGBMs that had been previously analyzed by TCGA consortium have been classified into the mesenchymal subtype of huGBM. Comparison of the transcriptional profiles of these seven huGBMs to those of the 159 unrelated samples notably revealed downregulation of *TAP1* (LFC=-0.84, FDR-adjusted p=0.008; Supplementary Table 14). Similar to the seven huGBM samples, the pathology reports for both neighboring kidney cancer samples revealed a diagnosis of clear cell renal cell carcinoma with sarcomatoid features (i.e., mesenchymal differentiation).

Discussion

Our genetic and histologic characterization of GL261-luc2 and CT2A-luc tumors revealed limited shared essential features with huGBM. Neither GL261-luc2 nor CT2A-luc models exhibited the diffusely infiltrative growth that is a defining hallmark of human diffuse gliomas including IDH-wildtype glioblastoma. Additionally, microvascular proliferation, *Tert* promoter mutations, *Egfr* amplification, or *Pten* loss (analogous to monosomy 10 in humans) – which are included as essential diagnostic criteria for WHO CNS grade 4 IDH-wildtype glioblastoma – were not observed in either model. Likewise, from the genetic perspective, while both models contained clonal hotspot mutations in RAS genes (*Kras* p.G12C in GL261-luc2 and *Nras* p.Q61L in CT2A-luc), which are important oncogenic drivers across multiple human cancers, such mutations have only been identified in <1% of huGBM tumors in TCGA. CT2A-luc did exhibit single-copy loss of *Cdkn2a/b*, although up to 40-50% of huGBMs have homozygous loss (41). These murine models demonstrated marked hypermutation, whereas most newly diagnosed and recurrent huGBMs demonstrate a modest tumor mutational burden (<10 mutations/MB) (42). Although huGBM patients with *de novo* hypermutation (i.e., as a result of germline DNA mismatch repair or POL-E deficiencies) arise occasionally and have been observed to respond to ICB, the more frequent condition of temozolomide-induced acquired hypermutation (noted in approximately 20% of

10.3389/fimmu.2023.1297932

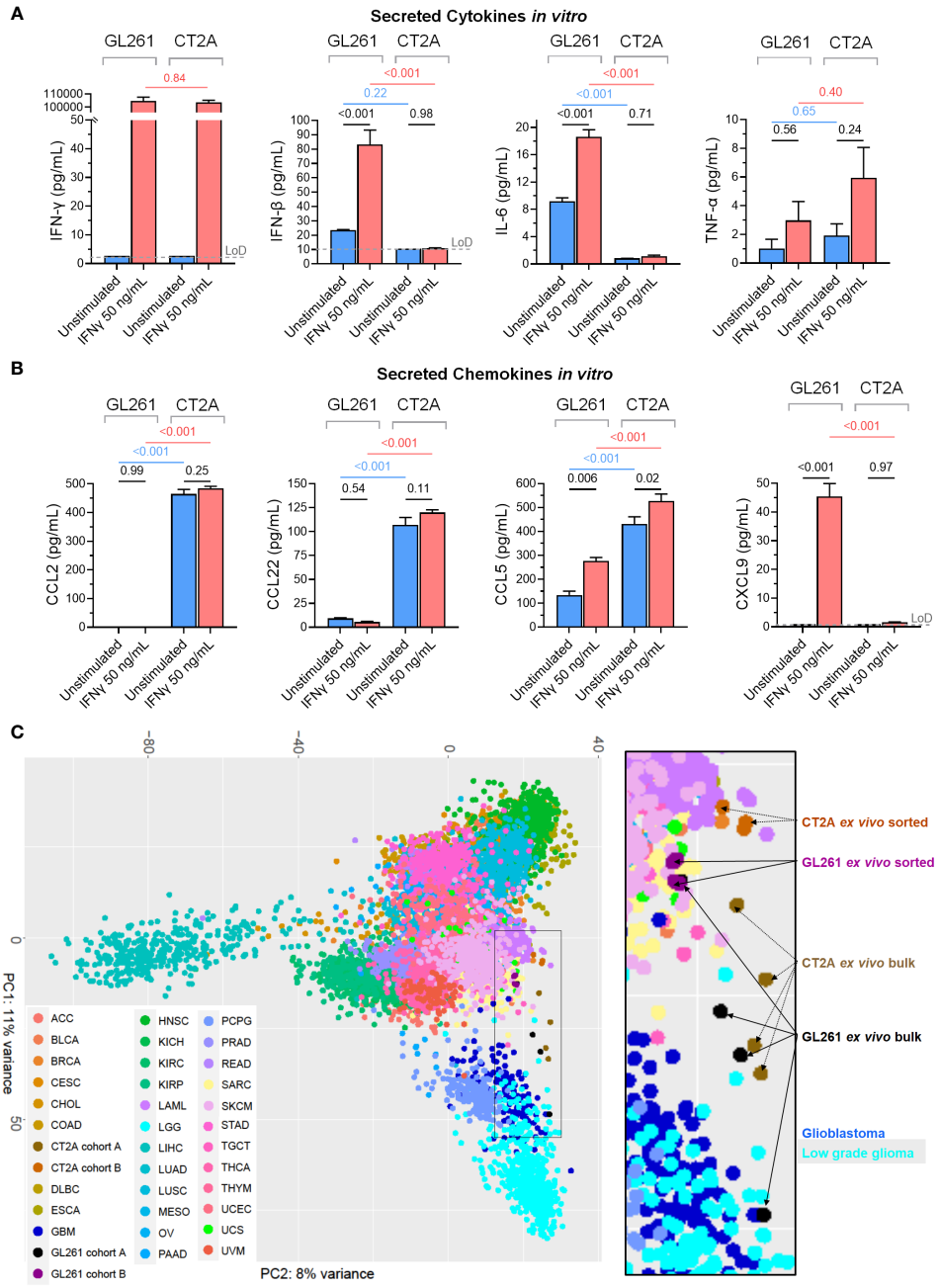

FIGURE 5
The secreted immunomodulatory protein profiles and relationship to human cancers of GL261-luc2 and CT2A-luc models. **(A, B)** Secreted **(A)** cytokines (IFN-γ, IFN-β, IL-6, TNF-α) and **(B)** chemokines (CCL2, CCL22, CCL5, CXCL9) were profiled from the conditioned media of the *in vitro* GL261-luc2 and CT2A-luc cultures from the Figure 3F experiment, which had been cultured for 24 hours without (*blue*) or with (*red*) IFN-γ (50 ng/mL). The experiment was conducted in triplicate, with secreted peptide concentrations graphed as mean ± standard error and compared using one-way ANOVA. The assay's limit of detection (LoD; *grey dashed line*) was displayed and analyzed for samples whose values were above the LoD. For assessment of IFN-γ secretion, the IFNγ-stimulated samples still contained the experimentally administered IFN-γ. P values were adjusted for multiple testing using the Holm-Šídák method. The cell lines were also evaluated for IL-23, IL-10, GM-CSF, IL-17A, IL-1α, IL-1β, IL-12p70, IL-27, CCL3, CCL4, CXCL10, CCL20, CXCL1, CCL11, CCL17, CXCL5, and CXCL13; displayed in Supplementary Figure 6. **(C)** Unsupervised principal component analysis of whole transcriptome expression of the *ex vivo* bulk (Cohort A) and *ex vivo* tumor sorted (Cohort B) GL261-luc2 and CT2A-luc samples alongside RNA sequencing of all human cancer samples from TCGA. The 500 genes that were most differentially expressed between mouse and human tumor samples were excluded to help minimize species-level effects. Inset = higher magnification. OncoTree cancer type definitions were detailed previously (39). Supplementary Figure 7A shows the corresponding unsupervised principal component analysis without the exclusion of the 500 genes that were most differentially expressed between mouse and human tumor samples.

recurrent huGBMs) has not been associated with a favorable response (42, 43).

To overcome the limitations of carcinogen-induced huGBM models, a diverse array of genetically engineered immunocompetent mouse models have been developed in recent years which more accurately recapitulate the molecular, histopathologic, and therapeutic features of huGBM – which have been reviewed elsewhere (13). However, the ability of such models to fully reflect the complex immunosuppressive TME and behavior of huGBM remains unclear. In this context, we found that the transcriptional profiles of GL261-luc2 and CT2A-luc tumors appear to more closely resembled human gliomas than other cancer types in TCGA – although the comparison of interspecies RNA sequencing data is beset by multiple limitations. Across our transcriptional and proteomic analyses, CT2A-luc was distinguished from GL261-luc2 by its mesenchymal differentiation and by its marked deficits in interferon response and antigen presentation pathways. In humans, several cancer types can manifest epithelial-mesenchymal transformation *de novo* or in response to treatment, including a subset of human IDH-wildtype glioblastomas that exhibit a mesenchymal histological subtype (i.e., gliosarcoma) and/or transcriptional profile and have been associated with worse survival (44, 45). In a large longitudinal analysis of gliomas (including 168 patients with RNA sequencing data for at least 2 timepoints), 38% and 45% of IDH-wild type diffuse gliomas displayed a mesenchymal cell state at initial and recurrent timepoints, respectively (45). We observed that multiple mesenchymal huGBMs from TCGA clustered more closely to CT2A-luc tumors than to other huGBMs, including a recurrent tumor that had acquired a mesenchymal cell state whereas its corresponding non-mesenchymal primary tumor clustered separately from CT2A-luc.

Mesenchymal huGBMs are also characterized by dense myeloid cell infiltrates, which have been well-described in the tumor microenvironment of CT2A (17, 40, 45, 46). For instance, using flow cytometric analysis, Liu et al. showed that tumor-associated macrophages comprise a substantially greater proportion (approximately 5-6x) of tumor-infiltrating CD45+ immune cells in CT2A tumors than GL261 tumors. Additionally, mass cytometry by time of flight (CyTOF) analyses by Khalsa et al. suggested that the CT2A TME features a greater proportion of resident macrophages (CD11b+ F4/80+ CD64+ Ly6C–) and infiltrating macrophages (CD11b+ F4/80+ CD64+ Ly6C+) than GL261. Single-cell RNA sequencing of TILs by Khan et al. found that GL261 is enriched with progenitor exhausted CD8+ T cells, whereas CT2A was enriched with terminally exhausted CD8+ T cells and regulatory CD4+ T cells (47). Although the tumors' immune cell composition was not an aim of our study, analysis of our bulk tumors' RNA profiles also identified a higher estimated proportion of monocytes in CT2A-luc than GL261-luc2. Consistent with these findings, we observed that CT2A-luc secreted multiple chemokines involved in myeloid cell and regulatory T cell chemoattraction in the huGBM tumor microenvironment (e.g., CCL-2 and CCL-22) (48, 49). In the tumor microenvironment of human gliomas, CCL2 has been shown to recruit both CCR4+ Treg and CCR2+ Ly6C+ monocytic myeloid-derived suppressive cells (48). Additionally, CCL22 has been shown to recruit differentiated Tregs into the glioblastoma TME (49).

The role of mesenchymal differentiation and response to immunotherapy is unclear in huGBM, with prior analyses of bulk RNA sequencing data identifying an association between the mesenchymal RNA subtype of huGBM and expression of both immune suppressive and proinflammatory gene signatures (50). However, when we compared the transcriptional profiles of CT2A-luc to human cancer samples, we identified a subset of mesenchymal huGBMs that indeed displayed a similar loss of antigen presentation and processing machinery – suggesting that mesenchymal glioblastomas may comprise a more complex spectrum of cell states with regards to immunotherapeutic resistance.

Whereas GL261 is sensitive to various immunotherapeutic modalities, CT2A is broadly resistant to single-agent immunotherapies aimed at T cell responses – including immune checkpoint inhibitors, vaccine therapy, and oncolytic virotherapy – which can be explained by our findings of deficits in antigen presentation machinery and interferon response in CT2A-luc (12, 17–21). The immunotherapeutic resistance of CT2A persists even with the ectopic expression of luciferase, which has been shown to confer increased immunogenicity to cell lines (51). Accordingly, ectopic expression of luciferase is a notable limitation of these models. Luciferase expression with bioluminescent imaging was used herein to ensure consistent tumor engraftment and sizes for all therapeutic and *ex vivo* experiments, and thereby avoid bias in our analyses due to differences in tumor engraftment or growth. An analysis of the tumor-immune microenvironment of GL261 tumors versus GL261-luc2 tumors found no significant differences in the presence of infiltrating immune cell populations (52).

Defects in antigen presentation machinery have been well-described across a spectrum of human cancer types – including mutations in *TAP1* and *PSMB8* like the ones we observed in CT2A-luc (53). Furthermore, in multiple cancer types such as melanoma (54–57), NSCLC (58), and Merkel cell carcinoma (59), the loss of MHC class I expression and defects in antigen presentation machinery or IFNy-response pathways have been recurrently associated with resistance (both intrinsic and acquired) to immunotherapy. Interestingly, we observed that CT2A-luc also clustered alongside several cutaneous melanoma tumors in transcriptional space. Melanoma is commonly characterized by carcinogen (i.e., ultraviolet light)-induced hypermutation and sensitivity to immune checkpoint inhibitors. However, only 20-50% of patients with advanced melanoma experience durable responses to immune checkpoint inhibitors (60, 61). Multiple mechanisms of immunotherapy resistance in melanoma have been elucidated (62), among them being MHC class I downregulation in conjunction with de-differentiation (including mesenchymal differentiation and angiogenesis upregulation) that have been associated with innate and acquired resistance to PD-1 checkpoint blockade (57, 63).

We found that CT2A-luc intrinsically shared these mechanisms, but we also observed that exogenous IFN-γ treatment could at least partially restore MHC class I expression in CT2A-luc – suggesting that select multi-pronged immunotherapeutic strategies may overcome CT2A's inherent

resistance to immunotherapy. Indeed, when PD-1 and CTLA-4 inhibitors were combined, we noted a modest therapeutic benefit in CT2A-luc tumor-bearing mice. In light of these findings, investigation of therapeutic combinations that address CT2A's distinctive processes, such as immune contexture (e.g. myeloid-targeting immunotherapies), angiogenesis (e.g. bevacizumab), and mesenchymal phenotype (e.g. ritanserin) may help identify strategies that translate to the treatment of analogous cancer types in humans. Other studies have reported success with such combination approaches in CT2A, including PD-(L)1 inhibition with either adjuvanted neoantigen vaccination, bacterial antigen-armed oncolytic measles virotherapy, GITR agonist, or ectopic VEGF-C expression (17, 21, 64, 65). Building on our results, future studies that functionally dissect the individual contribution of each of the features detailed herein to CT2A's overall resistance to immunotherapy will be informative. In particular, the enhancement of IFN-γ signaling warrants additional study for multi-modal therapeutic strategies in both CT2A and the human cancer contexts that it models. To overcome the obstacles posed by the blood-brain barrier, half-life in the interstitial fluid, and targeted localization to the tumor environment, such studies likely need to incorporate novel drug delivery technologies (e.g. convection-enhanced delivery, encapsulation in microspheres/nanoparticles, IFN-γ protein vs. mRNA delivery, etc.) or stimulation of IFN-γ release from existing cells in the tumor microenvironment. Pre-implantation stimulation of CT2A cells with IFN-γ also faces experimental challenges that should be taken into consideration, including if IFN-γ exposure leads to MHC class I upregulation *in vitro*, those CT2A tumors may be less likely to engraft in health mice and the effects of IFN-γ may only be transient.

Taken together, our findings indicate that although the clinical contexts that can be modeled by GL261 and CT2A for huGBM are limited, CT2A-luc may provide an informative preclinical model in immuno-oncology for investigating therapeutic strategies that can overcome immunotherapy resistance of cancers due to antigen presentation machinery loss, upregulated angiogenesis, and mesenchymal differentiation.

Data availability statement

WES data were deposited to the SRA repository (PRJNA1056465) and RNA sequencing data were deposited to the GEO repository (GSE215123). Mass spectrometry data were deposited to the ProteomeXchange Consortium via the PRIDE partner repository as PXD036720.

Ethics statement

Ethical approval was not required for the study involving humans in accordance with the local legislation and institutional requirements. Written informed consent to participate in this study was not required from the participants or the participants' legal guardians/next of kin in accordance with the national legislation and the institutional requirements. The animal study was approved by Dana-Farber Cancer Institute and Harvard Medical School Animal Care and Use Committees. The study was conducted in accordance with the local legislation and institutional requirements.

Author contributions

JI: Writing – original draft, Writing – review & editing, Conceptualization, Data curation, Formal analysis, Investigation, Methodology. NR: Conceptualization, Data curation, Formal analysis, Investigation, Methodology, Software, Validation, Visualization, Writing – review & editing. RA: Conceptualization, Formal analysis, Investigation, Writing – review & editing, Data curation. EP: Conceptualization, Investigation, Writing – review & editing, Data curation, Formal analysis, Methodology. PG: Conceptualization, Formal analysis, Investigation, Supervision, Visualization, Writing – review & editing, Data curation. MN: Conceptualization, Data curation, Formal analysis, Investigation, Visualization, Writing – original draft, Writing – review & editing, Validation. MS: Formal analysis, Investigation, Visualization, Writing – review & editing, Conceptualization, Data curation, Methodology. BE: Investigation, Writing – review & editing, Data curation, Validation. KS: Investigation, Writing – review & editing, Data curation. RP: Investigation, Writing – review & editing, Data curation, Formal analysis, Methodology. MD: Investigation, Writing – review & editing, Formal analysis, Methodology. SK: Investigation, Writing – review & editing, Formal analysis. KY: Investigation, Writing – review & editing, Formal analysis, Methodology. GB: Investigation, Writing – review & editing, Formal analysis, Methodology. RJ: Investigation, Writing – review & editing, Supervision. MS: Investigation, Writing – review & editing, Methodology, Supervision. DN: Supervision, Writing – review & editing, Methodology. FW: Methodology, Supervision, Investigation, Writing – review & editing, Conceptualization. EC: Investigation, Writing – review & editing, Conceptualization, Data curation, Funding acquisition, Methodology, Resources. GF: Investigation, Writing – review & editing, Conceptualization, Funding acquisition, Methodology, Resources, Supervision. AS: Investigation, Writing – review & editing, Conceptualization, Funding acquisition, Methodology, Resources, Supervision. CW: Conceptualization, Funding acquisition, Investigation, Methodology, Project administration, Supervision, Visualization, Writing – original draft, Writing – review & editing, Resources. DR: Conceptualization, Data curation, Funding acquisition, Investigation, Methodology, Project administration, Resources, Supervision, Visualization, Writing – original draft, Writing – review & editing.

Funding

The author(s) declare financial support was received for the research, authorship, and/or publication of this article. We gratefully acknowledge the following organizations for funding support: National Institutes of Health (P01CA236749 [to DR, CW, ALS, GF, EAC, DN, and MLS]; K12CA090354 [to JBI];

K22CA258410 [to MD]); Conquer Cancer Foundation/Sontag Foundation (JBI); BCured Foundation (DR); DFCI Medical Oncology grant (DR); The Jennifer Oppenheimer Cancer Research Initiative (DR); The Ben and Catherine Ivy Foundation (DR); Hope It's A Beach Thing (DR); and the Pan Mass Challenge (Erica's Entourage and CRUS11TOUR, DR); Brigham Research Institute NextGen award (JBI); MIT Center for Precision Cancer Medicine (RA and FW); Ludwig Center at MIT (RA); National Cancer Institute P01 CA163205 (EAC); National Cancer Institute P01 CA236749 (EAC); National Institutes of Health R01NS110942 (EAC); The Sandra Jelin Plouffe Fund to Advance Glioblastoma Research (EAC); The Oligodendroglioma Fund (EAC); The Daniel E. Ponton Fund (EAC); The MIT Koch Institute Bridge Grant (EAC); Alliance for Cancer Gene Therapy (EAC). National Foundation for Cancer Research (RJ); the Ludwig Center at Harvard Medical School (RJ); the Jane's Trust Foundation (RJ); the Nile Albright Research Foundation (RJ); and the NIH grants R35-CA197743, R01-CA269672, R01CA259253, U01CA261842 and U01-CA224348 (RJ), R01-CA208205 (RJ), Department of Defense fellowship W81XWH-19-1-0723 (SK).

Acknowledgments

We thank Chhayheng Chhoeu, Eric Lim, Mohammad Uduman, Min Wu, Yan Gao, Carolyn Smith, and Ivy Xiaoyu Chen for technical assistance; and Orr Ashenberg, Sudhir Thakurela, Liz Perez, Simon Gritsch, Michelle Bookstaver, Ana Anderson, Kai Wucherpfennig, Vijay Kuchroo, Gavin Dunn, Hiroshi Nakashima, Sarah Klein, Peter Sorger, Sean Lawlor, and Nicholas Haining for helpful discussions.

Conflict of interest

MLS is equity holder, scientific co-founder, and advisory board member of Immunitas Therapeutics. EAC is an advisor to Amacathera, Bionaut Labs, Genenta, Inc., Insightec, Inc., DNAtrix Inc., Seneca Therapeutics, Synthetic Biologics. EAC has equity options in Bionaut Laboratories, DNAtrix, Immunomic Therapeutics, Seneca Therapeutics, Synthetic Biologics, Ternalys Therapeutics. EAC is co-founder and on the Board of Directors of Ternalys Therapeutics. EAC also is a named inventor on patents related to oncolytic HSV1 and noncoding RNAs. MCS has equity options and is a current employee of GSK. MN is a current employee of AbbVie. DN has stock ownership in Madrigal Pharmaceuticals. RJ received consultant fees from Cur, Elpis, Innocoll, SPARC, and SynDevRx,; owns equity in Accurius, Enlight, and SynDevRx; is on the Board of Trustees of Tekla Healthcare Investors, Tekla Life Sciences Investors, Tekla Healthcare Opportunities Fund, and Tekla World Healthcare Fund; and received a research grant from Boehringer Ingelheim. AS currently has funding from Quark, Merck, AbbVie, Moderna and Vertex unrelated to the submitted work. AS serves on advisory boards for Surface Oncology, SQZ Biotechnologies, Selecta, Elpiscience, Monopteros, Bicara, Fibrogen, and Alixis. AS also is on scientific advisory boards for the Massachusetts General Cancer Center, Program in Cellular and Molecular Medicine at Boston Children's Hospital, the Human Oncology and Pathogenesis Program at Memorial Sloan Kettering Cancer Center, Glaxo Smith Kline and Janssen. AS is an academic editor for the Journal of Experimental Medicine. AS has patents/pending royalties on the PD-1 pathway from Roche and Novartis. GF has patents/pending royalties on the PD-L1/PD-1 pathway from Roche, Merck MSD, Bristol-Myers-Squibb, Merck KGA, Boehringer-Ingelheim, AstraZeneca, Dako, Leica, Mayo Clinic, Eli Lilly, and Novartis. GF has served on advisory boards for Roche, Bristol-Myers-Squibb, Origimed, Triursus, iTeos, NextPoint, IgM, Jubilant, Trillium, GV20, IOME, and Geode. GF has equity in Nextpoint, Triursus, Xios, iTeos, IgM, Trillium, Invaria, GV20, and Geode. CW is an equity holder of BioNTech, Inc. DR receives institutional support through Dana-Farber Cancer Institute from Acerta Phamaceuticals, Agenus, Bristol-Myers Squibb, Celldex, EMD Serono, Enterome, Epitopoietic Research Corporation, Incyte, Inovio, Insightec, Novartis, Omniox, and Tragara; and is an advisor/consultant for Abbvie, Advantagene, Agenus, Agios, Amgen, AnHeart Therapeutics, Avita Biomedical, Bayer, Boston Biomedical, Boehringer Ingelheim, Bristol-Myers Squibb, Celldex, Deciphera, Del Mar Pharma, DNAtrix, Ellipses Pharma, EMD Serono, Genenta, Genentech/Roche, Hoffman-LaRoche, Imvax, Inovio, Kintara, Kiyatec, Medicenna Biopharma, Merck, Merck KGaA, Monteris, Neuvogen, Novartis, Novocure, Oncorus, Oxigene, Regeneron, Stemline, Sumitono Dainippon Pharma, Pyramid, Taiho Oncology, Vivacitas Oncology, and Y-mabs Therapeutics.

The remaining authors declare that the research was conducted in the absence of any commercial or financial relationships that could be construed as a potential conflict of interest.

Publisher's note

Supplementary material

The Supplementary Material for this article can be found online at: https://www.frontiersin.org/articles/10.3389/fimmu.2023.1297932/full#supplementary-material

References

1. Ribas A, Wolchok JD. Cancer immunotherapy using checkpoint blockade. *Science* (2018) 359(6382):1350–5. doi: 10.1126/science.aar4060

2. Ostrom QT, Shoaf ML, Cioffi G, Waite K, Kruchko C, Wen PY, et al. National-level overall survival patterns for molecularly-defined diffuse glioma types in the United States. *Neuro-Oncol* (2022), noac198.25(4):799–807. doi: 10.1093/neuonc/noac198

3. Iorgulescu JB, Sun C, Neff C, Cioffi G, Gutierrez C, Kruchko C, et al. Molecular biomarker-defined brain tumors: epidemiology, validity, and completeness in the United States. *Neuro-Oncol* (2022) 24(11):1989–2000 noac113. doi: 10.1093/neuonc/noac113

4. Lim M, Weller M, Idbaih A, Steinbach J, Finocchiaro G, Raval RR, et al. Phase 3 trial of chemoradiotherapy with temozolomide plus nivolumab or placebo for newly diagnosed glioblastoma with methylated MGMT promoter. *Neuro-Oncol* (2022) 24 (11):1935–49. noac116. doi: 10.1093/neuonc/noac116

5. Reardon DA, Brandes AA, Omuro A, Mulholland P, Lim M, Wick A, et al. Effect of nivolumab vs bevacizumab in patients with recurrent glioblastoma: the checkMate 143 phase 3 randomized clinical trial. *JAMA Oncol* (2020) 6(7):1003–10. doi: 10.1001/jamaoncol.2020.1024

6. Omuro A, Vlahovic G, Lim M, Sahebjam S, Baehring J, Cloughesy T, et al. Nivolumab with or without ipilimumab in patients with recurrent glioblastoma: results from exploratory phase I cohorts of CheckMate 143. *Neuro-Oncol* (2018) 20(5):674–86. doi: 10.1093/neuonc/nox208

7. Harary M, Reardon DA, Iorgulescu JB. Efficacy and safety of immune checkpoint blockade for brain metastases. *CNS Oncol* (2019) 8(2):CNS33. doi: 10.2217/cns-2018-0018

8. Iorgulescu JB, Harary M, Zogg CK, Ligon KL, Reardon DA, Hodi FS, et al. Improved risk-adjusted survival for melanoma brain metastases in the era of checkpoint blockade immunotherapies: results from a national cohort. *Cancer Immunol Res* (2018) 6(9):1039–45. doi: 10.1158/2326-6066.CIR-18-0067

9. Flores C, Dunn G, Fecci P, Lim M, Mitchell D, Reardon DA. Is there a role for immunotherapy in central nervous system cancers? *Hematol Oncol Clin North Am* (2022) 36(1):237–52. doi: 10.1016/j.hoc.2021.09.002

10. Lim M, Xia Y, Bettegowda C, Weller M. Current state of immunotherapy for glioblastoma. *Nat Rev Clin Oncol* (2018) 15(7):422–42. doi: 10.1038/s41571-018-0003-5

11. Chongsathidkiet P, Jackson C, Koyama S, Loebel F, Cui X, Farber SH, et al. Sequestration of T cells in bone marrow in the setting of glioblastoma and other intracranial tumors. *Nat Med* (2018) 24(9):1459–68. doi: 10.1038/s41591-018-0135-2

12. Iorgulescu JB, Gokhale PC, Speranza MC, Eschle BK, Poitras MJ, Wilkens MK, et al. Concurrent dexamethasone limits the clinical benefit of immune checkpoint blockade in glioblastoma. *Clin Cancer Res Off J Am Assoc Cancer Res* (2021) 27(1):276–87. doi: 10.1158/1078-0432.CCR-20-2291

13. Haddad AF, Young JS, Amara D, Berger MS, Raleigh DR, Aghi MK, et al. Mouse models of glioblastoma for the evaluation of novel therapeutic strategies. *Neuro-Oncol Adv* (2021) 3(1):vdab100. doi: 10.1093/noajnl/vdab100

14. Ausman JI, Shapiro WR, Rall DP. Studies on the chemotherapy of experimental brain tumors: development of an experimental model. *Cancer Res* (1970) 30(9):2394–400.

15. Seyfried TN, El-Abbadi M, Roy ML. Ganglioside distribution in murine neural tumors. *Mol Chem Neuropathol* (1992) 17(2):147–67. doi: 10.1007/BF03159989

16. Johanns TM, Ward JP, Miller CA, Wilson C, Kobayashi DK, Bender D, et al. Endogenous neoantigen-specific CD8 T cells identified in two glioblastoma models using a cancer immunogenomics approach. *Cancer Immunol Res* (2016) 4(12):1007–15. doi: 10.1158/2326-6066.CIR-16-0156

17. Liu CJ, Schaettler M, Blaha DT, Bowman-Kirigin JA, Kobayashi DK, Livingstone AJ, et al. Treatment of an aggressive orthotopic murine glioblastoma model with combination checkpoint blockade and a multivalent neoantigen vaccine. *Neuro-Oncol* (2020) 22(9):1276–88. doi: 10.1093/neuonc/noaa050

18. Reardon DA, Gokhale PC, Klein SR, Ligon KL, Rodig SJ, Ramkissoon SH, et al. Glioblastoma eradication following immune checkpoint blockade in an orthotopic, immunocompetent model. *Cancer Immunol Res* (2016) 4(2):124–35. doi: 10.1158/2326-6066.CIR-15-0151

19. Speranza MC, Passaro C, Ricklefs F, Kasai K, Klein SR, Nakashima H, et al. Preclinical investigation of combined gene-mediated cytotoxic immunotherapy and immune checkpoint blockade in glioblastoma. *Neuro-Oncol* (2018) 20(2):225–35. doi: 10.1093/neuonc/nox139

20. Kim JE, Patel MA, Mangraviti A, Kim ES, Theodros D, Velarde E, et al. Combination therapy with anti-PD-1, anti-TIM-3, and focal radiation results in regression of murine gliomas. *Clin Cancer Res Off J Am Assoc Cancer Res* (2017) 23 (1):124–36. doi: 10.1158/1078-0432.CCR-15-1535

21. Panagioti E, Kurokawa C, Viker K, Ammayappan A, Anderson SK, Sotiriou S, et al. Immunostimulatory bacterial antigen-armed oncolytic measles virotherapy significantly increases the potency of anti-PD1 checkpoint therapy. *J Clin Invest* (2021) 131(13):141614. doi: 10.1172/JCI141614

22. Manguso RT, Pope HW, Zimmer MD, Brown FD, Yates KB, Miller BC, et al. *In vivo* CRISPR screening identifies Ptpn2 as a cancer immunotherapy target. *Nature* (2017) 547(7664):413–8. doi: 10.1038/nature23270

23. Pellegatta S, Poliani PL, Corno D, Menghi F, Ghielmetti F, Suarez-Merino B, et al. Neurospheres enriched in cancer stem-like cells are highly effective in eliciting a dendritic cell-mediated immune response against Malignant gliomas. *Cancer Res* (2006) 66(21):10247–52. doi: 10.1158/0008-5472.CAN-06-2048

24. Petitprez F, Levy S, Sun CM, Meylan M, Linhard C, Becht E, et al. The murine Microenvironment Cell Population counter method to estimate abundance of tissue-infiltrating immune and stromal cell populations in murine samples using gene expression. *Genome Med* (2020) 12(1):86. doi: 10.1186/s13073-020-00783-w

25. Stopfer LE, Mesfin JM, Joughin BA, Lauffenburger DA, White FM. Multiplexed relative and absolute quantitative immunopeptidomics reveals MHC I repertoire alterations induced by CDK4/6 inhibition. *Nat Commun* (2020) 11:2760. doi: 10.1038/s41467-020-16588-9

26. Andreatta M, Alvarez B, Nielsen M. GibbsCluster: unsupervised clustering and alignment of peptide sequences. *Nucleic Acids Res* (2017) 45(W1):W458–63. doi: 10.1093/nar/gkx248

27. Krug K, Mertins P, Zhang B, Hornbeck P, Raju R, Ahmad R, et al. A curated resource for phosphosite-specific signature analysis *[S]. *Mol Cell Proteomics* (2019) 18 (3):576–93. doi: 10.1074/mcp.TIR118.000943

28. Eid S, Turk S, Volkamer A, Rippmann F, Fulle S. KinMap: a web-based tool for interactive navigation through human kinome data. *BMC Bioinf* (2017) 18(1):16. doi: 10.1186/s12859-016-1433-7

29. Datta M, Chatterjee S, Perez EM, Gritsch S, Roberge S, Duquette M, et al. Losartan controls immune checkpoint blocker-induced edema and improves survival in glioblastoma mouse models. *Proc Natl Acad Sci U S A* (2023) 120(6):e2219199120. doi: 10.1073/pnas.2219199120

30. Love MI, Huber W, Anders S. Moderated estimation of fold change and dispersion for RNA-seq data with DESeq2. *Genome Biol* (2014) 15(12):550. doi: 10.1186/s13059-014-0550-8

31. Kolde R. Pheatmap: pretty heatmaps. *R Package Version* (2012) 1(2):726.

32. Gutman DA, Cobb J, Somanna D, Park Y, Wang F, Kurc T, et al. Cancer Digital Slide Archive: an informatics resource to support integrated in silico analysis of TCGA pathology data. *J Am Med Inform Assoc JAMIA* (2013) 20(6):1091–8. doi: 10.1136/amiajnl-2012-001469

33. Cerami E, Gao J, Dogrusoz U, Gross BE, Sumer SO, Aksoy BA, et al. The cBio cancer genomics portal: an open platform for exploring multidimensional cancer genomics data. *Cancer Discovery* (2012) 2(5):401–4. doi: 10.1158/2159-8290.CD-12-0095

34. Yi L, Zhou C, Wang B, Chen T, Xu M, Xu L, et al. Implantation of GL261 neurospheres into C57/BL6 mice: a more reliable syngeneic graft model for research on glioma-initiating cells. *Int J Oncol* (2013) 43(2):477–84. doi: 10.3892/ijo.2013.1962

35. Tate JG, Bamford S, Jubb HC, Sondka Z, Beare DM, Bindal N, et al. COSMIC: the catalogue of somatic mutations in cancer. *Nucleic Acids Res* (2019) 47(D1):D941–7. doi: 10.1093/nar/gky1015

36. Lee CL, Mowery YM, Daniel AR, Zhang D, Sibley AB, Delaney JR, et al. Mutational landscape in genetically engineered, carcinogen-induced, and radiation-induced mouse sarcoma. *JCI Insight* (2019) 4(13):128698. doi: 10.1172/jci.insight.128698

37. Ljunggren HG, Stam NJ, Ohlén C, Neefjes JJ, Höglund P, Heemels MT, et al. Empty MHC class I molecules come out in the cold. *Nature* (1990) 346(6283):476–80. doi: 10.1038/346476a0

38. Zhou F. Molecular mechanisms of IFN-gamma to up-regulate MHC class I antigen processing and presentation. *Int Rev Immunol* (2009) 28(3–4):239–60. doi: 10.1080/08830180902978120

39. Kundra R, Zhang H, Sheridan R, Sirintrapun SJ, Wang A, Ochoa A, et al. OncoTree: A cancer classification system for precision oncology. *JCO Clin Cancer Inform* (2021) 5):221–30. doi: 10.1200/CCI.20.00108

40. Khalsa JK, Cheng N, Keegan J, Chaudry A, Driver J, Bi WL, et al. Immune phenotyping of diverse syngeneic murine brain tumors identifies immunologically distinct types. *Nat Commun* (2020) 11(1):3912. doi: 10.1038/s41467-020-17704-5

41. Cancer Genome Atlas Research Network. Mastrogianakis G, et al. Comprehensive genomic characterization defines human glioblastoma genes and core pathways. *Nature* (2008) 455(7216):1061–8.

42. Touat M, Li YY, Boynton AN, Spurr LF, Iorgulescu JB, Bohrson CL, et al. Mechanisms and therapeutic implications of hypermutation in gliomas. *Nature* (2020) 580(7804):517–23. doi: 10.1038/s41586-020-2209-9

43. Johanns TM, Miller CA, Dorward IG, Tsien C, Chang E, Perry A, et al. Immunogenomics of hypermutated glioblastoma: A patient with germline POLE deficiency treated with checkpoint blockade immunotherapy. *Cancer Discovery* (2016) 6(11):1230–6. doi: 10.1158/2159-8290.CD-16-0575

44. Kavouridis VK, Ligon KL, Wen PY, Iorgulescu JB. Survival outcomes associated with MGMT promoter methylation and temozolomide in gliosarcoma patients. *J Neurooncol* (2022) 158(1):111–6. doi: 10.1007/s11060-022-04016-5

45. Varn FS, Johnson KC, Martinek J, Huse JT, Nasrallah MP, Wesseling P, et al. Glioma progression is shaped by genetic evolution and microenvironment interactions. *Cell* (2022) 185(12):2184–99.e16. doi: 10.1016/j.cell.2022.04.038

46. Hara T, Chanoch-Myers R, Mathewson ND, Myskiw C, Atta L, Bussema L, et al. Interactions between cancer cells and immune cells drive transitions to mesenchymal-like states in glioblastoma. *Cancer Cell* (2021) 39(6):779–92.e11. doi: 10.1016/j.ccell.2021.05.002

47. Khan SM, Desai R, Coxon A, Livingstone A, Dunn GP, Petti A, et al. Impact of CD4 T cells on intratumoral CD8 T-cell exhaustion and responsiveness to PD-1 blockade therapy in mouse brain tumors. *J Immunother Cancer* (2022) 10(12):e005293. doi: 10.1136/jitc-2022-005293

48. Chang AL, Miska J, Wainwright DA, Dey M, Rivetta CV, Yu D, et al. CCL2 produced by the glioma microenvironment is essential for the recruitment of regulatory T cells and myeloid-derived suppressor cells. *Cancer Res* (2016) 76(19):5671–82. doi: 10.1158/0008-5472.CAN-16-0144

49. Jacobs JFM, Idema AJ, Bol KF, Grotenhuis JA, de Vries IJM, Wesseling P, et al. Prognostic significance and mechanism of Treg infiltration in human brain tumors. *J Neuroimmunol* (2010) 225(1–2):195–9. doi: 10.1016/j.jneuroim.2010.05.020

50. Doucette T, Rao G, Rao A, Shen L, Aldape K, Wei J, et al. Immune heterogeneity of glioblastoma subtypes: extrapolation from the cancer genome atlas. *Cancer Immunol Res* (2013) 1(112):112–22. doi: 10.1158/2326-6066.CIR-13–0028

51. Noffsinger B, Witter A, Sheybani N, Xiao A, Manigat L, Zhong Q, et al. Technical choices significantly alter the adaptive immune response against immunocompetent murine gliomas in a model-dependent manner. *J Neurooncol* (2021) 154(2):145–57. doi: 10.1007/s11060-021-03822-7

52. Sanchez VE, Lynes JP, Walbridge S, Wang X, Edwards NA, Nwankwo AK, et al. GL261 luciferase-expressing cells elicit an anti-tumor immune response: an evaluation of murine glioma models. *Sci Rep* (2020) 10:11003. doi: 10.1038/s41598-020-67411-w

53. DhatChinamoorthy K, Colbert JD, Rock KL. Cancer immune evasion through loss of MHC class I antigen presentation. *Front Immunol* (2021) 12:636568. doi: 10.3389/fimmu.2021.636568

54. Zaretsky JM, Garcia-Diaz A, Shin DS, Escuin-Ordinas H, Hugo W, Hu-Lieskovan S, et al. Mutations associated with acquired resistance to PD-1 blockade in melanoma. *N Engl J Med* (2016) 375(9):819–29. doi: 10.1056/NEJMoa1604958

55. Rodig SJ, Gusenleitner D, Jackson DG, Gjini E, Giobbie-Hurder A, Jin C, et al. MHC proteins confer differential sensitivity to CTLA-4 and PD-1 blockade in untreated metastatic melanoma. *Sci Transl Med* (2018) 10(450):eaar3342. doi: 10.1126/scitranslmed.aar3342

56. Sade-Feldman M, Jiao YJ, Chen JH, Rooney MS, Barzily-Rokni M, Eliane JP, et al. Resistance to checkpoint blockade therapy through inactivation of antigen presentation. *Nat Commun* (2017) 8(1):1136. doi: 10.1038/s41467-017-01062-w

57. Lee JH, Shklovskaya E, Lim SY, Carlino MS, Menzies AM, Stewart A, et al. Transcriptional downregulation of MHC class I and melanoma de- differentiation in resistance to PD-1 inhibition. *Nat Commun* (2020) 11:1897. doi: 10.1038/s41467-020-15726-7

58. Gettinger S, Choi J, Hastings K, Truini A, Datar I, Sowell R, et al. Impaired HLA class I antigen processing and presentation as a mechanism of acquired resistance to immune checkpoint inhibitors in lung cancer. *Cancer Discovery* (2017) 7(12):1420–35. doi: 10.1158/2159-8290.CD-17-0593

59. Paulson KG, Voillet V, McAfee MS, Hunter DS, Wagener FD, Perdicchio M, et al. Acquired cancer resistance to combination immunotherapy from transcriptional loss of class I HLA. *Nat Commun* (2018) 9(1):3868. doi: 10.1038/s41467-018-06300-3

60. Lamba N, Ott PA, Iorgulescu JB. Use of first-line immune checkpoint inhibitors and association with overall survival among patients with metastatic melanoma in the anti–PD-1 era. *JAMA Netw Open* (2022) 5(8):e2225459. doi: 10.1001/jamanetworkopen.2022.25459

61. Larkin J, Chiarion-Sileni V, Gonzalez R, Grob JJ, Rutkowski P, Lao CD, et al. Five-year survival with combined nivolumab and ipilimumab in advanced melanoma. *N Engl J Med* (2019) 381(16):1535–46. doi: 10.1056/NEJMoa1910836

62. Iorgulescu JB, Braun D, Oliveira G, Keskin DB, Wu CJ. Acquired mechanisms of immune escape in cancer following immunotherapy. *Genome Med* (2018) 10(1):87. doi: 10.1186/s13073-018-0598-2

63. Plaschka M, Benboubker V, Grimont M, Berthet J, Tonon L, Lopez J, et al. ZEB1 transcription factor promotes immune escape in melanoma. *J Immunother Cancer* (2022) 10(3):e003484. doi: 10.1136/jitc-2021-003484

64. Amoozgar Z, Kloepper J, Ren J, Tay RE, Kazer SW, Kiner E, et al. Targeting Treg cells with GITR activation alleviates resistance to immunotherapy in murine glioblastomas. *Nat Commun* (2021) 12:2582. doi: 10.1038/s41467-021-22885-8

65. Song E, Mao T, Dong H, Boisserand LSB, Antila S, Bosenberg M, et al. VEGF-C-driven lymphatic drainage enables brain tumor immunosurveillance. *Nature* (2020) 577(7792):689–94. doi: 10.1038/s41586-019-1912-x

frontiers | Frontiers in Immunology

TYPE Perspective
PUBLISHED 07 February 2024
DOI 10.3389/fimmu.2024.1299044

OPEN ACCESS

EDITED BY
Michael Barish,
Beckman Research Institute, United States

REVIEWED BY
Kaushik Banerjee,
University of Michigan, United States

*CORRESPONDENCE
L. S. Lamb
larry@in8bio.com

RECEIVED 22 September 2023
ACCEPTED 22 January 2024
PUBLISHED 07 February 2024

CITATION
Nabors LB, Lamb LS, Goswami T, Rochlin K and Youngblood SL (2024) Adoptive cell therapy for high grade gliomas using simultaneous temozolomide and intracranial mgmt-modified γδ t cells following standard post-resection chemotherapy and radiotherapy: current strategy and future directions. *Front. Immunol.* 15:1299044. doi: 10.3389/fimmu.2024.1299044

Adoptive cell therapy for high grade gliomas using simultaneous temozolomide and intracranial mgmt-modified γδ t cells following standard post-resection chemotherapy and radiotherapy: current strategy and future directions

L. B. Nabors[1], L. S. Lamb[2]*, T. Goswami[2], K. Rochlin[2] and S. L. Youngblood[2]

[1]Department of Neurology, University of Alabama at Birmingham, Birmingham, AL, United States, [2]IN8Bio, Inc., New York, NY, United States

Cellular therapies, including chimeric antigen receptor T cell therapies (CAR-T), while generally successful in hematologic malignancies, face substantial challenges against solid tumors such as glioblastoma (GBM) due to rapid growth, antigen heterogeneity, and inadequate depth of response to cytoreductive and immune therapies, We have previously shown that GBM constitutively express stress associated NKG2D ligands (NKG2DL) recognized by gamma delta (γδ) T cells, a minor lymphocyte subset that innately recognize target molecules via the γδ T cell receptor (TCR), NKG2D, and multiple other mechanisms. Given that NKG2DL expression is often insufficient on GBM cells to elicit a meaningful response to γδ T cell immunotherapy, we then demonstrated that NKG2DL expression can be transiently upregulated by activation of the DNA damage response (DDR) pathway using alkylating agents such as Temozolomide (TMZ). TMZ, however, is also toxic to γδ T cells. Using a p140K/MGMT lentivector, which confers resistance to TMZ by expression of O(6)-methylguanine-DNA-methyltransferase (MGMT), we genetically engineered γδ T cells that maintain full effector function in the presence of therapeutic doses of TMZ. We then validated a therapeutic system that we termed Drug Resistance Immunotherapy (DRI) that combines a standard regimen of TMZ concomitantly with simultaneous intracranial infusion of TMZ-resistant γδ T cells in a first-in-human Phase I clinical trial (NCT04165941). This manuscript will discuss DRI as a rational therapeutic approach to newly diagnosed GBM and the importance of repeated administration of DRI in combination with the standard-of-care Stupp regimen in patients with stable minimal residual disease.

KEYWORDS

glioblastoma, genetic engineering, DNA damage (DDR), T cells gamma delta, cell therapy

Introduction

Newly diagnosed GBM, like many cancers, is first treated with a combination of surgery, induction radiation and chemotherapy followed by maintenance chemotherapy and subsequently monitored for recurrent disease, which is almost without exception a certainty. Once the recurrent tumor is evident and, depending on tumor characteristics and patient eligibility, clinical trials become available. Unfortunately, once the recurrent tumor becomes visible to imaging protocols it is already well past our ability to prevent the eventual uncontrolled proliferation and ultimately death. Upon recurrence, despite single or multi-agent chemotherapy, or surgery, nothing has shown an overall survival benefit and the median survival is approximately 8 months. Therefore, generating deeper tumor responses and delaying the time to tumor regrowth at first diagnosis are the best means to improve overall survival and quality of life for patients. We present a novel approach in which we seek to recapitulate the natural immunosurveillance function of innate recognition and control of GBM with primary standard-of-care therapy to create advantages for immune recognition and persistent surveillance.

The immune system and glioblastoma

The concept of cancer immunosurveillance predicts that the immune system can recognize precursors of cancer and, in most cases, destroy these precursors before they become clinically apparent. Animals that possess naturally occurring or experimentally induced defects leading to loss of recombination-activating gene 2 (RAG2), αβ T cells, γδ T cells, invariant NKT cells, interferon-γ (IFNγ) receptor 1 (1); signal transducer and activator of transcription 1 (STAT1), perforin; or tumor-necrosis factor (TNF)-related apoptosis-inducing ligand (TRAIL) (2) are more susceptible to spontaneous development of cancer or carcinogenic stimuli. Accordingly, the immune system is known to generate a coordinated response against pre-malignant cell clusters and developing tumors. For instance, the DDR evident in GBM and several other cancers can induce expression of tumor-associated stress receptors including NKG2D ligands (NKG2DL) such as MHC-class-I-polypeptide-related sequence A (MICA) and UL-16 binding proteins (ULBP) 1-8 thereby sensitizing malignant cells to killing by the immune system's NKG2D receptor-expressing first responders, such as NK cells, NKT cells, γδ T cells and some $CD8^+$ αβ T cells. T cell-mediated adaptive immune responses are also induced in concert with this broad-based stress-associated response as tumor-associated antigens (TAA) are presented to T cells via MHC class I or II on antigen presenting cells (APC) which then trigger T cell activation and expression of co-stimulatory molecules and secretion of chemokines and cytokines. Clonal expansion of TAA-specific T cells then occurs as well as other immune effector cells that regulate different aspects of the immune response. Direct cell-mediated cytotoxicity as well as an indirect antibody complement-mediated cytotoxicity (3) are both employed in the adaptive response. Despite heightened immune function in the premalignant stage, tumor cells can escape and disseminate. In particular, GBM exists in an environment that is generally protected from a robust immune response given the relatively immune privileged nature of the brain when compared to other systemic cancers and can grow undetected until its mass is of sufficient size to provoke symptomatic neurologic dysfunction.

The core standard of care for primary GBM was defined in 2005 by Stupp (4) and remains to date, the most widely used treatment regimen. With some variation, the Stupp regimen begins with gross total resection, the extent of which is dependent on retaining function of nearby areas of the brain that execute critical sensory and/or motor functions. Following resection, the patient recovers for 3-4 weeks and then receives a 6-week therapeutic combination of targeted radiation and daily TMZ, followed by six 28-day maintenance cycles consisting of five consecutive days of oral TMZ at the initiation of each cycle. The median survival from diagnosis for patients receiving this regimen is 15 months although this figure is variable and largely dependent on the genotypic characteristics of the tumor. Despite the gains achieved by primary debulking, radiation therapy, and maintenance, this regimen unfortunately enables the selection of resistant genomic variants that will eventually outlast every therapy presently available for recurrent disease.

Since the immune system is known to respond to and combat tumors including GBM, it would seem logical that adjunct immunotherapy regimens might be effective in reducing tumor burden and improving progression free survival (PFS). Preclinical models have suggested effectiveness, however, GBM has been remarkably resistant to immunotherapy protocols including checkpoint inhibition and CAR-T therapies that have been advanced to the clinic. This may be partially due to the natural interaction between the brain and the immune system which is inherently biased against destructive inflammatory responses. The GBM tumor microenvironment (TME) contains a large proportion of immunosuppressive myeloid cells that can attenuate the T cell responses required for effective anti-tumor responses. Accordingly, immune checkpoint blockade has shown little efficacy in the adjuvant setting (5), although the neoadjuvant setting has shown some promise (6). Despite the remarkable outcomes seen with hematologic malignancies, immune cell therapies such as chimeric antigen receptor (CAR) T cell therapies have been generally disappointing in solid tumors to-date. CAR-T programs targeting the interleukin-13 receptor (IL13R)α2 (7), epidermal growth factor receptor variant III (EGFRvIII) (8) and other potential targets have been generally well-tolerated and have produced extended stable disease and/or long-term remission in some patients with recurrent GBM. However, the biologic characteristics of GBM discussed above including the immunosuppressive tumor microenvironment, tumor-derived systemic immunosuppression, antigenic heterogeneity, on-target off-tumor toxicities, and T cell exhaustion have been formidable barriers to successful immunotherapy of GBM.

γδ T cells and the recognition of malignant disease – multiple weapons, multiple targets

γδ T cells are thought to be multi-specific, and antigen recognition demonstrates remarkable diversity (9). These T cells

can recognize malignant cells through less specific mechanisms that do not require prior antigen exposure or priming, a function that is shared by other innate immune cells such as macrophages and NK cells. Unfortunately, the tumor responses of adoptive cellular therapies against hematopoietic cancers have not, with rare exceptions, been replicated in solid tumors such as GBM. The immunogenic heterogeneity of solid tumors even within a single tumor has frustrated attempts to target specific TAA (7, 10, 11) and has called for strategies that can more broadly distinguish and target malignant cells while still limiting the potential for damage to the host. More recently, Barish (12) showed that tumor antigen heterogeneity creates a significant challenge to tumor eradication. Their cohort of 44 high-grade brain tumor samples demonstrated four major histological regions of interest and significant antigen diversity within each individual region. Moreover, a CAR-T targeting three individual antigens, IL-13Rα2, EGFR and HER2 was still predicted to leave at least 7% of the tumor remaining (12). Additionally, Larson (13) demonstrated that loss of the interferon-γ receptor (IFNγR) signaling pathway rendered glioblastoma resistant to killing by CAR-T cells due to a reduction of the duration of cell binding and avidity. Consequently, the potential antineoplastic effect of γδ T cells, a minor T cell subset with distinct innate recognition properties, has recently become an area of intense investigation.

It is now known that γδ T cells play a critical role in tumor immunosurveillance (14–17) and in the immune response to cancer (18–23). In many instances, γδ T cells that are cytotoxic to a specific tumor type will cross-react with other tumors but not with the tumor's non-transformed counterpart (21, 22, 24). Furthermore, the VγVδ2 subset of γδ T cells can respond early to infection or transformation and recruit adaptive responses from CD4+ and CD8 + T cells by internalizing antigens, processing them and displaying the antigens complexed with major histocompatibility complexes on their cell surface (25). As professional antigen presenting cells, γδ T cell lymphocytes express equivalent levels of costimulatory molecules and CCR7, home to lymph nodes and are equally potent at promoting proliferative responses in αβ T cells when compared to dendritic cells (9). Activating ligands for γδ T cells as well as the process by which they recognize stressed or malignant cells are complex and incompletely understood but are fundamentally different from both αβ T cells and NK cells (26–29).

The most prevalent circulating population of γδ T cells express an invariant Vγ9Vδ2 TCR (30). Vγ9/Vδ2+ T cells are thought to be activated via the T cell receptor (TCR) principally by three groups of non-peptide antigens: alkylphosphates such as isopentenyl pyrophosphate (IPP) generated by eukaryotic isoprenoid biosynthesis using the mevalonate pathway (31), alkylamines (32), and synthetic aminobisphosphonates (N-BP) (33, 34). Additionally, both Vδ1+ and Vδ2+ T cells express NKG2D, a C-type, lectin-like homodimeric activating receptor also expressed by NK cells and some αβCD8+ T cells. NKG2D is a ligand for MHC class-I like proteins such as major histocompatibility complex class I-related chain A/B (MICA/B), the UL-16 binding proteins (ULBP1-6) and MutS homologue 2 (MSH2). These NKG2D ligands provide a powerful danger signal to the immune system and are upregulated in response to cellular stress including infection and malignant transformation (35, 36). NKG2D ligation has been thought to play a costimulatory role in the activation of γδ T cells (37, 38), however, recent findings indicate that NKG2D ligation may be sufficient to independently activate certain γδ T cell subsets (39, 40). NKG2D activation is an important factor in tumor recognition and lysis by Vγ9Vδ2+ T cells, potentially playing a costimulatory role in cooperation with TCR-dependent activation (37, 41), although direct ligation of the Vγ9Vδ2+ receptor by the NKG2D ligand ULBP-4 has been reported (42). In some situations, NKG2D activation may be the primary stimulus, while TCR stimulation has a secondary role or is not required (40, 43).

Resetting the clock - amplifying and extending the innate "first responder" paradigm

We have recently shown that ex vivo activated murine γδ T cells, when delivered intracranially during a period of minimal disease, failed to prevent tumor progression in a syngeneic GL261 mouse model (44) although they showed strong *in vitro* cytotoxic function against the same cell line. Prior to that study, we had also shown ex vivo human expanded and activated γδ T cells to be significantly effective in a human cell line xenograft model using a similar protocol (45). The apparent discordance was resolved by our observation that murine NKG2DL RAE-1 and MULT-1 are significantly downregulated in the hypoxic environment of the brain compared to that in the normoxic environment of ex vivo cell culture. Based on the observations of others who had shown that chemotherapy creates a favorable environment for a follow-on anti-tumor immune response, we then examined whether standard cytoreductive chemotherapy such as TMZ could increase stress antigen expression. Indeed, we were able to force transient upregulation of NKG2DL on chemotherapy resistant GBM cell lines with exposure to a therapeutic concentration of TMZ (46). The transient nature of this effect, however, precluded the timing of cell therapy administration outside of a pharmacokinetic point beyond which the cytotoxic effect on lymphocytes would also be at issue, particularly in a standard-of-care environment that would require five consecutive daily doses of TMZ. With that in mind, we generated a TMZ-resistant product by transducing γδ T cells with a p140K-MGMT expressing lentivector, a technique that had been previously used to build TMZ resistance into hematopoietic stem cells. TMZ-modified γδ T cells showed negligible losses and robust killing potential that was significantly improved in co-culture with GBM cell lines in TMZ-supplemented culture media (46). Finally, we tested the combination of intracranial therapy with MGMT-modified γδ T cells and TMZ against classical and mesenchymal primary and recurrent PDXT models in immunodeficient mice (47). Results showed significantly improved tumor-free survival at 150 days in mice with primary GBM PDXT receiving combination therapy over either single agent γδ T cells or TMZ for both classical and mesenchymal subtypes. Histopathology following sacrifice of survivors demonstrated an ability to target the heterogeneity of GBM tumors, with no discernable residual disease. Recurrent

models fared poorly with a small effect of combination therapy noted in classical GBM subtype and no effect in mesenchymal PDXT. A separate safety study showed that the combination was not cytotoxic against cultured astrocytes exposed to radiation and/or TMZ chemotherapy and that NKG2DL were not upregulated on normal brain tissue from humans or mice exposed to stereotactic radiotherapy (48).

Clinical trial design

These concepts – treatment of minimal residual primary tumor with innate γδ T cells following forced upregulation of tumor NKG2DL – are currently being explored in a Phase I clinical trial as a collaboration between the University of Alabama at Birmingham (UAB) and IN8Bio, Inc. The Stupp standard of care regimen is an ideal treatment platform to test the concept of repeated applications of high dose γδ T cell therapy in the setting of minimal residual disease. Figure 1 details the Phase I trial design. Adult newly diagnosed GBM patients with adequate organ function and KPS>70% undergo gross total resection at which time a Rickham catheter (Integra LifeSciences; Princeton, NJ) is inserted into the resection cavity with a subcutaneous injection port placed under the skull. The patient then recovers for 3-4 weeks after which time an autologous mononuclear cell leukapheresis is obtained. Vγ9Vδ2 γδ T cells are expanded and activated using a proprietary manufacturing process (DeltEx^{TM} DRI; IN8Bio, Inc., New York, NY) in media supplemented with Zoledronate (Novartis; Basel, Switzerland) and IL-2 (Miltenyi Biotech) in an automated bioreactor (Prodigy^{TM}: Miltenyi Biotec; Bergisch Gladbach, Germany) and transduced with the p140K-MGMT lentivector (Miltenyi Lentigen; Gaithersburg, MD). The final cell product is then harvested and cryopreserved in dose aliquots containing 1 x 10^7 γδ T cells/cryovial.

It is well known that the circulating γδ T cell population is reduced in GBM patients by the dual-suppressing effects of exhaustion and tumor-derived systemic immunosuppression. Although zoledronate-mediated *in vivo* γδ T cell expansion has resulted in transient improvement for sensitive tumors (49), we have demonstrated that zoledronate + IL-2 mediated *in vivo* expansion of γδ T cells (50) results in only a moderate increase in the circulating γδ T cell count and expansion of the Treg population. Spacing resection and product collection provides time for recovery of cellular immunity as tumor-derived immunosuppressive cytokines decrease in the setting of minimal residual disease. Additionally, intracranial placement of the γδ T cells at the tumor site avoids the dilution and trapping of the cell product in the systemic microcirculation.

Dose administration begins on the first day of the first cycle of maintenance therapy where the patient receives the cell product through the intracranial Rickham catheter within 4 hours of intravenous (IV) TMZ. The remaining four TMZ doses are given orally, and the cycle repeats up to six times. In this dose escalation study, cohort 1 receives a single dose of γδ T cells on day 1 of Cohort 1 of maintenance while Cohort 2 receives γδ T cells on day one of cycles1-3 and Cohort 3 receives γδ T cells on cycles 1-6 along with temozolomide. In addition to standard of care diagnostic monitoring, patients are assessed at regular intervals for tumor genomics, histopathology, lymphocyte subsets, and serum cytokines. The primary endpoint is safety; secondary endpoints include progression free (PFS) and overall survival (OS). Dose limiting toxicities (DLTs) are defined as treatment related ≥ grade 3 cardiopulmonary or hepatic toxicity, grade 4 toxicity exceeding 72 hours or neurologic deterioration that exceeds 2 weeks.

This Phase I clinical trial (NCT04165941) is ongoing with anticipated completion of enrollment in 2023. Interim findings (51) for 15 enrolled patients (53% male; median age 69 (range: 21-76); 80% IDH-WT,66.7% MGMT unmethylated) of which 8 had

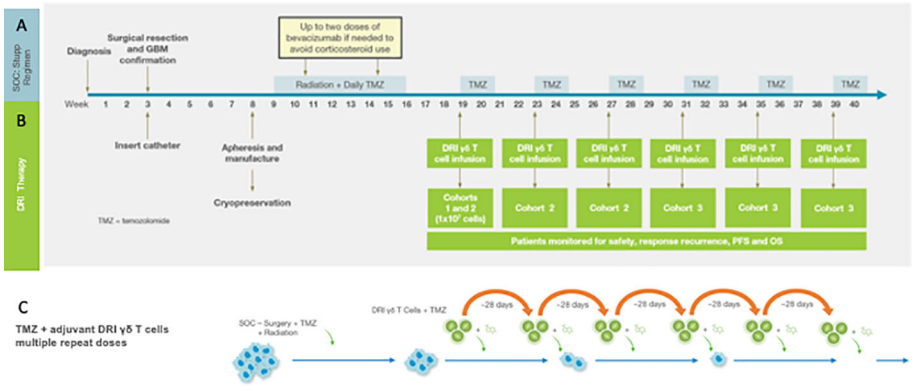

FIGURE 1
The Phase I Drug Resistant Immunotherapy trial is combined with the standard of care Stupp regimen consisting of resection + radiation/TMZ chemotherapy followed by six 28-day cycles of oral maintenance TMZ **(A)**. For the DRI protocol **(B)** a Rickham catheter is inserted into the tumor cavity following resection. Peripheral blood mononuclear cells (PBMC) for manufacturing of the cell product 3-4 weeks following tumor resection and prior to induction chemotherapy and radiotherapy (see text). The MGMT-modified γδ T cell product is infused on the first day of each maintenance cycle (depending on cohort-see text) within 4h of intravenous TMZ. **(C)** outlines the strategy that informs the clinical trial in which the tumor mass is reduced to minimal residual disease, the DDR and subsequent upregulated stress antigen expression then activated by TMZ and simultaneously targeted with a high local dose of MGMT-modified γδ T cells. Oral TMZ dosing continues for the remaining 4 days of the cycle and then repeated to provide continued pressure on tumor survival and proliferation.

been treated (N = 3 in C1, 4 in C2, 1 in C3) were presented at the 2023 American Society of Clinical Oncology conference.

Biologic impediments, potential solutions, and future directions

Our design addresses several obstacles to effective prolonged tumor reduction that must be considered when developing γδ T cell-based cellular therapies (52). The first is that circulating γδ T cells from GBM patients are reduced in number and show impairment of proliferative function, thus limiting the applicability of autologous infusion therapies or strategies that rely solely on *in vivo* stimulation and expansion of γδ T cells (50). A separate though related problem is the sensitivity of normal γδ T cells to activation-induced cell death (AICD), which could impact the longevity of ex vivo expanded γδ T cells once infused (53). These issues have been anticipated and adopted into the manufacturing and therapeutic strategy. GBM-derived suppression of peripheral immunosuppression is known to decrease significantly following tumor resection (54), therefore the autologous cell product is obtained postoperatively and immediately prior to primary chemo/radiotherapy when immune recovery has occurred after tumor removal. Most importantly, given the heterogeneity of solid tumors, a more effective use of cell therapy may require a multi-pronged approach that relies on a more logical combinations and sequencing of each agent. Indeed, the rapid ability of tumors to expand requires rapid extraction and interruption of growth with surgery, chemotherapy and radiation and subsequent use of immunotherapy to eliminate residual tumor cells that may or may not be chemotherapy resistant. Once T cells have been successfully manufactured and infused, they can encounter an array of defensive measures that are generated by the tumor. Indeed, T cells must traverse the tumor vasculature (52), and survive tumor-derived inhibitory factors such as TGF-β and IL-10 which can inhibit antigen presentation, T cell activation, and expand of CD3+CD4+FoxP3+ regulatory T cells (55–57)„ which have recently been implicated in the direct suppression of γδ T cell function (58). Tumor-derived proinflammatory factors also recruit monocyte-derived suppressor cells (MDSC) and mesenchymal stromal cells (MSC) into the tumor microenvironment (59) which can impair Vγ9Vδ2+ responses to phosphoantigen (60). Matrix metalloprotease derived proteolytic shedding of soluble NKG2D ligands can bind NKG2D (and possibly the γδ TCR) resulting in receptor endocytosis and inhibition of γδ T cell function (61). The repeated combination of TMZ chemotherapy and local application of MGMT modified γδ T cells over several months against small, undetectable malignant cell clusters should both reduce NKG2DL shedding, improve vulnerability to lysis by γδ T cells and inhibit formation of a vascularized and immunosuppressive tumor mass (62). Additionally, tumor-mediated effector-to-suppressor functional reprogramming of γδ T cells, which effectively results in a tumor-promoting γδ T cells phenotype, has been extensively documented for the Vδ1+ T cell population. Similar evidence for this effect for the Vγ9Vδ2+ population has not been documented in animal models or humans. Additionally, the cell therapy discussed herewith is intended for patients with minimal residual disease following subtotal resection and high-dose chemo/radiotherapy, which leaves the patient with no visible residual disease by standard imaging techniques, thereby lessening the potential effect of microenvironment that would be more characteristic of a bulky tumor. Finally, there is no evidence that expanded and activated Vδ2 T cell products are susceptible to reprogramming from effector to suppressor phenotype.

Additional combinations of chemotherapy, biologics, and CAR-T modifications to γδ T cells may further improve outcomes as these approaches move earlier in the treatment plan. Checkpoint inhibition, as shown earlier to be generally ineffective as a combination therapy with standard of care, presents an interesting biologic case if combined with γδ T cells. Tomogane (63) and Hoeres (64) recently examined the function of ex vivo expanded and activated γδ T cells across a variety of cell lines and found a decoupling between the anti-tumor cytotoxicity of γδ T cells and γδ T cell expression of PD-1 in that PD-1 blockade did not improve γδ T cell cytotoxicity against tumor lines. Interestingly, however, Tomogane showed a that a subset of PD-L1^{high} tumor lines were rendered more sensitive to ADCC-mediated γδ T cell lysis by PD-L1 blockade. Hoeres also showed that although PD-1 blockade did not improved cell-based cytotoxicity, it did upregulate IFN-γ production which could improve anti-tumor effect *in vitro*. We have previously shown (47) that PD-L1 is upregulated on GBM PDXT following treatment with TMZ which, as the review has noted, may impair DRI efficacy to some degree. Taken together, the probability exists that a neoadjuvant PD-1/PD-L1 regimen could improve overall γδ T cell function against a subset of PD-L1^{high} tumors although practical implementation would require further modeling.

Although we are hopeful that the strategy discussed above will lead to meaningful extension of PFS, we are cognizant of the unique challenges that GBM presents. The military principle of attacking a lightly defended position with overwhelming force and maintaining sustained pressure to prevent reinforcements (65) informs our strategy of repeated combination chemotherapy with a high dose of MGMT modified γδ T cells against a small population of residual primary tumor cells. With this approach we hope to minimize the immunosuppressive effect of the tumor, reduce the avenues for escape, and provide a path to sustained remission.

Data availability statement

The original contributions presented in the study are included in the article/supplementary material. Further inquiries can be directed to the corresponding author.

Ethics statement

The studies involving humans were approved by Western IRB. The studies were conducted in accordance with the local legislation and institutional requirements. The participants provided their written informed consent to participate in this study.

Author contributions

LN: Investigation, Project administration, Resources, Writing – review & editing. TG: Project administration, Writing – review & editing, Methodology, Visualization. KR: Methodology, Project administration, Writing – review & editing, Investigation. SY: Investigation, Methodology, Project administration, Writing – review & editing, Resources. LL: Investigation, Project administration, Resources, Conceptualization, Funding acquisition, Supervision, Writing – original draft, Writing – review & editing.

Funding

The author(s) declare that no financial support was received for the research, authorship, and/or publication of this article.

Conflict of interest

The concepts and work contained in this manuscript were conceived at the University of Alabama at Birmingham UAB by LL and licensed by IN8Bio at which LL has been employed as of 1 January 2019. KR, TG, and SY are also employees of IN8Bio, Inc. LN is faculty at UAB and has received funding from IN8Bio to conduct the referenced clinical trial as an IIT.

Publisher's note

References

1. Billiau A, Heremans H, Vandekerckhove F, Dijkmans R, Sobis H, Meulepas E, et al. Enhancement of experimental allergic encephalomyelitis in mice by antibodies against IFN-gamma. *J Immunol* (1988) 140:1506–10. doi: 10.4049/jimmunol.140.5.1506

2. Zitvogel L, Tesniere A, Kroemer G. Cancer despite immunosurveillance: immunoselection and immunosubversion. *Nat Rev Immunol* (2006) 6:715–27. doi: 10.1038/nri1936

3. Spurrell EL, Lockley M. Adaptive immunity in cancer immunology and therapeutics. *Ecancermedicalscience* (2014) 8:441. doi: 10.3332/ecancer.2014.441.eCollection2014

4. Stupp R, Mason WP, van den Bent MJ, Weller M, Fisher B, Taphoorn MJ, et al. Treatment of Cancer Brain, G. Radiotherapy and G. National Cancer Institute of Canada Clinical Trials, Radiotherapy plus concomitant and adjuvant temozolomide for glioblastoma. *N Engl J Med* (2005) 352:987–96. doi: 10.1056/NEJMoa043330

5. Khasraw M, Reardon DA, Weller M, Sampson JH. PD-1 Inhibitors: Do they have a Future in the Treatment of Glioblastoma? *Clin Cancer Res* (2020) 26:5287–96. doi: 10.1158/1078-0432.CCR-20-1135

6. Cloughesy TF, Mochizuki AY, Orpilla JR, Hugo W, Lee AH, Davidson TB, et al. Neoadjuvant anti-PD-1 immunotherapy promotes a survival benefit with intratumoral and systemic immune responses in recurrent glioblastoma. *Nat Med* (2019) 25:477–86. doi: 10.1038/s41591-018-0337-7

7. Brown CE, Alizadeh D, Starr R, Weng L, Wagner JR, Naranjo A, et al. Regression of glioblastoma after chimeric antigen receptor T-cell therapy. *N Engl J Med* (2016) 375:2561–9. doi: 10.1056/NEJMoa1610497

8. O'Rourke DM, Nasrallah MP, Desai A, Melenhorst JJ, Mansfield K, Morrissette JJD, et al. A single dose of peripherally infused EGFRvIII-directed CAR T cells mediates antigen loss and induces adaptive resistance in patients with recurrent glioblastoma. *Sci Transl Med* (2017) 9. doi: 10.1126/scitranslmed.aaa0984

9. Vantourout P, Hayday A. Six-of-the-best: unique contributions of gammadelta T cells to immunology. *Nat Rev Immunol* (2013) 13:88–100. doi: 10.1038/nri3384

10. Reuben A, Spencer CN, Prieto PA, Gopalakrishnan V, Reddy SM, Miller JP, et al. Wargo, Genomic and immune heterogeneity are associated with differential responses to therapy in melanoma. *NPJ Genom Med* (2017) 2. doi: 10.1038/s41525-017-0013-8

11. Jimenez-Sanchez A, Memon D, Pourpe S, Veeraraghavan H, Li Y, Vargas HA, et al. Heterogeneous tumor-immune microenvironments among differentially growing metastases in an ovarian cancer patient. *Cell* (2017) 170:927–938 e20. doi: 10.1016/j.cell.2017.07.025

12. Barish M WL, Ahai Y, D'Apuzzo M, Briti A, Chiang B, Aguilar B, et al. Heterogeneous antigen expression and multiantigen targeting potential for immunotherapy of high-grade glioma., Immunobiology of Primary and Metastatic CNS Cancer: Multidisciplinary Science to Advance Cancer Immunotherapy, American Association of Cancer Research, San Diego, CA. (2018), 38.

13. Larson RC, Kann MC, Bailey SR, Haradhvala NJ, Llopis PM, Bouffard AA, et al. CAR T cell killing requires the IFNgammaR pathway in solid but not liquid tumours. *Nature* (2022) 604:563–70. doi: 10.1038/s41586-022-04585-5

14. Zocchi MR, Poggi A. Role of gammadelta T lymphocytes in tumor defense. *Front Biosci* (2004) 9:2588–604. doi: 10.2741/1419

15. Kabelitz D, Wesch D, He W. Perspectives of gammadelta T cells in tumor immunology. *Cancer Res* (2007) 67:5–8. doi: 10.1158/0008-5472.CAN-06-3069

16. Girardi M, Oppenheim DE, Steele CR, Lewis JM, Glusac E, Filler R, et al. Regulation of cutaneous Malignancy by gammadelta T cells. *Science* (2001) 294:605–9. doi: 10.1126/science.1063916

17. Liu Z, Eltoum IE, Guo B, Beck BH, Cloud GA, Lopez RD. Protective immunosurveillance and therapeutic antitumor activity of gammadelta T cells demonstrated in a mouse model of prostate cancer. *J Immunol* (2008) 180:6044–53. doi: 10.4049/jimmunol.180.9.6044

18. Ferrarini M, Pupa SM, Zocchi MR, Rugarli C, Menard S. Distinct pattern of HSP72 and monomeric laminin receptor expression in human lung cancers infiltrated by gamma/delta T lymphocytes. *Int J Cancer* (1994) 57:486–90. doi: 10.1002/ijc.2910570408

19. Choudhary A, Davodeau F, Moreau A, Peyrat MA, Bonneville M, Jotereau F. Selective lysis of autologous tumor cells by recurrent gamma delta tumor-infiltrating lymphocytes from renal carcinoma. *J Immunol* (1995) 154:3932–40. doi: 10.4049/jimmunol.154.8.3932

20. Zhao X, Wei YQ, Kariya Y, Teshigawara K, Uchida A. Accumulation of gamma/delta T cells in human dysgerminoma and seminoma: roles in autologous tumor killing and granuloma formation. *Immunol Invest* (1995) 24:607–18. doi: 10.3109/08820139509066861

21. Xu C, Zhang H, Hu H, He H, Wang Z, Xu Y, et al. Gammadelta T cells recognize tumor cells via CDR3delta region. *Mol Immunol* (2007) 44:302–10. doi: 10.1016/j.molimm.2006.03.010

22. Corvaisier M, Moreau-Aubry A, Diez E, Bennouna J, Mosnier JF, Scotet E, et al. V gamma 9V delta 2 T cell response to colon carcinoma cells. *J Immunol* (2005) 175:5481–8. doi: 10.4049/jimmunol.175.8.5481

23. Zocchi MR, Ferrarini M, Rugarli C. Selective lysis of the autologous tumor by delta TCS1+ gamma/delta+ tumor-infiltrating lymphocytes from human lung carcinomas. *Eur J Immunol* (1990) 20:2685–9. doi: 10.1002/eji.1830201224

24. Bryant NL, Suarez-Cuervo C, Gillespie G, Markert JM, Nabors LB, Meleth S, et al. Characterization and immunotherapeutic potential of γδ T cells in patients with glioblastoma neuro-oncology. (2009) 11:357–67. doi: 10.1215/15228517-2008-111

25. Anderson J, Gustafsson K, Himoudi N, Yan M, Heuijerjans J. Licensing of gammadeltaT cells for professional antigen presentation: A new role for antibodies in regulation of antitumor immune responses. *Oncoimmunology* (2012) 1:1652–4. doi: 10.4161/onci.21971

26. Hayday AC. [gamma][delta] cells: a right time and a right place for a conserved third way of protection. *Annu Rev Immunol* (2000) 18:975–1026. doi: 10.1146/annurev.immunol.18.1.975

27. Boismenu R, Havran WL. An innate view of gamma delta T cells. *Curr Opin Immunol* (1997) 9:57–63. doi: 10.1016/S0952-7915(97)80159-8

28. Chien YH, Konigshofer Y. Antigen recognition by gammadelta T cells. *Immunol Rev* (2007) 215:46–58. doi: 10.1111/j.1600-065X.2006.00470.x

29. O'Brien RL, Roark CL, Jin N, Aydintug MK, French JD, Chain JL, et al. gammadelta T-cell receptors: functional correlations. *Immunol Rev* (2007) 215:77–88. doi: 10.1111/j.1600-065X.2006.00477.x

30. Parker CM, Groh V, Band H, Porcelli SA, Morita C, Fabbi M, et al. Evidence for extrathymic changes in the T cell receptor gamma/delta repertoire. *J Exp Med* (1990) 171:1597–612. doi: 10.1084/jem.171.5.1597

31. Morita CT, Beckman EM, Bukowski JF, Tanaka Y, Band H, Bloom BR, et al. Direct presentation of nonpeptide prenyl pyrophosphate antigens to human gamma delta T cells. *Immunity* (1995) 3:495–507. doi: 10.1016/1074-7613(95)90178-7

32. Bukowski JF, Morita CT, Brenner MB. Human gamma delta T cells recognize alkylamines derived from microbes, edible plants, and tea: implications for innate immunity. *Immunity* (1999) 11:57–65. doi: 10.1016/S1074-7613(00)80081-3

33. Kunzmann V, Bauer E, Feurle J, Weissinger F, Tony HP, Wilhelm M. Stimulation of gammadelta T cells by aminobisphosphonates and induction of antiplasma cell activity in multiple myeloma. *Blood* (2000) 96:384–92. doi: 10.1182/blood.V96.2.384.013k07_384_392

34. Miyagawa F, Tanaka Y, Yamashita S, Mikami B, Danno K, Uehara M, et al. Essential contribution of germline-encoded lysine residues in Jgamma1.2 segment to the recognition of nonpeptide antigens by human gammadelta T cells. *J Immunol* (2001) 167:6773–9. doi: 10.4049/jimmunol.167.12.6773

35. Gleimer M, Parham P. Stress management: MHC class I and class I-like molecules as reporters of cellular stress. *Immunity* (2003) 19:469–77. doi: 10.1016/S1074-7613(03)00272-3

36. Raulet DH. Roles of the NKG2D immunoreceptor and its ligands. *Nat Rev Immunol* (2003) 3:781–90. doi: 10.1038/nri1199

37. Das H, Groh V, Kuijl C, Sugita M, Morita CT, Spies T, et al. MICA engagement by human Vgamma2Vdelta2 T cells enhances their antigen-dependent effector function. *Immunity* (2001) 15:83–93. doi: 10.1016/S1074-7613(01)00168-6

38. Bauer S, Groh V, Wu J, Steinle A, Phillips JH, Lanier LL, et al. Activation of NK cells and T cells by NKG2D, a receptor for stress-inducible MICA [see comments]. *Science* (1999) 285:727–9. doi: 10.1126/science.285.5428.727

39. Whang MI, Guerra N, Raulet DH. Costimulation of dendritic epidermal gammadelta T cells by a new NKG2D ligand expressed specifically in the skin. *J Immunol* (2009) 182:4557–64. doi: 10.4049/jimmunol.0802439

40. Rincon-Orozco B, Kunzmann V, Wrobel P, Kabelitz D, Steinle A, Herrmann T. Activation of V gamma 9V delta 2 T cells by NKG2D. *J Immunol* (2005) 175:2144–51. doi: 10.4049/jimmunol.175.4.2144

41. Wrobel P, Shojaei H, Schittek B, Gieseler F, Wollenberg B, Kalthoff H, et al. Lysis of a broad range of epithelial tumour cells by human gamma delta T cells: involvement of NKG2D ligands and T-cell receptor- versus NKG2D-dependent recognition. *Scand J Immunol* (2007) 66:320–8. doi: 10.1111/j.1365-3083.2007.01963.x

42. Kong Y, Cao W, Xi X, Ma C, Cui L, He W. The NKG2D ligand ULBP4 binds to TCRgamma9/delta2 and induces cytotoxicity to tumor cells through both TCRgammadelta and NKG2D. *Blood* (2009) 114:310–7. doi: 10.1182/blood-2008-12-196287

43. Nitahara A, Shimura H, Ito A, Tomiyama K, Ito M, Kawai K. NKG2D ligation without T cell receptor engagement triggers both cytotoxicity and cytokine production in dendritic epidermal T cells. *J Invest Dermatol* (2006) 126:1052–8. doi: 10.1038/sj.jid.5700112

44. Beck BH, Kim H, O'Brien R, Jadus MR, Gillespie GY, Cloud GA, et al. Dynamics of circulating gammadelta T cell activity in an immunocompetent mouse model of high-grade glioma. *PloS One* (2015) 10:e0122387. doi: 10.1371/journal.pone.0122387

45. Bryant NL, Gillespie GY, Lopez RD, Markert JM, Cloud GA, Langford CP, et al. Preclinical evaluation of ex vivo expanded/activated gammadelta T cells for immunotherapy of glioblastoma multiforme. *J Neurooncol* (2011) 101:179–88. doi: 10.1007/s11060-010-0245-2

46. Lamb LS Jr., Bowersock J, Dasgupta A, Gillespie GY, Su Y, Johnson A, et al. Engineered drug resistant gammadelta T cells kill glioblastoma cell lines during a chemotherapy challenge: a strategy for combining chemo- and immunotherapy. *PloS One* (2013) 8:e51805. doi: 10.1371/journal.pone.0081805

47. Lamb LS, Pereboeva L, Youngblood S, Gillespie GY, Nabors LB, Markert JM, et al. A combined treatment regimen of MGMT-modified gammadelta T cells and temozolomide chemotherapy is effective against primary high grade gliomas. *Sci Rep* (2021) 11:21133. doi: 10.1038/s41598-021-00536-8

48. Pereboeva L, Harkins L, Wong S, Lamb LS. The safety of allogeneic innate lymphocyte therapy for glioma patients with prior cranial irradiation. *Cancer Immunol Immunother* (2015) 64:551–62. doi: 10.1007/s00262-015-1662-z

49. Dieli F, Vermijlen D, Fulfaro F, Caccamo N, Meraviglia S, Cicero G, et al. Targeting human gammadelta T cells with zoledronate and interleukin-2 for immunotherapy of hormone-refractory prostate cancer. *Cancer Res* (2007) 67:7450–7. doi: 10.1158/0008-5472.CAN-07-0199

50. Pressey JG, Adams J, Harkins L, Kelly D, You Z, Lamb LS Jr. *In vivo* expansion and activation of gammadelta T cells as immunotherapy for refractory neuroblastoma: A phase 1 study. *Med (Baltimore)* (2016) 95:e4909. doi: 10.1097/MD.0000000000004909

51. Mina Lobbous TG, Lamb LS, Rochlin K, Pillay T, Youngblood S, ter Haak M, et al. INB-200 phase I study of gene modified autologous gamma-delta (γδ) T cells in patients with newly diagnosed glioblastoma multiforme (GBM) receiving maintenance temozolomide (TMZ). *J Clin Oncol* (2023) 41.

52. Martinet L, Poupot R, Fournie JJ. Pitfalls on the roadmap to gammadelta T cell-based cancer immunotherapies. *Immunol Lett* (2009) 124:1–8. doi: 10.1016/j.imlet.2009.03.011

53. Siegers GM, Lamb LS Jr. Cytotoxic and regulatory properties of circulating Vdelta1+ gammadelta T cells: a new player on the cell therapy field? *Mol Ther* (2014) 22:1416–22. doi: 10.1038/mt.2014.104

54. Bryant NL, Suarez-Cuervo C, Gillespie GY, Markert JM, Nabors LB, Meleth S, et al. Characterization and immunotherapeutic potential of gammadelta T-cells in patients with glioblastoma. *Neuro Oncol* (2009) 11:357–67. doi: 10.1215/15228517-2008-111

55. Smyth MJ, Strobl SL, Young HA, Ortaldo JR, Ochoa AC. Regulation of lymphokine-activated killer activity and pore-forming protein gene expression in human peripheral blood CD8+ T lymphocytes. Inhibition by transforming growth factor-beta. *J Immunol* (1991) 146:3289–97. doi: 10.4049/jimmunol.146.10.3289

56. Inge TH, McCoy KM, Susskind BM, Barrett SK, Zhao G, Bear HD. Immunomodulatory effects of transforming growth factor-beta on T lymphocytes. Induction of CD8 expression in the CTLL-2 cell line and in normal thymocytes. *J Immunol* (1992) 148:3847–56. doi: 10.4049/jimmunol.148.12.3847

57. Jachimczak P, Bogdahn U, Schneider J, Behl C, Meixensberger J, Apfel R, et al. The effect of transforming growth factor-beta 2-specific phosphorothioate-anti-sense oligodeoxynucleotides in reversing cellular immunosuppression in Malignant glioma. *J Neurosurg* (1993) 78:944–51. doi: 10.3171/jns.1993.78.6.0944

58. Kunzmann V, Kimmel B, Herrmann T, Einsele H, Wilhelm M. Inhibition of phosphoantigen-mediated gammadelta T-cell proliferation by CD4+ CD25+ FoxP3+ regulatory T cells. *Immunology* (2009) 126:256–67. doi: 10.1111/j.1365-2567.2008.02894.x

59. Umansky V, Blattner C, Gebhardt C, Utikal J. The role of myeloid-derived suppressor cells (MDSC) in cancer progression. *Vaccines (Basel)* (2016) 4. doi: 10.3390/vaccines4040036

60. Martinet L, Fleury-Cappellesso S, Gadelorge M, Dietrich G, Bourin P, Fournie JJ, et al. A regulatory cross-talk between Vgamma9Vdelta2 T lymphocytes and mesenchymal stem cells. *Eur J Immunol* (2009) 39:752–62. doi: 10.1002/eji.200838812

61. Groh V, Wu J, Yee C, Spies T. Tumour-derived soluble MIC ligands impair expression of NKG2D and T-cell activation. *Nature* (2002) 419:734–8. doi: 10.1038/nature01112

62. Chitadze G, Lettau M, Luecke S, Wang T, Janssen O, Furst D, et al. NKG2D- and T-cell receptor-dependent lysis of Malignant glioma cell lines by human gammadelta T cells: Modulation by temozolomide and A disintegrin and metalloproteases 10 and 17 inhibitors. *Oncoimmunology* (2016) 5:e1093276. doi: 10.1080/2162402x.1093276

63. Tomogane M, Sano Y, Shimizu D, Shimizu T, Miyashita M, Toda Y, et al. Human Vgamma9Vdelta2 T cells exert anti-tumor activity independently of PD-L1 expression in tumor cells. *Biochem Biophys Res Commun* (2021) 573:132–9. doi: 10.1016/j.bbrc.2021.08.005

64. Hoeres T, Holzmann E, Smetak M, Birkmann J, Wilhelm M. PD-1 signaling modulates interferon-gamma production by Gamma Delta (gammadelta) T-Cells in response to leukemia. *Oncoimmunology* (2019) 8:1550618. doi: 10.1080/2162402X.2018.1550618

65. Home T. *Mastering the Art of Command: Admiral Chester W. Nimitz and Victory in the Pacific*. Annapolis: Naval Institute Press (2022).

frontiers | Frontiers in Immunology

TYPE Original Research
PUBLISHED 21 February 2024
DOI 10.3389/fimmu.2024.1342625

OPEN ACCESS

EDITED BY
Divya Nagarajan,
Uppsala University, Sweden

REVIEWED BY
Rio Sugimura,
The University of Hong Kong,
Hong Kong SAR, China
Sweta Ghosh,
University of Louisville, United States

*CORRESPONDENCE
Margarita Gutova
MGutova@coh.org

RECEIVED 22 November 2023
ACCEPTED 29 January 2024
PUBLISHED 21 February 2024

CITATION
Gutova M, Hibbard JC, Ma E, Natri HM, Adhikarla V, Chimge N-O, Qiu R, Nguyen C, Melendez E, Aguilar B, Starr R, Yin H, Rockne RC, Ono M, Banovich NE, Yuan Y-C, Brown CE and Kahn M (2024) Targeting Wnt signaling for improved glioma immunotherapy.
Front. Immunol. 15:1342625.
doi: 10.3389/fimmu.2024.1342625

Targeting Wnt signaling for improved glioma immunotherapy

Margarita Gutova[1]*, Jonathan C. Hibbard[2], Eric Ma[2], Heini M. Natri[3], Vikram Adhikarla[4], Nyam-Osor Chimge[5], Runxiang Qiu[1], Cu Nguyen[5], Elizabeth Melendez[5], Brenda Aguilar[2], Renate Starr[2], Holly Yin[5], Russel C. Rockne[4], Masaya Ono[6], Nicholas E. Banovich[3], Yate-Ching Yuan[7], Christine E. Brown[2] and Michael Kahn[5]

[1]Department of Stem Cell Biology and Regenerative Medicine, City of Hope Beckman Research Institute, Duarte, CA, United States, [2]Department of Hematology & Hematopoietic Cell transplantation (T cell Therapeutic Research Laboratories), City of Hope Beckman Research Institute, Duarte, CA, United States, [3]Translational Genomics Research Institute (TGen), Phoenix, AZ, United States, [4]Division of Mathematical Oncology, Department of Computational and Quantitative Medicine, City of Hope Beckman Research Institute, Duarte, CA, United States, [5]Cancer Biology and Molecular Medicine, City of Hope Beckman Research Institute, Duarte, CA, United States, [6]National Cancer Center, Tokyo, Japan, [7]Department of Computational and Quantitative Medicine, City of Hope Beckman Research Institute, Duarte, CA, United States

Introduction: Despite aggressive standard-of-care therapy, including surgery, radiation, and chemotherapy, glioblastoma recurrence is almost inevitable and uniformly lethal. Activation of glioma-intrinsic Wnt/β-catenin signaling is associated with a poor prognosis and the proliferation of glioma stem-like cells, leading to malignant transformation and tumor progression. Impressive results in a subset of cancers have been obtained using immunotherapies including anti-CTLA4, anti-PD-1, and anti-PD-L1 or chimeric antigen receptor (CAR) T cell therapies. However, the heterogeneity of tumors, low mutational burden, single antigen targeting, and associated antigen escape contribute to non-responsiveness and potential tumor recurrence despite these therapeutic efforts. In the current study, we determined the effects of the small molecule, highly specific Wnt/CBP (CREB Binding Protein)/β-catenin antagonist ICG-001, on glioma tumor cells and the tumor microenvironment (TME)–including its effect on immune cell infiltration, blood vessel decompression, and metabolic changes.

Methods: Using multiple glioma patient-derived xenografts cell lines and murine tumors (GL261, K-Luc), we demonstrated *in vitro* cytostatic effects and a switch from proliferation to differentiation after treatment with ICG-001.

Results: In these glioma cell lines, we further demonstrated that ICG-001 downregulated the CBP/β-catenin target gene *Survivin/BIRC5*–a hallmark of Wnt/CBP/β-catenin inhibition. We found that in a syngeneic mouse model of glioma (K-luc), ICG-001 treatment enhanced tumor infiltration by $CD3^+$ and $CD8^+$ cells with increased expression of the vascular endothelial marker CD31 (PECAM-1). We also observed differential gene expression and induced immune cell infiltration in tumors pretreated with ICG-001 and then treated with CAR T cells as compared with single treatment groups or when ICG-001 treatment was administered after CAR T cell therapy.

Discussion: We conclude that specific Wnt/CBP/β-catenin antagonism results in pleotropic changes in the glioma TME, including glioma stem cell differentiation, modulation of the stroma, and immune cell activation and recruitment, thereby suggesting a possible role for enhancing immunotherapy in glioma patients.

KEYWORDS

glioma, Wnt signaling, pathway, ICG-001, immunotherapy, NanoString gene expression, proteomics, differentiation

1 Introduction

Despite aggressive standard of care therapy, including surgery, radiation, and chemotherapy, glioblastoma (GBM) recurrence is almost inevitable and uniformly lethal (1–3). In glioma, Wnt pathway activation has been associated with a poor prognosis and progressive neurological deficits (4). Wnt signaling is associated with the proliferation of stem-like cells (5–7) as well as stark resistance to chemotherapy, radiotherapy, and immunotherapy in GBM (5–9). Unbiased profiling studies demonstrate a strong negative correlation between cancer cell stemness and antitumor immunity signatures across 21 types of solid tumors, with reduced anticancer immune cell tumor infiltration (i.e., $CD8^+$ T cells, natural killer cells, and B cells) and increased tumor-associated macrophages (10). β-catenin transcriptional activation, involving its translocation to the nucleus, is a hallmark of Wnt pathway activation and has been identified in 19% of adult and in 30% of pediatric gliomas (11). A resistance mechanism observed in immunologically "cold tumors", including gliomas, involves aberrant activation of the Wnt/β-catenin signaling pathway (12, 13). Enhanced tumor-intrinsic Wnt/β-catenin signaling appears to be a common mechanism mediating cancer immune evasion and is associated with the presence of an immunosuppressive cell subset and the prevention of effective dendritic cell presentation and T-effector cell recruitment and function (14). Increased expression of β-catenin inversely correlates with the presence of $CD8^+$ T cells and dendritic cells in multiple tumor types, including glioma (13, 15). Furthermore, Wnt pathway activation is correlated with tumor stemness, hypoxia, and poor treatment outcome (16, 17). The hostile tumor microenvironment (TME) is associated with decreased tumor antigen presentation and reduced or lost efficacy of various therapies, including adoptive T cell immunotherapy (18–22). Therefore, targeted downregulation of Wnt/β-catenin signaling–thereby enhancing the response to immunotherapy in patients with relapsed and refractory tumors–is an attractive therapeutic approach.

Glioma stem cells (GSC), via secretion of the Wnt-induced signaling protein 1 (WISP1), can further facilitate a 'cold' TME by promoting the survival of both GSC and tumor-associated macrophages (TAM) (14). Activation of Wnt/β-catenin signaling causes tumor cell proliferation, enhanced invasiveness via upregulation of JNK, and accumulation of metalloproteases, with concomitant neuronal degeneration due to decreased requisite Wnt signaling maintenance (23–25). Clinical and preclinical data suggest that curative immunotherapy must not only address immunotolerance and target tumor antigens, but also circumvent intrinsic and evolving barriers of adaptive and acquired immune escape mechanisms (12, 15). The hostile TME leads to a loss of therapeutic efficacy of immunotherapy, tumor antigen vaccination, and adoptive T cell transfer immunotherapy (including CAR T cell) approaches (13, 26–28). Support for the concept that increased Wnt/β-catenin activity plays a role in CAR T response in glioblastoma was provided by a patient who had a complete initial response to CAR T cell therapy; however upon relapse and antigen loss, tumor samples demonstrated the activation of several genes in the Wnt/β-catenin pathway (including Wnt 11 and Wnt 2A) (19, 29). Currently, WNT inhibitors in clinical trials include PORCN inhibitors, WNT ligand antagonists, FZD antagonists, and CBP/β catenin antagonists tested in various solid tumors and leukemia (30). The refractory nature of gliomas provides compelling motivation for the development of novel therapeutic interventions including CAR T cell therapy for glioma and other devastating malignancies (18, 19, 31–33). Taken together, our results demonstrate that inhibition of Wnt/CBP/β-catenin signaling can induce glioma cell differentiation *in vitro* and *in vivo*, modify the TME, and affect immune cell populations in the TME, shifting towards more effective dendritic cell presentation and a more effective T cell response, thereby potentially enhancing immunotherapeutic interventions in glioma patients.

2 Materials and methods

2.1 *In vitro* experiments

PBT tumor cells lines are derived from patients with brain tumors (IRB07074) dissociated and grown in DMEM/F12 medium, supplemented with heparin, hepes, glutamax, and B27. Epidermal growth factor (EFG) and fibroblast growth factor (FGF) are added at the time of culture, as described previously (34). ICG-001 was provided by M. Kahn's laboratory. Co-culture assay of PBT cell lines were grown as described above and seeded to 100,000 cells/2

ml in 6-well plates. ICG-001 was added to cell cultures in concentrations 0, 5, and 10 μM for 24–72h, as described previously (35).

2.2 RT-PCR analysis

RNA was extracted using the Total RNA Kit according to the manufacturer's instructions (Qiagen, RNeasy PowerSoil). cDNA was generated with the High-Capacity cDNA Reverse Transcription Kit (Applied Biosystems). Quantitative RT-PCR was performed using Power SYBR Green PCR Master Mix (Applied Biosystems). Amplification of human *Kif20A* was performed on RNA samples isolated from PBT147 and PBT030 cells treated with ICG-001 at concentrations of 0, 5, and 10 μM. All data was normalized to the PBT147-24H-0 drug control sample. Human *Kif20A* RT-PCR primers used for RT-PCR analysis were: Forward: TGGTACGCAAGAACCTGC; Reverse: GATCAGGGTTGTGTC CGT. Human GAPDH primers were used as controls: Forward: GGATTTGGTCGTATTGGG; Reverse: GGAAGATGGTGA TGGGATT.

2.3 Proteomics data analysis

The normalized distributions of protein levels were heavily skewed to the right, so we performed a logarithmic transformation of the data, which resulted in an approximate normal distribution of protein levels. The densities of the log-transformed normalized protein level for each cell line/dose are shown in Supplementary Figure 3. To examine the effect of ICG-001, we calculated the difference in log normalized levels for each protein between the four treated samples and the appropriate untreated sample (PBT147 and PBT030 cell lines were treated with ICG001 at 0, 5, and 10 μM, and cells were collected after 24 or 72 h for protein analysis), which corresponds to examining the log of the fold changes in each protein after treatment. For each of the two cell lines (PBT147 and PBT030), we plotted the log fold change for each protein at 5μM against the log fold change at 10μM. These plots are shown in Supplementary Figure 3A, with the points colored-coded by cell line.

2.4 Animal studies

Anesthesia: For tumor models, mice were anesthetized by intraperitoneal (i.p.) injection of Ketamine/Xylazine and gaseous Isoflurane prior to tumor injection. Kluc [0.1×10^5 were prepared in PBS–/– (2 μL per mouse)] and injected orthotopically in the brain parenchyma of female NSG mice via stereotactic injection. Tumor growth was monitored at least once a week via optical imaging (Spectral Instruments Imaging, LagoX) and flux signals were analyzed with Aura Imaging software (LagoX). For imaging, mice were injected intraperitoneally with 150 μL d-luciferin potassium salt (Perkin Elmer) suspended in PBS at 4.29 mg/mouse. Once flux signals reached desired levels, CAR T cells were prepared in PBS and mice were treated either by intratumoral/intracranial injection in 3 μL final volume. At desired time points or at moribund status, mice were euthanized, and tissues were processed for IHC as described below. Syngeneic mice (C57BL/6) of 8–12 weeks of age were implanted with subcutaneous K-Luc tumors (n=8). 7 days later, when tumors became palpable and after confirmation of tumor presence with BLU imaging, mice were implanted with Alzet minipumps. Pumps continuously provided a daily dose of ICG-001 (50 mg/kg/day). Tumor tissues were harvested on days 7, 14, and 21 post pump implantations, and tumors were prepared for IHC (paraffin sections) and NanoString analysis. Control mice were not treated with ICG-001 pumps, and tumors from control mice were harvested on day 7, 14 and 21 to match ICG-001-treated tumors.

2.5 Immunohistochemistry

Three immune cell markers (CD3, CD8, CD31, Abcam) were evaluated with IHC on whole tumor sections. IHC Staining was performed in the City of Hope Pathology Core according to the manufacturer's instructions (n=6 mice). After IHC staining, slides were scanned using the NanoZoomer 2.0-HT slide scanner at 10× magnification (Hamamatsu Photonics). Scanned slides were then imported into Qupath as Brightfield H-DAB images for analysis. Tumor section annotations were manually outlined with the brush and wand tools. Once all tumor areas were selected, total cell count, positive cell count per area, and total area were counted using the Positive Cell Detection tool with the settings optimized for each CD3, CD8 and CD31 staining (Figure 1). All data were extracted from QuPath and further calculations and quantifications were done with Microsoft Excel and Prism.

2.6 Qupath quantification method

After IHC staining, the slides were scanned using the NanoZoomer 2.0-HT slide scanner (Hamamatsu Photonics). Scanned slides were then imported into Qupath as *Brightfield H-DAB* images for analysis. Tumor section annotations were manually outlined with the brush and wand tool. Once all tumor areas were selected, total cell count, positive cell detection, positive %, and total area were counted using the Positive Cell Detection tool with the auto settings (Figures 1D, H, L). All data were then extracted from Qupath and further calculations and quantifications were done with Microsoft Excel and Prism.

2.7 NanoString data analysis

Raw gene count was averaged across three brain tissue samples from CAR T treated mice and across two brain tissue samples from CAR T + ICG001 treated groups. Brain tissue was isolated during euthanasia, and tumors were dissected and snap frozen in liquid nitrogen. Total RNA was isolated from K-Luc tumor tissue and analyzed by NanoString (NanoString nCount mouse PanCancer Immune profiling paneled assays, https://nanostring.com/products/

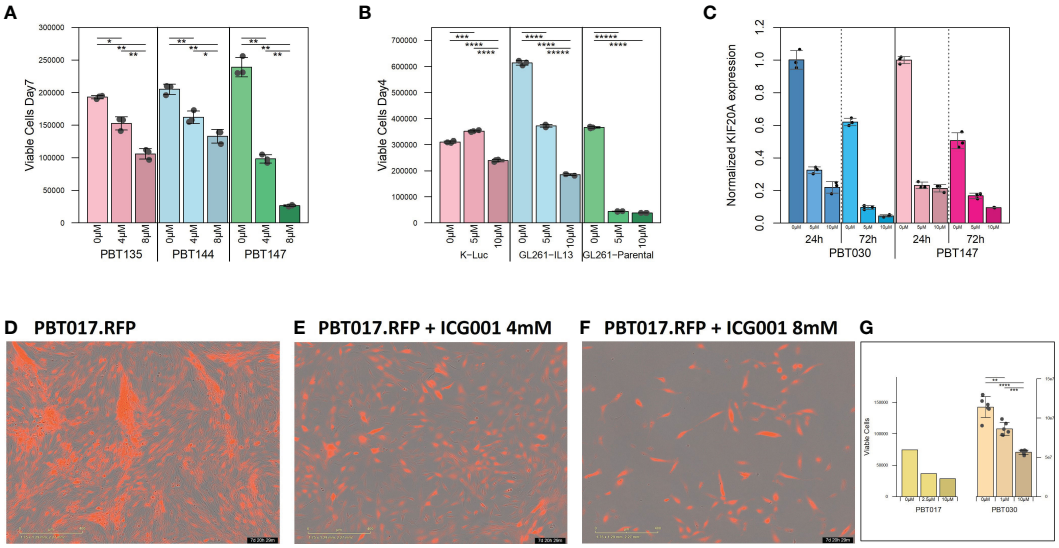

FIGURE 1
Cytostatic effect of ICG-001 in human and mouse glioma cell lines *in vitro*. **(A)** Growth kinetics of human PBT glioma lines (PBT135, PBT144, and PBT147) treated with ICG-001 (0, 5, 10 μM) for 7 days (n=3); and **(B)** mouse glioma cells (K-luc, GL261-IL13, and GL261) treated with ICG-001 (0-10 μM) for 4 days (n=3). Scale bars represent SD of triplicate samples from 2 independent experiments. **(C)** Expression of target gene KIF20 post-ICG-001 treatment (5, 10 μM) by RT-PCR using KIF20A-specific primers (n=3). **(D–F)** Live images taken by IncuCyte of PBT017 glioma expressing red fluorescent protein untreated or treated with ICG-001 (0, 4, 8 μM). **(G)** Analysis and quantification of IncuCyte images (10x) for PBT017.RFP (PBT017 expressing red fluorescent protein-RFP) glioma cells and PBT030 quantified using phase images. P values denoted by *<0.05, **<0.01, ***<0.001, ****<0.0001, *****<0.00001.

ncounter-assays-panels/oncology/pancancer-immune-profiling). Multiplex gene expression analysis was performed in mice for 770 genes from different immune cell types, common checkpoint inhibitors, CT antigens, and genes covering both the adaptive and innate immune response. The panel measures many features of the immune response to facilitate rapid development of clinical actionable gene expression profiles in the context of cancer immunotherapy. Comparisons between brain tissue and ICG001-treated tissue were determined by the nonparametric *U*-test, and $\log_2$ |fold change| ≥ 1.5, -Log_{10} P-value < 0.05 using the Benjamini-Hochberg method to be statistically significant. Log2 normalized counts and expression ratios were generated using nSolver 4.0 and advanced analysis 2.0 (NanoString Technologies, Inc.) as well as ROSALIND analysis platform v3.38.0.1.

2.8 ROSALIND® NanoString gene expression methods

Data was analyzed by ROSALIND® version 3.38.0.1 (https://www.rosalind.bio/), with a HyperScale architecture developed by ROSALIND, Inc. (San Diego, CA). Read Distribution percentages, violin plots, identity heatmaps, and sample MDS plots were generated as part of the QC step. Normalization, fold changes and p-values were calculated using criteria provided by NanoString. ROSALIND® follows the nCounter® Advanced Analysis protocol of dividing counts within a lane by the geometric mean of the normalizer probes from the same lane. Housekeeping probes for normalization were selected based on the geNorm algorithm as implemented in the NormqPCR R library1. Abundance of various cell populations was calculated on ROSALIND using the NanoString Cell Type Profiling Module. ROSALIND was used to perform a filtering of Cell Type Profiling results to include results that have significant scores ($p \leq 0.05$). Fold changes and p-values were calculated using the fast method, as described in the nCounter® Advanced Analysis 2.0 User Manual. P-value adjustment was performed using the Benjamini-Hochberg method of estimating false discovery rates (FDR). Clustering of genes for the final heatmap of differentially expressed genes was performed using the Partitioning Around Medoids (PAM) method using the fpc R library2 that takes into consideration the direction and type of all signals on a pathway (the position, role and type of every gene, etc.). Hypergeometric distribution was used to analyze the enrichment of pathways, gene ontology, domain structure, and other ontologies. The topGO R library3, was used to determine local similarities and dependencies between GO terms in order to perform Elim pruning correction. Several database sources were referenced for enrichment analysis, including Interpro4, NCBI5, MSigDB6,7, REACTOME8, and WikiPathways9. Enrichment was calculated relative to a set of background genes relevant for the experiment (ACTB, GAPDH).

3 Results

3.1 Cytostatic effect of ICG-001 in human and mouse glioma cell lines *in vitro*

We initially tested the effects of the specific small molecule CBP/β-catenin antagonist ICG-001 *in vitro* as a single agent on 5 human PBT and 3 mouse glioma lines. Treatment with ICG-001 (0–10 μM) showed a concentration-dependent cytostatic effect in

10.3389/fimmu.2024.1342625

all tested human patient-derived glioma cell lines (PBT017, PBT030, PBT135, PBT144, and PBT147) (Figures 1A, D–F) and all murine-derived glioma cell lines (K-luc, GL261-parental, and GL261.IL13Rα2 engineered) (Figure 1B). We found that the KIF20A gene was downregulated in the PBT030 and PBT147 lines upon treatment of glioma cells with ICG-001 (Figure 1C). KIF20A, a mitotic kinesin, plays an important role in controlling the mode of division of neural progenitor cells (NPC) in both normal brain cells and brain tumor cells, and KIF20A knockdown induces a transition from proliferative to differentiative divisions in NPC (36, 37). Consistent with ICG-001-induced differentiation of PBT147 and PBT030 lines, ICG-001 treatment led to a significant reduction in the expression of *KIF20A*, as measured by qPCR (Figure 1C) (36), further confirming that the differentiating effects of ICG-001 on glioma lines are not cell line dependent. Additionally, all glioma lines exhibited a more differentiated phenotype based on their elongated cell morphology, with decreased proliferation and loss of clonal expansion, as shown by the PBT017.RFP human glioma cell line, imaged and quantified by Incucyte (Figures 1D–G). We also correlated human Wnt gene family with CD3 mRNAseq expression using public TCGA GBM datasets and RNA-seq data [downloaded from the GDC portal (https://portal.gdc.cancer.gov/)] (Supplementary Figures 1A, B). Upregulation of the Wnt pathway in glioma was inversely correlated with CD3 cell infiltration (Supplementary Figure 1B). A strong negative correlation was found among Wnt genes-APC, AXIN1, AXIN2, GSK3BTCF4 and CD3 score and a positive correlation was found for LEF1, CDC42 and CD3.

3.2 ICG-001 specifically targets Wnt/CBP/β-catenin transcription in glioma

Decreased expression of the Wnt/CBP/β-catenin target gene *BIRC5/Survivin*, with concomitant upregulation of the Wnt/p300/β-catenin target gene *EphB2*, is a hallmark of specific CBP/β-catenin inhibition (Figure 2A) (38). In our studies, we used *EphB2* and *BIRC5/Survivin* as a biomarker of the response to ICG-001. *BIRC5/Survivin* expression was also previously used as a biomarker for pharmacokinetic/pharmacodynamic (PK/PD) activity of the Wnt pathway in circulating tumor cells in the first-in-human clinical trial of the second-generation CBP/β-catenin specific antagonist PRI-724 (39). We demonstrated that *BIRC5/Survivin* gene expression was selectively downregulated and *EphB2* was upregulated in our experiments in both human and mouse glioma cell lines post ICG-001 treatment, as shown by qPCR, which was further confirmed using a Survivin-luciferase reporter assay for PBT017 and PBT030 cell lines *in vitro* (Figure 2B). ICG-001's selective effects on the expression of *BIRC5/Survivin* and *EphB2* serve as an indicator of on target activity *in vitro* in the human and mouse G261, GL261.IL13Ra2, and K-luc cell lines (Figures 2A, C).

3.3 ICG-001 specifically targets glioma cell metabolism via Wnt/CBP/β-catenin modulation

The N-termini of the two human Kat3 coactivators, CBP and p300, provide a highly evolutionarily conserved hub to integrate

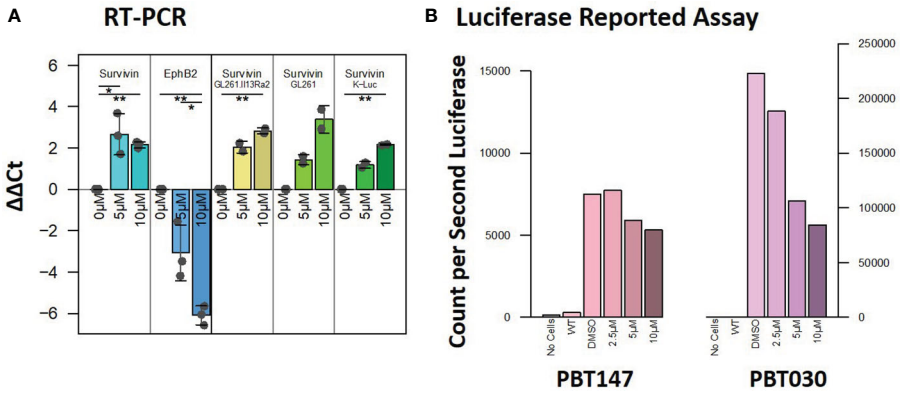

C ***BIRC5* and *EphB2* Expression in Glioma**

ICG-001	GL261/BIRC5	GL261-IL13/BIRC5	K-Luc/BIRC5	PBT030/BIRC5	PBT030/EphB2
0	0	0	0	0	0
5uM	1.4	2.1	1.2	2.7	-3.1
10uM	3.4	2.8	2.2	2.2	-6.1

FIGURE 2
Expression of the target genes *BIRC5/Survivin* and *EphB2* post-ICG-001 treatment (0, 5, 10 mM) as detected by RT-PCR and Luciferase Reporter Assay. **(A)** Survivin and *EphB2* mRNA levels in PBT017 and PBT030 human glioma lines and mouse GL-261 and K-Luc lines treated with ICG-001 for 3 days (0, 5, 10 μM). **(B)** Luciferase reporter assay indicating downregulation of luciferase reported gene in PBT017 and PBT030 cell lines upon treatment with ICG-001 at 0, 5, and 10 μM in triplicates. **(C)** *Survivin/BIRC5* relative expression upon treatment with ICG001. P values denoted by *<0.05, **<0.01, ***<0.001, ****<0.0001, *****<0.00001.

10.3389/fimmu.2024.1342625

multiple signaling cascades that coordinate cellular metabolism with the regulation of symmetric versus asymmetric division of somatic stem cells and cancer stem cells, cellular proliferation, and differentiation status and function (40). More specifically, small molecule inhibition of the N-terminal region of CBP enhances p300/β-catenin mediated transcription, which is a prerequisite for increased mitochondrial oxidative metabolism during the initiation of cellular differentiation (40, 41). To explore ICG-001's impact on metabolic changes associated with glioma differentiation after disrupting the CBP/β-Catenin interaction, we treated patient-derived GBM cell lines PBT147 and PBT030 with ICG-001 (0, 5, or 10 μM) for 24 and 72 h (Figure 3). RNA isolated from the treated PBT cells was analyzed using the NanoString nCounter metabolic panel (NanoString Technologies) (42). We used Rosalind software v.3.38.0.1 to analyze differential gene expression between PBT030 and PBT147 cell lines (Figures 3A–D). Furthermore, we analyzed gene and pathway expression in ICG-001 treated PBT samples as compared with untreated controls (Figures 3E, F). Statistically significant genes and pathways were analyzed using $\log_2$ Fold Change ≥ 1.5, < -1.5 and $-\text{Log}_{10}$ p-Adj <0.05 filter. First, we demonstrated differences between PBT030 and PBT147 patient-derived lines (X-axis shift on MDS plot) and that ICG-001 treatment caused a similar shift in gene expression on the Y-axis among untreated and ICG-001-treated cell lines (Figure 3A). We detected genes upregulated in PBT030 cells, such as SOX2, MYCN, NOS2, RUNX2, and VEGFA, while PBT147 cells upregulated level of PTEN, STAT6, CA9 and TLR2, demonstrating differences among PBT cell lines, which can be explained by various driving mutations and heterogeneity in glioma lines (Figures 3A–D and Supplementary Figures 2A, B).

Next, we tested if ICG-001 drives a similar metabolic shift in both lines. Fully consistent with our previous studies (40), we found similar changes in several genes and metabolic pathways after treatment of PBT030 and PBT147 with ICG-001–an increase in amino acid transporters, hypoxia, glutamine metabolism, MAPK, autophagy, mitochondrial respiration, cytokine and chemokine signaling, and arginine metabolism in both lines (Supplementary Figure 7). The PBT030 line demonstrated a decrease of tryptophan/kynurenine, fatty acid synthesis and oxidation, glycolysis, and the pentose phosphate pathway (Supplementary Figure 7). Similarly, in PBT147 lines treated with ICG-001, an increase in glutamine metabolism, autophagy, amino acid transport and synthesis, and MAPK, and strong down regulation in cell cycle, pentose phosphate, fatty acid synthesis, and oxidation was observed. (Supplementary Figure 7). This change in tumor cell metabolism may provide CD8 effector cells with the ability to effectively compete metabolically within the TME (43), which increases the likelihood of immune cell infiltration into the otherwise hostile TME (44). Consistent with our *in vitro* data (Figures 1 and 2), we also observed downregulation of cell cycle-

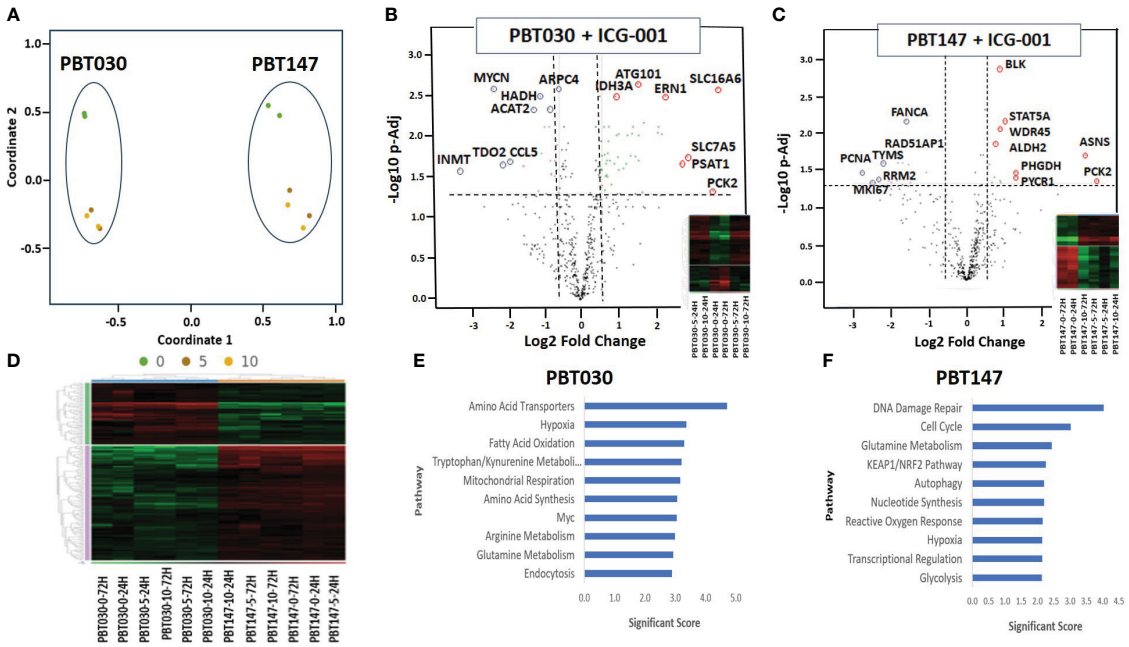

FIGURE 3
NanoString analysis of human metabolic pathways after treatment with ICG-001. **(A)** Multidimensional scaling (MDS) plot of visual representation of the patterns of proximities among PBT030 and PBT147 human cell lines treated with ICG-001 at 2 time points (24 hrs & 72 hrs) and 3 doses (0μM, 5μM, 10 μM) [n=2] separately on the Y-axis. X-axis indicated clustering of PBT030 and PBT147 cell lines each separately. **(B)** Volcano plot showing difference in expression for PBT030 between ICG-001 treated vs untreated, with the x-axis showing log2 fold change and the y-axis showing the negative log10 of p-adj value and heatmap; mRNA represented by red circles for significantly upregulated genes and blue circles for significantly down-regulated human genes. Full list of differentially expressed genes is shown in Supplementary Table 2 **(C)** Volcano plot showing difference in expression for PBT147 between ICG-001 treated vs untreated, with the x-axis showing log2 fold change and the y-axis showing the negative log10 of p-adj value and heatmap; mRNA represented by red circles for significantly upregulated genes and blue circles for significantly down-regulated genes. Full list of differentially expressed genes are shown in Supplementary Table 2. **(D)** Heat map of differentially expressed genes when comparing PBT030 and PBT147 cell lines (selected glioma gene list). **(E, F)** Bar chart of functional analysis showing the top 10 significance score predicted using ROSALIND Gene Set Analysis with NanoString annotations for PBT030 and PBT147 human cell lines treated with ICG-001.

related genes post ICG-001 treatment in PBT030 (PRIM2, NPM1) and PBT147 cell lines (including KIAA0101-PCNA, MKI67, RRM2, TYMS, CLSPN, CDCA8, UBE2C, EXO1, BRCA1, BRCA2, BRIP1, and PRIM1), which is associated with cytostasis and metabolic changes required for the switch from proliferation to differentiation (Figures 3B, C) (40). Fatty acid oxidation–the metabolic pathway preferred by quiescent stem-like cells (45)—was decreased in all treated cell lines at all timepoints and all doses. Furthermore, ALDH2 (PBT147), ACAT2, and HADH were downregulated in PBT030 cells, indicating that CBP/β-Catenin inhibition directs GSC activation and differentiation via metabolic reprogramming. These metabolic changes have been shown to be critical for the transition of quiescent to activated CSC (46) and their subsequent differentiation to bulk tumor cells (36). Upregulation of the p53 tumor suppressive pathway and mitochondrial respiration (up-PBT030-PPARGC1A, MCP1, PDP1, ME2, IDH3A, UQCR11, FAHD1, SOD2, and ATP6V1F), and glutamine metabolism (up-PBT030-PSAT1, GOT1, SERINC1; PBT147-ASNS, PYCR1, and PHGDH)—hallmarks of cell differentiation–were also observed at both time points, at both the 5- and 10-μM doses and in both cell lines (Supplementary Figure 2). A full list of up and downregulated genes with $\log_2$ Fold Change ≥ 1.5, < -1.5 and -Log_{10} p-Adj 0.05 filter is shown in Supplementary Figure 2. Selected data is shown for PBT147 and PBT030 in Figures 4B, C, E, F, and Supplementary Figure 7.

3.4 Proteomic analysis of glioma cell lines PBT147 and PBT030 upon treatment with ICG-001

To see the effect of ICG-001 treatment on the protein level in glioma cell lines, PBT147 and PBT030 cells were treated with ICG-001 at 0, 5, and 10 μM for 72 h (Figure 4). We collected cells and conducted global proteomic analyses after treatment (Figure 4). Using 2-DICAL, we detected 1,553 common proteins expressed in both PBT030 and PBT147 lines (47). The resulting data was quantile normalized and differential protein expression was further analyzed by ANOVA. Differentially expressed proteins were subjected to pathway enrichment analysis utilizing the KEGG database. Pathways with statistically significant enrichment (p-value <0.0001) following 5 μM or 10 μM ICG-001 treatments are represented in Figure 4. Both PBT147 and PBT030 cell lines demonstrated upregulation of pathways involved in neurogenesis, autophagy, regulation of the actin skeleton, and protein synthesis in the ER (Figures 4A, B). Consistent with the activation of quiescent stem-like cells, ICG-001 treatment of PBT147 and PBT030 induced metabolic reprogramming with increased ATP production, and an increase in protein translation and differentiation (48) (Supplementary Figure 3). Specifically, we found increased protein expression of APOD (lipid metabolism and neuroprotection), AAAS (metabolic protein transport), MFGM (promotes phagocytosis of apoptotic cells, wound healing), PDPR (metabolism), PGM1 (metabolism-glycosylation), RRAGA (metabolism), RRAGB (regulator of TOR signaling), RTC1 (metabolism), SERC, and SYMC, and downregulation of MCM6 (cell cycle, DNA replication), GSTM5 (oxidative stress, metabolism), SORCN (Proto-oncogene), FADS2 (fatty acid metabolism), and PSD7 (cytoskeletal remodeling) upon treatment of PBT147 and PBT030 with ICG-001. We postulate that these metabolic changes in tumor cells post ICG-001 treatment, leading towards a more differentiated glioma phenotype, modulate the TME and influence CAR T cell efficacy.

3.5 ICG-001 specifically enhances tumor T cell recruitment

We anticipated that modulation of the cold TME by ICG-001 should enhance the recruitment of T cells into the TME, because upregulation of the Wnt pathway has been shown to be involved in immune evasion (Figure 5) (49). To test this hypothesis, we used a subcutaneous model of syngeneic K-Luc glioma cells implanted into C57BL/6 mice. Mice received 1×10^6 tumor cells and were either untreated or treated with ICG-001 on day 7 after tumor implantation (delivered by subcutaneous Alzet minipumps, 50 mg/kg/day) (Figures 5A–C). The tumors were harvested and evaluated for

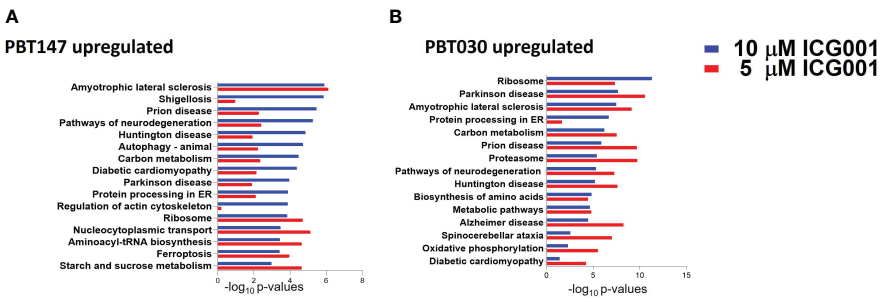

FIGURE 4
Proteomics analysis of PBT147 and PBT030 cell lines treated with ICG-001 (0-10 μM) for 72h. **(A)** Up-regulated protein density was calculated by the difference in log normalized levels for each protein between the four treated samples (ICG001 5, 10 mM at 24 and 72h) and the appropriate untreated sample control. **(B)** Calculating the difference in log levels corresponds to the log of the fold changes in each pathway. For both cell lines, the log fold-change is plotted for each protein at 5 μM against the log fold-change at 10 μM. These plots are shown in **(A)**, with the points color-coded by ICG001 concentrations. This highlights a positive linear relationship between the log fold changes at 5μM and 10μM in both cell lines. The dose effect is significantly greater in PBT030 than PBT147, with the same increase in dose, usually resulting in a greater fold-change.

10.3389/fimmu.2024.1342625

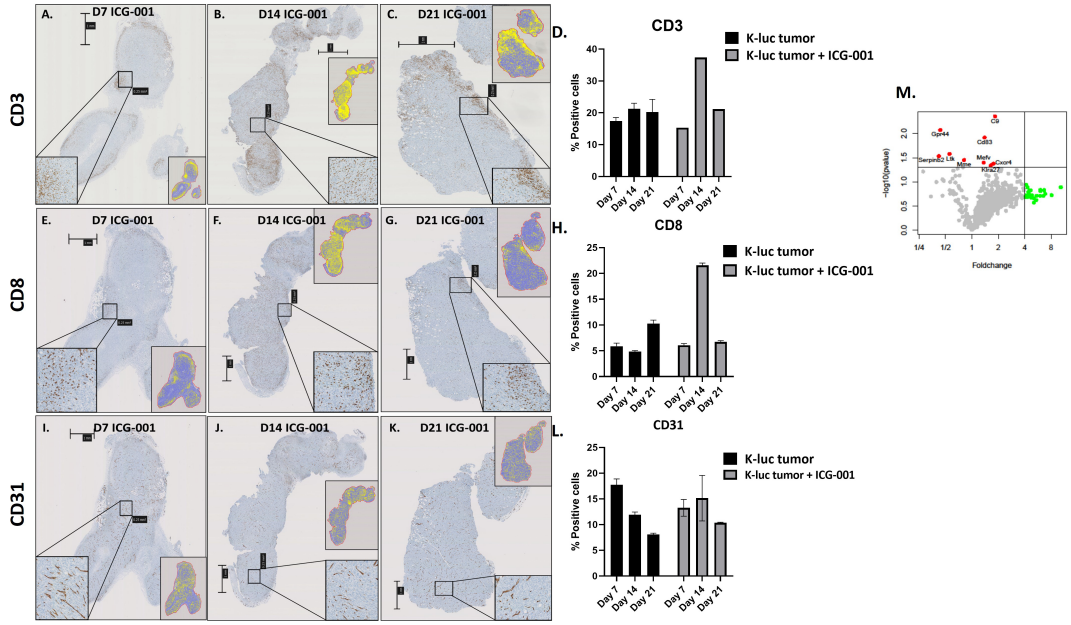

FIGURE 5
IHC analysis of immune cells in syngeneic models of subcutaneous glioma (K-Luc). **(A–C, E–G, I–K)** Mice bearing subcutaneous K-luc glioma tumors were treated with ICG-001 (50 mg/kg/day) for 7, 14, or 21 days using Alzet minipumps. At the end of treatment, tumor tissue was excised and IHC stained for CD3 cells to evaluate recruitment and patterns of CD3, CD8, and CD31 distribution. **(D, H, L)** Quantification of tumor coverage was performed using QuPath for mouse CD3, CD8, and CD31 positive cells on days 7, 14, 21 post minipump implantation. Pairwise comparison was performed to access the CD31 expression on days 7, 14 and 21 (P-value 0.314, 0.624, 0.0016 respectively). Control animals were treated with no pumps. Scale bars are SD of duplicate sections (n=4). **(M)** NanoString analysis of mouse immune panel genes in subcutaneous K-Luc tumors at days 7 and 21, as compared with untreated controls (untreated tumors were also collected on days 7 and 21).

CD3, CD8, and CD31 by immunohistochemistry (IHC) on days 7, 14, and 21 post-Alzet minipump implantation (ICG-001 release by Alzet pump continues for 28 days post implantation) and compared to the tumors from untreated controls that were harvested on the same days (Figures 5E–G, I–K). We observed an increase in host immune cells, including $CD3^+$ and $CD8^+$ T cells, infiltrating tumors by day 14 post-ICG-001 treatment (Figures 5D, H). A time-dependent increase in CD31 expression was also observed, when compared with controls (Figure 5L).

NanoString gene expression analysis of subcutaneous tumors from ICG-001-treated mice (daily release of ICG-001 by Alzet pump is 50 mg/kg/day) versus untreated (harvested on the same days 7, 14, 21) tumors identified genes that were significantly upregulated ($p \leq 0.05$), such as C9, CD83, Gpr44, Cxcr4, and others (Figure 5M and Supplementary Table 1) with a demonstrated fold-change increase (>=4) such as Dmbt1, Nsr1, Irf4, Klrg1, Gzmb, and others (Figure 5M). On day 7 and 14 post Azlet pump implantation, we observed upregulation of tumor suppressor gene DMBT1 and the chemotactic factor CCL24, which displays chemotactic activity on resting T lymphocytes, and both GZMA and GMZB, which are associated with cytotoxic T cell activation on day 7 and 14 post Alzet pump implantation (Supplementary Table 1) was observed. These results further support our hypothesis that specific downregulation of Wnt/CBP/β-catenin signaling along with reprogramming of the TME may enhance the efficacy of tumor immunotherapy, increase recruitment of host T-cells, and improve immunotherapy to solid tumors (50).

3.6 ICG-001 treatment regimen added before or after CAR T cell therapy in intracranial, syngeneic K-luc glioma

To understand the effect of ICG-001 on tumor metabolism alone and in combination with IL13Rα2–CAR T cells, we established orthotopic immunocompetent mouse models of syngeneic glioma using K-Luc glioma cells and engineered murine IL13Rα2-targeted CAR T cells (51). The murine IL13Rα2- targeted CAR T cells (mIL13BBζ CAR T cells) were characterized by FACS and contained comparable numbers of CD4+ and CD8+ T-cell subsets, with a mixture of early memory (CD62L+) and effector (CD62L–) T-cell populations, as described previously (51). We developed intracranial tumors by administration of K-luc glioma cells (0.1×10^6) into the right frontal lobe of C57BL/6 mice. The K-luc tumor line derived from a spontaneous glioma arising from *Nf1, Trp53* mutant mice (KR158) is poorly immunogenic, as indicated by its unresponsiveness to anti–PD-1 checkpoint therapy (52). This line has been further engineered to express the murine IL13Rα2 and used to recapitulate invasive glioma in syngeneic mouse models. On day 14 post-tumor implantation, mice received intratumoral administration of CAR T cells at a sub-therapeutic dose (1×10^6) (cF11240 Mouse T cell mIL13-mCD8h-mCD8tm3-m41BB-mZeta-T2A-mCD19t(CO)_MSCV) (n=14). Treatment groups were as follows: 1) Tumor only [GR1]; 2) Tumor + ICG-001 (D16-[MI-GR2]); 3) Tumor + CAR Ts (D14–[MC-GR3]); 4) Tumor + CAR Ts (D14) and ICG-001 (D16—[MCI-GR4]) (n=14); 5) Tumor + ICG-001 (D7)+ CAR Ts (D14–

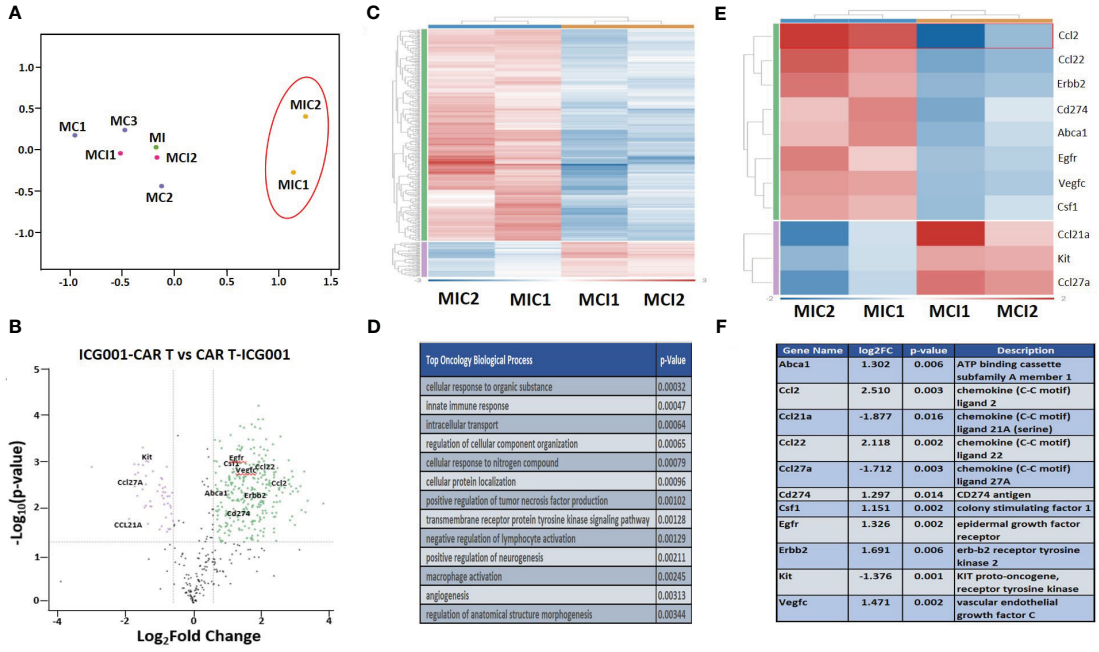

Top Oncology Biological Process	p-Value
cellular response to organic substance	0.00032
innate immune response	0.00047
intracellular transport	0.00064
regulation of cellular component organization	0.00065
cellular response to nitrogen compound	0.00079
cellular protein localization	0.00096
positive regulation of tumor necrosis factor production	0.00102
transmembrane receptor protein tyrosine kinase signaling pathway	0.00128
negative regulation of lymphocyte activation	0.00129
positive regulation of neurogenesis	0.00211
macrophage activation	0.00245
angiogenesis	0.00313
regulation of anatomical structure morphogenesis	0.00344

Gene Name	log2FC	p-value	Description
Abca1	1.302	0.006	ATP binding cassette subfamily A member 1
Ccl2	2.510	0.003	chemokine (C-C motif) ligand 2
Ccl21a	-1.877	0.016	chemokine (C-C motif) ligand 21A (serine)
Ccl22	2.118	0.002	chemokine (C-C motif) ligand 22
Ccl27a	-1.712	0.003	chemokine (C-C motif) ligand 27A
Cd274	1.297	0.014	CD274 antigen
Csf1	1.151	0.002	colony stimulating factor 1
Egfr	1.326	0.002	epidermal growth factor receptor
Erbb2	1.691	0.006	erb-b2 receptor tyrosine kinase 2
Kit	-1.376	0.001	KIT proto-oncogene, receptor tyrosine kinase
Vegfc	1.471	0.002	vascular endothelial growth factor C

FIGURE 6
NanoString analysis of nCounter mouse Pan Cancer immune profile gene expression within ICG-001, CAR T, CAR T + ICG-001 and ICG-001 + CAR T treatment groups. **(A)** Multidimensional scaling (MDS) plot for the samples treatments with ICG001[MI] (ICG001 only), 3 treatments with CAR Ts [MC] (CART only), 2 treatments with ICG001 and then CAR Ts [MIC] (ICG001 first then CART), and 2 treatments with CAR Ts and ICG001 [MCI] (CART first then ICG001). **(B)** Volcano plot showing difference in expression of |Fold Change|>1.5 & p-value<0.05 between ICG001-CAR T and CAR T-ICG001 treated mice, with the x-axis showing log2 fold change using cutoff and the y-axis showing the negative log10 of p-value for the 11 selected mouse brain tumor genes of interest. **(C)** Heatmap of differential expression gene comparison between ICG001 + CAR T and CAR T + ICG001 using filtering |FC |≥ 1.5 & p-value ≤ 0.05 label highlighted. **(D)** The top statistic significant ROSALIND oncology collection biologic process based on the differential expression gene expression comparison between ICG001 + CAR T and CAR T + ICG001. **(E)** The heatmap of differential expression gene comparison between ICGCART & CARTICG for the 11 selected brain tumor genes of interest which are also labelled on Volcano plot. **(F)** The description and log2(fold change) & p-value for the 11 selected brain tumor genes of interest.

[MIC-GR5]). Tumor-bearing mice in GR5 were pretreated with ICG-001 (starting on Day 7 post tumor implantation for 28 days) 1 week prior to CAR T administration [MIC-GR5]. ICG-001 was given via Alzet subcutaneous minipump delivering a dose of 50 mg/kg/day over 28 days. Otherwise, pumps were implanted on day 16, 2 days post CAR T administration (D14) in the treatment group GR4. Mice were monitored until they developed tumors larger than 0.5 cm^2. Normalized RNA concentration per tumor tissue (1 mg) was used for NanoString analysis. NanoString pathway analysis revealed the top genes that were up- or downregulated in CAR T vs CAR T + ICG-001 groups using a mouse immune panel to detect metabolic changes in mouse K-luc tumors and to visualize endogenous immune cells infiltration upon inhibition of Wnt with ICG-001 (nCounter_Mouse_PanCancer_Immune_Profiling_Panel). Once tumors reached the predetermined criteria for euthanasia, they were harvested, isolated, and subjected to IHC and NanoString analysis to detect differentially expressed genes in ICG + CAR T [MIC-GR5] versus CAR T + ICG-001[MCI-GR4] (Figure 6). Rosalind analysis (https://www.rosalind.bio) revealed that gene expression of all CAR T, ICG001, and CAR T+ ICG-001 treated tumors were clustered together on the MDS plot, whereas ICG-001 pretreated and CAR T treated tumors demonstrated very different gene expression profiles on the MDS plot (Figure 6A). The volcano plot shows difference in expression of selected genes between ICG-001 + CART versus CART+ ICG-001 with the x-axis of log2 fold change and y-axis of the negative log10 of p-value. We observed downregulation of Kit, CD27A, and CCl23A, and upregulation of CCL2, VEGFC, Erbb2, Cd274, CCL22, and CSF1, contributing to improved T cell trafficking (Figure 6B). The full list of differentially regulated genes is presented in Supplementary Table 1. The top up and downregulated genes are displayed in Figures 6E, F and the top biological processes affected are displayed in Figure 6D. These changes demonstrate the reprogramming of tumors pre-treated with ICG-001 and then CAR T and changes in metabolic pathways and genes, shifting to a more differentiated, immune responsive tumor.

3.7 ICG-001 treatment regimen affects immune cell infiltration when added before or after CAR T cell therapy: cell line profiling using NanoString analysis

Next, we compared CD45, Macrophages, and NK cell infiltration within tumors treated with 2 different schedules of administration of ICG-001 [CAR T + ICG001[GR4] versus ICG-001 + CAR Ts[GR5]]. We compared groups treated with ICG-001 only, CAR T only, and CAR T [D14] + ICG-001[D16] in comparison with ICG-001[D7] only or CAR T only treated groups[D14]. We found increased infiltration of CD45+ macrophages and NK-CD56dim (natural killer cells responsible

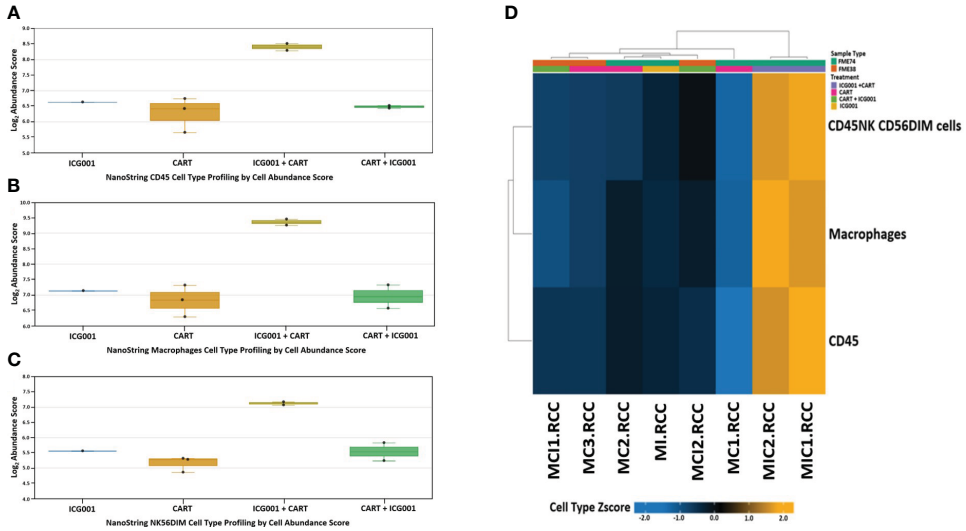

FIGURE 7
NanoString nCounter mouse cell line PanCancer immune profiling: Genes previously shown to be characteristic of various cell populations by measuring cells population abundance based on the NanoString Cell Type Profiling Module. **(A–C)** Bar graph charts showing abundance scores of CD45, NK-CD56, and Macrophage cell type populations across all samples for genes that are characteristic and grouped by cell population abundance. **(D)** Heat map of gene clustering and cell profile in groups treated with ICG001 (MI), CAR T + ICG001 (MCI1, MCI2), ICG001+ CAR Ts (MIC1, MIC2), and CAR Ts only (MC1, MC2, MC3). Genes previously shown to be characteristic of CD45, NK-CD56, and Macrophage cell population abundance across all samples for ICG001+ CAR Ts (MIC1, MIC2) shows positive Z-score differently comparing from samples of ICG001 (MI), CAR T + ICG001 (MCI1, MCI2), and CAR Ts only (MC1, MC2, MC3) with negative Z-score.

for cytolytic activity and target cell killing) cells in the ICG-001 +CAR T group [GR5] (Figures 7A–D). Cell type profiler analysis identified clearly different immune cell infiltration in the GR5 [ICG-001 + CAR T] treated group when compared with controls (GR1 [ICG001], GR2 [CAR T], and GR4 [CAR T + ICG001] treated groups). We also observed an increase in the expression of the gene PTPRC encoding CD45RA that plays role in lymphocyte function, and an increase in KLRG1- cells contributing to an increase in all memory T cell lineages, including peripheral memory and tissue-resident memory cells, which should enhance long-term protective immunity (53) (Supplementary Figure 4A). Upregulation of the SELL (aka E-selectin CD62L) gene T_{scm} CD45RA$^+$, IL7R$^+$, CCR7$^+$, CD62L$^+$, KLRG$^-$ was found within a group treated with ICG-001 first and then CAR T [ICG001 + CAR T], which is a marker associated with the T cell memory phenotype (Supplementary Figure 4B). We also found upregulation of IL7R- Interleukin-7 receptor (IL7R), which provides the potential for long-term survival of both CD62L^{high} central memory T cells and Th1 effector cells (Supplementary Figure 4C) (54). CCR7 is important in the migration of memory CD8+ T cells and survival in their niches (Supplementary Figures 4D, E).

3.8 Combination of ICG-001 with CAR T cells enhances cytotoxicity to glioma *in vitro*

We next tested the efficacy of a titrated dose of CAR T cells ± ICG-001 to induce tumor cell killing *in vitro* (Supplementary Figure 5). We evaluated the combination of HER2-engineered CAR T (HER2-CAR T) cells and PBT106 tumor cells (high expressing HER2) in combination with IGC-001 using an *in vitro* co-culture assay. ICG-001, in combination with HER2-CAR T cells, demonstrated synergistic cytotoxicity in several patient-derived glioma lines that expressed high levels of the tumor antigen HER2 (Supplementary Figure 5). ICG-001 combined with HER2-CAR T cells demonstrated synergistic killing in a CAR T cell concentration-dependent fashion (Supplementary Figure 5A). Enhanced killing was observed with the combination of HER2-CAR T cells and ICG-001 at effector/target cell ratios of both 1:2 and 1:4 (Supplementary Figures 5B, C). Furthermore, CBP/β-catenin antagonism with ICG-001 was not toxic to T cells *in vitro* or *in vivo*, providing important insights for the advancement of CAR T cell therapy combined with CBP/β-catenin antagonism for the treatment for brain tumors (Supplementary Figure 6).

4 Discussion

Tumors evolve a variety of mechanisms to escape immune surveillance, including evading immune recognition, promoting regulatory cell expansion, coopting inhibitory signals, and secreting suppressive factors. Impressive results in a subset of cancers have been obtained using immunotherapies such as checkpoint inhibitors (i.e. anti-CTLA4, anti-PD-1, and anti-PD-L1) and CAR T therapies. Still, only a subset of patients respond to these immunotherapies, and the response rate in certain tumor types, including glioma, is very low, and relapse remains a significant concern (55). The Wnt/β-catenin signaling pathway, which is a critical regulator of both somatic stem cells and cancer

stem/tumor initiating cells, has been correlated with resistance to radiation and cytotoxic and targeted chemotherapy. Wnt/β-catenin pathway signaling is also correlated with immunotherapy resistance in melanoma (15, 56, 57) and across other tumor types (12). Tumor-intrinsic Wnt/β-catenin signaling mediates cancer immune evasion by preventing T-cell and/or dendritic cell infiltration, migration, and function, and thereby resistance to immunotherapies (12, 13, 16, 58).

Wnt/β-catenin signaling also plays an essential role in the development and maintenance of multiple organ systems, including the brain. A dichotomous role for Wnt signaling in stem cells, organ development, maintenance, and repair is a commonly observed phenomenon, with Wnt signaling playing critical roles in the processes of both cell proliferation and differentiation. We have previously demonstrated that aberrant Kat3 coactivator usage (i.e., enhanced CBP usage at the expense of p300 by β-catenin) is responsible for the improper termination of the wound healing process by maintaining epithelial cell proliferation and inhibiting differentiation (59). Small molecule CBP/β-catenin antagonists, which target a fundamental control switch in stem cell biology, can overcome cytotoxic or targeted chemotherapy and immunotherapy resistance (28, 60) through forced symmetric differentiation, thereby eliminating CSCs while having beneficial effects on the normal somatic stem cell population, which preferentially divides asymmetrically (25, 59). By binding with high affinity (K_d~1nM) and specificity to the N-terminus of CBP, the small molecule CBP/β-catenin antagonist ICG-001 can safely correct aberrant Wnt signaling to initiate differentiation via p300/β-catenin transcription (25).

The concept of combining a specific small molecule CBP/β-catenin antagonist with immunotherapy to reverse Wnt/β-catenin-mediated cancer immune evasion has been previously explored preclinically in NAFLD-associated liver cancer (60) and colorectal cancer to liver metastasis (28). However, using a CBP/β-catenin antagonist to induce the differentiation of GSC without damaging effects on somatic stem cells (41) is novel. Although ICG-001 has high biochemical specificity for the N-terminus of CBP, its mechanism of action is highly pleiotropic via the modulation of enhancers and super-enhancers in multiple cell types beyond tumor cells themselves, including mesenchymal, endothelial, and immune cell populations (40, 59, 61).

In using human glioma xenograft models with patient-derived tumors in [NSG NOD-*scid* IL2Rgamma^{null}] mice, we previously found that IL13BBζ-CAR T cells improved anti-tumor activity and T cell persistence as compared to first-generation IL13ζ-CAR CD8(+) T cells that had shown evidence for bioactivity in patients (21). However, our studies were not limited by the tumor target-specific CARs, and can be expanded to various CAR therapies as well (62). To overcome known limitations of the use of CAR T cell therapy for glioma, such as antigen escape and the need for increased T cell persistence and potency, in the current manuscript, we tested a novel combination therapeutic approach with the Wnt/CBP/β-catenin antagonist ICG-001 to enhance the expression of genes involved in antigen presentation and the adaptive immune response.

Establishing the proof-of-concept that ICG-001 can safely target aberrant Wnt/β-catenin signaling in glioma in combination with CAR T cell therapy could provide a novel means of broadening the tumor response to CAR T cell therapy while decreasing the resistance and relapse arising post-CAR T cell therapy in solid tumors. However to date, targeting aberrant Wnt signaling clinically with anything other than a specific CBP/β-catenin antagonist has demonstrated significant on-target associated toxicities (59). We also separately analyzed the immune subsets and Wnt/β-catenin pathway activation in the TME of brain tumors [BTs] in preclinical models using novel techniques such as gene expression profiles and proteomics to elucidate downstream target genes.

Key genes involved in glioma cell differentiation, including ASCL1 and PTPRZ1-MET, have been shown to contribute to the development of a glioma stem cell phenotype, which is thought to be the source of resistance and relapse after initial treatment with checkpoint inhibitors (63, 64). Furthermore, reprogramming the immune landscape with a single gene in non-cancer cells identified S100A8 as a regulator of an immune suppressive T and myeloid cell subtype (65). We have also demonstrated infiltration of CD45, Macrophages, and NK cells into the tumor stroma, and upregulation of KLRG1, Sell, Ccr7, and IL7r upon the treatment with ICG-001 and then CAR Ts (66).

5 Conclusion

These studies have demonstrated that CBP/β-catenin antagonists induce significant differences in the expression of genes and proteins involved in proliferation and differentiation of tumor cells and of critical metabolic pathways. These promising studies provide the basis for future development of this multi-targeted approach, with the goal of developing a breakthrough treatment for patients with brain tumors.

Data availability statement

The original contributions presented in the study are publicly available. This data can be found via the following link: https://www.ncbi.nlm.nih.gov/geo/query/acc.cgi?acc=GSE252155.

Ethics statement

The animal study was approved by Institutional AnimalAnimal Care and Use Committee 18059. The study was conducted in accordance with the local legislation and institutional requirements.

Author contributions

MG: Conceptualization, Data curation, Resources, Supervision, Writing – original draft, Writing – review & editing, Investigation, Methodology, Project administration. JH: Data curation, Formal

analysis, Investigation, Methodology, Writing – original draft, Validation, Visualization. EMa: Investigation, Methodology, Validation, Visualization, Writing – review & editing. HN: Data curation, Investigation, Methodology, Writing – review & editing. VA: Data curation, Formal analysis, Investigation, Methodology, Writing – review & editing. NC: Data curation, Formal analysis, Writing – review & editing. RQ: Data curation, Methodology, Writing – review & editing. CN: Data curation, Methodology, Writing – review & editing. EMe: Data curation, Investigation, Methodology, Writing – review & editing. BA: Data curation, Funding acquisition, Investigation, Methodology, Writing – review & editing. RS: Data curation, Methodology, Project administration, Writing – review & editing. MO: Data curation, Writing – review & editing, Formal analysis. HY: Methodology, Writing – review & editing, Software, Data curation, Funding acquisition. RR: Formal analysis, Investigation, Writing – review & editing, Conceptualization, Methodology, Software, Validation. NB: Investigation, Formal analysis, Writing – review & editing. YCY: Data curation, Formal analysis, Investigation, Methodology, Software, Visualization, Writing – review & editing. CB: Conceptualization, Data curation, Investigation, Supervision, Writing – review & editing, Formal analysis, Funding acquisition, Resources. MK: Data curation, Formal analysis, Writing – review & editing, Conceptualization, Investigation, Project administration, Supervision, Validation, Visualization, Writing – original draft.

Funding

The author(s) declare financial support was received for the research, authorship, and/or publication of this article. This work was supported by the Andrew McDonough B+ Foundation, Uncle Kory Foundation, National Institutes of Health grants P30CA033572 and the Albert & Bettie Sacchi Foundation (MG). Research reported in this publication included work performed in the Research Pathology Services and Light Microscopy & Digital Imaging Shared Resources supported by the National Cancer Institute of the NIH under grant number P30CA033572.

Acknowledgments

The authors would like to acknowledge the CoH Center for Informatics and for the utilization of the POSEIDON platforms for data exploration, visualization, analysis, and discovery. The authors also acknowledge the technical expertise of Dr. Brian Armstrong and the professional editing of Dr. Erin S. Keebaugh.

Conflict of interest

MK is a cofounder and holds equity in 3 + 2 Pharmaceuticals.

The remaining authors declare that the research was conducted in the absence of any commercial or financial relationships that could be construed as a potential conflict of interest.

Publisher's note

Author disclaimer

The content is solely the responsibility of the authors and does not necessarily represent the official views of the National Institutes of Health.

Supplementary material

The Supplementary Material for this article can be found online at: https://www.frontiersin.org/articles/10.3389/fimmu.2024.1342625/full#supplementary-material

References

1. Sharma P, Siddiqui BA, Anandhan S, Yadav SS, Subudhi SK, Gao J, et al. The next decade of immune checkpoint therapy. *Cancer Discovery* (2021) 11(4):838–57. doi: 10.1158/2159-8290.CD-20-1680

2. Zhao J, Chen AX, Gartrell RD, Silverman AM, Aparicio L, Chu T, et al. Immune and genomic correlates of response to anti-PD-1 immunotherapy in glioblastoma. *Nat Med* (2019) 25(3):462–9. doi: 10.1038/s41591-019-0349-y

3. Muldoon LL, Soussain C, Jahnke K, Johanson C, Siegal T, Smith QR, et al. Chemotherapy delivery issues in central nervous system Malignancy: a reality check. *J Clin Oncol* (2007) 25(16):2295–305. doi: 10.1200/JCO.2006.09.9861

4. Martin-Orozco E, Sanchez-Fernandez A, Ortiz-Parra I, Ayala-San Nicolas M. WNT signaling in tumors: the way to evade drugs and immunity. *Front Immunol* (2019) 10:2854. doi: 10.3389/fimmu.2019.02854

5. Kahlert UD, Maciaczyk D, Doostkam S, Orr BA, Simons B, Bogiel T, et al. Activation of canonical WNT/beta-catenin signaling enhances *in vitro* motility of glioblastoma cells by activation of ZEB1 and other activators of epithelial-to-mesenchymal transition. *Cancer Lett* (2012) 325(1):42–53. doi: 10.1016/j.canlet.2012.05.024

6. Kahlert UD, Suwala AK, Koch K, Natsumeda M, Orr BA, Hayashi M, et al. Pharmacologic Wnt inhibition reduces proliferation, survival, and clonogenicity of glioblastoma cells. *J Neuropathol Exp Neurol* (2015) 74(9):889–900. doi: 10.1097/NEN.0000000000000227

7. Kahlert UD, Bender NO, Maciaczyk D, Bogiel T, Bar EE, Eberhart CG, et al. CD133/CD15 defines distinct cell subpopulations with differential *in vitro* clonogenic activity and stem cell-related gene expression profile in *in vitro* propagated glioblastoma multiforme-derived cell line with a PNET-like component. *Folia Neuropathol* (2012) 50(4):357–68. doi: 10.5114/fn.2012.32365

8. Huang M, Zhang D, Wu JY, Xing K, Yeo E, Li C, et al. Wnt-mediated endothelial transformation into mesenchymal stem cell-like cells induces chemoresistance in glioblastoma. *Sci Transl Med* (2020) 12(532):eaay7522. doi: 10.1126/scitranslmed.aay7522

9. Paw I, Carpenter RC, Watabe K, Debinski W, Lo HW. Mechanisms regulating glioma invasion. *Cancer Lett* (2015) 362(1):1–7. doi: 10.1016/j.canlet.2015.03.015

10. Miranda A, Hamilton PT, Zhang AW, Pattnaik S, Becht E, Mezheyeuski A, et al. Cancer stemness, intratumoral heterogeneity, and immune response across cancers. *Proc Natl Acad Sci U S A* (2019) 116(18):9020–9. doi: 10.1073/pnas.1818210116

11. Zhang M, Wang D, Su L, Ma J, Wang S, Cui M, et al. Activity of Wnt/PCP regulation pathway classifies patients of low-grade glioma into molecularly distinct subgroups with prognostic difference. *Front Oncol* (2021) 11:726034. doi: 10.3389/fonc.2021.726034

12. Luke JJ, Bao R, Sweis RF, Spranger S, Gajewski TF. WNT/beta-catenin pathway activation correlates with immune exclusion across human cancers. *Clin Cancer Res* (2019) 25(10):3074–83. doi: 10.1158/1078-0432.CCR-18-1942

13. Gajewski TF, Corrales L, Williams J, Horton B, Sivan A, Spranger S. Cancer immunotherapy targets based on understanding the T cell-inflamed versus non-T cell-inflamed tumor microenvironment. *Adv Exp Med Biol* (2017) 1036:19–31. doi: 10.1007/978-3-319-67577-0_2

14. Tao W, Chu C, Zhou W, Huang Z, Zhai K, Fang X, et al. Dual Role of WISP1 in maintaining glioma stem cells and tumor-supportive macrophages in glioblastoma. *Nat Commun* (2020) 11(1):3015. doi: 10.1038/s41467-020-16827-z

15. Spranger S, Bao R, Gajewski TF. Melanoma-intrinsic beta-catenin signalling prevents anti-tumour immunity. *Nature* (2015) 523(7559):231–5. doi: 10.1038/nature14404

16. Chen P, Hsu WH, Han J, Xia Y, DePinho RA. Cancer stemness meets immunity: from mechanism to therapy. *Cell Rep* (2021) 34(1):108597. doi: 10.1016/j.celrep.2020.108597

17. Wiese M, Hamdan FH, Kubiak K, Diederichs C, Gielen GH, Nussbaumer G, et al. Combined treatment with CBP and BET inhibitors reverses inadvertent activation of detrimental super enhancer programs in DIPG cells. *Cell Death Dis* (2020) 11(8):673. doi: 10.1038/s41419-020-02800-7

18. Brown CE, Badie B, Barish ME, Weng L, Ostberg JR, Chang WC, et al. Bioactivity and safety of IL13Ralpha2-redirected chimeric antigen receptor CD8+ T cells in patients with recurrent glioblastoma. *Clin Cancer Res* (2015) 21(18):4062–72. doi: 10.1158/1078-0432.CCR-15-0428

19. Brown CE, Alizadeh D, Starr R, Weng L, Wagner JR, Naranjo A, et al. Regression of glioblastoma after chimeric antigen receptor T-cell therapy. *N Engl J Med* (2016) 375(26):2561–9. doi: 10.1056/NEJMoa1610497

20. Priceman SJ, Tilakawardane D, Jeang B, Aguilar B, Murad JP, Park AK, et al. Regional delivery of chimeric antigen receptor-engineered T cells effectively targets HER2(+) breast cancer metastasis to the brain. *Clin Cancer Res* (2018) 24(1):95–105. doi: 10.1158/1078-0432.CCR-17-2041

21. Brown CE, Aguilar B, Starr R, Yang X, Chang WC, Weng L, et al. Optimization of IL13Ralpha2-targeted chimeric antigen receptor T cells for improved anti-tumor efficacy against glioblastoma. *Mol Ther* (2018) 26(1):31–44. doi: 10.1016/j.ymthe.2017.10.002

22. Zhang X, Zhang W, Mao XG, Zhen HN, Cao WD, Hu SJ. Targeting role of glioma stem cells for glioblastoma multiforme. *Curr Med Chem* (2013) 20(15):1974–84. doi: 10.2174/0929867311320150004

23. Portela M, Venkataramani V, Fahey-Lozano N, Seco E, Losada-Perez M, Winkler F, et al. Glioblastoma cells vampirize WNT from neurons and trigger a JNK/MMP signaling loop that enhances glioblastoma progression and neurodegeneration. *PloS Biol* (2019) 17(12):e3000545. doi: 10.1371/journal.pbio.3000545

24. Kahn M. Wnt signaling in stem cells and cancer stem cells: A tale of two coactivators. *Prog Mol Biol Transl Sci* (2018) 153:209–44. doi: 10.1016/bs.pmbts.2017.11.007

25. Kahn M. Can we safely target the WNT pathway? *Nat Rev Drug Discovery* (2014) 13(7):513–32. doi: 10.1038/nrd4233

26. Spranger S, Dai D, Horton B, Gajewski TF. Tumor-residing Batf3 dendritic cells are required for effector T cell trafficking and adoptive T cell therapy. *Cancer Cell* (2017) 31(5):711–23 e4. doi: 10.1016/j.ccell.2017.04.003

27. Horton BL, Williams JB, Cabanov A, Spranger S, Gajewski TF. Intratumoral CD8(+) T-cell apoptosis is a major component of T-cell dysfunction and impedes antitumor immunity. *Cancer Immunol Res* (2018) 6(1):14–24. doi: 10.1158/2326-6066.CIR-17-0249

28. Osawa Y, Kojika E, Nishikawa K, Kimura M, Osakaya S, Miyauchi H, et al. Programmed cell death ligand 1 (PD-L1) blockade attenuates metastatic colon cancer growth in cAMP-response element-binding protein (CREB)-binding protein (CBP)/beta-catenin inhibitor-treated livers. *Oncotarget* (2019) 10(32):3013–26. doi: 10.18632/oncotarget.26892

29. Jonsson VD, Ng RH, Dulleru N, Hibbard J, Wang D, Aguilar B, et al. CAR T cell therapy drives endogenous locoregional T cell dynamics in a responding patient with glioblastoma. *BioRxiv* (2021). doi: 10.1101/2021.09.22.460392

30. Jung YS, Park JI. Wnt signaling in cancer: therapeutic targeting of Wnt signaling beyond beta-catenin and the destruction complex. *Exp Mol Med* (2020) 52(2):183–91. doi: 10.1038/s12276-020-0380-6

31. Garvin JH Jr., Selch MT, Holmes E, Berger MS, Finlay JL, Flannery A, et al. Phase II study of pre-irradiation chemotherapy for childhood intracranial ependymoma. Children's Cancer Group protocol 9942: a report from the Children's Oncology Group. *Pediatr Blood Cancer* (2012) 59(7):1183–9. doi: 10.1002/pbc.24274

32. Zhao X, Liu Z, Yu L, Zhang Y, Baxter P, Voicu H, et al. Global gene expression profiling confirms the molecular fidelity of primary tumor-based orthotopic xenograft mouse models of medulloblastoma. *Neuro Oncol* (2012) 14(5):574–83. doi: 10.1093/neuonc/nos061

33. Khasraw M, Reardon DA, Weller M, Sampson JH. PD-1 Inhibitors: Do they have a Future in the Treatment of Glioblastoma? *Clin Cancer Res* (2020) 26(20):5287–96. doi: 10.1158/1078-0432.CCR-20-1135

34. Brown CE, Starr R, Martinez C, Aguilar B, D'Apuzzo M, Todorov I, et al. Recognition and killing of brain tumor stem-like initiating cells by CD8+ cytolytic T cells. *Cancer Res* (2009) 69(23):8886–93. doi: 10.1158/0008-5472.CAN-09-2687

35. Brown CE, Warden CD, Starr R, Deng X, Badie B, Yuan YC, et al. Glioma IL13Ralpha2 is associated with mesenchymal signature gene expression and poor patient prognosis. *PloS One* (2013) 8(10):e77769. doi: 10.1371/journal.pone.0077769

36. Geng A, Qiu R, Murai K, Liu J, Wu X, Zhang H, et al. KIF20A/MKLP2 regulates the division modes of neural progenitor cells during cortical development. *Nat Commun* (2018) 9(1):2707. doi: 10.1038/s41467-018-05152-1

37. Qiu R, Wu J, Gudenas B, Northcott PA, Wechsler-Reya RJ, Lu Q. Depletion of kinesin motor KIF20A to target cell fate control suppresses medulloblastoma tumour growth. *Commun Biol* (2021) 4(1):552. doi: 10.1038/s42003-021-02075-4

38. Manegold P, Lai KKY, Wu Y, Teo JL, Lenz HJ, Genyk YS, et al. Differentiation therapy targeting the beta-catenin/CBP interaction in pancreatic cancer. *Cancers (Basel)* (2018) 10(4). doi: 10.3390/cancers10040095

39. Anthony B, El-Khoueiry YN, Yang D, Cole S, Kahn M, Berg MZ, et al. A phase I first-in-human study of PRI-724 in patients (pts) with advanced solid tumors. *J Clin Oncol* (2013) 31(15 supplemental). doi: 10.1200/jco.2013.31.15_suppl.2501

40. Hu X, Ono M, Chimge NO, Chosa K, Nguyen C, Melendez E, et al. Differential Kat3 usage orchestrates the integration of cellular metabolism with differentiation. *Cancers (Basel)* (2021) 13(23). doi: 10.3390/cancers13235884

41. Thomas PD, Kahn M. Kat3 coactivators in somatic stem cells and cancer stem cells: biological roles, evolution, and pharmacologic manipulation. *Cell Biol Toxicol* (2016) 32(1):61–81. doi: 10.1007/s10565-016-9318-0

42. Geiss GK, Bumgarner RE, Birditt B, Dahl T, Dowidar N, Dunaway DL, et al. Direct multiplexed measurement of gene expression with color-coded probe pairs. *Nat Biotechnol* (2008) 26(3):317–25. doi: 10.1038/nbt1385

43. Bantug GR, Galluzzi L, Kroemer G, Hess C. The spectrum of T cell metabolism in health and disease. *Nat Rev Immunol* (2018) 18(1):19–34. doi: 10.1038/nri.2017.99

44. Vancurova I, Uddin MM, Zou Y, Vancura A. Combination therapies targeting HDAC and IKK in solid tumors. *Trends Pharmacol Sci* (2018) 39(3):295–306. doi: 10.1016/j.tips.2017.11.008

45. Knobloch M, Pilz GA, Ghesquiere B, Kovacs WJ, Wegleiter T, Moore DL, et al. A fatty acid oxidation-dependent metabolic shift regulates adult neural stem cell activity. *Cell Rep* (2017) 20(9):2144–55. doi: 10.1016/j.celrep.2017.08.029

46. Thomas TM, Yu JS. Metabolic regulation of glioma stem-like cells in the tumor micro-environment. *Cancer Lett* (2017) 408:174–81. doi: 10.1016/j.canlet.2017.07.014

47. Ono M, Kamita M, Murakoshi Y, Matsubara J, Honda K, Miho B, et al. Biomarker discovery of pancreatic and gastrointestinal cancer by 2DICAL: 2-dimensional image-converted analysis of liquid chromatography and mass spectrometry. *Int J Proteom* (2012) 2012:897412. doi: 10.1155/2012/897412

48. Nyam-Osor Chimge M-HC, Nguyen C, Wu X, Gonzales G, Ogana H, Hurwitz S, et al. Deeply quiescent CML LSC depend on FAO yet avoid deleterious ROS by suppressing mitochondrial complex I. *Curr Mol Pharmacol* (2023) 17(1):e060923220758. doi: 10.2174/1874467217666230906092236

49. Duan Q, Zhang H, Zheng J, Zhang L. Turning Cold into Hot: Firing up the Tumor Microenvironment. *Trends Cancer* (2020) 6(7):605–18. doi: 10.1016/j.trecan.2020.02.022

50. Chryplewicz A, Scotton J, Tichet M, Zomer A, Shchors K, Joyce JA, et al. Cancer cell autophagy, reprogrammed macrophages, and remodeled vasculature in glioblastoma triggers tumor immunity. *Cancer Cell* (2022) 40(10):1111–27 e9. doi: 10.1016/j.ccell.2022.08.014

51. Alizadeh D, Wong RA, Gholamin S, Maker M, Aftabizadeh M, Yang X, et al. IFNgamma is critical for CAR T cell-mediated myeloid activation and induction of endogenous immunity. *Cancer Discovery* (2021) 11(9):2248–65. doi: 10.1158/2159-8290.CD-20-1661

52. Alizadeh D, Wong RA, Gholamin S, Maker M, Aftabizadeh M, Yang X, et al. IFNg is critical for CAR T cell mediated myeloid activation and induction of endogenous immunity. *Cancer Discovery* (2021) 11(9):2248–65. doi: 10.1158/2159-8290.CD-20-1661

53. Herndler-Brandstetter D, Ishigame H, Shinnakasu R, Plajer V, Stecher C, Zhao J, et al. KLRG1(+) effector CD8(+) T cells lose KLRG1, differentiate into all memory T cell lineages, and convey enhanced protective immunity. *Immunity* (2018) 48(4):716–29 e8. doi: 10.1016/j.immuni.2018.03.015

54. Colpitts SL, Dalton NM, Scott P. IL-7 receptor expression provides the potential for long-term survival of both CD62Lhigh central memory T cells and Th1 effector cells during Leishmania major infection. *J Immunol* (2009) 182(9):5702–11. doi: 10.4049/jimmunol.0803450

55. Andersen BM, Reardon DA. Immunotherapy approaches for adult glioma: knowledge gained from recent clinical trials. *Curr Opin Neurol* (2022) 35(6):803–13. doi: 10.1097/WCO.0000000000001118

56. Li H, van der Leun AM, Yofe I, Lubling Y, Gelbard-Solodkin D, van Akkooi ACJ, et al. Dysfunctional CD8 T cells form a proliferative, dynamically regulated compartment within human melanoma. *Cell* (2020) 181(3):747. doi: 10.1016/j.cell.2020.04.017

57. Sade-Feldman M, Yizhak K, Bjorgaard SL, Ray JP, de Boer CG, Jenkins RW, et al. Defining T cell states associated with response to checkpoint immunotherapy in melanoma. *Cell* (2019) 176(1-2):404. doi: 10.1016/j.cell.2018.12.034

58. Chen L, Chiang YC, Chan LS, Chau WY, Lung ML, Kahn M, et al. The CBP/beta-Catenin Antagonist, ICG-001, Inhibits Tumor Metastasis via Blocking of the miR-134/ITGB1 Axis-Mediated Cell Adhesion in Nasopharyngeal Carcinoma. *Cancers (Basel)* (2022) 14(13). doi: 10.3390/cancers14133125

59. Kahn M. Taking the road less traveled - the therapeutic potential of CBP/beta-catenin antagonists. *Expert Opin Ther Targets* (2021) 25(9):701–19. doi: 10.1080/14728222.2021.1992386

60. Wong AM, Ding X, Wong AM, Xu M, Zhang L, Leung HH, et al. Unique molecular characteristics of NAFLD-associated liver cancer accentuate beta-catenin/TNFRSF19-mediated immune evasion. *J Hepatol* (2022) 77(2):410–23. doi: 10.1016/j.jhep.2022.03.015

61. Wiese M, Walther N, Diederichs C, Schill F, Monecke S, Salinas G, et al. The beta-catenin/CBP-antagonist ICG-001 inhibits pediatric glioma tumorigenicity in a Wnt-independent manner. *Oncotarget* (2017) 8(16):27300–13. doi: 10.18632/oncotarget.15934

62. Wang D, Starr R, Chang WC, Aguilar B, Alizadeh D, Wright SL, et al. Chlorotoxin-directed CAR T cells for specific and effective targeting of glioblastoma. *Sci Transl Med* (2020) 12(533). doi: 10.1126/scitranslmed.aaw2672

63. Azzarelli R, McNally A, Dell'Amico C, Onorati M, Simons B, Philpott A. ASCL1 phosphorylation and ID2 upregulation are roadblocks to glioblastoma stem cell differentiation. *Sci Rep* (2022) 12(1):2341. doi: 10.1038/s41598-022-06248-x

64. Matjasic A, Zupan A, Bostjancic E, Pizem J, Popovic M, Kolenc D. A novel PTPRZ1-ETV1 fusion in gliomas. *Brain Pathol* (2020) 30(2):226–34. doi: 10.1111/bpa.12776

65. Abdelfattah N, Kumar P, Wang C, Leu JS, Flynn WF, Gao R, et al. Single-cell analysis of human glioma and immune cells identifies S100A4 as an immunotherapy target. *Nat Commun* (2022) 13(1):767. doi: 10.1038/s41467-022-28372-y

66. Yeo AT, Shah R, Aliazis K, Pal R, Xu T, Zhang P, et al. Driver mutations dictate the immunologic landscape and response to checkpoint immunotherapy of glioblastoma. *Cancer Immunol Res* (2023) 11(5):629–45. doi: 10.1158/2326-6066.CIR-22-0655

Frontiers in Immunology

Explores novel approaches and diagnoses to treat immune disorders.

The official journal of the International Union of Immunological Societies (IUIS) and the most cited in its field, leading the way for research across basic, translational and clinical immunology.

Discover the latest Research Topics

See more →

Frontiers

Avenue du Tribunal-Fédéral 34
1005 Lausanne, Switzerland
frontiersin.org

Contact us

+41 (0)21 510 17 00
frontiersin.org/about/contact